

Characterization of ergodicity breaking in disordered quantum systems

Dissertation
zur Erlangung des akademischen Grades
Doctor rerum naturalium
(Dr. rer. nat.)

vorgelegt
der Fakultät Mathematik und für Naturwissenschaften
der Technischen Universität Dresden

von
Giuseppe De Tomasi
geboren am 20 Oktober 1987 in Vizzolo Predabissi, Italien

Wissenschaftlicher Betreuer:
Prof. J.H. Bardarson und Prof. Dr. Frank Pollmann

Dresden, October 2018

Eingereicht am 07. Mai 2018

Gutachter:

1. Dr. Markus Heyl
2. Prof. Dr. Roland Ketzmerick
3. Prof. Dr. Roderich Moessner
4. Prof. Dr. Frank Pollmann

Verteidigt am 20. August 2018

Abstract

The interplay between quenched disorder and interaction effects opens the possibility in a closed quantum many-body system of a phase transition at finite energy density between an ergodic phase, which is governed by the laws of statistical physics, and a localized one, in which the degrees of freedom are frozen and ergodicity breaks down. The possible existence of a quantum phase transition at finite energy density is strongly questioning our understanding of the fundamental laws of nature and has generated an active field of research called many-body localization.

This thesis consists of three parts and is dedicated to the understanding and characterization of the phenomenon of many-body localization, approaching it from complementary facets. In particular, borrowing methods and tools from different fields, we analyze timely problems.

The first part of the thesis is devoted to detecting the many-body localization transition and to characterize both the ergodic and the localized phase it separates. Here we provide a characterization from two different perspectives: the first one is based on the study of local entanglement properties. In the second one, using tools from quantum-chaos theory, we attempt to answer the question of understanding time-irreversibility, and thus probing the breaking of ergodicity. We analyze experimentally viable observables. Moreover, we propose two different quantities to distinguish an Anderson insulating phase from a many-body localized one, which is one of the issues in experiments.

The second part focuses on understanding the existence of a putative subdiffusive multifractal phase. Analyzing the quantum dynamics of the system in this region of the phase diagram, we point out the importance of finite-size effects, questioning the existence of this multifractal phase. We speculate with a possible scenario in which the diffusivity and thus ergodicity could be restored in the thermodynamic limit. Furthermore, we find that the propagation is highly non-Gaussian, which could have an important effect on understanding the critical point of the according transition. We tackle this problem also from a different angle. A possible toy-model to understand many-body localization entails the Anderson model on a random-regular graph. Also in the latter model the possible existence of an intermediate multifractal phase has been conjectured. There, studying the survival return probability of a particle with time, we give a new characterization of multifractal phases and give indication of the possible existence of this phase. Nevertheless, we also outline possible caveats.

In the last part of this thesis we study the interplay between symmetry and correlated disorder in a non-interacting fermionic system. We show another possible mechanism for breaking localization. In particular, we focus on studying information and particle transport, emphasizing how the two types of propagation can be different.

List of Publications

- **G. De Tomasi**, F. Pollmann, M. Heyl, “*Solving efficiently the dynamics of many-body localized systems at strong disorder*”. arXiv:1810.04178.
- S. Bera, **G. De Tomasi**, I. M. Khaymovich, A. Scardicchio, “*Return probability for the Anderson model on the random regular graph*”. arXiv:1805.12354.
- **G. De Tomasi**, M. Amini, S. Bera, I. M. Khaymovich, V. E. Kravtsov, “*Survival probability in Generalized Rosenzweig-Porter random matrix ensemble*”. arXiv:1805.06472.
- Shreya Vardhan, **Giuseppe De Tomasi**, Markus Heyl, Eric J. Heller, Frank Pollmann. “*Characterizing time-irreversibility in disordered fermionic systems by the effect of local perturbations*”. Phys. Rev. Lett. 119, 016802 (2017).
- Soumya Bera, **Giuseppe De Tomasi**, Felix Weiner, Ferdinand Evers. “*Density propagator for many-body localization: finite size effects, transient subdiffusion, and exponential decay*”. Phys. Rev. Lett. 118, 196801 (2017).
- **Giuseppe De Tomasi**, Soumya Bera, Jens H. Bardarson, Frank Pollmann. “*Quantum Mutual Information as a Probe for Many-Body Localization*”. Phys. Rev. Lett. 118, 016804 (2017).
- **Giuseppe De Tomasi**, Sthitadhi Roy, Soumya Bera. “*Generalized Dyson model: nature of zero mode and its implication in dynamics*”. Phys. Rev. B 94, 144202 (2016).

Acknowledgements

I would like to thank Prof. Dr. Jens H. Bardarson and Prof. Dr. Frank Pollmann for strongly supporting me in the time of my Ph.D. studies. Moreover, I would like to thank everyone with whom I have collaborated, Prof. Dr. Bera Soumya, Dr. Sthitadhi Roy, Dr. Mohsen Amini, Dr. Ivan M. Khaymovich, Dr. Markus Heyl, Prof. Dr. Antonello Scardicchio, Felix Weiner, Prof. Ferdinand Evers, Prof. Dr. Eric J. Heller, Shreya Vardhan and Prof. Dr. Vladimir E. Kravtsov. For reviews and comments made on this thesis I am very grateful to Prof. Soumya Bera, Dr. Ivan M. Khaymovich, Dr. Sthitadhi Roy, Dr. Jad C. Halimeh, Daniel Trapin, Dr. Robert J. Slager, Srivatsa N. S. Prasanna and Talía Lezama. I would like to thank the visitors program, the administrative staff and the IT department of MPIPKS

Contents

Abstract	i
List of Publications	ii
Acknowledgements	iii
I Introduction	1
1 Anderson Localization	5
1.1 The locator Expansion	6
1.2 Self-consistent theory of localization	11
1.2.1 Anderson localization on a Bethe lattice	13
1.3 Anderson Localization in one dimension	15
1.3.1 Localization length and density of states	17
1.3.2 Landauer formalism	18
1.4 Aubry-André-Harper model	19
1.5 Multifractal wavefunctions	21
2 Many-Body Localization	23
2.1 Integrable closed quantum many-body systems and the concept of non-integrability	24
2.2 Quantum Thermalization in closed quantum systems	26
2.2.1 Eigenstate thermalization hypothesis	29
2.2.1.1 Thermalization in Random Matrices	30
2.2.1.2 Thermalization in generic closed quantum many-body systems	30
2.2.1.3 Numerical evidence for the eigenstate thermalization hypothesis	31
2.3 Many-Body-Localization	34
2.3.1 Localization in Fock Space	36
2.3.2 Numerical evidence of Many-Body Localization	38
2.3.2.1 Analysis of the level statistics	39
2.3.2.2 Eigenstates analysis	41

2.3.2.3	Integrals of motion	43
2.3.2.4	Many-body mobility edges	45
2.3.2.5	Absence of transport	46
2.3.2.6	Unbounded growth of Entanglement	47
II Detecting the Many-Body Localization transition and characterization of the ergodic and many-body localized phases		50
3	Quantum Mutual Information as a Probe for Many-Body Localization	52
3.1	Models	53
3.2	Quantum Mutual Information	54
3.3	Quantum mutual information for the Aubry-André-Harper model	56
3.4	Quantum mutual information for many-body localization	58
3.4.1	Unbounded spread of quantum mutual information	60
3.5	Summary	62
4	Characterizing time-irreversibility in disordered fermionic systems	64
4.1	Models and methods	65
4.2	Non-interacting models	67
4.2.1	Loschmidt Echo for non-interacting models	67
4.2.2	Difference of the local density profile in non-interacting models	72
4.3	Spinless t-V chain	74
4.3.1	Loschmidt echo for the t-V chain	74
4.3.2	Difference of the local density profile in the Spinless t-V chain	76
4.3.3	An effective model for many-body localized systems	78
4.4	Summary	82
III Study of Multifractal phases in Many-Body and Anderson localization on hierarchical tree-structures		83
5	Subdiffusion, mobility edges, and finite-size effects in many-body localized systems	85
5.1	Model and methods	86
5.2	Mean square displacement	87
5.3	Flowing of the dynamical exponent	88
5.4	Return probability	91
5.5	Density propagator	92
5.6	Numerical Tests	93
5.6.1	Chebyshev-representation of the density matrix $\hat{\rho}(\varepsilon)$	94
5.6.2	Stochastic trace evaluation and convergence	95
5.7	Summary	97
6	Typical versus mean properties as a sensitive probe of multifractal states	100
6.1	Models and methods	102

6.2	Return probability for the power-law banded matrices and for the Rosenzweig-Porter random matrices	105
6.3	Return probability in a random regular graph	107
6.4	Summary	112
IV	Role of Symmetry and Correlation in the disorder	113
7	The generalized Dyson model	115
7.1	Model and localization length	115
7.2	Dynamical properties	119
7.2.1	Dyson II	120
7.2.2	Generalized Dyson model	121
7.3	Summary	123
8	Conclusions and Outlooks	125
A	Appendix	129
A.1	Time evolution: Chebyshev expansion	129
A.2	Bipartite entanglement entropy for non-interacting spinless fermions . . .	130
	Bibliography	131
	Erklärung	143

In memory of my Father

Part I

Introduction

The deep relation between thermodynamics and probability theory allows one to describe extremely complex systems composed of a huge number of degrees of freedom by the knowledge of only few thermodynamic parameters [119]. The resulting concept of *classical statistical physics* is a self-consistent framework which is strongly based on the underlying ergodic hypothesis [53, 119]. The ergodic hypothesis states that the time that the system spends in a region composed by its allowed microstates is proportional to the volume of the region. Moreover, the dominance in probability of “typical” microstates, makes the laws of thermodynamics a very intuitive concept.

Indeed, nobody will expect to see particles going back to an atypical initial condition in a generic classical system. Nevertheless, the applicability as well as the foundations of statistical physics for a closed quantum many-body system are not well understood [40]. On the one hand, recent advancements of controlled experimental techniques suggest that generic closed quantum systems can thermalize [78], in the sense that the local degrees of freedom in the long-time limit can be described by the laws of statistical physics. On the other hand, thermalization can fail in strongly disordered closed interacting many-body systems [17, 62]. The discovery of a class of generic systems in which statistical physics breaks down questions our understanding of the fundamental laws of nature.

The breaking of ergodicity is intimately connected with the phenomenon of Anderson localization, in which non-interacting quantum particles subjected to a disordered potential can be localized due to destructive interference [9]. Whether interactions will delocalize the particles, and thus restore ergodicity, has puzzled physicists for many decades, culminating in the discovery of a new type of quantum phase transition, which may occur also at finite energy density [17, 62]. Indeed, the interplay between interactions and quantum interference due to the presence of a disordered potential can drive the system into a transition separating an ergodic phase, in which a mechanical statistical description is possible, and a localized phase, in which its degrees of freedom are frozen and ergodicity breaks down.

In the last few years many attempts have been undertaken with the aim of understating and characterizing this transition, hence generating a fast moving field called *many-body localization* (MBL) [106]. Furthermore, this result, besides questioning our understanding of the applicability of statistical physics, is drastically changing the perspective of condensed-matter physics. Condensed-matter theory, traditionally focuses on understanding low-temperature properties. Hence, the possibility of a quantum phase transition at finite energy density is redirecting the attention to the study of highly-excited states, and thus facilitating the development of new ideas and methods, including new analytical treatments and new numerical techniques [77, 152, 153, 159]. Moreover, the

recent progress in experimental techniques in cold atoms and trapped ions provides for a perfect playground to confirm and to stimulate new concepts, producing in less than ten years of the discovery of MBL its first experimental evidence [24, 97, 129, 137].

Despite many efforts to characterize the two phases and to classify the transition, still little is known about fundamental aspects of the problem [106]. Most of the difficulties emerge due to the lack of powerful techniques to tackle interacting disordered systems at finite energy density. Indeed, many of the standard methods both numerical and analytical were developed to understand quantum phase transitions at the level of the ground state. These methods fail badly due to the exponential growth in complexity of the problem with system size. Furthermore, with the aim to solve the problem came up many surprising results. For example the diffusive behavior expected in the ergodic phase has not been confirmed by numerical simulations, rather a subdiffusive phase composed by critical states has been found [15, 60, 94, 96, 132, 150]. Hence, MBL still remains a changing unsolved problem.

The main aim of this thesis is to analyze the phenomena of MBL from complementary different facets attempting to solve timely problems. This thesis is organized as follows:

In the first part (Part I), we introduce the main concepts and methods that we will use throughout the thesis. In particular, in Chapter 1 we give an introduction of Anderson localization, focusing on models in hierarchical tree-structures and one-dimensional lattices.

In Chapter 2, we introduce the concepts of thermalization in closed quantum many-body systems. Here, we state and show numerical evidence of the *eigenstate thermalization hypothesis* [40, 138], which is the most accredited theory attempting to explain thermalization in generic closed quantum systems. After that, we define the MBL problem and report on several numerical characterizations of the highly excited quantum phase transition. We give particular attention to the original idea of mapping this problem to an Anderson localization model on a hierarchical tree-structure (localization in Fock space). In Parts II-IV we present the results of the thesis.

In Part II, we focus on detecting the MBL transition and on characterizing both the ergodic and the MBL phase. In Chapter 3 we focus on the study of local entanglement properties. Here, borrowing tools from quantum-information theory, we demonstrate how the quantum-mutual information can be efficiently used to detect the transition and to uniquely describe the two phases. In Chapter 4, with the aim of characterizing time-irreversibility in MBL systems, using tools from quantum-chaos theory, we give a new characterization of the two phases. In both chapters we study only quantities that in principle could be measured in an experimental setup. Moreover, we propose new

methods to distinguish a non-interacting Anderson phase from an MBL phase, which is a rather timely and relevant issue.

In Part III, we study the possible existence of an intermediate phase which is neither ergodic nor localized, but composed of critical states (multifractal), which give rise to subdiffusive transport. Specially, in Chapter 5, studying the dynamical property of the system we question the existence of this phase, showing that its apparent signatures could be just a finite-size effect and proposing a possible alternative scenario. In Chapter 6, we tackle this problem from a different angle. A toy-model to understand MBL systems could be the Anderson model on a random regular graph [7, 41, 57, 82, 145]. Also for this toy-model, an intermediate multifractal phase could exist [7, 41, 82]. Studying the wavepacket dynamics we provide evidence of its existence. Moreover, we propose a new method to characterize multifractal phases.

In the last Part IV, we investigate the interplay between correlated disorder and symmetry for a new model of non-interacting fermions. We emphasize how this interplay can lead to a delocalization-localization transition at a specific single-particle energy. We study the non-equilibrium dynamics, showing that information can propagate slower than particles.

Finally, in Chapter 8 we summarize the results of this thesis, underlining open issues and proposing new possible research directions.

Chapter 1

Anderson Localization

Anderson Localization is a wave-phenomenon in which transport in a non-interacting system can be suppressed due to the presence of a quenched disorder potential [9, 147]. The existence of Anderson localization for a quantum system is intimately connected to the particle-wave duality in quantum mechanics [126]. A classical particle subject to a random potential $U(x)$ will have a different kind of propagation depending on its kinetic energy, K . Indeed, if its kinetic energy is larger than $U(x)$ ($K > U(x)$), the particle will propagate through the system. Instead, if its kinetic energy is smaller than $U(x)$ ($K < U(x)$), the particle will be able only to visit a bounded portion of the system and it will oscillate back and forth in this allowed region [86]. Quantum mechanics changes drastically this scenario, where a quantum particle behaves like a wave and it will be able to tunnel through also higher potential barriers than its kinetic energy [126]. Nevertheless, at the same time, a part of it will also be reflected by small potential barriers. The reflected and the transmitted parts of the wavefunction will not only interfere constructively but also destructively. At first approximation, this transmitted-reflected phenomenon will take place randomly and hence the motion of the particle may be approximated as a random walker where the particle diffuses through the system. Nevertheless, this expectation turns out to be incorrect in the presence of strong enough disorder. Indeed, if the disorder is strong enough, destructive interference will dominate the constructive one and the transport will be completely suppressed, even if the kinetic energy of the quantum particle is larger than the disordered potential. This phenomenon was for the first time discovered by P.W. Anderson in his seminal work [9].

In this chapter, we will give an introduction to Anderson localization focusing on the main results which are the conceptual backbone of this thesis.

1.1 The locator Expansion

In the seminal work of P.W. Anderson a tight-binding model is considered in a cubic lattice subject to a random potential. The Hamiltonian reads

$$\hat{\mathcal{H}} = -J \sum_{\langle \mathbf{x}, \mathbf{y} \rangle} |\mathbf{x}\rangle \langle \mathbf{y}| + \sum_{\mathbf{x}} \mu_{\mathbf{x}} |\mathbf{x}\rangle \langle \mathbf{x}|, \quad (1.1)$$

$|\mathbf{x}\rangle$ represents a state completely localized in the site \mathbf{x} , $\{\mu_{\mathbf{x}}\}$ are random variables uniformly distributed between $[-W/2, W/2]$ and the notation $\langle \mathbf{x}, \mathbf{y} \rangle$ indicates that sites \mathbf{x} and \mathbf{y} are nearest neighbors. In the literature, the tight-binding model with uncorrelated disordered potential is often referred as the Anderson model [51]. The idea is to consider a particle initially localized in a site (without loss of generality, we will take $|\mathbf{0}\rangle$) and calculate the return probability in time, defined by:

$$|\mathcal{G}_{\mathbf{0}, \mathbf{0}}(t)|^2 = |\langle \mathbf{0} | e^{-i\hat{\mathcal{H}}t} | \mathbf{0} \rangle|^2. \quad (1.2)$$

If the system is localized, $\lim_{T \rightarrow \infty} 1/T \int_0^T |\mathcal{G}_{\mathbf{0}, \mathbf{0}}(t)|^2 > 0$, since its amplitude does not completely diffuse through the system. Nevertheless, at this point it is important to underline that even if $\lim_{T \rightarrow \infty} 1/T \int_0^T |\mathcal{G}_{\mathbf{0}, \mathbf{0}}(t)|^2 > 0$, the particle can propagate through the system, since $|\mathcal{G}_{\mathbf{0}, \mathbf{0}}(t)|^2$ is a local probe and it does not detect the propagation outside the starting point. The last statement is connected to the fact that the system can be only partially localized, in the sense that only for some energies the system is localized [51].

$\mathcal{G}_{\mathbf{0}, \mathbf{0}}(t)$ is the Green's function in the space-time domain. However, to analyze the problem better, it is necessary to consider it in the energy domain

$$\begin{aligned} \mathcal{G}_{\mathbf{x}, \mathbf{y}}(E) &= \int \frac{dt}{2\pi} e^{iEt} \mathcal{G}_{\mathbf{x}, \mathbf{y}}(t) \\ &= -i \lim_{\eta \rightarrow 0} \int_0^{\infty} dt e^{i(E+i\eta)t} \mathcal{G}_{\mathbf{x}, \mathbf{y}}(t) \\ &= \langle \mathbf{x} | (E - \hat{\mathcal{H}} + i0^+)^{-1} | \mathbf{y} \rangle, \end{aligned} \quad (1.3)$$

where $\mathcal{G}_{\mathbf{x}, \mathbf{y}}(t) = \langle \mathbf{x} | e^{-i\hat{\mathcal{H}}t} | \mathbf{y} \rangle$.

The formal solution for $\mathcal{G}_{\mathbf{x}, \mathbf{y}}(E)$ is given by

$$\mathcal{G}_{\mathbf{x}, \mathbf{y}}(E) = \frac{\delta_{\mathbf{x}, \mathbf{y}}}{E - \mu_{\mathbf{x}}} + \frac{J_{\mathbf{x}, \mathbf{y}}}{(E - \mu_{\mathbf{x}})(E - \mu_{\mathbf{y}})} + \sum_{\mathbf{x}_1} \frac{J_{\mathbf{x}, \mathbf{x}_1} J_{\mathbf{x}_1, \mathbf{y}}}{(E - \mu_{\mathbf{x}})(E - \mu_{\mathbf{x}_1})(E - \mu_{\mathbf{y}})} + \dots, \quad (1.4)$$

where we have defined the matrix elements $J_{\mathbf{x}, \mathbf{y}}$, to be equal to J if \mathbf{x} and \mathbf{y} are linked in the 3D lattice structure, but zero otherwise. The Green's function can be rewritten

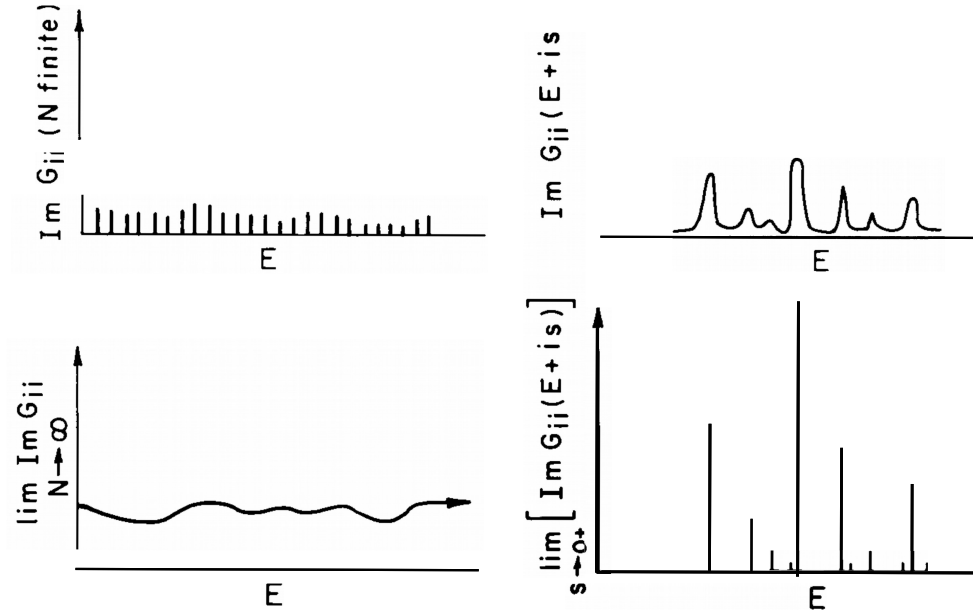


FIGURE 1.1: The left-column shows the behavior of the imaginary part of the Green's function in the case in which the system is delocalized, while the right-column shows the case in which the system is localized [116]. In the figure N is the volume of the system.

defining the self-energy $\Sigma_{\mathbf{x},\mathbf{x}}(E)$

$$\mathcal{G}_{\mathbf{x},\mathbf{x}}(E) = \frac{1}{E - \mu_{\mathbf{x}} - \Sigma_{\mathbf{x},\mathbf{x}}(E)}, \quad (1.5)$$

with

$$\Sigma_{\mathbf{x},\mathbf{x}}(E) = \sum_{n=1}^{\infty} \sum_{\mathbf{x}_1, \mathbf{x}_2, \dots, \mathbf{x}_n \neq \mathbf{x}} \frac{J_{\mathbf{x},\mathbf{x}_1} J_{\mathbf{x}_1,\mathbf{x}_2} \cdots J_{\mathbf{x}_n,\mathbf{x}}}{(E - \mu_{\mathbf{x}_1})(E - \mu_{\mathbf{x}_2}) \cdots (E - \mu_{\mathbf{x}_n})}. \quad (1.6)$$

Broadening the energy ($E \rightarrow E + i\eta$) with $\eta > 0$ to ensure convergence, the real part of the self-energy ($\text{Re}(\Sigma_{\mathbf{x},\mathbf{x}}(E + i\eta))$) gives a renormalization of the site energies $\{\mu_{\mathbf{x}}\}$, while the imaginary part of the self-energy ($\text{Im}(\Sigma_{\mathbf{x},\mathbf{x}}(E + i\eta))$) determines the decay of $\mathcal{G}_{\mathbf{0},\mathbf{0}}(t)$ with time. We have to distinguish two cases depending on the behavior of $\text{Im}(\Sigma_{\mathbf{x},\mathbf{x}}(E + i\eta))$:

1. If $\lim_{\eta \rightarrow 0} \text{Im} \Sigma_{\mathbf{0},\mathbf{0}}(E + i\eta)$ exists and it is a regular function of E , then by the Riemann-Lebesgue theorem

$$\lim_{t \rightarrow \infty} \mathcal{G}_{\mathbf{0},\mathbf{0}}(t) \rightarrow 0.$$

The return probability decays to zero with time and thus the system is delocalized.

2. A different possibility is that $\lim_{\eta \rightarrow 0} \text{Im} \Sigma_{\mathbf{0}, \mathbf{0}}(E + i\eta)$ is not a regular function of E . Let's consider the case in which we truncate Eq. 1.6 only to second order in J

$$\lim_{\eta \rightarrow 0} \text{Im} \Sigma_{\mathbf{0}, \mathbf{0}}(E + i\eta) \approx - \lim_{\eta \rightarrow 0} \sum_{\langle \mathbf{x}_1 \rangle} \frac{J^2 \eta}{(E - \mu_{\mathbf{x}_1})^2 + \eta^2} = -\pi J^2 \sum_{\langle \mathbf{x}_1 \rangle} \delta(E - \mu_{\mathbf{x}_1}),$$

the sum $\sum_{\langle \mathbf{x}_1 \rangle}$ runs over the six neighboring sites of $\{\mathbf{0}\}$.

$$i\mathcal{G}_{\mathbf{0}, \mathbf{0}}(t) = - \lim_{\eta \rightarrow 0} \int i \frac{dE}{2\pi} \left(E + i\eta - \mu_{\mathbf{0}} - \sum_{\langle \mathbf{x}_1 \rangle} \frac{J^2}{E + i\eta - \mu_{\mathbf{x}_1}} \right)^{-1} e^{-iEt} = \sum_j C_j e^{-i\tilde{E}_j t}, \quad (1.7)$$

where $\{\tilde{E}_j\} \in \mathbb{R}$ are respectively the poles of the integrand function. In this case $|\mathcal{G}_{\mathbf{0}, \mathbf{0}}(t)|^2$ does not decay and thus the system is localized.

At this point we find that if the system is localized, then $\lim_{\eta \rightarrow 0} \text{Im} \Sigma_{\mathbf{0}, \mathbf{0}}(E + i\eta)$ must have a non-regular part.

To get a better physical understanding, let's define the local density of states

$$n(E, \mathbf{0}) = \sum_l |\psi_l(\mathbf{0})|^2 \delta(E - \epsilon_l), \quad (1.8)$$

where $\{\psi_l(\mathbf{x})\}$ are the eigenstates of $\hat{\mathcal{H}}$ (Eq. 1.1) with eigenenergies $\{\epsilon_l\}$. The local density of state is connected to the Green's function by the relation [50]

$$n(E, \mathbf{0}) = - \lim_{\eta \rightarrow 0} \frac{1}{\pi} \text{Im} \mathcal{G}_{\mathbf{0}, \mathbf{0}}(E + i\eta).$$

So far we have defined localization only considering the transport properties of the system, nevertheless it will turn out (at least for this kind of systems with uncorrelated disorder and without special symmetry [121]) that if transport is absent, then the eigenstates of $\hat{\mathcal{H}}$ (Eq. 1.1) are exponentially localized $\psi_l(\mathbf{x}) \sim e^{-|\mathbf{x} - \mathbf{x}_{\text{loc}}|/\xi_{\text{loc}}}$, where \mathbf{x}_{loc} is the center of localization and ξ_{loc} is the localization length. In other words, if the system is localized then its eigenstates will have a finite support in space ($\sim \xi_{\text{loc}}$) which does not scale with the volume of the system. On the contrary, if the system is delocalized, then $\{\psi_l(\mathbf{x})\}$ will be to first approximation, spread out in the entire system and their amplitudes will be uniform $|\psi_l(\mathbf{x})|^2 \sim 1/V$, where V is the volume for a finite system.

Let's consider a finite system of volume V , whose spectrum is always discrete

$$\text{Im} \mathcal{G}_{\mathbf{0}, \mathbf{0}}(E + i\eta, V) = - \sum_l^V |\psi_l(\mathbf{0})|^2 \frac{\eta}{(E - \epsilon_l)^2 + \eta^2}. \quad (1.9)$$

If the system is delocalized,

$$\text{Im}\mathcal{G}_{\mathbf{0},\mathbf{0}}(E + i\eta, V) \sim -\frac{1}{V} \sum_l^V \frac{\eta}{(E - \epsilon_l)^2 + \eta^2}.$$

Thus, for a finite system and for a finite η , $n(E, \mathbf{0})$ will be a sum ($\sim \mathcal{O}(V)$) of Lorentzians with a height $\sim \mathcal{O}(1/V\eta)$. In the limit $V \rightarrow \infty$ and $\eta \rightarrow 0$ with $V \cdot \eta \sim \mathcal{O}(1)$, $n(E, \mathbf{0})$ will be a smooth finite function of E . Instead, for a localized system, in the sum of Eq. 1.9 contribute only energies such that the distance between the site $\mathbf{0}$ and the localized center of the respective eigenstates is within the localization length

$$\text{Im}\mathcal{G}_{\mathbf{0},\mathbf{0}}(E + i\eta, V) \sim -\frac{1}{\xi_{\text{loc}}} \sum_{l: |\mathbf{x}_{\text{loc}}(l)| < \xi_{\text{loc}}} \frac{\eta}{(E - \epsilon_l)^2 + \eta^2}.$$

In this case, $\text{Im}\mathcal{G}_{\mathbf{0},\mathbf{0}}(E + i\eta, V)$ will be sum of a finite number ($\sim \mathcal{O}(\xi_{\text{loc}})$) of Lorentzians with height $\sim \mathcal{O}(1/\xi_{\text{loc}}\eta)$. Thus, for a localized system, in the limit $V \rightarrow \infty$ and $\eta \rightarrow 0$, $n(E, \mathbf{0})$ is not a regular function. Figure 1.1 [116] is a graphical representation of what we have discussed, it shows the behavior of the imaginary part of the Green's function in the case in which the system is delocalized (left-column) and in which the system is localized (right-column). Moreover, it is important to note that so far we did not average over disorder configurations $\{\mu_{\mathbf{x}}\}$, indeed the average over disorder will wash out the difference in Eq. 1.9 between extended states and localized states. Averaging over disorder is equivalent to making an average over space in the limit $V \rightarrow \infty$, it is called self-averaging and it can be proved rigorously that for the imaginary part of the Green's function it holds [92], that

$$\overline{\text{Im}\mathcal{G}_{\mathbf{0},\mathbf{0}}(E + i\eta, V)} \sim \frac{1}{V} \sum_{\mathbf{x}} \sum_l^V |\psi_l(\mathbf{x})|^2 \frac{\eta}{(E - \epsilon_l)^2 + \eta^2} \sim \mathcal{O}(1/V\eta),$$

where the overline indicates the average over the disorder configurations. The averaged local density of states is always a smooth function regardless if the system is localized or not. For this reason, to understand if the system is localized or not, one can not just study the averaged local density of states, but one must also study the entire probability distribution. Moreover, since $\text{Im}\mathcal{G}_{\mathbf{0},\mathbf{0}}(E + i\eta) \propto \text{Im}\Sigma_{\mathbf{0},\mathbf{0}}(E + i\eta)$, P.W. Anderson studied the probability distribution of $\text{Im}\Sigma_{\mathbf{0},\mathbf{0}}(E + i\eta)$ [9].

Let $P_{E,\eta}(\Gamma)$ be the probability distribution of $\Gamma = -\text{Im}\Sigma_{\mathbf{0},\mathbf{0}}(E + i\eta)$. We have seen that for a localized system, Γ must not be regular (*e.g.*, sum of delta-functions), which implies that with probability one Γ must be zero, so $\lim_{\eta \rightarrow 0} P_{E,\eta}(\Gamma > 0) \rightarrow 0$.

In general, Γ is a sum of Lorentzians, and with high probability ($\sim 1 - \mathcal{O}(\eta)$), we have $\Gamma = \eta J^2/W^2$ (second order perturbation theory in J/W), which implies

$$\frac{J^2}{W^2} P_{E,\eta}(J^2/W^2) \sim \mathcal{O}(1) \Rightarrow P_{E,\eta}(\eta J^2/W^2) \sim W^2/(\eta J^2) \quad \text{“Typical-condition”}.$$

Nevertheless, with a small probability $\mathcal{O}(\eta/W)$, the energy E is in resonance with an on-site energy and so $\Gamma \sim J^2/\eta$

$$\frac{J^2}{\eta} P_{E,\eta}(J^2/\eta) \sim \mathcal{O}(\eta/W) \Rightarrow P_{E,\eta}(J^2/\eta) \sim \eta^2/(WJ^2) \quad \text{“Rare events-condition”}.$$

Moreover, we have seen that the average over disorder configurations of Γ is always finite ($\Gamma > 0$) independently if the system is localized or not. Thus, its probability distribution must have long-tail, so we can assume that $P_{E,\eta}(\Gamma) \sim 1/\Gamma^\alpha$. Matching the “Typical” and “Rare” events conditions, we have

$$P_{E,\eta}(\Gamma) \sim \frac{J}{W} \sqrt{\eta/\Gamma^3}. \quad (1.10)$$

Furthermore, the imaginary part of the self-energy can be expressed using the so called path-representation [92, 128]

$$\text{Im}\Sigma_{\mathbf{0}}(E + i\eta) = -\eta \left| \sum_{path} A_{path} \right|^2 + \mathcal{O}(\eta^3), \quad A_{path} = \prod_{\mathbf{x}_j \in path} \frac{J}{E - \mu_{\mathbf{x}_j}},$$

where the sum runs over all possible paths that start from $\mathbf{0}$ and that never return back. Thus $\Gamma = \eta A$, as $\eta \rightarrow 0$ the only possibility to have a finite Γ is that A diverges in probability as the length of the paths goes to infinity. To analyze the probability distribution of A , P.W. Anderson makes the following simplifications:

1. Only the center of the band is considered ($E = 0$).
2. The paths are statistically independent.
3. Only non self-crossing paths are considered.

Using these approximations and using a generalization of the central limit theorem in the case in which random variables do not have a finite variance, it is possible to estimate the probability distribution ($P_n(A)$) of A with the restriction that A contains only paths with fixed length n [9]

$$P_n(A) \sim \frac{[evK \ln(1/v)]^n}{A^{2-1/\ln 1/v}} \exp \left[-C \frac{[evK \ln(1/v)]^n}{A^{1-1/\ln 1/v}} \right], \quad (1.11)$$

K is the constant that determines how many non self-crossing paths of length n exist ($V \sim CK^n$) and $v = J/W$. Thus in the limit $n \rightarrow \infty$, if $evK \ln(1/v) < 1$ $\lim_{n \rightarrow \infty} P_n(A) \rightarrow 0$ and thus the system is localized. Instead, if $evK \ln(1/v) > 1$, $P_n(A)$ diverges as $n \rightarrow \infty$ and it is a sign that perturbation theory breaks down and that the system could be delocalized. The critical value of W is determined by

$$evK \ln(1/v) = 1 \Rightarrow \frac{eKJ}{W_c} \ln \frac{W_c}{J} = 1 \quad (1.12)$$

It is important to note that this estimate for the critical value is an upper-bound, since it is derived doing perturbation theory from the localized phase. In the second part of his work, P.W. Anderson tried to remove the simplification of considering only non self-crossing paths by introducing a cut-off on the probability distribution of the random variables $\{\mu_{\mathbf{x}}\}$ ($|\mu_{\mathbf{x}}| > \delta(W) > 0$ for $E = 0$) [9] in order to avoid resonant processes. By introducing this cut-off, it is possible to obtain a redefined formula for the critical point

$$\frac{2KJ}{W_c(1 - (J/W_c)^2)} \ln \frac{W_c}{J} = 1. \quad (1.13)$$

Recapitulating, P.W. Anderson proved that the tight-binding model with diagonal uncorrelated disorder has a transition between extended states and localized states in a cubic lattice (localization-delocalization transition). Nevertheless, the assumption that the paths are statistically independent is mathematically incorrect [142] and also the introduction of the cut-off is difficult to motivate [1]. For this reason more than 10 years later R. Abou-Chacra, D. J. Thouless and P. W. Anderson proposed a different approach the so-called ‘‘self-consistent theory of localization’’.

1.2 Self-consistent theory of localization

In 1973, R. Abou-Chacra, D. J. Thouless and P. W. Anderson in their work [1] proved the existence of the localization-delocalization transition solving self-consistently a set of equations for the self-energy. It can be proved that the self-energy can be expressed in the following way [52]

$$\begin{aligned} \Sigma_{\mathbf{x},\mathbf{x}}(E) = & \sum_{\mathbf{y} \neq \mathbf{x}} \frac{J_{\mathbf{x},\mathbf{y}} J_{\mathbf{y},\mathbf{x}}}{E - \mu_{\mathbf{y}} - \Sigma_{\mathbf{y},\mathbf{y}}^{(\mathbf{x})}(E)} \\ & - \sum_{\mathbf{y} \neq \mathbf{x}} \sum_{\mathbf{z} \neq \mathbf{x},\mathbf{y}} \frac{J_{\mathbf{x},\mathbf{z}} J_{\mathbf{z},\mathbf{y}} J_{\mathbf{y},\mathbf{x}}}{(E - \mu_{\mathbf{z}} - \Sigma_{\mathbf{z},\mathbf{z}}^{(\mathbf{x},\mathbf{y})}(E))(E - \mu_{\mathbf{y}} - \Sigma_{\mathbf{y},\mathbf{y}}^{(\mathbf{x})}(E))} + \dots, \end{aligned} \quad (1.14)$$

where $\Sigma_{\mathbf{x},\mathbf{x}}^{(\mathbf{x}_1, \mathbf{x}_2, \dots, \mathbf{x}_n)}(E)$ is the self-energy of the same system, but where the sites $(\mathbf{x}_1, \mathbf{x}_2, \dots, \mathbf{x}_n)$ have been removed. Also the ‘‘reduced’’ self-energies $\{\Sigma_{\mathbf{x},\mathbf{x}}^{(\mathbf{x}_1, \mathbf{x}_2, \dots, \mathbf{x}_n)}(E)\}$

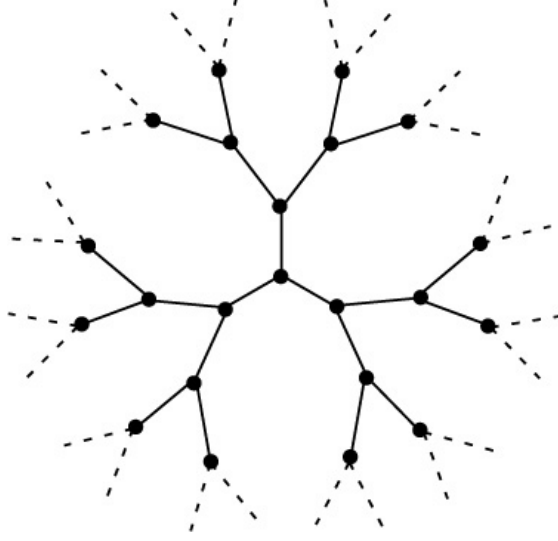


FIGURE 1.2: The figure shows a Bethe Lattice with $K = 2$, [13].

can be expressed likewise as in Eq. 1.15.

$$\Sigma_{\mathbf{y},\mathbf{y}}^{(\mathbf{x})}(E) = \sum_{\mathbf{z} \neq \mathbf{x},\mathbf{y}} \frac{J_{\mathbf{y},\mathbf{z}} J_{\mathbf{z},\mathbf{y}}}{E - \mu_{\mathbf{y}} - \Sigma_{\mathbf{z},\mathbf{z}}^{(\mathbf{x},\mathbf{y})}(E)} + \dots \quad (1.15)$$

The main approximation is to consider only the first terms of these expansions

$$\begin{aligned} \Sigma_{\mathbf{x},\mathbf{x}}(E) &= \sum_{\mathbf{y} \neq \mathbf{x}} \frac{J_{\mathbf{x},\mathbf{y}} J_{\mathbf{y},\mathbf{x}}}{E - \mu_{\mathbf{y}} - \Sigma_{\mathbf{y},\mathbf{y}}^{(\mathbf{x})}(E)}, \\ \Sigma_{\mathbf{y},\mathbf{y}}^{(\mathbf{x})}(E) &= \sum_{\mathbf{z} \neq \mathbf{x},\mathbf{y}} \frac{J_{\mathbf{y},\mathbf{z}} J_{\mathbf{z},\mathbf{y}}}{E - \mu_{\mathbf{z}} - \Sigma_{\mathbf{z},\mathbf{z}}^{(\mathbf{x},\mathbf{y})}(E)}, \end{aligned} \quad (1.16)$$

generally

$$\Sigma_{\mathbf{x}_n, \mathbf{x}_n}^{(\mathbf{x}_1, \dots, \mathbf{x}_{n-1})}(E) = \sum_{\mathbf{z} \neq \mathbf{x}_1, \dots, \mathbf{x}_{n-1}} \frac{J_{\mathbf{x}_n, \mathbf{z}} J_{\mathbf{z}, \mathbf{x}_n}}{E - \mu_{\mathbf{z}} - \Sigma_{\mathbf{z}, \mathbf{z}}^{(\mathbf{x}_1, \dots, \mathbf{x}_{n-1})}(E)}. \quad (1.17)$$

Moreover, making the approximation that removing one site from the system does not change the self-energy

$$\Sigma_{\mathbf{x},\mathbf{x}}(E) = \sum_{\mathbf{y}} \frac{J_{\mathbf{x},\mathbf{y}} J_{\mathbf{y},\mathbf{x}}}{E - \mu_{\mathbf{y}} - \Sigma_{\mathbf{y},\mathbf{y}}(E)}. \quad (1.18)$$

As we have already discussed, we have to study the probability distribution of the self-energy. After a broadening of the energy $E \rightarrow E + i\eta$

$$\begin{aligned} \text{Re}\Sigma_{\mathbf{x},\mathbf{x}}(E) &= \sum_{\mathbf{y}} \frac{|J_{\mathbf{x},\mathbf{y}}|^2 (E - \mu_{\mathbf{y}} - \text{Re}\Sigma_{\mathbf{y},\mathbf{y}}(E))}{(E - \mu_{\mathbf{y}} - \text{Re}\Sigma_{\mathbf{y},\mathbf{y}}(E))^2 + (\eta + \text{Im}\Sigma_{\mathbf{y},\mathbf{y}}(E))^2}, \\ \text{Im}\Sigma_{\mathbf{x},\mathbf{x}}(E) &= - \sum_{\mathbf{y}} \frac{|J_{\mathbf{x},\mathbf{y}}|^2 (\eta + \text{Im}\Sigma_{\mathbf{y},\mathbf{y}}(E))}{(E - \mu_{\mathbf{y}} - \text{Re}\Sigma_{\mathbf{y},\mathbf{y}}(E))^2 + (\eta + \text{Im}\Sigma_{\mathbf{y},\mathbf{y}}(E))^2}. \end{aligned} \quad (1.19)$$

It is possible to find an integral equation for the joint probability distribution of $\text{Re}\Sigma_{\mathbf{x},\mathbf{x}}(E)$ and $\text{Im}\Sigma_{\mathbf{x},\mathbf{x}}(E)$ [1]. This integral equation for the joint distribution is too difficult to be exactly solved for a generic system [1]. Nevertheless, there exists a case where the approximations that have been done so far are justifiable [1, 128] and where this integral equation can be solved. Namely, the case of Anderson localization on a Bethe lattice.

1.2.1 Anderson localization on a Bethe lattice

A Bethe lattice is a tree-like structure without loops with fixed connectivity (K), see Fig. 1.2. This special structure being free from loops, makes the self-consistent approximation in Eq. 1.15 an accurate assumption [1, 128]. Indeed, removing a point in the graph does not modify its local and global structure in the limit of large K . Furthermore Eq. 1.19 can be further simplified

$$\begin{aligned}\text{Re}\Sigma_{x,x}(E) &\sim J^2 \sum_{y=1}^K \frac{1}{E - \mu_y - \text{Re}\Sigma_{y,y}(E)}, \\ \text{Im}\Sigma_{x,x}(E) &\sim J^2 \sum_{y=1}^K \frac{\eta - \text{Im}\Sigma_{y,y}(E)}{(E - \mu_y - \text{Re}\Sigma_{y,y}(E))^2}.\end{aligned}\tag{1.20}$$

In the last approximation, it has been supposed that the system is localized and thus $\text{Im}\Sigma_{x,x}(E) \sim \mathcal{O}(\eta)$. Moreover, by neglecting $\text{Re}\Sigma_{y,y}(E)$ in $\text{Im}\Sigma_{x,x}(E)$ since $\text{Re}\Sigma_{y,y}(E) \sim \mathcal{O}(J^2/W)$, $\{\text{Re}\Sigma_{x,x}(E)\}_x$ and $\{\text{Im}\Sigma_{x,x}(E)\}_x$ become independent random variables

$$\begin{aligned}\text{Re}\Sigma_{x,x}(E) &\sim J^2 \sum_{y=1}^K \frac{1}{E - \mu_y - \text{Re}\Sigma_{y,y}(E)}, \\ \text{Im}\Sigma_{x,x}(E) &\sim J^2 \sum_{y=1}^K \frac{\eta - \text{Im}\Sigma_{y,y}(E)}{(E - \mu_y)^2}.\end{aligned}\tag{1.21}$$

It is interesting to note, that the last approximation, which is valid only in a localized phase, ensures that $\text{Im}\Sigma_{x,x}(E)$ is not an analytic function (Cauchy - Riemann equations), which as we discussed, is one of the main ingredients to have localized states. Finally, considering the case in which $\{\mu_x\}$ are uniformly distributed between $[-W/2, W/2]$, we have

$$P(\text{Im}\Sigma_0) = \frac{1}{W^K} \int_{-W/2}^{W/2} d\mu_1 P(\Sigma_1) \cdots \int_{-W/2}^{W/2} d\mu_K P(\Sigma_K) \delta \left(\text{Im}\Sigma_0 - J^2 \sum_{y=1}^K \frac{1 + \text{Im}\Sigma_{y,y}(E)}{(E - \mu_y)^2} \right)\tag{1.22}$$

where we made the rescaling $\text{Im}\Sigma_0 \rightarrow -\eta \text{Im}\Sigma_0$. Note, that the double indexing in $\Sigma_{0,0}$ is dropped employing a single collective index Σ_0 . Tacking the Laplace transform ($f(s)$)

of $P(\text{Im}\Sigma_0)$ to transform sums into products

$$f(s) = \left[\int_{-W/2}^{W/2} \frac{d\mu}{W} f\left(J^2 \frac{s}{(E-\mu)^2}\right) e^{-\frac{sJ^2}{(E-\mu)^2}} \right]^K. \quad (1.23)$$

As we have already discussed, $P(\text{Im}\Sigma_0)$ must decay as a power law (Eq. 1.10), $P(\text{Im}\Sigma_0) \sim 1/(\text{Im}\Sigma_0)^\alpha$. It implies that its Laplace transform will have the form $f(s) \sim 1 - (\text{constant})s^\beta$ for $s \ll 1$ and $\beta = \alpha - 1$. The normalization condition for the probability distribution of $\text{Im}\Sigma_0$ ($\int d\text{Im}\Sigma_0 P(\text{Im}\Sigma_0) = 1$) leads to the restriction $\beta \in [0, 1/2]$. Thus

$$KJ^{2\beta} \int_{E-W/2}^{E+W/2} \frac{dx}{W} \frac{1}{x^{2\beta}} = 1. \quad (1.24)$$

Considering $E = 0$ (center of the band), we find the condition

$$\frac{K}{(1-2\beta)} \frac{(2J)^{2\beta}}{W^{2\beta}} = 1. \quad (1.25)$$

We are looking at the lower value of W , such that there exists a $\beta \in [0, 1/2]$ which satisfies Eq. 1.25. It is possible to show that it satisfies the following [1] equation

$$\frac{W_c}{J} = 2Ke \log \frac{W_c}{2J} \quad (1.26)$$

The last equation give an estimation for the critical value W_c for the localization-delocalization transition on a Bethe lattice.

Recently, V.E. Kravtsov et al. [82], removing the assumption of neglecting $\text{Re}\Sigma_{x,x}(E)$ in $\text{Im}\Sigma_{x,x}(E)$ (Eq. 1.20), refined the equation for the critical point W_c , finding

$$2K \log \frac{W_c}{2J} = \frac{W_c}{2J} - \frac{2J}{W_c}. \quad (1.27)$$

In this section we have shown that on a Bethe lattice a localization-delocalization transition happens. The approximate formula for the critical point W_c (Eq. 1.27) turns out to be a good approximation in the limit of K large. Nevertheless, the critical value for $K = 2$ (Fig. 1.2) using Eq. 1.27 is at $W_c \approx 17.6$ for $J = 1$, what is in good agreement with numerical simulations [41, 82].

The limiting case $K = 1$ (one-dimensional chain) is also exactly solvable and in the next section, we will introduce the main tools used to analyze and solve this case.

1.3 Anderson Localization in one dimension

In the early sixties, N.F. Mott and W.D. Twose [105], following the work of Anderson [9], conjectured that in one-dimensional systems ($K = 1$) all single-particle eigenstates are localized for any amount of uncorrelated disorder. This statement was given a mathematically rigorous proof by M. Goldshtein et al. in the seventies [58]. Moreover, this case is for us of particular interest, since many of the results that we will state (Chapter 3-7) are for one-dimensional systems.

The Schrödinger equation for the tight-binding model (Eq. 1.1 with $J = 1$) in one-dimension reads

$$-\psi_{x-1} - \psi_{x+1} + \mu_x \psi_x = E\psi_x \quad (1.28)$$

If the disordered potential is absent then the solution of Eq. 1.28 is given by

$$E = 2 \cos(k), \quad \psi_x \sim A_1 e^{ikx} + A_2 e^{-ikx}. \quad (1.29)$$

The solution is a linear combination of plane-waves and thus the eigenstates are delocalized in space, in the sense that they are spread over the entire system. Eq. 1.28 can be solved recursively

$$\begin{pmatrix} \psi_{x+1} \\ \psi_x \end{pmatrix} = \begin{pmatrix} \mu_x - E & -1 \\ 1 & 0 \end{pmatrix} \begin{pmatrix} \psi_x \\ \psi_{x-1} \end{pmatrix}, \quad (1.30)$$

defining

$$A_x = \begin{pmatrix} \mu_x - E & -1 \\ 1 & 0 \end{pmatrix}, \quad (1.31)$$

we have

$$\begin{pmatrix} \psi_{x+1} \\ \psi_x \end{pmatrix} = A_x A_{x-1} \cdots A_1 \begin{pmatrix} \psi_1 \\ \psi_0 \end{pmatrix}. \quad (1.32)$$

$\begin{pmatrix} \psi_1 \\ \psi_0 \end{pmatrix}$ is the boundary condition of the Schrödinger equation. If the system is localized, we expect the eigenstates to decay exponentially fast in space $\psi_x \sim e^{-x/\xi_{\text{loc}}}$. It is possible to prove that for a fixed energy E there exists a one dimensional vector space $\mathbb{V} \subset \mathbb{R}^2$, such that if $\begin{pmatrix} \psi_1 \\ \psi_0 \end{pmatrix} \in \mathbb{V}$ then, for any amount of disorder, we have $\psi_x \sim e^{-x/\xi_{\text{loc}}}$ with

$$\xi_{\text{loc}}^{-1} = - \lim_{x \rightarrow \infty} \frac{1}{x} \log \|A_x A_{x-1} \cdots A_1 \begin{pmatrix} \psi_1 \\ \psi_0 \end{pmatrix}\| > 0 \quad \text{iff} \quad \begin{pmatrix} \psi_1 \\ \psi_0 \end{pmatrix} \in \mathbb{V}, \quad (1.33)$$

where we have introduced the norm of a vector $\|\mathbf{v}\| = \sqrt{|v_1|^2 + |v_2|^2}$. The one dimensional vector space depends on the specific random configuration $\{\mu_x\}$, the value of ξ_{loc}^{-1} (self-averaging) does not and it depends only on the energy E . Moreover, since $\det(A_x) = 1 \forall x$, we have

$$\xi_{\text{loc}}^{-1} = \lim_{x \rightarrow \infty} \frac{1}{x} \log \|A_x A_{x-1} \cdots A_1 \begin{pmatrix} \psi_1 \\ \psi_0 \end{pmatrix}\| > 0 \quad \text{iff} \quad \begin{pmatrix} \psi_1 \\ \psi_0 \end{pmatrix} \notin \mathbb{V}, \quad (1.34)$$

The last statement means that for almost any choice of the boundary condition and for a fixed energy E , the solution will diverge $\psi_x \sim e^{x/\xi_{\text{loc}}}$. The last statement can be reformulated in the following way

$$\xi_{\text{loc}}^{-1}(E) = \lim_{x \rightarrow \infty} \frac{1}{x} \log \|A_x A_{x-1} \cdots A_1\| > 0 \quad \text{with probability one} \quad (1.35)$$

Formally, $\xi_{\text{loc}}^{-1}(E)$ is the Lyapunov exponent of the product of matrices $\{A_x\}$. Moreover, in the literature the method that we explained is called “*transfer matrix technique*”. We will use this technique in several points in this thesis (Chapters 3,7).

The main theorems and assumptions which were used by M. Goldshtein et al. [58] to prove that for any amount of uncorrelated disorder $\xi_{\text{loc}}^{-1}(E) > 0$ are:

1. The matrices $\{A_x\}$ are independently and equally distributed.
2. The Oseledec-Ruelle Theorem (multiplicative ergodic Theorem) [118].
3. Fürstenberg’s Theorem [56].

Nevertheless, there is a point in the proof that it is of particular interest because it shows the generality of this theory. Moreover, this part of the proof is the only part where the actual form of the matrices $\{A_x\}$ are used. In this part one needs to show that, there exist at least an element in the matrix group constructed by the matrices $\{A_x\}_1^\infty$ that acts as a contraction in a two dimensional sphere $\mathbb{S}^1/\{+, -\}$ ($v, w \in \mathbb{S}^1$, $v \sim w$ if $v = \pm w$). Let’s consider the following element in the group

$$(A_x A_y^{-1})^n = \begin{pmatrix} 1 & n(\mu_y - \mu_x) \\ 0 & 1 \end{pmatrix}, \quad (1.36)$$

with $\mu_x \neq \mu_y$.

$$\lim_{n \rightarrow \infty} \frac{(A_x A_y^{-1})^n \begin{pmatrix} v_1 \\ v_2 \end{pmatrix}}{\|(A_x A_y^{-1})^n \begin{pmatrix} v_1 \\ v_2 \end{pmatrix}\|} \rightarrow \begin{pmatrix} \pm 1 \\ 0 \end{pmatrix}. \quad (1.37)$$

We have found an element in the group that contracts any elements in $\mathbb{S}^1/\{+, -\}$ in just one point. Furthermore, since it is the only point of the proof where the form of matrices are used, it underlines two important points.

1. Any kind of uncorrelated disorder (also binary disorder $\mu_x \in \{W_1, W_2\}$) will give a finite localization length ($\xi_{\text{loc}}^{-1}(E) > 0$).
2. The element $(A_x A_y^{-1})^n$ does not depend on the energy E , what implies that $\xi_{\text{loc}}^{-1}(E) > 0 \forall E$.

Furthermore, a perturbative calculation shows that in the weak disorder limit ($W \ll 1$) the localization length is given by [44, 80]

$$\xi_{\text{loc}}^{-1}(E) = \frac{W^2}{24(4 - E^2)}, \quad |E| < 2. \quad (1.38)$$

Nevertheless, numerical simulations show that the numerical prefactor for $\xi_{\text{loc}}^{-1}(E = 0)$ is different, $\xi_{\text{loc}}^{-1}(E = 0) = W^2/105$ [44, 114]. The origin of this discrepancy is due to an anomalous effect at $E = 0$, in which second order perturbation theory breaks down.

Finally, it is important to note that the assumption that the matrices $\{A_x\}$ are statistically independent is fundamental. For example, if one considers the model with binary disorder in which the random on-site energies $\{\mu_x\}$ appear in identical pairs $(\mu_{x1}, \mu_{x1}, \mu_{x2}, \mu_{x2}, \dots)$, then there are values of E for which $\xi_{\text{loc}}^{-1}(E) = 0$ [25, 48, 55].

1.3.1 Localization length and density of states

In the last section, we have introduced a technique to understand the behavior of the localization length in one-dimensional systems. In this section we show a relation between the localization length and the density of states in one-dimensional systems [37, 65, 143].

Let's consider a chain of length L and fix the boundary condition $\begin{pmatrix} \psi_1 \\ \psi_0 \end{pmatrix}$, then the solution ψ_L due to the recursive relation Eq. 1.32 is a polynomial of degree $L - 1$ of the energy E

$$\psi_L(E) = C \prod_{j=1}^{L-1} (E_j - E) = C \prod_{j=1}^{L-1} |E_j - E| e^{i\pi\theta(E-E_j)}, \quad (1.39)$$

$\{E_j\}$ are the roots of $\psi_L(E)$ and $\theta(x)$ is the step function. Taking the logarithmic of $\psi_L(E)$ and dividing by L we have,

$$\frac{1}{L} \log \psi_L(E) = \frac{1}{L} \sum_{j=1}^{L-1} \log |E_j - E| + \frac{i\pi}{L} \sum_{j=1}^{L-1} \theta(E - E_j) + \frac{1}{L} \log C. \quad (1.40)$$

It can be proved that the roots $\{E_j\}$ are indeed distributed like the eigenvalues of the system [65]. Thus, we can replace the sum in the limit of large L by an integral over the density of states $\rho(E)$ and taking the average over the disorder ($\frac{1}{L} \log \psi_L(E)$ is not self averaging)

$$\lim_{L \rightarrow \infty} \frac{1}{L} \overline{\log \psi_L(E)} = \int_{-\infty}^{\infty} dE' \rho(E') \log |E - E'| + i\pi \int_{-\infty}^E dE' \rho(E'). \quad (1.41)$$

taking the real and the imaginary part, we have

$$\begin{cases} \xi_{\text{loc}}^{-1}(E) = \int_{-\infty}^{\infty} dE' \rho(E') \log |E - E'|, \\ \frac{1}{\pi} \text{Im} \left[\lim_{L \rightarrow \infty} \overline{\frac{1}{L} \log \psi_L(E)} \right] = \int_{-\infty}^E dE' \rho(E'). \end{cases} \quad (1.42)$$

These relations are called the Herbert-Jones-Thouless formulae [65, 143]. These formulae are general, in the the sense that they hold for any one-dimensional system, and we will use them later in order to analyze several models (Chapter 7).

1.3.2 Landauer formalism

We have shown that for any amount of uncorrelated disorder in one-dimensional systems (without special symmetry, and with finite-range hopping) localization occurs. In this section, we show that this system describes a perfect insulator called the Anderson insulator.

In 1970, Landauer [87] studied the conductivity of one-dimensional chains with disordered potential. Let's consider a one-dimensional chain of length L subject to a random potential, in which the two ends are coupled to two reservoirs. Applying a small difference of potential ΔV between the two reservoirs, an electric current (\mathbf{j} = intensity flux) will flow through the system (without loss of generality, suppose that the potential in the left-reservoir is higher than the one in the right). At zero temperature ($T = 0$) the difference in the electron density is given by

$$\Delta n = n(E_F + q_e \Delta V) - n(E_F) = q_e \left. \frac{\partial n}{\partial E} \right|_{E_F} \Delta V, \quad (1.43)$$

where E_F is the Fermi energy and q_e is the charge of an electron, moreover, for one-dimensional systems $\left. \frac{\partial n}{\partial E} \right|_{E_F} = (\pi v_F)^{-1}$, v_F is the Fermi velocity. Since the potential is higher in the left part, the current will flow from left to right, and part of it will be reflected with a rate \tilde{R} and part of it will be transmitted with a rate \tilde{T} , ($\tilde{R} + \tilde{T} = 1$).

Thus the difference in the electron density is given by

$$\Delta n = \frac{2\tilde{R}\mathbf{j}}{q_e v_F} = \frac{q_e \Delta V}{\pi v_F}, \quad (1.44)$$

giving the relation

$$\mathbf{j} = \frac{q_e^2 \Delta V}{2\pi \tilde{R}}. \quad (1.45)$$

The conductivity G is defined as $I/\Delta V$ where I is the current that has been transmitted $\mathbf{j}\tilde{T}$

$$G = \frac{q_e^2 \tilde{T}}{2\pi \tilde{R}}. \quad (1.46)$$

The idea is to relate the coefficient \tilde{T} with the localization length ξ_{loc} . Without loss of generality, the point in the chain $x \in [0, L-1]$ are the sites subject to the random potential, while in the two reservoirs the wavefunction are given by

$$\begin{cases} \psi_x = \begin{matrix} e^{ikx} \\ \text{injected} \end{matrix} + \begin{matrix} r e^{-ikx} \\ \text{reflected} \end{matrix} & x = -1, -2, \dots \\ \psi_x = \begin{matrix} t e^{ikx} \\ \text{transmitted} \end{matrix} & x = L, L+1, \dots \end{cases} \quad (1.47)$$

where $\tilde{R} = |r|^2$ and $\tilde{T} = |t|^2$. Using the recursive Eq. 1.32 with $E = 2 \cos(k)$

$$\mathbf{z}(L) = A_{L-1} A_{L-2} \cdots A_0 \mathbf{z}(-1), \quad (1.48)$$

where we have defined

$$\mathbf{z}(L) = \begin{pmatrix} t e^{ik(L+1)} \\ t e^{ikL} \end{pmatrix}, \quad \mathbf{z}(-1) = \begin{pmatrix} 1+r \\ e^{-ik} + r e^{ik} \end{pmatrix}. \quad (1.49)$$

Let's note that $\|\mathbf{z}(L)\| \propto t$, thus using Eq. 1.33

$$G \sim |t|^2 \sim e^{-2L/\xi_{\text{loc}}}. \quad (1.50)$$

As expected, the system being localized, G decays exponentially with L , and thus the system is an insulator (Anderson insulator).

1.4 Aubry-André-Harper model

In an experimental setup (*e.g.*, cold-atoms, trapped ions) [80, 97, 129, 137] it is not easy to simulate systems with uncorrelated disorder, and usually some sort of correlation between on-site energies is present. Thus, whether the localization persists in the presence of correlated disorder, is an important question that has been the center of intensive

research [70]. Indeed, even with on-site disorder, where all single-particle eigenstates are exponentially localized in one dimension [58, 105], correlations in the disorder can either partially or completely destroy localization [38, 48, 70, 71, 85]. Nevertheless, there exists a model defined in a one-dimensional lattice with a quasi-periodic potential (which can be considered a kind of correlated disorder), in which a localization-delocalization transition occurs. Moreover, the system with this quasi-periodic potential can be simulated in an experimental setup [97, 129].

The Schrödinger equation reads

$$-\psi_{x-1} - \psi_{x+1} + W \cos(2\pi\alpha x)\psi_x = E\psi_x, \quad (1.51)$$

where $W \cos(2\pi\alpha x)$ is the quasi-periodic potential with $\alpha = \frac{1+\sqrt{5}}{2}$ (Golden ratio), this model is called Aubry-André-Harper model (AAH) [12]. We will study this model in different parts of this thesis (Chapters 3, 4). The AAH model has an important symmetry the so-called self-dual symmetry. Defining $\{\phi_k\}$ by

$$\psi_x = \sum_k e^{i2\pi\alpha kx} \phi_k, \quad (1.52)$$

the Schrödinger equation for the rotated wavefunctions $\{\phi_k\}$ reads

$$-\frac{W}{2}\phi_{k-1} - \frac{W}{2}\phi_{k+1} + 2\cos(2\pi\alpha k)\phi_k = E\phi_k. \quad (1.53)$$

At $W = 2$ the Schrödinger equation for $\{\psi_x\}$ and $\{\phi_k\}$ are the same, this special value of W is called the self-dual point. It is possible to prove that exactly at $W = 2$ the system has a localization-delocalization transition.

$$\begin{cases} \xi_{\text{loc}}^{-1}(E) > 0, & W > 2, \\ \xi_{\text{loc}}^{-1}(E) = 0, & W < 2. \end{cases}$$

In 1980, S. Aubrey and G. André proved an important property of the density of states [12], which is a direct consequence of the duality transformation (Eq. 1.52)

$$\rho_W(E) = \rho_{4/W}(2E/W), \quad (1.54)$$

where we added a sub-script W on the density of states to indicate the value of the potential strength of the system. Finally, using the Herbert-Jones-Thouless formulae (Eq. 1.42) we have

$$\xi_{\text{loc},W}^{-1}(E) = \xi_{\text{loc},4/W}^{-1}(2E/W) + \log W/2. \quad (1.55)$$

Thus, since $\xi_{\text{loc},W}^{-1}(E) \geq 0$ and $\xi_{\text{loc},4/W}^{-1}(2E/W) \geq 0$, we have for $W > 2$

$$\xi_{\text{loc},W}^{-1}(E) \geq \log W/2. \quad (1.56)$$

The last equation implies that the system is exponentially localized for $W > 2$, moreover, it implies that its dual solution is extended (since it is its Fourier transform), thus $\xi_{\text{loc},4/W}^{-1}(2E/W) = 0$.

$$\xi_{\text{loc},W}^{-1}(E) = \log W/2. \quad (1.57)$$

In summary, the system is exponentially localized for $W > 2$ and extended for $W < 2$, moreover the localization length $\xi_{\text{loc},W}^{-1}(E)$ does not depend on the energy E .

1.5 Multifractal wavefunctions

We have seen that the eigenstates of a system in which disorder is present can be localized or delocalized. We have described, that the delocalized wavefunctions span uniformly the system, whereas the localized wavefunctions, are confined in a restricted region of the system.

Nevertheless, at the critical point of an Anderson transition, the amplitude of the eigenstates present strong fluctuations in space [51]. Indeed, at criticality the wavefunctions are not extended (delocalized) neither localized, and they are called multifractal wavefunctions. Multifractal wavefunctions are characterized by an infinite number of exponents $\{\tau_q\}$. Defining the generalized inverse participation ratio (IPR_q)

$$IPR_q = \sum_x^V |\psi(x)|^{2q}, \quad q \geq 1, \quad (1.58)$$

for a system of volume V , we have

$$\overline{IPR_q} \sim V^{-\tau_q}, \quad (1.59)$$

where the overline indicates the average over disorder configurations. The set of exponents $\{\tau_q\}$ are usually parameterized by introducing the multifractal exponents $\{D_q\}$

$$\tau_q = D_q(q - 1). \quad (1.60)$$

If the system is extended (ergodic) $D_q = 1$, while if the system is localized $D_q = 0$. For multifractal states D_q is a non trivial function of q , and $0 \leq D_q \leq 1$. Moreover, one can

also define the anomalous dimension exponents $\{\Delta_q\}$

$$\tau_q = (q - 1) + \Delta_q. \quad (1.61)$$

The most studied exponent is Δ_2 , and it can be related to the behavior of the two point correlation function [30]

$$V^2 \overline{|\psi_\epsilon(x)|^2 |\psi_{\epsilon+\omega}(x')|^2} \sim \left(\frac{|x - x'|}{V_\omega} \right)^{-\Delta_2}, \quad (1.62)$$

where $V_\omega \sim (\rho\omega)^{-1}$ with ρ the density of states.

Defining the probability distribution of the squared amplitude of the wavefunction

$$P(|\psi|^2) \sim \frac{1}{|\psi|^2} V^{-1+f(-\frac{\log |\psi|^2}{\log V})}, \quad (1.63)$$

the $\{IPR_q\}$ (Eq 1.58) can be obtained by calculating different moments of the probability distributions $P(|\psi|^2)$. Indeed,

$$\overline{IPR_q} \sim \int d\alpha V^{-q\alpha+f(\alpha)}. \quad (1.64)$$

Evaluating the integral using the saddle-point approximation

$$\overline{IPR_q} \sim V^{-\tau_q}, \quad \tau_q = q\alpha - f(\alpha), \quad q = f'(\alpha). \quad (1.65)$$

In other words, τ_q is the the Legendre transform of the function f . The function $f(\alpha)$ measure the fractal dimension of the wavefunction

$$\#\{x : |\psi(x)|^2 \sim V^{-\alpha}\} \sim V^{f(\alpha)}. \quad (1.66)$$

For a completely ergodic system ($|\psi(x)|^2 \sim V^{-1}$), $f(\alpha)$ will be not regular function, with $f(\alpha = 1) = 1$ but $f(\alpha) = -\infty$ otherwise. For multifractal-states $f(\alpha)$ is a convex function, and its maximum is shifted to $\alpha_0 \geq 1$.

In this section, we described the main definitions and tools to characterize multifractal states. We will use this definition mostly in Chapter 6, where we will inspect the possible existence of a multifractal phase in the Anderson model on a Bethe lattice.

Chapter 2

Many-Body Localization

In Chapter 1, we have seen that the presence of strong quenched disorder can localize a non-interacting quantum system. Whether localization persists when interactions between degrees of freedom are introduced, has been a fundamental question since the time of the discovery of Anderson localization [9]. Indeed, the original motivation of the seminal work of Anderson was to study interacting spin models [9]. During several decades, this question has generated important debates and interesting directions of research [5, 6, 54], without finding a definitive accepted answer. In 2006, D.M. Basko, I.L. Aleiner and B.L. Altshuler showed in their seminal work [17] that the localized phase is robust if a weak interaction is taken into account. Moreover, they also found the existence of a new type of localization-delocalization transition, which occurs even at finite energy density [17, 62]. The last result brought new emphasis, giving rise to a new field of research called many-body localization (MBL) [106]. As we will describe, this problem is intimately connected with the understanding of the fundamental laws of statistical mechanics. Hence, shedding light on the MBL problem, could bring new insights on the fundamental laws of nature.

The aim of this chapter is to give a self contained explanation of MBL, especially focusing on recent results, which will be used later in the thesis. This chapter is organized as follows. First, we explain the concept of integrability and non-integrability in closed quantum many-body systems. Next, we give the definition of thermalization in closed quantum systems. This topic is strictly linked with a conjecture called the “eigenstate thermalization hypothesis” [40, 138], which is the most accredited theory attempting to understand thermalization in closed systems from a quantum-mechanical perspective. Second, we define what many-body localization means. In the last part, we collect several results which underline different aspects of MBL.

2.1 Integrable closed quantum many-body systems and the concept of non-integrability

The aim of this section is to introduce the concept of (non-)integrability in quantum systems.

A quantum many-body system is considered integrable, when it can be described by an algebraic number in volume of commuting constants of motion and couplings between them. Although, the exact definition of integrability in a quantum system is still under debate, a review concerning possible definitions and caveats for different definitions can be found in [28]. For many practical purposes, an integrable quantum system is a non-interacting quantum system (its Hamiltonian is quadratic in the creation and annihilation fermionic (bosonic) operators), or a system which can be solved using Bethe ansatz [74]. Moreover, these systems are fine-tuned, in the sense that any generic random perturbation will drastically change some properties of these systems (*e.g.*, transport properties).

In this chapter and in the next ones, we focus mainly on one-dimensional lattice models with local Hilbert space of dimension two (*e.g.*, fermionic and spin-1/2 chains). For this reason let's consider a generic one-dimensional lattice system of length L described by a Hamiltonian $\hat{\mathcal{H}}$. Since $\hat{\mathcal{H}}$ is defined up to an additive constant, we can consider the case in which $\text{Tr}[\hat{\mathcal{H}}] = 0$. The Hilbert space where $\hat{\mathcal{H}}$ is defined is $(\mathbb{C}^2)^{\otimes L}$ and its dimension is $\mathfrak{D} = 2^L$. Let $\{E_n\}$ and $\{|E_n\rangle\}$ be the eigenvalues and eigenvectors of $\hat{\mathcal{H}}$. We can always construct L integrals of motion in the following way

$$\hat{\tau}_j^z = \sum_n a_n^j |E_n\rangle \langle E_n| \quad 1 \leq j \leq L, \quad (2.1)$$

with $\{(a_1^1, a_1^2, \dots, a_1^L), \dots, (a_{2L}^1, a_{2L}^2, \dots, a_{2L}^L)\}$ all possible sequences of length L composed by $\{-1, 1\}$. The following relations hold

$$\begin{aligned} (\hat{\tau}_j^z)^\dagger &= \hat{\tau}_j^z, & (\hat{\tau}_j^z)^3 &= \hat{\tau}_j^z, \\ [\hat{\tau}_i^z, \hat{\tau}_j^z] &= 0, & \forall i, j, \end{aligned} \quad (2.2)$$

and

$$[\hat{\mathcal{H}}, \hat{\tau}_j^z] = 0. \quad (2.3)$$

Moreover, it can be shown that the Hamiltonian $\hat{\mathcal{H}}$ can be expressed in terms of $\{\hat{\tau}_j^z\}$ [117]

$$\hat{\mathcal{H}} = \sum_i b_i^{(1)} \hat{\tau}_i^z + \sum_{i < j} b_{i,j}^{(2)} \hat{\tau}_i^z \hat{\tau}_j^z + \dots + b_{1,2,\dots,L}^{(L)} \hat{\tau}_1^z \hat{\tau}_2^z \dots \hat{\tau}_L^z, \quad (2.4)$$

where

$$\begin{aligned} b_i^{(1)} &= \frac{1}{2^L} \text{Tr}[\hat{\mathcal{H}} \hat{\tau}_i^z] = \frac{1}{2^L} \sum_n E_n a_n^i, \\ b_{i,j}^{(2)} &= \frac{1}{2^L} \text{Tr}[\hat{\mathcal{H}} \hat{\tau}_i^z \hat{\tau}_j^z] = \frac{1}{2^L} \sum_n E_n a_n^i a_n^j, \end{aligned} \quad (2.5)$$

and generally

$$b_{i,j,\dots,k}^{(m)} = \frac{1}{2^L} \text{Tr}[\hat{\mathcal{H}} \hat{\tau}_i^z \hat{\tau}_j^z \cdots \hat{\tau}_k^z] = \frac{1}{2^L} \sum_n E_n a_n^i a_n^j \cdots a_n^k. \quad (2.6)$$

Therefore, any system can be expressed in the following way

$$\hat{\mathcal{H}} = \sum_j^L \sum_{i_1 < i_2 < \cdots < i_j} b_{i_1, i_2, \dots, i_j}^{(j)} \hat{\tau}_{i_1}^z \hat{\tau}_{i_2}^z \cdots \hat{\tau}_{i_j}^z. \quad (2.7)$$

In other words, we constructed a function which assigns to any eigenstates $\{|E_n\rangle\}$ a sequence of $\{-1, 1\}$,

$$\mathbf{f}(|E_n\rangle) \rightarrow (a_n^1, a_n^2, \dots, a_n^L). \quad (2.8)$$

Thus,

$$\begin{aligned} \hat{\tau}_j^z &= \sum_n \mathbf{f}_j(|E_n\rangle) |E_n\rangle \langle E_n| \quad 1 \leq j \leq L, \\ \mathbf{f}_j(|E_n\rangle) &= a_n^j. \end{aligned} \quad (2.9)$$

It is important to clarify that the construction of \mathbf{f} is not unique, and consequently the choice of $\{\hat{\tau}_j^z\}$. Once the function \mathbf{f} is defined, we can construct an entire set of operators which obey the Pauli-matrix commutation relations [126]: $\{\hat{\tau}_j^x\}$ and $\{\hat{\tau}_j^y\}$

$$[\hat{\tau}_i^\alpha, \hat{\tau}_j^\beta] = i \delta_{i,j} \epsilon_{\alpha\beta\gamma} \hat{\tau}_j^\gamma \quad \alpha, \beta, \gamma \in \{x, y, z\}, \quad (2.10)$$

where $\epsilon_{\alpha\beta\gamma}$ is the anti-symmetric Levi-Civita tensor [126].

We say that the system is integrable (strongly-integrable) if there exists a map \mathbf{f} and a variable \tilde{L} ($1 \leq \tilde{L} < L$) which does not depend on L , such that

$$\hat{\mathcal{H}} = \sum_j^{\tilde{L}} \sum_{i_1 < i_2 < \cdots < i_j} b_{i_1, i_2, \dots, i_j}^{(j)} \hat{\tau}_{i_1}^z \hat{\tau}_{i_2}^z \cdots \hat{\tau}_{i_j}^z. \quad (2.11)$$

We need to know only L constants of motion $\{\hat{\tau}_j^z\}$ and an algebraic number in L of coefficients $\{b_i^{(1)}, b_{i,j}^{(2)}, \dots, b_{i_1, \dots, i_{\tilde{L}}}^{(\tilde{L})}\}$ to describe the system.

Non-interacting quantum systems are included in the definition of integrable systems.

For example, let's consider a one-dimensional fermionic quantum many-body system (*e.g.*, the Anderson-model, or the AAH-model in Chapter 1)

$$\hat{\mathcal{H}} = \sum_{x,y} \hat{c}_x^\dagger \Omega_{x,y} \hat{c}_y, \quad (2.12)$$

where $\{\hat{c}_j^\dagger\}$ ($\{\hat{c}_j\}$) are the fermionic creation (annihilation) operators ($\{\hat{c}_i^\dagger, \hat{c}_j\} = \delta_{i,j}$ and $\{\hat{c}_j^2 = 0\}$), and Ω is a bounded symmetric real matrix ($\|\Omega\| < \infty, \Omega_{x,y} = \Omega_{y,x}$). Let $\{\phi_l(x)\}$ and $\{\epsilon_l\}$ be respectively the single-particle eigenstates and eigenvalues

$$\sum_y \Omega_{x,y} \phi_l(y) = \epsilon_l \phi_l(x). \quad (2.13)$$

Defining the operators

$$\hat{\eta}_l^\dagger = \sum_x \phi_l(x) \hat{c}_x^\dagger, \quad (2.14)$$

we have:

$$\hat{\mathcal{H}} = \sum_l \epsilon_l \hat{\eta}_l^\dagger \hat{\eta}_l. \quad (2.15)$$

Thus, a non-interacting system is integrable in the sense of the above definition with $\tilde{L} = 1$.

2.2 Quantum Thermalization in closed quantum systems

In this section we define, what it means for a closed quantum system to thermalize.

Let's consider a strongly interacting isolated (closed) quantum many-body system of volume V . Isolated here means that the system is neither coupled to an external bath, nor to a reservoir. The system is described by a Hamiltonian $\hat{\mathcal{H}}$ and we are interested in its highly-excited eigenstates, meaning that we will not just focus on its low-energy properties, but rather on eigenstates that belong to a finite energy density. Let $|\psi\rangle$ be the initial state in which the system is prepared. The density matrix is simply given by

$$\hat{\rho}(0) = |\psi(0)\rangle\langle\psi(0)|, \quad (2.16)$$

and it is a pure state since $\hat{\rho}^2(0) = \hat{\rho}(0)$.

The quantum time evolution of the system is described by

$$i \frac{d\hat{\rho}(t)}{dt} = [\hat{H}, \hat{\rho}(t)], \quad (2.17)$$

whose solution is given by

$$\hat{\rho}(t) = \hat{U}(t)|\psi(0)\rangle\langle\psi(0)|\hat{U}^\dagger(t), \quad (2.18)$$

which is also a pure state.

We are interested in the long-time dynamics of the system and aim to know if the system will eventually thermalize or not. If the system thermalizes, then the local memory of the initial state will be completely lost. In this case the long-time dynamics of the evolved state will be described by an equilibrium statistical density matrix (Boltzmann density matrix), which depends only on few thermodynamic parameters, like the temperature T , chemical potential μ etc..

$$\lim_{\tilde{T} \rightarrow \infty} \lim_{V \rightarrow \infty} \frac{1}{\tilde{T}} \int_0^{\tilde{T}} dt \hat{\rho}(t) \rightarrow \frac{e^{-\beta(\hat{\mathcal{H}} + \mu \hat{N} + \dots)}}{Z}, \quad (2.19)$$

Z is the partition function, $\beta = 1/T$ and \hat{N} is the particle-number operator.

It is important to give some remarks:

1. The definition requires

$$\lim_{\tilde{T} \rightarrow \infty} \lim_{V \rightarrow \infty} \left\| \frac{1}{\tilde{T}} \int_0^{\tilde{T}} dt \hat{\rho}(t) - \frac{e^{-\beta(\hat{\mathcal{H}} + \mu \hat{N} + \dots)}}{Z} \right\| \rightarrow 0. \quad (2.20)$$

It is called convergence in the strong sense.

However, the strong-convergence is usually a too strict definition. Indeed, two density matrices could describe the same physical system even if the norm of their difference is not zero. A less demanding convergence is called convergence in the weak-sense

$$\lim_{\tilde{T} \rightarrow \infty} \lim_{V \rightarrow \infty} \frac{1}{\tilde{T}} \int_0^{\tilde{T}} dt \text{Tr} [\hat{\rho}(t) \hat{A}] \rightarrow \text{Tr} \left[\frac{e^{-\beta(\hat{\mathcal{H}} + \mu \hat{N} + \dots)}}{Z} \hat{A} \right] \quad \forall \hat{A} \text{ observable.} \quad (2.21)$$

The weak-convergence is definitely more appropriate and more physical, since in an experimental setup usually only local observables are possible to be measured.

2. In the definition that we have given (Eq 2.19), we used the grand-canonical ensemble. Nevertheless, any other thermodynamic ensembles (*i.e.* micro-canonical, canonical) will give the same results, due to the equivalence between ensembles [119].

3. We considered only time-averaged quantities, nevertheless it is also important that the temporal fluctuations decay to zero in the thermodynamic limit

$$\lim_{\tilde{T} \rightarrow \infty} \lim_{V \rightarrow \infty} \frac{1}{\tilde{T}} \int_0^{\tilde{T}} dt \left(\text{Tr} [\hat{\rho}(t)\hat{A}] - \frac{1}{\tilde{T}} \int_0^{\tilde{T}} dt \text{Tr} [\hat{\rho}(t)\hat{A}] \right)^2 \rightarrow 0 \quad (2.22)$$

$\forall \hat{A}$ bounded observable.

4. The limits, $V \rightarrow \infty$ and $\tilde{T} \rightarrow \infty$ should be taken simultaneously (*i.e.* $V/\tilde{T} = \text{constant}$).
5. The temperature T is not a well defined concept in a closed system, in this case T is the parameter which controls the energy density in the system.

Nevertheless, a pure state can never thermalize, indeed the solution of Eq. 2.17 is still a pure state and a rank-one operator can not converge to a Boltzmann density matrix, which has rank larger than one. From a physical point of view it is also clear that the solution of Eq. 2.17 will always conserve the information about the initial density matrix [106]. Indeed, a closed system is meant to thermalize, if “*it acts as its own bath*” [40, 106]. The last statement means that the system will thermalize locally. Let \tilde{S} be a finite portion of the system (it contains only a finite number of degrees of freedom), tracing out all the degrees of freedom outside \tilde{S} (\tilde{S}^c), we can define a density matrix which acts only on the subsystem \tilde{S}

$$\hat{\rho}_{\tilde{S}}(t) = \text{Tr}_{\tilde{S}^c} [\hat{\rho}(t)]. \quad (2.23)$$

The support of the density-matrix $\hat{\rho}_{\tilde{S}}(t)$ is \tilde{S} , and in general $\hat{\rho}_{\tilde{S}}(t)$ is not a pure state. We will say that a closed system will thermalize in the strong-sense if

$$\lim_{\tilde{T} \rightarrow \infty} \lim_{\tilde{S}^c \rightarrow \infty} \frac{1}{\tilde{T}} \int_0^{\tilde{T}} dt \hat{\rho}_{\tilde{S}}(t) \rightarrow \text{Tr}_{\tilde{S}^c} \left[\frac{e^{-\beta(\hat{\mathcal{H}} + \mu\hat{N} + \dots)}}{Z} \right]. \quad (2.24)$$

The thermalization on the subsystem \tilde{S} can be defined also in the weak-sense (Eq. 2.21) considering only observables \hat{A} with support in \tilde{S} .

The thermodynamic parameters T , μ , etc. are calculated by the set of equations

$$\text{Tr}[\hat{\mathcal{H}}\hat{\rho}_{\tilde{S}}^{eq}(T, \mu, \dots)] = \langle \psi(0) | \hat{\mathcal{H}} | \psi(0) \rangle,$$

$$\text{Tr}[\hat{N}\hat{\rho}_{\tilde{S}}^{eq}(T, \mu, \dots)] = \langle \psi(0) | \hat{N} | \psi(0) \rangle,$$

$$\text{Tr}[\hat{\rho}_{\tilde{S}}^{eq}(T, \mu, \dots)] = \langle \psi(0) | \cdot | \psi(0) \rangle.$$

Let $\{|E_n\rangle\}$ be the eigenstates of $\hat{\mathcal{H}}$ with eigenenergies $\{E_n\}$, then

$$|\psi(t)\rangle = \sum_n C_n e^{-iE_n t} |E_n\rangle, \quad (2.25)$$

the coefficients $\{C_n\}$ are simply given by $\{\langle E_n|\psi(0)\rangle\}$, thus the only information about the initial state is encoded in $\{C_n\}$. Let \hat{A} be an observable with support in \tilde{S}

$$A(t) = \langle \psi(t) | \hat{A} | \psi(t) \rangle = \sum_n |C_n|^2 A_{n,n} + \sum_{n \neq m} C_m^* C_n e^{-i(E_m - E_n)t} A_{m,n}, \quad (2.26)$$

with $A_{m,n} = \langle E_m | A | E_n \rangle$. If there are no special symmetries and thus no energy degeneracy, then

$$\lim_{\tilde{T} \rightarrow \infty} \frac{1}{\tilde{T}} \int_0^{\tilde{T}} dt A(t) = \sum_n |C_n|^2 A_{n,n}. \quad (2.27)$$

If the system thermalizes

$$\sum_n |C_n|^2 A_{n,n} \approx A_{eq}, \quad (2.28)$$

where A_{eq} is the expectation value of \hat{A} at equilibrium (calculated with the Boltzmann density matrix). It is important to add few remarks concerning the choice of the initial state $|\psi(0)\rangle$ and on the choice of the subsystem.

1. The energy fluctuation must be sub-extensive in the number of degrees of freedom in the system

$$\delta E = \sqrt{\langle \psi(0) | \hat{\mathcal{H}}^2 | \psi(0) \rangle - (\langle \psi(0) | \hat{\mathcal{H}} | \psi(0) \rangle)^2} \sim V^{-\nu} \langle E \rangle \quad \nu > 0, \quad (2.29)$$

where $\langle E \rangle = \langle \psi(0) | \hat{\mathcal{H}} | \psi(0) \rangle \sim V$.

2. We have taken the sub-system \tilde{S} in such a way that the degrees of freedom inside \tilde{S} do not scale with the volume. This assumption could be relaxed as far as the scaling of the degrees of freedom of \tilde{S} scale sub-linearly with the volume.

2.2.1 Eigenstate thermalization hypothesis

In the previous section we defined what it means for a closed quantum system to thermalize. In this section, we state the eigenstate thermalization hypothesis (ETH). ETH is a conjecture on the structure of the eigenstates, which gives an explanation of thermalization in closed quantum system.

2.2.1.1 Thermalization in Random Matrices

Before providing the precise statement of ETH, let's consider the case in which the system is described by a symmetric random matrix. In this case, the entries of the Hamiltonian $\hat{\mathcal{H}}$ are independent equally distributed random variables. For this special case it is possible to prove that the diagonal elements of *any* observable \hat{A} expressed in the basis of the eigenstates of $\hat{\mathcal{H}}$ are given by [45]

$$A_{n,n} = \bar{A} + \frac{1}{\sqrt{\mathfrak{D}}} \mathcal{R}_{n,n}, \quad (2.30)$$

where \mathfrak{D} is the dimension of the matrix $\hat{\mathcal{H}}$, \bar{A} is the normalized trace of \hat{A} ($\bar{A} = \frac{1}{\mathfrak{D}} \text{Tr}[A]$), and $\{\mathcal{R}_{n,n}\}$ are sign-alternating independent random variables. Moreover, the coefficients $\{C_n\}$ (Eq 2.28) will be given by

$$C_n = \frac{e^{i\phi_n}}{\sqrt{\mathfrak{D}}} + \frac{S_n}{\mathfrak{D}}, \quad (2.31)$$

and $\{S_n\}$ are distributed in the same way as $\{\mathcal{R}_{n,n}\}$.

$$\sum_n |C_n|^2 A_{n,n} \approx \bar{A} + \sum_n \left(\frac{\mathcal{R}_{n,n}}{\mathfrak{D}\sqrt{\mathfrak{D}}} + \bar{A} \frac{e^{i\phi_n} S_n + c.c.}{\mathfrak{D}\sqrt{\mathfrak{D}}} + \bar{A} \frac{|S_n|^2}{\mathfrak{D}^2} + \frac{|S_n|^2 \mathcal{R}_{n,n}}{\mathfrak{D}^2 \sqrt{\mathfrak{D}}} \right), \quad (2.32)$$

since $\sum_n \mathcal{R}_{n,n} \sim \sqrt{\mathfrak{D}}$ (central limit theorem), we have

$$\sum_n |C_n|^2 A_{n,n} \approx \bar{A} + \mathcal{O}(\mathfrak{D}^{-1}). \quad (2.33)$$

From Eq. 2.33 follows that any observable \hat{A} will thermalize to the equilibrium value \bar{A} , defined as the expectation value of \hat{A} at infinite temperature. Since the system is described by a random matrix, its eigenstates are random vectors. Thus since all the eigenstates are statistically equivalent, they must have the same weight in the thermodynamic ensemble (infinite temperature ensemble). In other words, the ensemble density matrix will be proportional to the unity operator ($\hat{\rho}_{\text{eq}} = \mathbb{I}/\mathfrak{D}$).

2.2.1.2 Thermalization in generic closed quantum many-body systems

In 1994, M. Srednicki gave an ansatz for the matrix elements of an observable \hat{A} of a generic quantum many-body system [138]. This ansatz goes under the name of *eigenstate thermalization hypothesis*:

$$A_{m,n} = \bar{A}(\bar{E}) \delta_{n,m} + e^{-S(\bar{E})/2} f_A(\bar{E}, \omega) \mathcal{R}_{n,m}, \quad (2.34)$$

where $\bar{E} = \frac{E_n + E_m}{2}$, $\omega = E_n - E_m$, and $S(\bar{E}) > 0$ is the entropy of the system which scales with the volume ($S \sim V$) and $\{\mathcal{R}_{n,m}\}$ are independent equally distributed sign-alternating random variables. Furthermore, \bar{A} and f_A are smooth functions of their arguments and $\bar{A} = A_{eq}$ (Eq. 2.28). Since the off-diagonal elements of \hat{A} ($A_{n,m}$ with $n \neq m$) are proportional to $e^{-S(\bar{E})/2}$, they are exponentially small in volume compared with the diagonal elements. The last statement is an important property, indeed in Eq. 2.26 we defined thermalization in the limit \tilde{T} tends to infinity. Formally, it means that the time for equilibration \tilde{T}_{eq} will scale exponentially with the volume $\tilde{T}_{eq} \sim e^V$, since one needs to resolve the smallest difference between two eigenenergies ($\min_{n,m} |E_n - E_m| \sim e^{-\eta V}$). Nevertheless, the time for equilibration is usually finite, and this could be explained by the exponential suppression in volume of the off-diagonal elements of \hat{A} in Eq. 2.34. Moreover, the exponential suppression of the off-diagonal elements dominate the time-averaged fluctuations of $A(t)$

$$\sigma_A^2 = \lim_{\tilde{T} \rightarrow \infty} \frac{1}{\tilde{T}} \int_0^{\tilde{T}} dt [A(t)]^2 - \left(\frac{1}{\tilde{T}} \int_0^{\tilde{T}} dt A(t) \right)^2, \quad (2.35)$$

$$\sigma_A^2 = \sum_{m,n} |C_m|^2 |C_n|^2 |A_{m,m}|^2 \leq \max_{m,n} |A_{m,n}|^2 \sum_{m,n} |C_m|^2 |C_n|^2 = \max_{m,n} |A_{m,n}|^2 \sim e^{-S(\bar{E})}. \quad (2.36)$$

The time-averaged fluctuations are exponentially small in the number of degrees of freedom in the system. The last scaling gives important information about the typical value of the long-time dynamics of $A(t)$. Indeed, when the system thermalizes, $A(t)$ will be close to the equilibration value most of the time. Nevertheless, it can be proved that the fluctuations of the observable \hat{A} (bounded) decay algebraically in volume [40],

$$\delta A = \lim_{\tilde{T} \rightarrow \infty} \frac{1}{\tilde{T}} \int_0^{\tilde{T}} dt \langle \psi(t) | (\hat{A} - A_{eq})^2 | \psi(t) \rangle \sim V^{-1}. \quad (2.37)$$

2.2.1.3 Numerical evidence for the eigenstate thermalization hypothesis

In this section, we report some numerical results based on [40], which give strong evidence that in non-integrable many-body quantum systems ETH holds. We start showing an example that in integrable quantum systems ETH does not hold. In particular we consider a non-interacting fermionic system, described by the Hamiltonian in Eq. 2.15, in the case in which Ω is a bounded symmetric random matrix. Let $|E_n\rangle$ be an eigenstate of $\hat{\mathcal{H}}$, and it is specified by the occupation numbers $\langle E_n | \eta_l^\dagger \eta_l | E_n \rangle = a_n^l$ with $a_n^l \in \{0, 1\}$, where a_n^l assumes the value zero if the single-particle mode with eigenvalue ϵ_l is non-occupied and one otherwise. Let $|E_s\rangle = \eta_l^\dagger \eta_m |E_n\rangle$ be another eigenstate of $\hat{\mathcal{H}}$, where we assumed that the $m(l)$ -mode is occupied (not-occupied) in $|E_n\rangle$. Evaluating the

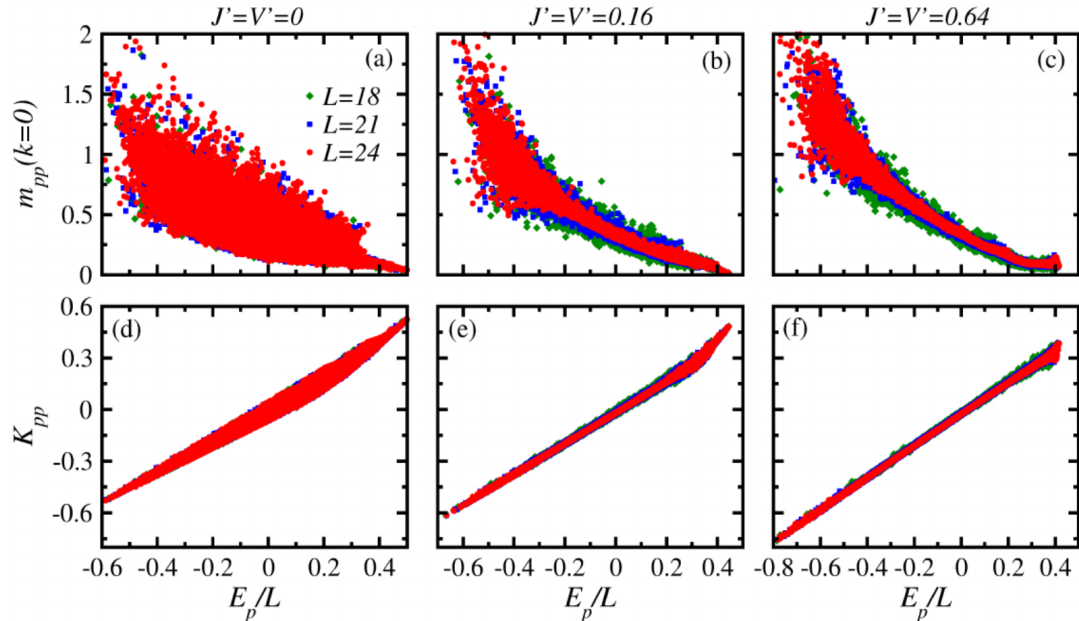


FIGURE 2.1: The panels show the diagonal elements in the basis of the eigenstates for two operators: $\hat{m}(k=0)$ (First row) and \hat{K} (Second row). The panels (a) and (d) show the case in which the system is integrable ($J' = V' = 0$), while (b),(c),(e) and (f) the non-integrable case ($J' = V' \neq 0$) [40].

off-diagonal element of the local operator $\hat{c}_x^\dagger \hat{c}_x$, we have

$$|\langle n | \hat{c}_x^\dagger \hat{c}_x | m \rangle| = |\psi_l(x) \psi_m(x)|, \quad (2.38)$$

since $\{\psi_l\}$ are the eigenvectors of the random matrix Ω , $|\langle E_n | \hat{c}_x^\dagger \hat{c}_x | E_s \rangle| \sim \mathcal{O}(1/L)$. Thus, the off-diagonal elements do not decay exponentially in L as predicted by ETH.

Nevertheless, numerical simulations give strong evidence for the validity of ETH for a large number of systems, ranging from strongly interacting fermionic (bosonic) lattice systems to ultra-cold quantum gases [3, 19, 20, 104, 120, 127]. In the following, we give few examples. Let's consider a non-integrable one-dimensional system of hard-core bosons with periodic boundary conditions, the Hamiltonian expressed in second-quantization reads [40]

$$\hat{\mathcal{H}} = \sum_{j=1}^L \{ -J(\hat{b}_j^\dagger \hat{b}_{j+1} + h.c.) + V(\hat{n}_j - 1/2)(\hat{n}_{j+1} - 1/2) - J'(\hat{b}_j^\dagger \hat{b}_{j+2} + h.c.) + V'(\hat{n}_j - 1/2)(\hat{n}_{j+2} - 1/2), \} \quad (2.39)$$

where $\{\hat{b}_j^\dagger\}$ ($\{\hat{b}_j\}$) are the creation (annihilation) operators for hard-core bosons ($[\hat{b}_i^\dagger, \hat{b}_j] = \delta_{i,j}$ and $\{\hat{b}_j^2 = 0\}$). The system is integrable if $J' = V' = 0$ and non-integrable otherwise (e.g., $J' = V' \neq 0$). The following local observables are considered:

1. The momentum mode occupation operator

$$\hat{m}(k) = \frac{1}{L} \sum_{i,j} e^{ik(i-j)} \hat{b}_i^\dagger \hat{b}_j. \quad (2.40)$$

2. The kinetic energy density operator

$$\hat{K} = \frac{1}{L} \sum_{j=1}^L \{-J(\hat{b}_j^\dagger \hat{b}_{j+1} + h.c.) - J'(\hat{b}_j^\dagger \hat{b}_{j+2} + h.c.)\}. \quad (2.41)$$

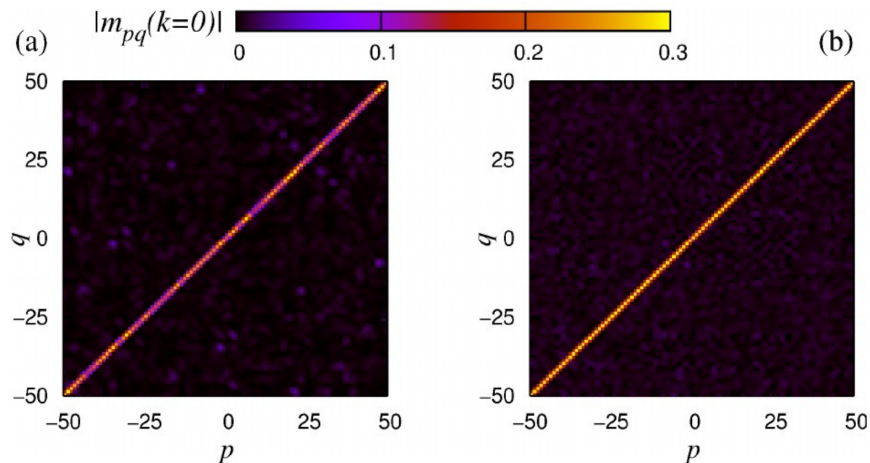


FIGURE 2.2: The panel (a) shows the matrix elements $m_{p,q}(k=0)$ for the integrable case with $L = 24$ and for 100 eigenstates $1 \leq p, q \leq 100$ with energy density close to $E/L = -0.16$. The panel (b) shows $m_{p,q}(k=0)$ for the non-integrable ($J' = V' = 0.32$) case with the same L , but with $E/L = -0.19$ [40].

Figure 2.1 [40] shows the diagonal element of $\hat{m}(k=0)$ and of \hat{K} in the eigenstates basis of $\hat{\mathcal{H}}$ as a function of energy density E/L . For $J' = V' = 0$ the system is integrable, and we can notice (panel (a) and (d)), that the diagonal elements of the two local operators are not smooth, and moreover the variance of the diagonal elements does not scale to zero with increasing system size. In contrast, in the other panels $J' = V' \neq 0$ the system is non-integrable, the diagonal elements are a smoother function of E/L compared with the integrable case. Furthermore, the curves become smoother with increasing the system size (Eq 2.37). Figure 2.2 [40] shows for a fixed system size and for a fixed energy density the matrix elements (diagonal and off-diagonal) of $\hat{m}(k=0)$, the eigenstates are labeled with the letters $\{p, q\}$ and they have been sorted by energy values. The first panel (Fig. 2.2 (a)) shows $\hat{m}_{p,q}(k=0)$ for the integrable case ($J' = V' = 0$), where it is visible that the diagonal elements $\hat{m}_{p,p}(k=0)$ present strong fluctuations, as we have already discussed. Moreover, the off-diagonal elements $\hat{m}_{p,q}(k=0)$ with $p \neq q$ are also affected by strong fluctuations, indeed there are some off-diagonal matrix elements which have the same order of magnitude as the diagonal elements, giving evidence that ETH breaks down. For the non-integrable case ($J' = V' \neq 0$), the diagonal elements

are approximately constant. The off-diagonal elements are highly suppressed compared to the diagonal ones as expected since they are proportional to an exponentially small value in L ($\sim e^{-S(\bar{E})/2}$). Moreover, they do not have strong fluctuations, indicating that their values depend only on the energy density.

2.3 Many-Body-Localization

We have stated ETH, which have used to show a possible explanation of thermalization in closed quantum systems. In this section, we introduce the concept of many-body localization (MBL).

MBL regards a class of closed interacting quantum many-body systems, which are robust against weak perturbations [107] and do not thermalize (ETH does not hold) [106]. We say that the system described by the Hamiltonian $\hat{\mathcal{H}}$ is many-body localized, if there exists a bijective map \mathbf{f} between the eigenstates of $\hat{\mathcal{H}}$ and the set of all possible sequences of $\{-1, 1\}$ of length L (Eq. 2.8), such that the Hamiltonian can be expressed in the following way

$$\hat{\mathcal{H}} = \sum_j^L \sum_{i_1 < i_2 < \dots < i_j} b_{i_1, i_2, \dots, i_j}^{(j)} \hat{\tau}_{i_1}^z \hat{\tau}_{i_2}^z \dots \hat{\tau}_{i_j}^z, \quad (2.42)$$

with $\{\hat{\tau}_j^z\}$ defined by \mathbf{f} as in Eq. 2.9, crucially with

$$b_{i_1, i_2, \dots, i_j}^{(j)} \sim e^{-\max |i_\alpha - i_\beta| / \xi}. \quad (2.43)$$

The couplings $\{b_i^{(1)}, b_{i,j}^{(2)}, \dots, b_{i_1, \dots, i_L}^{(L)}\}$ couple only exponentially weakly the integrals of motion $\{\hat{\tau}_i^z\}$.

Moreover, there is a set of L observables $\{\hat{A}_i\}$ such that

$$[\hat{A}_i, \hat{A}_j] = 0, \quad [\hat{A}_i, \hat{\tau}_j^\alpha] \neq 0 \quad \forall i, j \quad \forall \alpha \in \{x, y, z\}, \quad (2.44)$$

and

$$\left| \frac{1}{2^L} \text{Tr}[\hat{\tau}_i^z A_j] \right| \sim e^{-|i-j|/\xi_1}, \quad (2.45)$$

where the observables $\{\hat{\tau}_i^\alpha\}$, with $\alpha \in \{x, y\}$, have been constructed to satisfy Eq. 2.10.

The choice of the observables $\{\hat{A}_i\}$ defines the space in which the system can be defined to be localized. Indeed, the labels $\{i\}$ could be connected with physical labels. For example, they could be the site indices of the lattice and thus the observables $\{\hat{A}_i\}$ could be taken as local density operators $\{\hat{n}_i\}$ for fermionic systems or as Pauli matrices $\{\hat{\sigma}_i^z\}$ for spin systems. In this case, we say that the system is many-body localized in

space. Nevertheless, the labels $\{i\}$ could also be the momentum indices and for example $\{\hat{A}_i\}$ could be taken to be the momentum density operators. In the latter case, we say, that the system is many-body localized in momentum space.

The last point can be better explained with an example. Let's consider the following Hamiltonian

$$\hat{\mathcal{H}}^{(0)} = \sum_{i=1}^L h_i \hat{\sigma}_i^z, \quad (2.46)$$

$\{h_i\}$ are independent identically distributed random variables and L is the length of the chain. This model is integrable and it can be easily diagonalized. Its eigenstates are just the product states in the σ^z -basis. We could say that this model is trivially localized in space.

What happens to the eigenvectors of $\hat{\mathcal{H}}^{(0)}$ when the system is weakly perturbed ?

Let's consider the following perturbation

$$\hat{\mathcal{H}}^{(1)} = \sum_{i=1}^L \gamma_i \hat{\sigma}_i^x + \sum_{i=1}^{L-1} J_i \hat{\sigma}_i^z \hat{\sigma}_{i+1}^z, \quad (2.47)$$

where $\{\gamma_i\}$ and $\{J_i\}$ are independent identically distributed random variables. The perturbed Hamiltonian is defined by

$$\hat{\mathcal{H}} = \hat{\mathcal{H}}^{(0)} + \gamma \hat{\mathcal{H}}^{(1)}, \quad (2.48)$$

with $\gamma > 0$ the strength of the perturbation.

In 2016, J. Z. Imbrie, under minimal assumptions on the level energy statistics of $\hat{\mathcal{H}}$, proved that for weak γ ($\gamma \ll 1$) the system is still localized in space [68]. In the sense that:

1.

$$\lim_{L \rightarrow \infty} \frac{1}{2^L} \sum_n \overline{|\langle E_n | \hat{\sigma}_i^z | E_n \rangle|} = 1 - \mathcal{O}(\gamma^k) \quad \forall i, \quad (2.49)$$

where the overline indicates the average over the disorder configurations.

2.

$$\max_n |\langle E_n | \hat{O}_i \hat{O}_j | E_n \rangle - \langle E_n | \hat{O}_i | E_n \rangle \langle E_n | \hat{O}_j | E_n \rangle| \leq \gamma^{|i-j|/3}, \quad (2.50)$$

with probability $1 - (\gamma^k)^{1+(\log|i+j|)^2}$, where \hat{O}_i is any operator formed by the product of $\hat{\sigma}_i^x$ and $\hat{\sigma}_i^z$.

As a consequence, we could say that the eigenstates of $\hat{\mathcal{H}}$ for weak $\gamma \ll 1$, are close to the eigenstates of $\hat{\mathcal{H}}^{(0)}$.

Moreover, in his proof J. Z. Imbrie defines a map \mathbf{f} which connects the non-interacting eigenstates of $\hat{\mathcal{H}}^{(0)}$ with the eigenstates of $\hat{\mathcal{H}}$ constructing a unitary operator $\hat{\mathcal{U}}$ given by the product of local unitary operators such that

$$\hat{\mathcal{U}}^\dagger \hat{\mathcal{H}} \hat{\mathcal{U}} = \sum_j \sum_{i_1 < i_2 < \dots < i_j} b_{i_1, i_2, \dots, i_j}^{(j)} \hat{\sigma}_{i_1}^z \hat{\sigma}_{i_2}^z \dots \hat{\sigma}_{i_j}^z, \quad (2.51)$$

and

$$\hat{\tau}_i^z = \hat{\mathcal{U}} \hat{\sigma}_i^z \hat{\mathcal{U}}^\dagger, \quad [\hat{\tau}_i^z, \hat{\mathcal{H}}] = 0. \quad (2.52)$$

Recapitulating, for $\gamma \ll 1$, the model is many-body localized in the real-space, meaning

$$\left| \frac{1}{2^L} \text{Tr}[\hat{\tau}_i^\alpha \hat{\sigma}_j^\beta] \right| \sim e^{-|i-j|/\xi_{\alpha,\beta}} \quad \alpha, \beta \in \{x, y, z\}. \quad (2.53)$$

Furthermore, in many-body localized systems a weak form of integrability is restored. Indeed, we could define a system as weakly-integrable if for any $\epsilon > 0$ there exists a map \mathbf{f} and a variable $\tilde{L}(\epsilon)$ ($1 \leq \tilde{L}(\epsilon) < L$) which does not depend on L , such that

$$\begin{aligned} \|\hat{\mathcal{H}} - \hat{\mathcal{H}}_{\tilde{L}(\epsilon)}\| &\leq \epsilon, \quad \forall L \geq \tilde{L}(\epsilon), \\ \hat{\mathcal{H}}_{\tilde{L}(\epsilon)} &= \sum_j \sum_{i_1 < i_2 < \dots < i_j} b_{i_1, i_2, \dots, i_j}^{(j)} \hat{\tau}_{i_1}^z \hat{\tau}_{i_2}^z \dots \hat{\tau}_{i_j}^z. \end{aligned} \quad (2.54)$$

with $\lim_{\epsilon \rightarrow 0} \tilde{L}(\epsilon) \rightarrow \infty$.

Thus, many-body localized systems are weakly-integrable systems, nevertheless it is important to point out that our definition of weakly-integrability also include systems for which $b_{i_1, i_2, \dots, i_j}^{(j)} \sim 1/\max|i_\alpha - i_\beta|^\alpha$ with $\alpha > 1 + \delta$ for any $\delta > 0$ (power-law many-body localized system).

2.3.1 Localization in Fock Space

As we have described in the previous section, J. Z. Imbrie constructed a map which connects the eigenstates of $\hat{\mathcal{H}}^{(0)}$ with the eigenstates of $\hat{\mathcal{H}}$ via local small unitary operations [68]. It underlines that the final eigenstates of $\hat{\mathcal{H}}$ are adiabatically connected with the eigenstates of $\hat{\mathcal{H}}^{(0)}$ [18], in the same way that the localized eigenstates of an Anderson problem are connected with the site states of the lattice system [67]. Indeed, the original idea of mapping a non-extensive disordered quantum many-body system like a quantum dot to a localization problem in the Fock space has constructed a fundamental link between Anderson localization on hierarchical tree structures and many-body physics [6]. The MBL problem that we have described in the previous section, can be

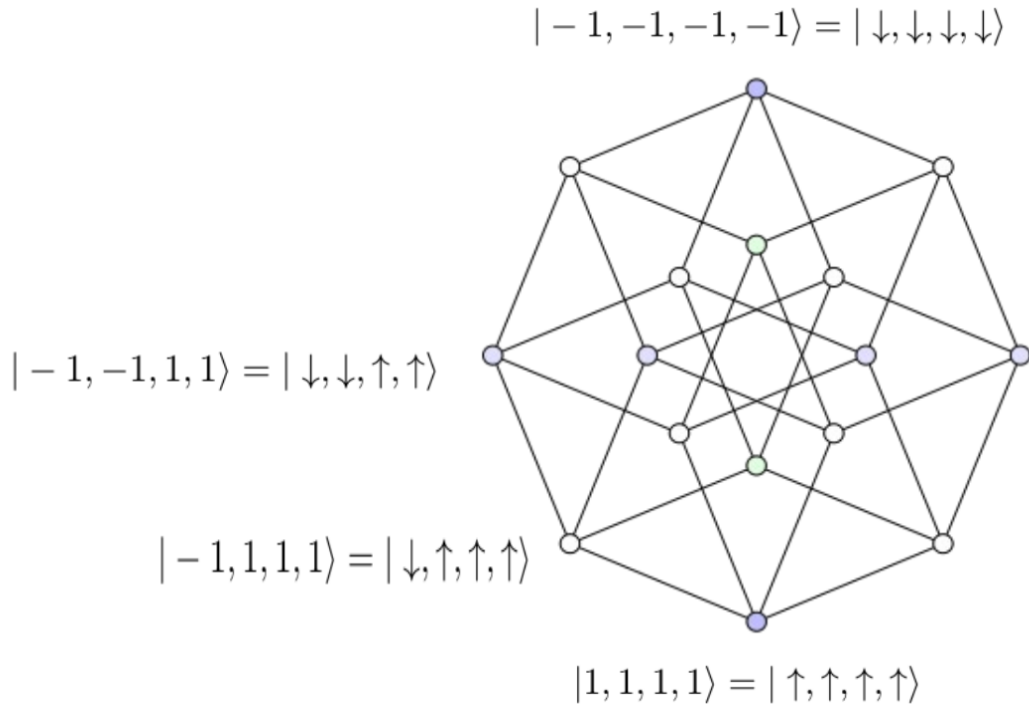


FIGURE 2.3: The Hamiltonian $\hat{\mathcal{H}}$ (Eq. 2.48) can be mapped to an Anderson localization problem in Fock space. The Figure shows a graphical representation of the Fock space graph with $L = 4$ in which $\hat{\mathcal{H}}$ can be mapped. Any point in this hypercube represents a product state in the σ^z -basis.

mapped onto an Anderson localization problem on a hypercube. Without loss of generality, let's consider the system defined by the Hamiltonian $\hat{\mathcal{H}}$ (Eq. 2.48). In the limit $\gamma \rightarrow 0$, $\hat{\mathcal{H}}$ is simply given by the sum of $\{\hat{\sigma}^z\}$ operators, and its eigenstates are product states in the σ^z -basis. Thus we can think of the σ^z -basis to be the sites of a hypercube. Turning on the perturbation ($\hat{\mathcal{H}}^{(1)}$) an effective hopping is introduced in the hypercube. This is illustrated in Fig. 2.3, which shows the system with $L = 4$, the number of sites is given by the dimension of the Hilbert space ($\mathfrak{D} = 2^L$) and a point in the hypercube represents a state in the Fock space in the σ^z -basis. The term $\sum_j \gamma_j \hat{\sigma}_j^x$ produces a hopping between different sites which differs by only one spin flip operation. The connectivity of this graph scales as L and the on-site energies in the graph are simply given by $\sum_i h_i a_i + \sum_i J_i a_i a_{i+1}$, with $a_j \in \{-1, 1\}$. Thus, $\hat{\mathcal{H}}$ can be mapped onto an “Anderson” model on a graph, in which the connectivity grows with L and in which the on-site energies are correlated random variables with typical fluctuations of order $\mathcal{O}(\sqrt{L})$. However, the difference between the on-site energies that are directly linked in the graph does not scale with L ($\sim \mathcal{O}(1)$).

One could ask if the system is localized in the sense of Anderson localization (Chapter 1) on the graph constructed in the Fock space. D.M. Basko, I.L. Aleiner and B.L. Altshuler

in their seminal work [17], demonstrated for a model of weakly-interacting disordered fermions that the system is localized in the sense of Anderson localization in the graph constructed taking the eigenstates of the non-interacting model. Remarkably, they also proved that a delocalization-localization transition happens as a function of disorder strength and energy density. This transition, which is called MBL transition, defines two phases: an ergodic phase where the eigenstates are delocalized in this Fock space graph and are thermal, and a many-body localized (MBL phase) in which the system is localized. Nevertheless, several works claim that a genuine localization in Fock space is not possible, meaning that the eigenstates are spread only on a sub-extensive portion of the Fock space (*e.g.*, $\sim \log \mathfrak{D}$, \mathfrak{D} is the dimension of the Hilbert space) [18, 93, 95].

In the next section, we show numerical results based on the works [16, 31, 95, 110, 130, 149], which give evidence of the existence of the two phases and thus of the MBL transition.

2.3.2 Numerical evidence of Many-Body Localization

The existence of a delocalization-localization transition has been confirmed in several works, which also underline the ergodicity breaking in the MBL phase.

Due to the exponential growth of the Hilbert space with system size, most of the numerical works focus on one-dimensional systems. The most studied model with an MBL transition is the spin-1/2 Heisenberg model [31, 95, 110, 130, 149]

$$\hat{\mathcal{H}} = \sum_i^L h_i \hat{S}_i^z + \sum_i^L J \hat{\mathbf{S}}_i \cdot \hat{\mathbf{S}}_{i+1}, \quad (2.55)$$

where $\hat{\mathbf{S}}_i = \{\hat{S}_i^x, \hat{S}_i^y, \hat{S}_i^z\}$, with $\hat{S}_i^\alpha = \frac{1}{2} \hat{\sigma}_i^\alpha$, and $\{h_i\}$ independent random fields equally distributed between $[-h, h]$ and L is the length of the chain. The Hamiltonian commutes with the total spin operator $\hat{S}_{\text{Tot}}^z = \sum_i^L \hat{S}_i^z$ ($[\hat{\mathcal{H}}, \hat{S}_{\text{Tot}}^z] = 0$), which implies the conservation of the magnetization in the z-direction. This model can be mapped onto the t-V spinless fermion chain via the Jordan-Wigner transformation [8]

$$\begin{aligned} \hat{\sigma}_j^+ &= e^{-i\pi \sum_k^{j-1} \hat{c}_k^\dagger \hat{c}_k} \hat{c}_j^\dagger, \\ \hat{\sigma}_j^- &= e^{+i\pi \sum_k^{j-1} \hat{c}_k^\dagger \hat{c}_k} \hat{c}_j, \\ \hat{\sigma}_j^z &= 2\hat{n}_j - 1. \end{aligned} \quad (2.56)$$

giving

$$\hat{\mathcal{H}} := -\frac{J}{2} \sum_{i=1}^L \hat{c}_i^\dagger \hat{c}_{i+1} + h.c. + \sum_{i=1}^L h_j \left(\hat{n}_i - \frac{1}{2} \right) + J \sum_{i=1}^L \left(\hat{n}_i - \frac{1}{2} \right) \left(\hat{n}_{i+1} - \frac{1}{2} \right). \quad (2.57)$$

In Chapters 3-5 we will use the Hamiltonian (Eq. 2.57) expressed in the particle lan-

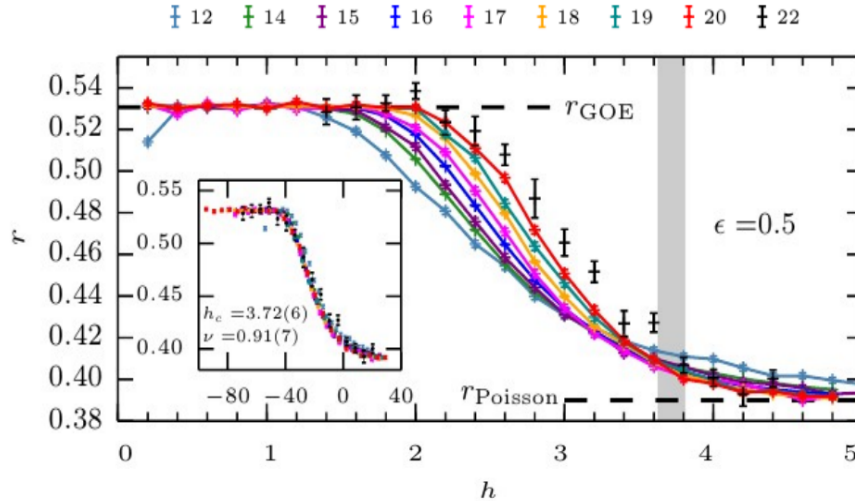


FIGURE 2.4: The panel shows r for several system sizes as a function of the disorder strength h for the Hamiltonian $\hat{\mathcal{H}}$ Eq. 2.55 [95].

guage.

2.3.2.1 Analysis of the level statistics

A powerful method to distinguish an ergodic phase from a localized phase is to study the energy spectrum of $\hat{\mathcal{H}}$ (Eq 2.55) [64]. The resistance to have crossing of levels (level repulsion) is a well known property of ergodic systems. Indeed, motivated by the Bohigas-Giannoni-Schmit conjecture [23] the statistic of level spacing of an ergodic system is expected to be the same as that of a random matrix belonging to the same symmetry class [64]. The probability distribution for the level spacing for random matrices in the Gaussian Orthogonal ensemble (GOE) is the Wigner-Dyson distribution [64], and thus we expect to find the same distribution in the ergodic phase. On the contrary, in the localized phase, due to existence of (quasi)-local integrals of motion, the energy levels will tend to cross each other (level-crossing). In this case, the probability distribution of the level spacing is expected to be Poissonian [51, 64]. To distinguish these two distributions (Wigner-Dyson, Poisson), it is useful to define the following quantity,

known as level spacing parameter [107]

$$\begin{aligned} r^{(n)} &= \min(\delta^{(n)}, \delta^{(n+1)}) / \max(\delta^{(n)}, \delta^{(n+1)}), \\ \delta^{(n)} &= E_{n+1} - E_n. \end{aligned} \quad (2.58)$$

It is possible to prove that in the case where the probability distribution is the Wigner-Dyson distribution, the average over the eigenstates index n of r is equal to $r_{\text{GOE}} \approx 0.5307$, while in the case of level-crossing $r_{\text{Poisson}} = 2 \log 2 - 1 \approx 0.3863$ [107]. Figure 2.4 [95] shows the level spacing parameter (r) as a function of the disorder strength h for several system sizes L for the Hamiltonian (Eq. 2.55). r has been obtained by averaging over disorder and over eigenstates with a fixed energy density ϵ which is defined by $\epsilon = (E - E_{\min}) / (E_{\max} - E_{\min})$ ($\epsilon = 0.5$, middle of the spectrum). For weak disorder, $r \approx r_{\text{GOE}}$ indicating that the system is ergodic, increasing the disorder strength the value of r drops monotonically to r_{Poisson} which for values $h \geq 4.5$ seems to be independent of system size. The curves for different system sizes L cross each other at a value around $h_c \approx 3.7$, giving a strong evidence of a possible transition. Indeed, it is possible to collapse the curves for different L making a finite-size scaling analysis with the use of a scaling-function of the form $g[L^{1/\nu}(h - h_c)]$, as shown in the inset of Fig. 2.4, with $\nu \approx 0.91$.

Nevertheless, recently it has been shown, that r can have the value r_{GOE} even if the probability distribution of the level spacing is not the Wigner-Dyson distribution [83]. This is one of the reasons why only an analysis of the level spacing parameter (r) is not sufficient to distinguish an ergodic from a localized phase. In the next sections we probe the existence of the transition using different approaches.

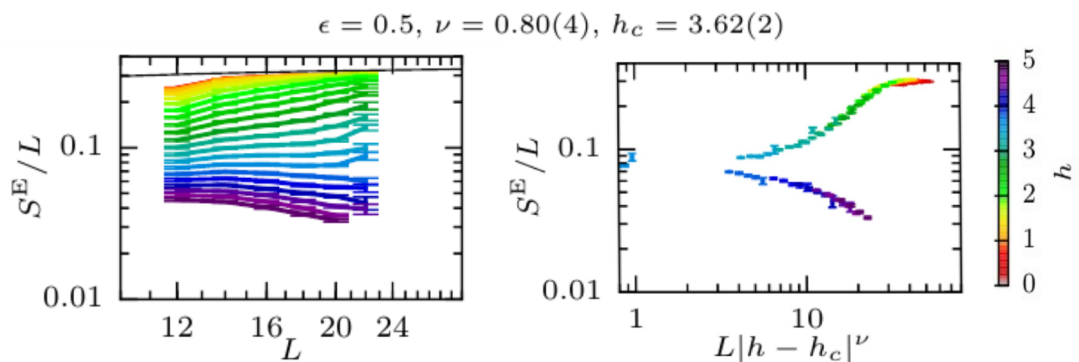


FIGURE 2.5: The panels show the renormalized with system size bipartite entanglement entropy S/L (S^E in the figure) as a function of L for several disorder strengths h and at energy density $\epsilon = 0.5$ [95].

2.3.2.2 Eigenstates analysis

In the previous section we showed how to detect the MBL transition studying the spectrum of the Hamiltonian. In this section, we show a complementary analysis, which consists in studying the eigenstates of Eq. 2.55.

We start with a probe borrowed from quantum-information theory [8]. This is the Von Neumann entanglement entropy (EE), which measures the spread of information of one-part of the system to the other. Dividing the system in two separated parts, the bipartite EE is defined by

$$\begin{aligned} S &= -\text{Tr}_{\tilde{A}}[\hat{\rho}_{\tilde{A}} \ln \hat{\rho}_{\tilde{A}}], \\ \hat{\rho}_{\tilde{A}} &= \text{Tr}_{\tilde{A}^c}[|E_n\rangle\langle E_n|], \end{aligned} \quad (2.59)$$

where $\tilde{A} = [1, \dots, \frac{L}{2}]$. The reduced density matrix $\hat{\rho}_{\tilde{A}}$ of eigenstates obeying ETH is expected to be thermal, and the EE will scale with the size of the system $S \sim L$. For localized eigenstates, we expect in one-dimensional system, that the EE will not scale with system size $S \sim \mathcal{O}(1)$. Indeed, if an eigenstate is localized in the real-space, then only closed by sites are entangled, hence the EE will scale only with the size of the boundary of the region traced out, thus implying for a generic system in d -dimensions, $S \sim L^{d-1}$. Figure 2.5 [95] shows S/L (S^E/L in the figure) as a function of L for several values of h averaged over disorder and over eigenstates in the middle of the spectrum ($\epsilon = 0.5$). A clear change in the behavior of S/L , at disorder value $h_c \approx 3.6$ is visible. For $h \leq h_c$, S/L is almost a constant as a function of L , giving indication that S is an extensive quantity. For $h \geq h_c$, S/L starts to decrease for large L implying that S is at least subextensive, in contrast with ETH. A collapse of several curves is possible, using a scaling-function of the form $g[L^{1/\nu}(h - h_c)]$, as shown in the inset of Fig. 2.5, suggesting the existence of the MBL transition.

A similar behavior can be observed for the bipartite fluctuation of a subsystem [135], which is defined by

$$\begin{aligned} \mathcal{F} &= \langle E_n | (\hat{S}_{\tilde{A}}^z)^2 | E_n \rangle - (\langle E_n | \hat{S}_{\tilde{A}}^z | E_n \rangle)^2, \\ \hat{S}_{\tilde{A}}^z &= \sum_i^{L/2} \hat{S}_i^z. \end{aligned} \quad (2.60)$$

\mathcal{F} measures the quantum fluctuations of the operator $\hat{S}_{\tilde{A}}^z$. For a localized system, since its degrees of freedom are frozen, we expect $\lim_{L \rightarrow \infty} \mathcal{F}/L \rightarrow 0$, while in a thermal phase \mathcal{F} will be an extensive quantity. Figure 2.6 [95] shows \mathcal{F} averaged over disorder as a function of h for several system sizes, but for a different energy density $\epsilon = 0.3$. Also

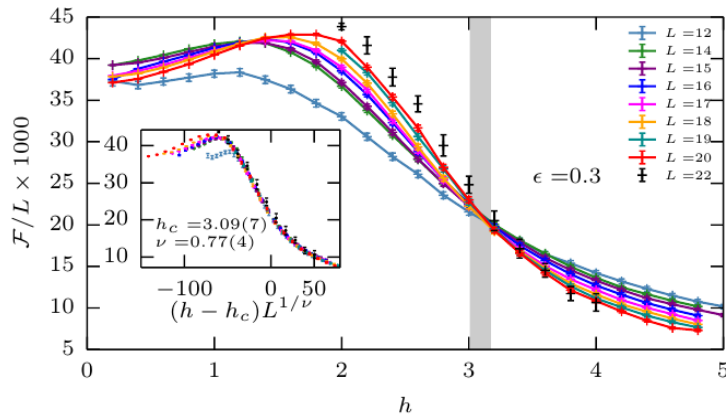


FIGURE 2.6: The panel shows \mathcal{F} (Eq. 2.60) for several L as a function of h , with $\epsilon = 0.3$ (energy density) [95].

in this case, at $h \approx h_c(\epsilon)$, a change in its behavior occurs as observed for the EE. This gives an indication that the MBL transition depends on the value of energy density $h_c(\epsilon = 0.3) \leq h_c(\epsilon = 0.5)$.

As we already discussed, in the ergodic phase the eigenstates are expected to be thermal, thus ETH should hold. A possible way to check if ETH holds is to consider expectation values of local observables for eigenstates which belong to the same energy density in the thermodynamic limit. For example defining

$$m_i^n = \langle E_n | \hat{S}_i^z | E_n \rangle, \quad (2.61)$$

$$|m_i^n - m_i^{n+1}| = |\langle E_n | \hat{S}_i^z | E_n \rangle - \langle E_{n+1} | \hat{S}_i^z | E_{n+1} \rangle|.$$

On the one hand if the eigenstate $|E_n\rangle$ is thermal, the expectation value of \hat{S}_i^z is just described by the energy density ϵ , and thus by ETH

$$|m_i^n - m_i^{n+1}| \sim e^{-\alpha L} \quad \alpha > 0. \quad (2.62)$$

On the other hand if the system is localized then the expectation value m_i^n will be different also for two eigenstates which belong to the same energy density. In fact, considering the limiting case of infinite disorder ($h \rightarrow \infty$), for which the system is trivially localized in the σ^z -basis, m_i^n takes with equal probability the values $\frac{1}{2}$ or $-\frac{1}{2}$, giving

$$|m_i^n - m_i^{n+1}| \sim \mathcal{O}(1). \quad (2.63)$$

Figure 2.7 [110] shows the logarithm of $|m_i^n - m_i^{n+1}|$ averaged over disorder configurations and over few eigenstates in the middle of the spectrum. For large disorder, $|m_i^n - m_i^{n+1}|$ is independent of L , while for weak disorder where ETH should hold, $|m_i^n - m_i^{n+1}|$ decays exponentially with L .

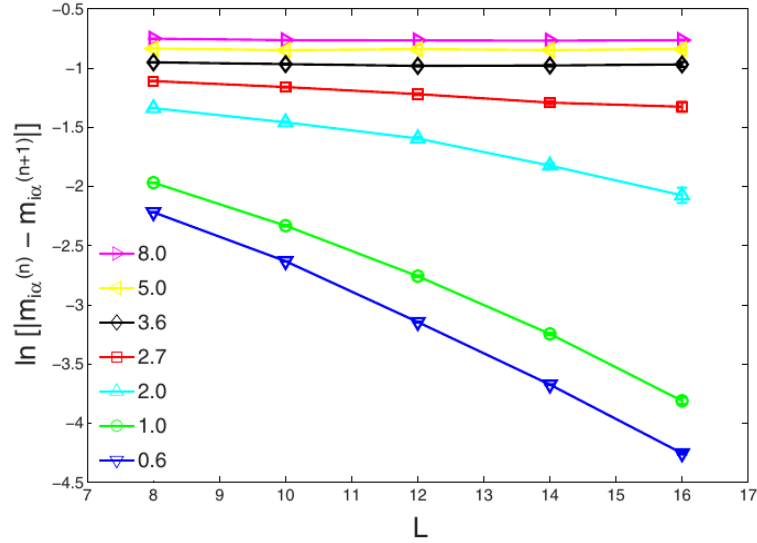


FIGURE 2.7: The panel shows the logarithm of $|m_i^n - m_i^{n+1}|$ averaged over disorder and over eigenstates in the middle of the spectrum for several values of h as a function of L . In the ergodic phase this difference decay exponentially with L (ETH), while in the localized phase $|m_i^n - m_i^{n+1}|$ does not decay [110].

2.3.2.3 Integrals of motion

We have seen that many-body localized systems are characterized by an extensive number of quasi-local integrals of motion. Several methods have been proposed to construct the quasi-local integrals of motion $\{\hat{\tau}_i^z\}$ for an MBL system [31, 123, 128]. In this section, we describe a method proposed by A. Chandran et al. [31], which constructs the integrals of motion considering the long-time evolution of a local-observable. The advantage of this method resides on its simple physical interpretation, however these integrals of motion do not obey the Pauli commutation relations.

Let's consider the system described by the Hamiltonian $\hat{\mathcal{H}}$ (Eq. 2.55), and the following initial state

$$\hat{\rho} = 2^{-L}(1 + \hat{\sigma}_i^z) \otimes \mathbb{I}_{i^c}, \quad (2.64)$$

where \mathbb{I}_{i^c} is the identity operator outside the site i . The density matrix $\hat{\rho}$ describes a state where the magnetization is zero outside the site i and one at site i . Moreover, all the other correlation functions are zero.

$$\begin{aligned} \text{Tr}[\hat{\rho}\hat{\sigma}_j^z] &= \delta_{i,j}, \\ \text{Tr}[\hat{\rho}\hat{\sigma}_j^z\hat{\sigma}_k^z] &= 0 \quad j \neq k. \end{aligned} \quad (2.65)$$

Let's consider the time evolution of the density matrix $\hat{\rho}(t) = \hat{U}^\dagger(t)\hat{\rho}\hat{U}(t)$, with $\hat{U}(t) = e^{-i\hat{\mathcal{H}}t}$. If the system is ergodic, in the long-time limit the local magnetization will be

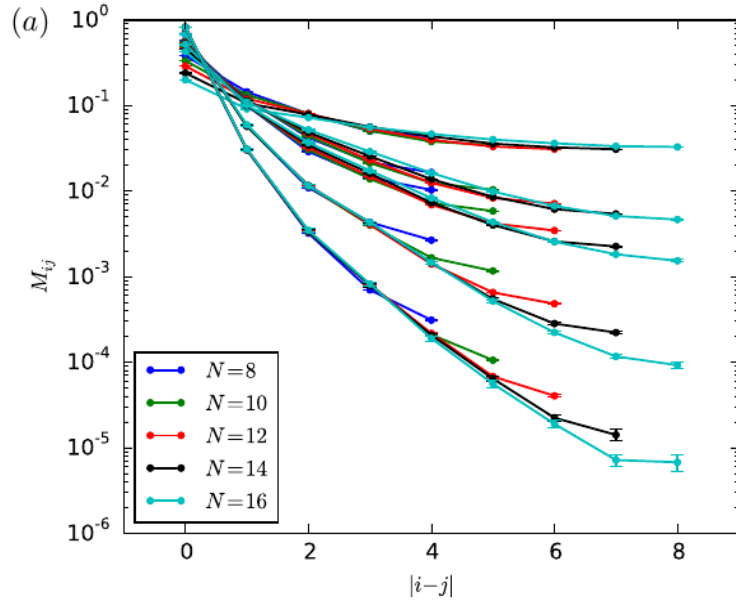


FIGURE 2.8: The panel shows $M_{i,j}$ (Eq. 2.69) as a function of $|i-j|$ for several L and several values of disorder strength $W \in \{2, 3, 3.5, 5, 7\}$ from top to bottom. It gives evidence that the integrals of motion that have been constructed are quasi-local in space [31].

the same at any site and since the total magnetization is conserved

$$\lim_{t \rightarrow \infty} \text{Tr}[\hat{\rho} \hat{\sigma}_j^z] \sim \frac{1}{L} \quad \text{“for ergodic systems”}. \quad (2.66)$$

In contrast, in the MBL phase, since ergodicity breaks down, even at long-time the evolved state will still remember the initial state ($\hat{\rho}(0)$) and thus one would expect that the profile of the magnetization will have an exponentially decaying envelop centered at the site i

$$\lim_{t \rightarrow \infty} \text{Tr}[\hat{\rho} \hat{\sigma}_j^z] \sim e^{-|i-j|/\xi} \quad \text{“for many-body localized systems”}. \quad (2.67)$$

This can be better formalized by taking the long-time average

$$\bar{\rho} = \lim_{\tilde{T} \rightarrow \infty} \frac{1}{\tilde{T}} \int_0^{\tilde{T}} dt \hat{\rho}(t). \quad (2.68)$$

Thus, we have

$$M_{i,j} = \text{Tr}[\bar{\rho} \hat{\sigma}_j^z] = \frac{1}{2L} \text{Tr}[\bar{\hat{\sigma}}_i^z \hat{\sigma}_j^z], \quad (2.69)$$

where

$$\bar{\hat{\sigma}}_i^z = \lim_{\tilde{T} \rightarrow \infty} \frac{1}{\tilde{T}} \int_0^{\tilde{T}} dt \hat{\sigma}_i^z(t). \quad (2.70)$$

Moreover, $\{\bar{\hat{\sigma}}_i^z\}$ are integrals of motion

$$[\hat{\mathcal{H}}, \hat{\sigma}_i^z] = 0 \quad [\hat{\sigma}_i^z, \hat{\sigma}_j^z] = 0, \quad \forall i, j. \quad (2.71)$$

Figure 2.8 [31] shows $M_{i,j}$ as a function of the distance $|i - j|$ for several L and W . As expected, for large values of W , $M_{i,j}$ decays exponentially in the distance between sites ($M_{i,j} \sim e^{-|i-j|/\xi}$), while for smaller values of W , $M_{i,j}$ is almost constant.

2.3.2.4 Many-body mobility edges

In this section, we summarize the results that we have reported, and we show the complete phase diagram for an MBL system [95]. The study of eigenstates and of the spectral properties of $\hat{\mathcal{H}}$ (Eq 2.55) give evidence for the existence of two phases. An ergodic phase in which the eigenstates are ergodic and ETH holds, and another phase called MBL phase where the eigenstates are localized and ergodicity breaks down. Furthermore, the ergodic phase is characterized by having Wigner-Dyson level spacing statistic ($r \approx r_{\text{GOE}}$) and the eigenstates are volume-law ($S \sim L$). The MBL phase has Poissonian level spacing statistics ($r \approx r_{\text{Poisson}}$) and its eigenstates are area-law ($S \sim L^0$). The localized phase is also characterized by the existence of an extensive number of quasi-local integrals of motion ($\{\hat{\tau}_i^z\}$). Moreover, we have also seen that

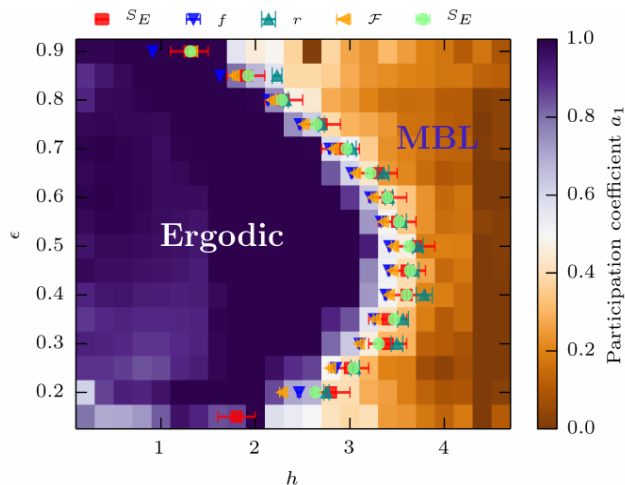


FIGURE 2.9: The panel shows the full phase diagram for the Hamiltonian Eq. 2.55 (disorder strength (h) - energy density ϵ) [95].

the critical value of the MBL transition (h_c) is energy density dependent $h_c(\epsilon)$. The collection of these results gives rise to the phase-diagram for the MBL transition of $\hat{\mathcal{H}}$ (Eq 2.55). Figure 2.9 [95] shows the phase diagram (disorder strength (h) - energy density ϵ). It gives evidence for the existence of an MBL transition also at a finite energy density (highly-excited quantum phase transition) and thus of the existence of a *many-body mobility edge* (MBME). In the literature, energy density and the word temperature are used interchangeably (quantum phase transition at finite temperature) [106].

In other words, for large values of h , the system is always localized ($h \geq h_c(\epsilon = 0.5) \approx 3.5$). For smaller values of h , the energy spectrum can host separated bands which are composed of ergodic states or of localized states.

Nevertheless, it is important to point out that recently the existence of MBME has been questioned [42]. W. De Roeck et al. [42], using perturbation theory and assuming that ETH holds in the ergodic phase, argued that thermal local-fluctuations in eigenstates could destabilize the localized phase, forbidding the existence of MBME.

In the next section, we show some properties of the quantum dynamics of many-body localized systems.

2.3.2.5 Absence of transport

MBL systems are characterized by having no transport, as has been shown in the seminal works [17, 62]. It can be showed numerically considering the spin-spin correlator

$$C(r, t) = \frac{1}{2L} \text{Tr}[\hat{S}_{L/2}^z(t) \hat{S}_{L/2+r}^z]. \quad (2.72)$$

The correlator $C(r, t)$ gives direct information on the d.c. conductivity of the model [149]. In the ergodic phase, diffusion should take place, and at long-time the correlator should have a Gaussian form, $C(r, t) \sim \frac{e^{-\frac{1}{2}(\frac{r}{Dt})^2}}{\sqrt{2\pi Dt}}$ with D the diffusion constant. For a localized system, at long-time $C(r, t)$ does not decay to zero, and it is expected to have the form $C(r, t) \sim e^{-r/\xi}$. Figure 2.10 (a) [149] shows $C(r, t)$ in a log scale for the non-

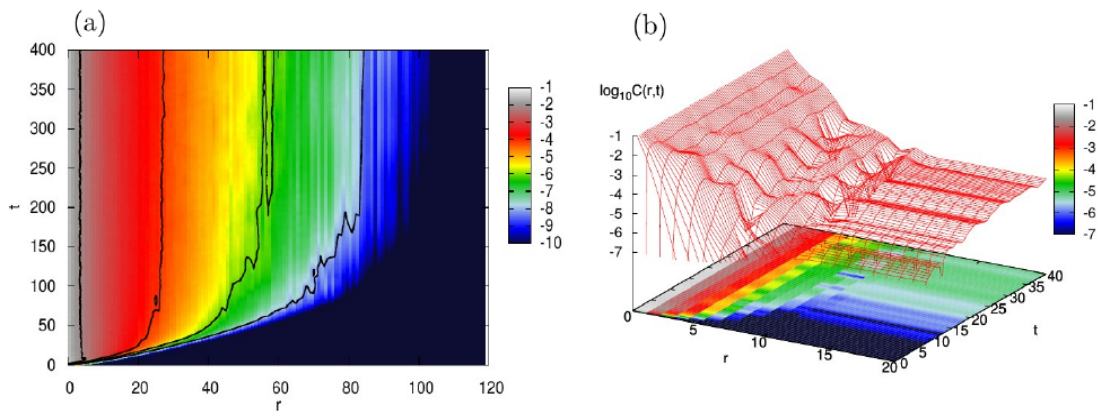


FIGURE 2.10: The panel (a) show the spin-spin correlator (Eq 2.72) for the non-interacting case. The panel (b) shows $C(r, t)$ for the interacting case in the localized phase. [149]

interacting case ($\hat{\mathcal{H}}^{(0)} = \sum_i^L h_i \hat{S}_i^z + \sum_i^L J(\hat{S}_i^x \hat{S}_{i+1}^x + \hat{S}_i^y \hat{S}_{i+1}^y)$) which can be mapped onto an Anderson model. At short time the propagation is ballistic ($t \leq 1/J$), while at long-time the propagation is frozen as expected for localized systems and $C(r, t) \sim e^{-r/\xi}$.

The same picture is unchanged if interaction is switched on (at least for strong disorder or weak interaction strengths) as is shown in Fig. 2.10 (b).

2.3.2.6 Unbounded growth of Entanglement

As we have already discussed, localized systems are characterized by the absence of transport (*e.g.*, spin-spin diffusion, energy diffusion). Nevertheless, MBL systems have the peculiarity that information can still propagate, contrary to a localized non-interacting system, in which information propagation is also absent. Indeed, starting with a random

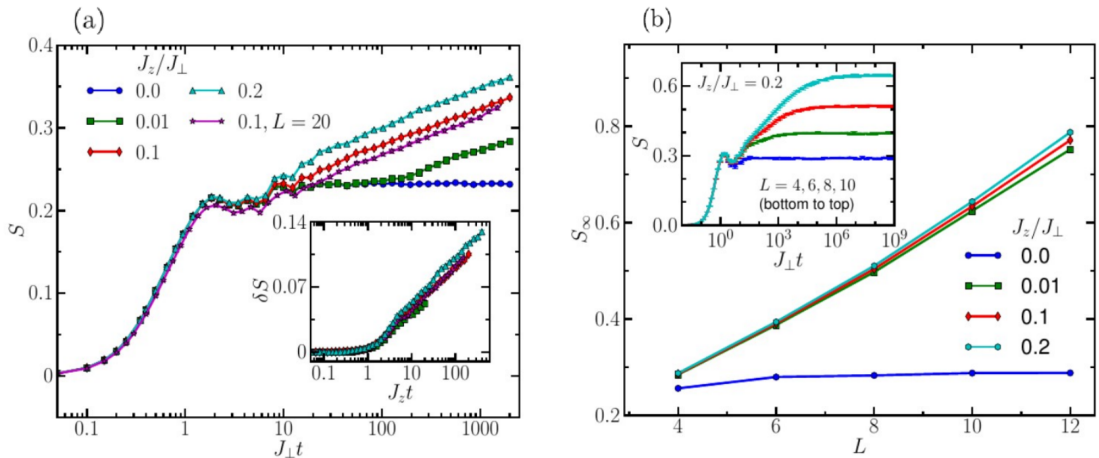


FIGURE 2.11: The panel (a) shows $S(t)$ as a function of t for several interaction strengths J_z for a fixed L . In this panel the system is always in a localized phase. for $J_z = 0$ the system is Anderson localized and information propagation is absent (also panel (b), $S_{\infty} \sim L^0$), while for $J_z \neq 0$ the system is interacting and $S(t) \sim \log(t)$. The panel (b) shows that the saturation value of $S(t)$ in the interacting case follows a volume-law ($S_{\infty} \sim L$) [16].

product state in the σ^z -basis and evolving it, the bipartite entanglement entropy grows logarithmically with time ($S(t) \sim \log(t)$) in the MBL phase. Contrary, for the non-interacting case, no propagation occurs ($\lim_{t \rightarrow \infty} S(t) \sim \text{constant}$). Figure 2.11 (a) [16] shows $S(t)$ as a function of t for several interaction strengths (J_z in the figure) for a fixed system size. As we anticipated, $S(t)$ for the non-interacting case just saturates to a constant. As the interaction is switched on, a slow logarithmic propagation of information is visible. It is important to note (Fig. 2.11 (b)) [16] that the long-time saturation value of $S(t)$ scales linearly with system size ($S_{\infty} = \lim_{t \rightarrow \infty} S(t) \sim L$). If the system is ergodic, then the entanglement will spread ballistically [94], and at long-time for finite systems, it will saturate to the value, $S_{\infty} = L \log 2 - \frac{1}{2} + \mathcal{O}(\frac{\log L}{L})$ [109]. Indeed, the evolved random product state in an ergodic system spreads in the Fock space, and its long-time limit can be approximated with a random state in the Fock space, and the bipartite entanglement entropy of a random state is $L \log 2 - \frac{1}{2} + \mathcal{O}(\frac{\log L}{L})$. Nevertheless, for an MBL system S_{∞} is smaller than the value expected for an ergodic system,

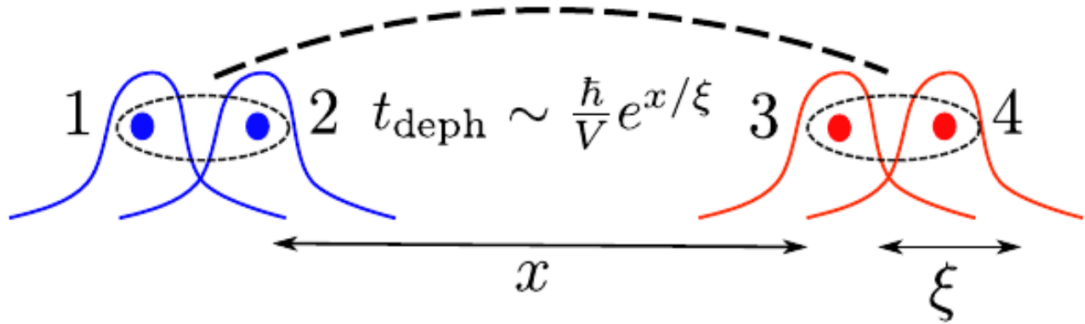


FIGURE 2.12: The panel shows a graphical representation of the dephasing mechanism due by interaction ($V \neq 0$), which is the reason of the log-information propagation in the MBL phase [130].

giving indication that even if the long-time evolved state is a volume-law state, it is non-thermal.

The reason of this slow logarithmic spread of information is due to a dephasing mechanism originating from interactions which is able to entangle degrees of freedom far away in space [130]. It is easier to understand this dephasing mechanism in the particle language rather than in spin language. If the interaction is absent, the eigenstates are Slater determinants of the single-particle eigenstates, and they are completely specified by the occupations of the single-particle levels. Moreover, the eigenvalues are sum of the single-particle eigenenergies. For weak interactions to first order approximation, the eigenstates are those of the non-interacting case, nevertheless, the interactions will correlate and dephase the eigenenergies. Let's consider the simple case in which only two particles are present in the system and consider the following initial state

$$|\psi_0\rangle = \frac{1}{2}(\hat{\eta}_1^\dagger \hat{\eta}_2^\dagger)(\hat{\eta}_3^\dagger \hat{\eta}_4^\dagger)|0\rangle, \quad (2.73)$$

where $\hat{\eta}_i^\dagger$ creates an excitation localized in space. Suppose that the distance between the support of the excitation (1,2) and (3,4) x is large ($x \gg \xi$) (Fig 2.12 [130]), where ξ is the localization length of the non-interacting problem. If the interaction is absent no entanglement will be generated during the time evolution. Nevertheless, the interactions generate a correlation between single-particle eigenenergies. With the use of first order perturbation theory, $E_{\alpha,\beta} = \epsilon_\alpha + \epsilon_\beta + \delta E_{\alpha,\beta}$, $\delta E_{\alpha,\beta} \sim C_{\alpha,\beta} J e^{-x/\xi}$. The reduced density matrix for the first particle is given by:

$$\hat{\rho}(t) = \frac{1}{2} \begin{pmatrix} 1 & F(t)/2 \\ F^*(t)/2 & 1 \end{pmatrix}, \quad (2.74)$$

where $F(t) = e^{-i\Omega t}(1 + e^{-i\delta\Omega t})$, with $\delta\Omega = \delta E_{1,4} - \delta E_{1,4} - \delta E_{1,3} + \delta E_{2,3}$ and $\Omega = \epsilon_1 - \epsilon_2 + \delta E_{1,3} - \delta E_{2,3}$. At time, $t = (2n + 1)2\pi/\delta\Omega$ the state will be maximally

entangled ($S = \log 2$). Moreover, the time to reach this value scales exponentially with x (distance between single-particle modes), giving rise to the logarithmic growth. This gives the main idea of the mechanism for which the presence of interaction produces entanglement propagation through the system.

Part II

Detecting the Many-Body
Localization transition and
characterization of the ergodic
and many-body localized phases

In the next two chapters we present two complementary methods to detect the MBL transition and to give a characterization of both the ergodic phase and the MBL phase. In the first approach, borrowing concepts from quantum-information theory, we show that the quantum-mutual information is an efficient probe to detect the MBL transition. In the second one, giving a characterization of time-irreversibility, we give a complementary description of the two phases. Moreover, we show, how these two methods can be used to distinguish an Anderson-insulating phase from an MBL localized phase.

Chapter 3

Quantum Mutual Information as a Probe for Many-Body Localization

As we have already discussed, several quantities have been proposed to characterize a many-body localized (MBL) phase and to detect the MBL transition (Chapter 2). Moreover, new advancements in experimental techniques allowed to obtain the first evidence of the existence of a localized phase and the presence of a transition [24, 97, 129, 137]. Nevertheless, one of the issues in the experiments has been to distinguish an Anderson insulator phase from an MBL phase. As we have shown in Chapter 2, the growth of the entanglement entropy after a global quench shows different behavior between the two phases: in the Anderson insulator phase it saturates and in the MBL phase it grows logarithmically. However, measuring entanglement entropy in an experimental setup is challenging due to its nonlocal nature [69]. Only few local measurements have been proposed to distinguish an Anderson insulator from an MBL phase. For example, M. Serbyn et. al. [131], considering the evolution of local observables after a quantum quench, found that the time-fluctuations decay algebraically with time in an MBL phase, while in the Anderson insulator phase the time-fluctuations do not decay. They relate this decay to the entanglement growth in an MBL phase, and moreover they relate the rate of the decay to a characteristic localization length. Nevertheless, usually the study of time-fluctuations are difficult in an experimental setup since the time scale to study them are too large, and thus the system can not longer be considered closed.

In this chapter, we demonstrate that the quantum mutual information (QMI) between two separated sites is a useful probe to study MBL, and moreover it can be used as a dynamical indicator to distinguish an Anderson insulator from an MBL phase. Moreover,

the QMI between two sites, being a local measurement, can in principle be used in an experimental setup to detect the transition and to distinguish between an Anderson insulator and an MBL phase, without the need to compute an extensive many body density matrix [8].

This chapter is structured as follows: In the first part of this chapter, with the aim to make it self-consistent, we describe the models that we will study. Then, we will define the QMI and explain its properties. In the second part, we will benchmark our conjectures in the non-interacting Aubrey-André-Harper model (Chapter 1), and in the disordered t-V spinless chain (Chapter 2). In the last part of this chapter, we will show how the QMI can be used as a dynamical indicator to distinguish an Anderson insulator from an MBL phase.

3.1 Models

The Hamiltonian reads

$$\begin{aligned} \hat{\mathcal{H}} = & -\frac{t}{2} \sum_{j=1}^{L-1} \hat{c}_j^\dagger \hat{c}_{j+1} + h.c. + \sum_{j=1}^L h_j \left(\hat{n}_j - \frac{1}{2} \right) \\ & + V \sum_{j=1}^{L-1} \left(\hat{n}_j - \frac{1}{2} \right) \left(\hat{n}_{j+1} - \frac{1}{2} \right) \end{aligned} \quad (3.1)$$

where \hat{c}_j^\dagger (\hat{c}_j) is the fermionic creation (annihilation) operator at site j and $\hat{n}_j = \hat{c}_j^\dagger \hat{c}_j$, $\{h_j\}$ are random fields, t and V are respectively the hopping and the interaction strength, L the system size and $N = \frac{L}{2}$ the number of fermions. We consider two different cases that have a metal-insulator transition:

1. The noninteracting AAH model (Chapter 1), which is obtained from $\hat{\mathcal{H}}$ (3.1) with $V = 0$, $t = 2$ and $h_j = W \cos(2\pi j\phi + \alpha)$ where $\alpha = \frac{1+\sqrt{5}}{2}$ is the golden ratio and ϕ is a random phase uniformly distributed in $[0, 2\pi]$. As we have shown in Chapter 1, the AAH model is known to have a metal-insulator transition at $W_c = 2$ (extended phase for $W \leq W_c$ and localized phase for $W > W_c$). The localization length close to the transition diverges as $\xi_{\text{loc}} \sim \log^{-1} \frac{W}{2}$ (Chapter 1).
2. The t-V spinless fermionic disordered chain (Chapter 2) is obtained by choosing $t = V = 1$, and $\{h_j\}$ independent random variables uniformly distributed in $[-W, W]$. This t-V chain is believed to have an MBL transition at a critical disorder strength $W_c = 3.5 \pm 1$ (extended for $W < W_c$ and localized for $W > W_c$), as discussed in Chapter 2.

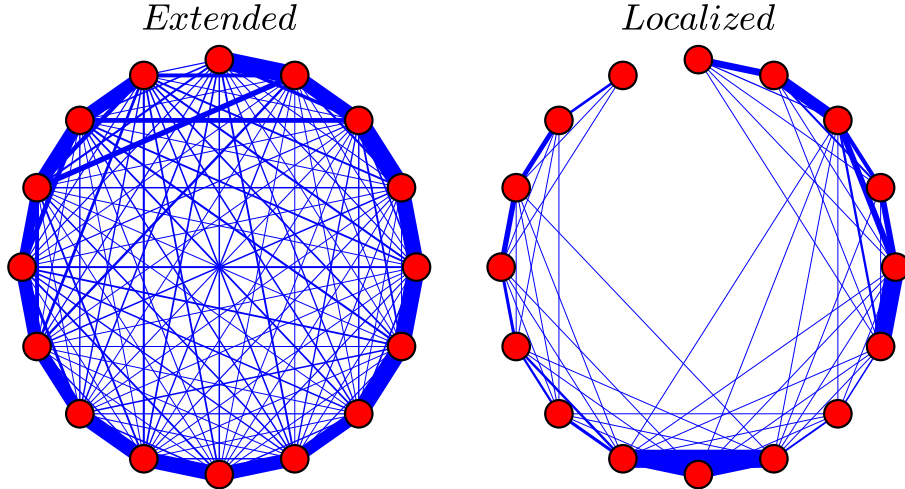


FIGURE 3.1: Qualitative behavior of the QMI in the two different phases of the interacting disorder model $\hat{\mathcal{H}}$ (3.1) for a fixed disorder configuration. $t = V = W = 1$ (left) and $t = V = 1$ $W = 5$ (right). The red dots represent the sites of the chain and the thickness of the blue bonds between sites $\{i, j\}$ is proportional to the magnitude of $\frac{\mathcal{I}([i], [j])}{\max_{i,j} \mathcal{I}([i], [j])}$ averaged over 16 eigenstates in the middle of the spectrum.

3.2 Quantum Mutual Information

The mutual information measures the total amount of classical and quantum correlations in the system and has been successfully used to study phase transitions [4, 11, 33, 66, 98–100, 136, 140, 146, 157, 158]. The QMI for two spatial subsets of the system $\mathcal{A}, \mathcal{B} \subseteq [1, L]$ is defined as [8]:

$$\mathcal{I}(\mathcal{A}, \mathcal{B}) := S(\mathcal{A}) + S(\mathcal{B}) - S(\mathcal{A} \cup \mathcal{B}) \quad (3.2)$$

where $S(\mathcal{A})$ is the Von Neumann entropy $S(\mathcal{A}) = -\text{Tr}[\rho_{\mathcal{A}} \log \rho_{\mathcal{A}}]$ with $\rho_{\mathcal{A}}$ the reduced density matrix of the subset \mathcal{A} calculated using an eigenstate of $\hat{\mathcal{H}}$. Figure 3.1 shows the typical behavior of $\mathcal{I}([i], [j])$ for a given disorder configuration in two different phases (extended/localized) for all possible combination of bonds $\{i, j\}$. The thickness of the lines that connect $i \leftrightarrow j$ represents the magnitude of $\frac{\mathcal{I}([i], [j])}{\max_{i,j} \mathcal{I}([i], [j])}$. In the extended phase (Fig. 3.1, left panel) the strongest bonds are the first neighbors $\{i, i+1\}$ but nevertheless all the other combinations of bonds have almost the same magnitude indicating that in the extended phase all sites are entangled with each other. Note that in the thermodynamic limit for ergodic infinite temperature states where a random-matrix assumption is supposed to be valid, we expect $\frac{\mathcal{I}([i], [j])}{\max_{i,j} \mathcal{I}([i], [j])}$ to be a constant independent of $\{i, j\}$. In contrast, in the localized phase (Fig. 3.1, right panel) each site is mainly entangled with neighboring sites and the QMI is almost zero for distant sites. Particularly, the QMI between two sites $\{i, j\}$ in a fermionic system with a fixed number of particles is given by

$$\mathcal{I}([i], [j]) := S([i]) + S([j]) - S([i] \cup [j]) \quad (3.3)$$

where

$$S([i]) = - \langle n_i \rangle \log \langle n_i \rangle - (1 - \langle n_i \rangle) \log \langle 1 - n_i \rangle, \quad (3.4)$$

$$S([i] \cup [j]) = - \langle n_i n_j \rangle \log \langle n_i n_j \rangle - \langle (1 - n_i)(1 - n_j) \rangle \log \langle (1 - n_i)(1 - n_j) \rangle - \lambda_+ \log \lambda_+ - \lambda_- \log \lambda_-, \quad (3.5)$$

and

$$\lambda_{\pm} = \frac{\langle (n_i + n_j)^2 \rangle \pm \sqrt{\langle n_i - n_j \rangle^2 + 4|\langle c_i^\dagger c_j \rangle|^2}}{2}, \quad (3.6)$$

where $\langle \cdot \rangle$ is the expectation value in an eigenstate of $\hat{\mathcal{H}}$. The computation of the QMI requires only the knowledge of two point correlation functions (*i.e.* $\langle n_i n_j \rangle$) and the expectation values of the local densities ($\langle n_i \rangle$).

Furthermore, in the case of one particle ($N=1$) the QMI reduces to

$$\begin{aligned} \mathcal{I}_j &= - |\psi_1|^2 \log |\psi_1|^2 - (1 - |\psi_1|^2) \log(1 - |\psi_1|^2) \\ &\quad - |\psi_j|^2 \log |\psi_j|^2 - (1 - |\psi_j|^2) \log(1 - |\psi_j|^2) \\ &\quad + (|\psi_1|^2 + |\psi_j|^2) \log(|\psi_1|^2 + |\psi_j|^2) \\ &\quad + (1 - |\psi_1|^2 - |\psi_j|^2) \log(1 - |\psi_1|^2 - |\psi_j|^2). \end{aligned} \quad (3.7)$$

To quantify this behavior, we focus our study on $\mathcal{I}_j = \mathcal{I}([1], [j+1])$, from which we can define a correlation length

$$\xi^{-1} := - \lim_{j \rightarrow \infty} \frac{1}{j} \overline{\log \frac{\mathcal{I}_j}{\mathcal{I}_1}} = \lim_{j \rightarrow \infty} \xi_j^{-1}, \quad (3.8)$$

where the overline stands for disorder average. We expect that in the localized phase \mathcal{I}_j decays exponentially in j ($\mathcal{I}_j \sim e^{-\frac{j}{\xi}}$), thus ξ^{-1} will be nonzero. Instead, in the extended phase we expect a decay of \mathcal{I}_j slower than exponential, implying ξ^{-1} is zero in the thermodynamic limit. The exponential decay of \mathcal{I}_j implies, via the Pinsker's inequality, that all two point correlation functions also decay exponentially with the distance [59]. This definition of a correlation length is related to the single particle localization length ξ_{loc} , which has been discussed in Chapter 1

$$\xi_{\text{loc}}^{-1} := - \lim_{j \rightarrow \infty} \frac{1}{j} \log \frac{|\psi_j|}{|\psi_1|}, \quad (3.9)$$

with ψ_j the single particle wave function evaluated at site j . Using Eq. 3.7, and assuming ψ_j is an exponential function of j

$$\log \mathcal{I}_j \sim \log |\psi_j|^2 + \log \left(1 - \log |\psi_j|^2 + \log \frac{|\psi_1|^2}{1 - |\psi_1|^2} \right)$$

for large j , implies

$$\xi \sim 2\xi_{\text{loc}}. \quad (3.10)$$

As a further measure of the spread of the QMI we interpret $\left\{ p_j = \frac{\mathcal{I}_j}{\sum_m \mathcal{I}_m} \right\}$ as the values of a discrete probability distribution and take its variance

$$\sigma^2 := \sum_j j^2 p_j - \left(\sum_j j p_j \right)^2. \quad (3.11)$$

Since we expect \mathcal{I}_j to decay exponentially fast with j in the localized phase, $\bar{\sigma}$ should saturate with system size in this phase. However, it is important to note that $\bar{\sigma}$ can still saturate for algebraically decaying \mathcal{I}_j (*i.e.*, $\mathcal{I}_j \sim \frac{1}{j^{3+\eta}}$ for any $\eta > 0$), thus this quantity can only be used to detect a lower bound of the transition point.

3.3 Quantum mutual information for the Aubry-André-Harper model

We start by benchmarking our expectations on the behavior of the QMI in different phases for the AAH model. We compute \mathcal{I}_j for this model using a free fermion technique (Appendix A) for eigenstates of $\hat{\mathcal{H}}$ constructed as a Slater determinant taking random single particle eigenstates, which implies an effective infinite temperature ensemble. The two lower panels of Fig. 3.2 show ξ_j^{-1} as a function of j , for two different values of W , in the extended phase ($W = 1.5$) and in the localized phase ($W = 2.2$). In the extended phase it decays to zero with a saturation point which scales as the inverse of the system size with a logarithmic correction due to the normalization of the single particle wave functions ($\xi^{-1} \sim \frac{\log L}{L}$). In the localized phase, ξ^{-1} saturates to a nonzero value, leading to a finite correlation length. The left upper panel of Fig. 3.2 shows ξ for different system sizes and different disorder strengths. In the localized phase for a fixed system size L , ξ was extrapolated from ξ_j by averaging over the values of j where it saturates, and in the extended phase we take $\xi = \xi_{j=L}$. As expected, in the extended phase ξ increases with system size, while in the localized phase it saturates to a constant. The left panel of Fig. 3.3 shows how the correlation length ξ grows with system size in the extended phase, $\xi \sim \frac{L}{\log L}$. The logarithmic correction is due to the normalization of the single particle wave function in the extended phase, which decays as $\frac{1}{\sqrt{L}}$. Moreover, the single

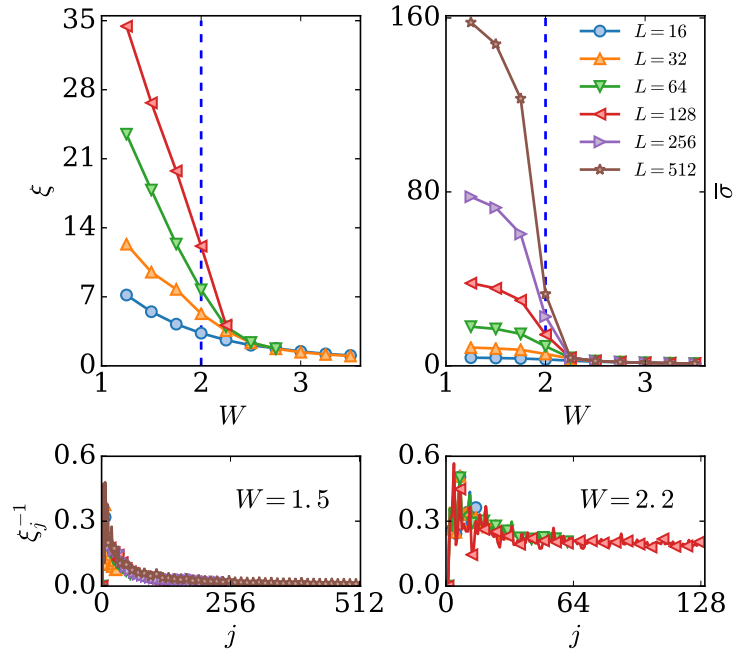


FIGURE 3.2: The upper left panel shows the localization length ξ for different system sizes as a function of disorder strength W for the AAH model. The dashed line at $W_c = 2$ represent the known transition point between extended and localized states (Chapter 1). For values below W_c , ξ increases with system size while for values above W_c it saturates. The right upper panel shows $\bar{\sigma}$ for different system sizes as a function of disorder strength W ; for values of W below W_c , $\bar{\sigma}$ grows with system size while for values above W_c it saturates. The lower panels show ξ_j^{-1} in two different phases: for $W = 1.5$ in the extended phase ξ_j^{-1} goes to zero as a function of j , while for $W = 2.2$ in the localized phase it saturates to a positive value implying a finite correlation length ξ .

particle localization length is known to diverge close to the critical point as $\xi_{\text{loc}} \sim \frac{1}{\log \frac{W}{2}}$. The right panel of Fig. 3.3 shows $\xi \sim \xi_{\text{loc}}$ close to the transition. It can be understood by the non existence of a single particle mobility edge in the AAH model, implying that the localization length of any particle diverges approaching W_c as $\frac{1}{\log \frac{W}{2}}$, and thus the correlation length ξ will be dominated by the divergence of ξ_{loc} . Furthermore we checked that ξ does not change if calculated from the center of the chain. Figure 3.4 shows the ξ_j^{-1} calculated from the mutual information of site $\frac{L}{2}$ with site j , in this case $\xi_j^{-1} = -\frac{1}{|L/2-j-1|} \log \frac{\mathcal{I}([\frac{L}{2}], [j+1])}{\mathcal{I}([\frac{L}{2}], [\frac{L}{2}+1])}$. As expected in the extended phase ($W = 1.5$) ξ_j^{-1} tends to zero as j increases. In the localized phase $W = 2.2$, ξ_j^{-1} saturates to a finite values which is consisted with the values that we have just showed. The right upper panel of Fig. 3.2 shows $\bar{\sigma}$ averaged over disorder realizations for different disorder strengths and different system sizes. For values of W greater than W_c , $\bar{\sigma}$ converges to a finite value, which implies that all the eigenstates are localized and have reached their maximum extension. However, for values below W_c , $\bar{\sigma}$ scales linearly with system size ($\bar{\sigma} \sim L$), with the consequence that $p_j \sim L^{-1}$, indicating that correlations are spread

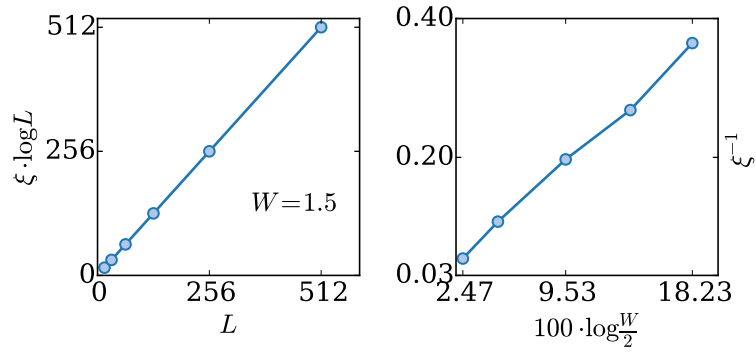


FIGURE 3.3: The left panel shows the localization length in the extended phase for the AAH-model for different system sizes, $\xi \sim \frac{L}{\log L}$. The right panel shows how ξ approaches the transition point ($W_c = 2$) as a function of W in the localized phase. In the localized phase ξ has been extrapolated choosing the system size L in which ξ saturates.

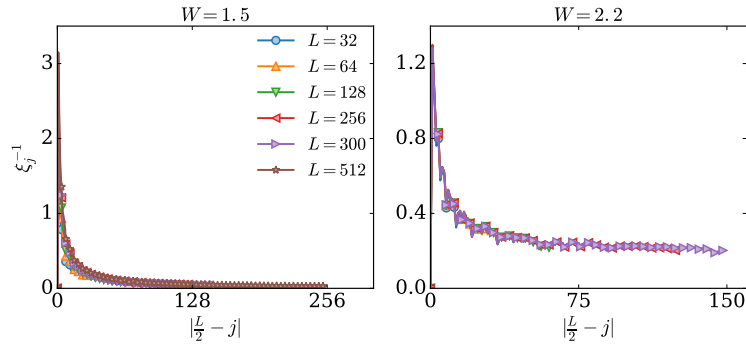


FIGURE 3.4: ξ_j^{-1} for two values of W calculated from the quantum mutual information of site $\frac{L}{2}$ with site j for the AAH-model.

uniformly at any distance. Figure 3.5 shows the full probability distribution (ρ) of σ for the AAH-model in the two different phases. For $W = 1.5$ in the extended phase, the probability shifts systematically with system size, indicating that all the states are extended. In contrast, for $W = 3.5$ in the localized phase ρ does not shift, indicating that the system is fully localized.

3.4 Quantum mutual information for many-body localization

In the previous section, we have shown that the QMI captures the salient features of the metal–insulator transition in the AAH model, we now study \mathcal{I}_j for the interacting

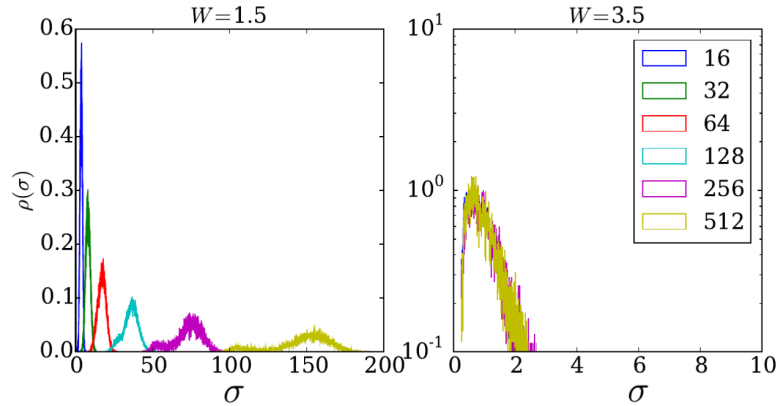


FIGURE 3.5: The probability distribution ρ of σ in the two different phase for different system sizes L for the AAH-model. The first panel ($W = 1.5$) is in the extended phase and ρ shifts to infinity with increasing L . The second panel ($W = 3.5$) is in the localized phase and ρ does not scale with L .

problem that has an MBL transition. For this model, we compute \mathcal{I}_j using exact diagonalization for eigenstates in the middle of the spectrum. The lower panels of Fig. 3.6 show ξ_j^{-1} for two different values of W . In the expected extended phase ($W = 1$), it goes to zero with increasing j and in the MBL phase ($W = 5$) it becomes constant for large j , indicating that the QMI decays exponentially with j . As for the AAH-model, for values of W where ξ_j becomes a constant with respect to j we average over those sites, and for values of W where ξ_j decays uniformly with j we take $\xi = \xi_{j=L}$. The left panel of Fig. 3.6 shows the extrapolation of the correlation length for different values of W and for different L . We note that for values $W < 4.0$, ξ does not converge for available system sizes, but it increases with L giving an indication of an extended phase and thus of a transition. As expected, ξ is a monotonically decreasing function of W , implying stronger localization for larger disorder. We also detect the extended and localized phases by studying $\bar{\sigma}$, as shown in the right upper panel of Fig. 3.6. Its behavior is similar to the case of the AAH model. For values $W \leq 4$, $\bar{\sigma}$ grows with L ($\bar{\sigma} \sim L$), implying $p_j \sim L^{-1}$, so there is equal probability of finding correlation at any distance. Figure 3.7 shows the scaling of $\bar{\sigma}$ for different system sizes in the extended phase. $\bar{\sigma}$ scales linearly with L indicating that $p_j \sim L^{-1}$, all sites are correlated with each other uniformly. Figure 3.8 shows the full probability distribution of σ in the two different phases, in the extended phase ($W = 1$) it shifts with system size, while in the MBL phase it is stable and has exponential tails. For $W > 4.0$, $\bar{\sigma}$ saturates with L indicating the presence of the two different phases.

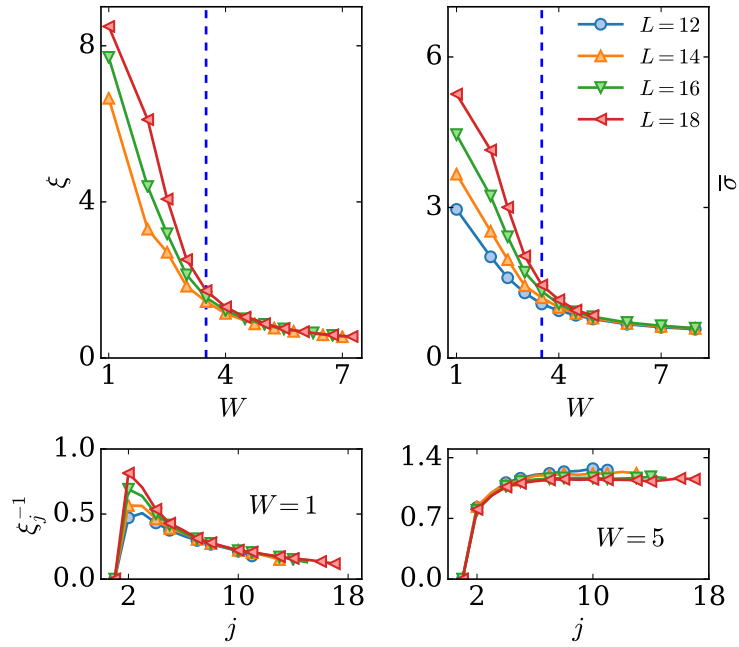


FIGURE 3.6: The top left panel shows the localization length ξ for different system sizes as a function of disorder strength W for the t-V model. The top right panel shows $\bar{\sigma}$ for different system sizes as a function of disorder strength W , for values $W < 4$ it grows with system size while for larger values it saturates. The vertical dashed line at $W_c = 3.5$ is the value for the expected transition [95, 110]. The bottom lower panels show ξ_j^{-1} in the two different phases. For $W = 1$ in the extended phase, ξ_j^{-1} goes to zero as a function of j , for $W > 4$ in the localized phase it starts to saturate to a positive value implying a finite correlation length.

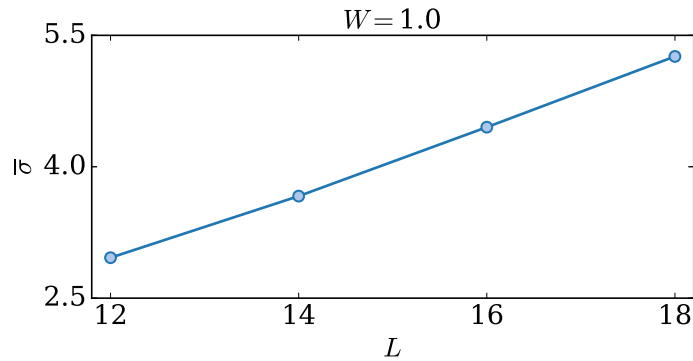


FIGURE 3.7: Scaling of $\bar{\sigma}$ for different system sizes in the extended phase ($W = 1$) for the t-V model.

3.4.1 Unbounded spread of quantum mutual information

We now show how \mathcal{I}_j can be used to distinguish between an Anderson insulator phase and an MBL phase. We perform a global quench from a random product state ($\prod_{s=1}^N c_{i_s}^\dagger |0\rangle$)

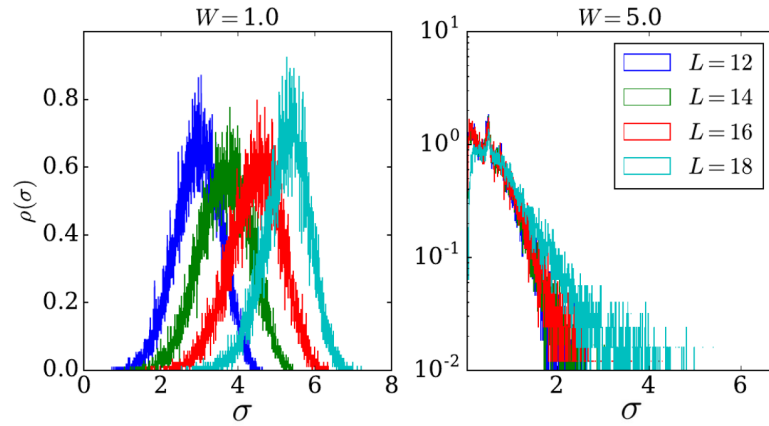


FIGURE 3.8: The probability distribution ρ of σ in the two different phases of the t-V model for different system sizes L . The first panel ($W = 1.0$) is in the extended phase and ρ shifts to infinity with increasing L . The second panel ($W = 5.0$) is in the localized phase and it does not scale with L .

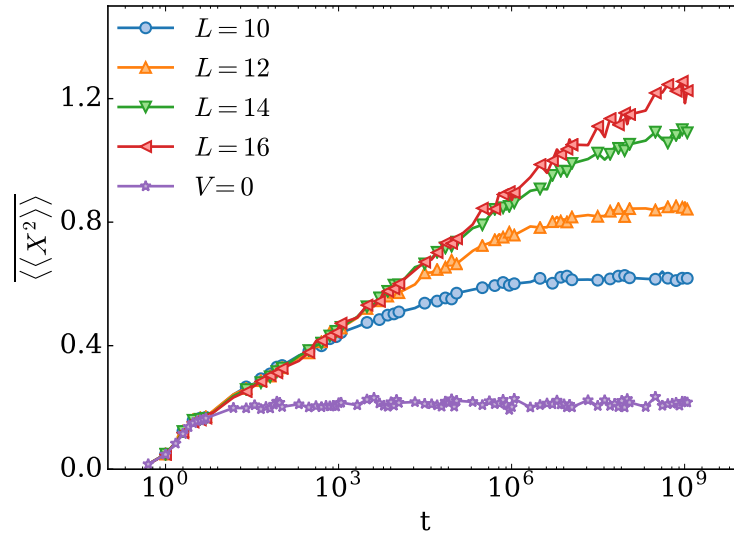


FIGURE 3.9: $\overline{\langle\langle X^2 \rangle\rangle}$ for different system sizes for $W = 6$, and for $V = 0$ (non-interacting). For $V = 0$ $\overline{\langle\langle X^2 \rangle\rangle}$ saturates at time of the order one and with system size. For $V \neq 0$, $\overline{\langle\langle X^2 \rangle\rangle} \sim \log(t)$.

and compute \mathcal{I}_j as a function of time. We study the following quantity,

$$\langle\langle X^2 \rangle\rangle := \sum_j j^2 \mathcal{I}_j(t) - \left(\sum_j j \mathcal{I}_j(t) \right)^2. \quad (3.12)$$

This quantity allows us to detect the spread of information under time evolution. At $t = 0$ the initial product state has no entanglement and $\langle\langle X^2 \rangle\rangle$ is zero. With the increase of time its value increases. Figure 3.9 shows $\langle\langle X^2 \rangle\rangle$ as a function of time t averaged over disorder and over random product states in the regime of strong localization $W = 6$. For

$V = 0$ (Anderson model) it saturates at a time of the order one ($\sim (\text{hopping strength})^{-1}$) as one would expect in an Anderson insulator phase. Using a free fermion technique (Appendix A), we compute $\langle\langle X^2 \rangle\rangle$ for large system sizes for the noninteracting Anderson model ($V = 0$), as shown in Fig. 3.10 to show that there is no propagation.

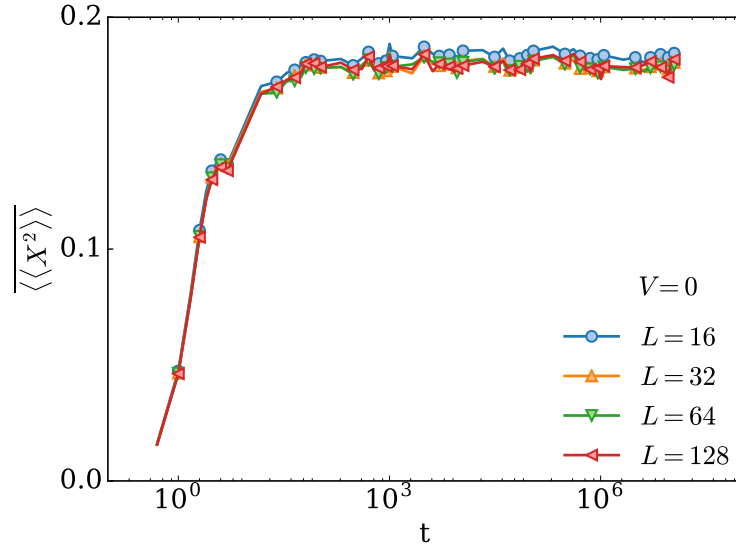


FIGURE 3.10: $\langle\langle X^2 \rangle\rangle$ as a function of time (t) for the Anderson model ($V = 0$) for $W = 6$.

In the MBL phase ($V \neq 0$) in contrast, it grows logarithmically, $\langle\langle X^2 \rangle\rangle \sim \log(t)$. The logarithmic growth can be understood from the mechanism of dephasing induced by interaction discussed in Chapter 2, in which the time needed to entangle separated portion of the system grows exponentially with their distance. We tested this by calculating the minimum time such that $\overline{\mathcal{I}}_j(t)$ starts to be bigger than some fixed threshold,

$$T_{\min}(j) := \min \{t | \overline{\mathcal{I}}_j(t) \geq 10^{-5}\} \quad (3.13)$$

and we plot it as a function of j in Fig. 3.11. In the extended phase (Fig. 3.11, left panel) T_{\min} grows algebraically with distance j , while in the MBL phase (Fig. 3.11, right panel) the time to entangle two separated portions of the system grows exponentially with their distance after an intermediate regime.

3.5 Summary

In this chapter we studied the QMI in fermionic systems having a localization-delocalization transition. First, we benchmarked our main conjectures on the scaling of the QMI as a function of the distance of two sites in the AAH-model. Second, we studied the QMI

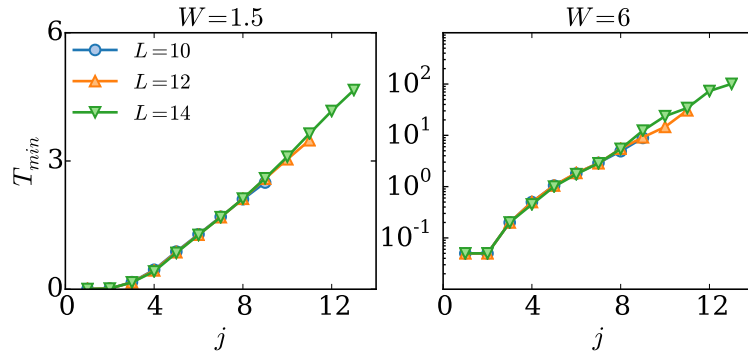


FIGURE 3.11: T_{\min} for different system size and in two different phases. For $W = 1.5$ extended phase, it grows algebraically. In the localized phase ($W = 6$) the time to entangled two separated region of the systems grows exponentially with their distance.

in a interacting model having an MBL transition. The QMI decays exponentially with the distance in the localized phase and slower than exponential in the extended phase. This allowed us to define a correlation length ξ , which is finite in the localized phase and diverging in the extended phase. This correlation length recovers the single particle localization length ξ_{loc} if the system is composed of only a single fermion. Furthermore, we defined the quantity σ , which can be seen as the variance of an appropriate probability distribution defined using the quantum mutual information. In both models, this quantity saturates to a finite value in the localized phase and diverges with system size in the extended phase. Finally we studied the non-equilibrium properties of the MBL system by performing a global quench from a random product state and following the time evolution of the mutual information. We showed that the spread of the QMI with time can be used as a dynamical indicator to distinguish an Anderson insulator phase from an MBL phase. In the Anderson phase it saturates with system size, while in the interacting case it grows logarithmically. We propose the QMI between two sites as a possible quantity which in principle can be measured in experiments, to detect the MBL transition, and moreover to distinguish between an Anderson insulator phase and an interacting localized phase.

Chapter 4

Characterizing time-irreversibility in disordered fermionic systems

In Chapter 3, we have characterized the two phases of an MBL system studying its local entanglement properties. In the following chapter, we will change perspective, and we give a complementary characterization of the two known phases, analyzing and quantifying time-irreversibility.

The existence of a “time-arrow” is one of the most intuitive phenomena in nature. Indeed, the second law of thermodynamics imposes strong constraints on the time-reversibility of non-adiabatic processes between thermodynamic states. Why time-irreversible processes exist even though the microscopic classical laws of motion are time-reversible, has been a question that has intrigued physicists for many decades [53]. The answer to this question is strongly connected to the existence of chaos in the classical phase-space [119], and thus the exponentially large sensitivity to small perturbations of the initial condition. Nevertheless, how time-irreversibility is revealed in quantum systems is a much less understood phenomena. Already, the sensitivity to initial conditions, giving rise to time-irreversibility in classical systems, cannot be used in quantum systems due to the unitary time evolution [63]. Indeed, the scalar product of any two evolving states is unchanged during the time evolution. To overcome this problem, in 1994, A. Peres [61, 111] in the context of quantum-chaos proposed to focus not on the stability of the choice of the initial conditions but rather on the stability of the quantum-dynamics when the Hamiltonian is weakly perturbed. The main idea is represented diagrammatically in Fig. 4.1 (a) [63]. An initial state $|\psi_0\rangle$ will be evolved with the Hamiltonian H_1 and then at time t , it will be evolved back with a different a Hamiltonian $H_2 = H_1 + \{\text{weak perturbation}\}$. Finally, taking the absolute module square to calculate the quantum return probability, we quantify how time-reversible the system

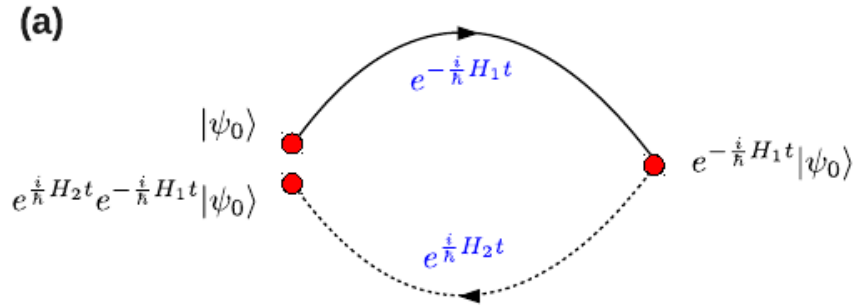


FIGURE 4.1: Diagrammatic explanation of the Loschmidt echo [63].

is. The described quantity is called the Loschmidt echo, and we will define it precisely later.

If the system is ergodic, the Loschmidt echo will have a fast decay with time (exponentially fast), since the system is governed by the laws of statistical mechanics. How time-irreversibility is affected by the breaking of ergodicity (*i.e.*, in MBL systems) is the main topic of this chapter. The chapter is organized as follows. Starting with the definitions of the models, we will then introduce the main methods to quantify time-irreversibility. First, we will apply these methods to non-interacting disordered fermionic models. Second, we will quantify time-irreversibility in an MBL system, focusing on the characterization of the ergodic and MBL phases.

4.1 Models and methods

We study the following Hamiltonian

$$\begin{aligned} \hat{\mathcal{H}} = & -\frac{t}{2} \sum_{x=-\frac{L}{2}}^{\frac{L}{2}-2} \hat{c}_x^\dagger \hat{c}_{x+1} + h.c. + \sum_{x=-\frac{L}{2}}^{\frac{L}{2}-1} h_x \left(\hat{n}_x - \frac{1}{2} \right) \\ & + V \sum_{x=-\frac{L}{2}}^{\frac{L}{2}-2} \left(\hat{n}_x - \frac{1}{2} \right) \left(\hat{n}_{x+1} - \frac{1}{2} \right), \end{aligned} \quad (4.1)$$

where $\{\hat{c}_x^\dagger\}$ ($\{\hat{c}_x\}$) are the fermionic creation (annihilation) operators, L the system size and $N = \frac{L}{2}$ the number of fermions.

In this chapter we consider three different cases, which have been described in detail in the introductory chapters (Chapters 1, 2):

1. The non-interacting Aubry-André-Harper (AAH) model, obtained from \hat{H} with $V=0$, $t=2$ and $h_x=W \cos(2\pi x\alpha+\phi)$ where $\alpha=\frac{1+\sqrt{5}}{2}$; ϕ is a random phase uniformly distributed in $[0, 2\pi]$. The AAH model has a localization-delocalization transition at $W_c=2$ (extended phase for $W \leq W_c$ and localized phase for $W > W_c$). The localization length close to the transition diverges as $\xi_{\text{loc}} \sim \log^{-1} \frac{W}{2}$ (Chapter 2).
2. The non-interacting Anderson model, given by $V=0$, $t=1$ and $\{h_x\}$ independent random variables uniformly distributed in $[-W, W]$. In the Anderson model, all the single-particle eigenstates are exponentially localized and $\xi_{\text{loc}} \sim W^{-2}$ in the weak disorder regime (Eq. 1.38).
3. The spinless disordered t-V chain which has been studied also in Chapters 2,3, obtained from the Anderson model by turning on the interaction with $V=1$. This t-V chain is believed to have a MBL transition at a critical disorder strength $W_c \approx 3.5$ (extended/ergodic for $W < W_c$ and localized for $W > W_c$) at infinite temperature.

In what follows we describe the quantities that we consider to characterize time-irreversibility perturbing the system. We focus on the study of spatially local perturbation of the Hamiltonian $\hat{\mathcal{H}}$, we define

$$\hat{\mathcal{H}}_\epsilon = \hat{\mathcal{H}} + 2\epsilon\hat{n}_0, \quad (4.2)$$

with $\epsilon > 0$. We would like to point out, that this perturbation is a zero density perturbation in the thermodynamic limit, meaning

$$\left| \frac{\|\|\hat{\mathcal{H}}\|\| - \|\|\hat{\mathcal{H}}_\epsilon\|\|}{L} \right| \sim \mathcal{O}(\epsilon/L). \quad (4.3)$$

A central object studied in this chapter is the Loschmidt echo (LE) [39, 46, 47, 72, 91, 115], which in related forms has already been studied in disordered systems [2, 22, 43, 125, 133]

$$\mathcal{L}(t) = |\langle \psi | e^{it\hat{\mathcal{H}}} e^{-it\hat{\mathcal{H}}_\epsilon} | \psi \rangle|^2. \quad (4.4)$$

The LE is a highly sensitive measure, since it involves a scalar product between two many-body wavefunctions. For example, the scalar product of two many-body wavefunctions can be zero even if they describe locally the same physical state. For this reason, to understand how states deviate in their local properties if evolved with $\hat{\mathcal{H}}$ and $\hat{\mathcal{H}}_\epsilon$, we study the difference of the local density profile (DLDP) [43, 76], defining

$$\mathcal{D}(t) = \sum_x |\delta\rho(x, t)|, \quad (4.5)$$

with

$$\delta\rho(x, t) = \langle \psi | e^{it\hat{\mathcal{H}}}\hat{n}_x e^{-it\hat{\mathcal{H}}} | \psi \rangle - \langle \psi | e^{it\hat{\mathcal{H}}_\epsilon}\hat{n}_x e^{-it\hat{\mathcal{H}}_\epsilon} | \psi \rangle, \quad (4.6)$$

Moreover, we are interested in the long-time behavior of $\mathcal{D}(t)$, which quantifies the long-time relative temporal fluctuations

$$\mathcal{D}_\infty = \lim_{T \rightarrow \infty} \frac{1}{T} \int_0^T ds \mathcal{D}(s). \quad (4.7)$$

For the initial state $|\psi\rangle$, we choose a product state in the occupation basis ($\prod_{s=1}^N c_{2s}^\dagger |0\rangle$) (charge-density state), which is easy to realize in experiments [129]. The strength of the perturbation ϵ is set equal to 0.1, so $\epsilon < \{t, W, V\}$. The average over disorder is indicated with an overline, *i.e.*, $\overline{\mathcal{D}(t)}$.

4.2 Non-interacting models

We start by quantifying time-irreversibility for the two non-interacting models.

4.2.1 Loschmidt Echo for non-interacting models

We compute the LE for these models using a free fermion technique (Wick's theorem [113]), which permits us to inspect large system sizes for long times. Figure 4.2 (a-c) shows the LE in the two phases of the AAH and in the Anderson model. In the extended phase of the AAH model ($W = 1.5$), the LE decays exponentially as $\mathcal{L}(t) \sim e^{-\Gamma t}$, revealing the strong effect of local small perturbations. In the localized phase for both models (AAH and Anderson models), the LE decays algebraically in time as $\mathcal{L}(t) \sim t^{-\beta}$. Note that in both phases, the long time saturation value is exponentially small in system size, *i.e.*, $\mathcal{L}(t \rightarrow \infty) \sim e^{-\eta L}$ (Anderson orthogonality theorem [10]). Still the two phases can be distinguished through the decay of the LE as a function of time. For the localized phase, Fig. 4.2 (b-c) also shows the relation between the exponent β and the microscopic parameter of the Hamiltonian (W), with a good collapse of the curves. For the Anderson model, we observe $\beta \propto W^{-2}$, indicating that β is proportional to ξ_{loc} at least in the weak disorder limit. For the AAH model, we find the scaling $\beta \propto (W \log \frac{W}{2})^{-1}$. Thus, β is again proportional to the localization length ξ_{loc} on approaching the localization-delocalization transition to leading order. The rescaled time in the LE deserves particular attention: the time scale for the onset of the algebraic decay is proportional to the localization length, which on approaching the localization-delocalization transition shifts to infinity in the thermodynamic limit.

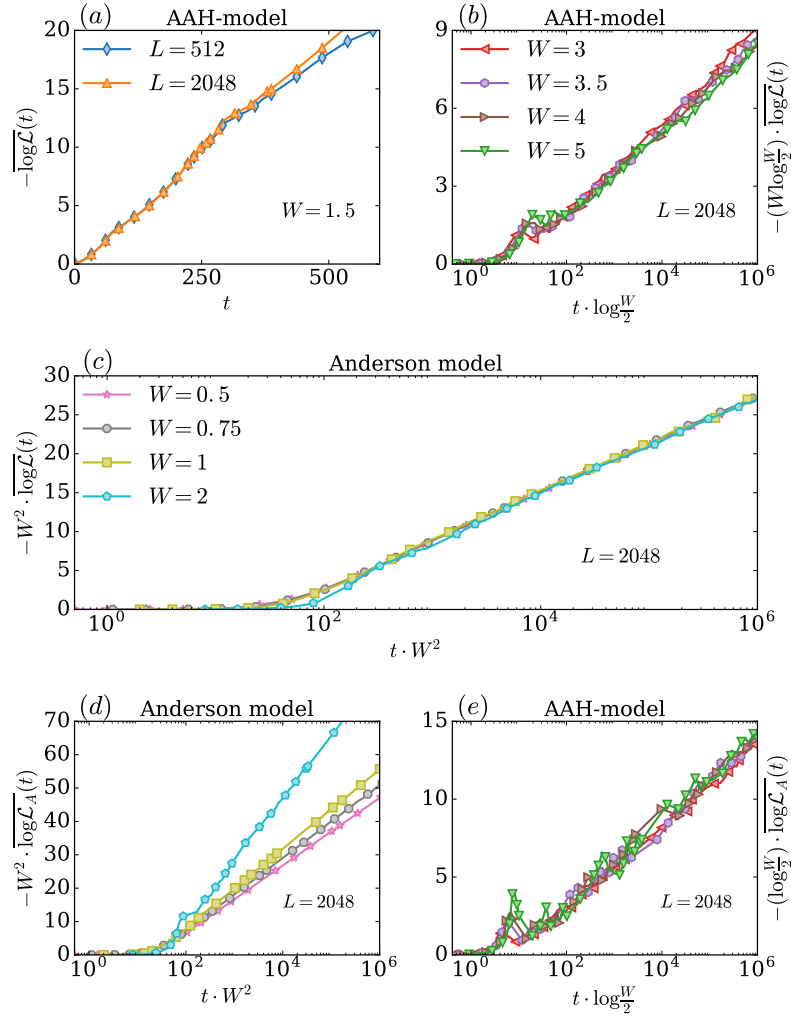


FIGURE 4.2: (a),(b): Behavior of $-\overline{\log \mathcal{L}(t)}$ for the AAH model in the extended phase ($W = 1.5$) ($\mathcal{L}(t) \sim e^{-\Gamma t}$) and in the localized phase for several values of W ($\mathcal{L}(t) \sim t^{-\beta}$). In the localized phase t and $\mathcal{L}(t)$ have been properly rescaled to underline the time scale on which the decays starts and the behavior of the exponent of the algebraic decay β . (c): $-\overline{\log \mathcal{L}(t)}$ for the Anderson model for several values of W ; here also a rescaling has been done on t and $\mathcal{L}(t)$. (d),(e): Panels show the approximate formula $\mathcal{L}_A(t)$ for the two non-interacting models and for the same values of W . The averages have been performed over 5000 random configurations of disorder.

We now present an analytical argument supporting the algebraic decay of the LE in the localized phase. In the Lehmann representation [113] the LE reads

$$\mathcal{L}(t) = \left| \sum_{n,m} \langle \psi | n \rangle \langle n | m_\epsilon \rangle \langle m_\epsilon | \psi \rangle e^{-it(E_n - E_m^{(\epsilon)})} \right|^2, \quad (4.8)$$

where E_n ($|n\rangle$) and $E_m^{(\epsilon)}$ ($|m_\epsilon\rangle$) are the eigenvalues (eigenvectors) of $\hat{\mathcal{H}}$ and $\hat{\mathcal{H}}_\epsilon$, respectively. The simple picture is that in the localized phase, the local perturbation causes an exponentially weak dephasing of the energies of the unperturbed Hamiltonian with

respect to the perturbed one, inducing the decay of the LE. The following approximations, which are equivalent to a first order expansion in ϵ [29], permit us to estimate the behavior of the LE and relate the power-law exponent β to the localization length. We confirmed this relation close to the localization-delocalization transition with exact numerics.

The main assumptions which we use are the following:

1. The perturbation modifies only the eigenenergies of $\hat{\mathcal{H}}_\epsilon$ but not its eigenfunctions, which are the same as those of the unperturbed Hamiltonian $\hat{\mathcal{H}}$. It is easy to see that the contribution to the change of the eigenfunctions is second order in the strength of the perturbation ϵ .
2. The behavior of the LE is independent of the initial choice of the product state.

Using the spectral representation for the time evolution and with the use of the first approximation $\langle n|m_\epsilon \rangle = \delta_{n,m}$,

$$\mathcal{L}(t) \approx \left| \sum_n |\langle n|\psi \rangle|^2 e^{-it(E_n - E_n^{(\epsilon)})} \right|^2, \quad (4.9)$$

and using the second approximation,

$$\mathcal{L}(t) \approx \left| \frac{1}{2^L} \sum_n e^{-it(E_n - E_n^{(\epsilon)})} \right|^2, \quad (4.10)$$

Using first-order perturbation theory in ϵ to estimate the energy difference

$$E_n - E_n^{(\epsilon)} = 2\epsilon \langle n|\hat{n}_0|n \rangle, \quad (4.11)$$

we get

$$\mathcal{L}(t) \approx \left| \frac{\sum_n e^{-i2t\epsilon \langle n|\hat{n}_0|n \rangle}}{2^L} \right|^2. \quad (4.12)$$

Moreover $\langle n|\hat{n}_0|n \rangle = \sum_{j=1}^L a_j^{(n)} |\phi_j(0)|^2$, where $\{\phi_j(0)\}$ are the single particle wavefunctions evaluated in the center of the the chain and $a_j^{(n)}$ takes only two values $\{1, 0\}$ depending on whether the single-particle eigenstate labeled with j is occupied or not in the state $|n \rangle$. The last expression is essentially a perturbation expansion in ϵ , $\mathcal{L}(t) = \mathcal{L}_A(t) + \mathcal{O}(\epsilon^2)$. Finally, defining $\mathcal{L}_A(t)$ by

$$\mathcal{L}_A(t) = \left| \frac{\sum_n e^{-i2t\epsilon \langle n|\hat{n}_0|n \rangle}}{2^L} \right|^2 = \prod_{j=1}^L \cos^2(\epsilon |\phi_j(0)|^2 t), \quad (4.13)$$

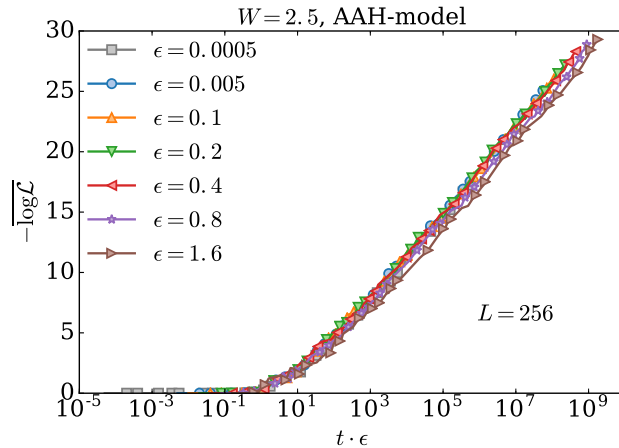


FIGURE 4.3: $-\overline{\log \mathcal{L}(t)}$ for different values of ϵ for the AAH model in the localized phase ($W = 2.5$). The time has been rescaled by ϵ as is suggested by the equation in main text $|\phi_j(0)|^2 t \epsilon \approx 1$.

where the subscript A underlines that this is an approximate formula. Since all single particle eigenstates are exponentially localized, after an appropriate relabeling of the index j , we assume that $|\phi_j(0)|^2 \sim \frac{e^{-j/\xi}}{\xi}$. Thus, the only factors that contribute significantly are the ones where $\epsilon |\phi_j(0)|^2 t \approx 1$

$$\mathcal{L}_A(t) \approx \prod_{j=1}^{\xi \log \frac{\epsilon t}{\xi}} \cos^2(\epsilon |\phi_j(0)|^2 t) \sim \left(\frac{\epsilon t}{\xi}\right)^{-c\xi}, \quad (4.14)$$

with $c > 0$.

We can confirm our analytical predictions by numerically studying Eq. 4.13. The last row of Fig. 4.2 (d,e) shows the algebraic decay with time of the LE from Eq. 4.13 as $\mathcal{L}_A(t) \sim t^{-\beta_A}$ for the two models and several values of W . Surprisingly, despite being a perturbative expansion in ϵ , $\mathcal{L}_A(t)$ reproduces the algebraic decay of the LE also for long times. The exponents β_A and β have the same dependence on the microscopic parameter W in the vicinity of the critical point, namely $\beta, \beta_A \sim W^{-2}$ as $W \rightarrow 0$ for the Anderson model and $\beta, \beta_A \sim \log^{-1} \frac{W}{2}$ as $W \rightarrow 2$ for the AAH model. Indeed, as shown in Fig. 4.2 (d-e), β_A is proportional to the localization length ($\beta_A \propto \xi_{\text{loc}}$). For the Anderson model, the deviation with increasing disorder strength W is just a sign that the perturbative expansion for ξ_{loc} is breaking down (Chapter 1).

Moreover, the approximate formula Eq. 4.14 describes well the rescaling of time, given by $t \rightarrow \frac{\epsilon t}{\xi}$. Figure 4.3 shows $\mathcal{L}(t)$ for several values of the perturbation strength ϵ for the AAH model in the localized phase ($W = 2.5$). $\mathcal{L}(t)$ decays algebraically, the exponent of the decay β does not depend on ϵ , and as suggested by the expression $|\phi_j(0)|^2 t \epsilon$, the time has been properly rescaled to make the curves collapse together. We can check

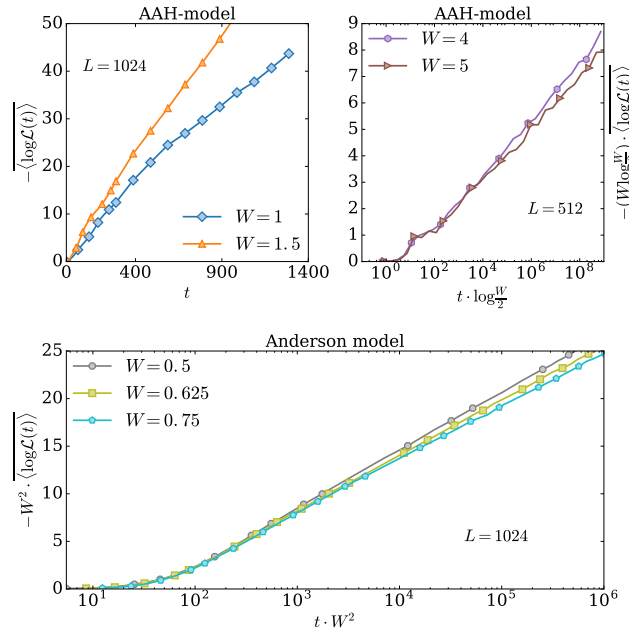


FIGURE 4.4: The panels show $-\log \mathcal{L}(t)$ averaged over random product states and disorder configurations for the AAH model and for the Anderson mode.

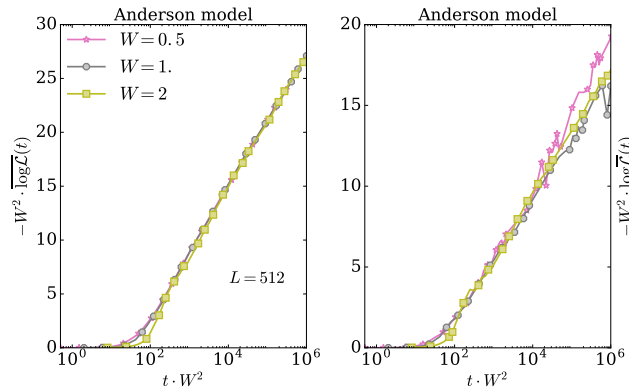


FIGURE 4.5: The panels shows $-\overline{\log \mathcal{L}(t)}$ (left) and $-\log \overline{\mathcal{L}(t)}$ (right) for the non interacting Anderson model for different values of W .

that our results are qualitatively independent of the choice of the initial product state, averaging the LE over random product states of the form $\prod_{s=1}^N c_{i_s}^\dagger |0\rangle$ (for any random configuration we calculate $\mathcal{L}(t)$ for 25 random product states), as shown in Fig. 4.4 (the average over random product states is indicated with $\langle \cdot \rangle$). Figure 4.4 shows that the behavior of $\mathcal{L}(t)$ is similar to the charge-density state, and the same scaling with the microscopic parameter W still works relatively well, and the deviations become relevant for long times ($t > 10^4$). It is also interesting to compare different way of performing the average. Figure 4.5 shows for the non-interacting Anderson model and for different disorder strengths $-\overline{\log \mathcal{L}(t)}$ and $-\log \overline{\mathcal{L}(t)}$. As expected from the inequality between the arithmetic mean and the geometric mean, $-\overline{\log \mathcal{L}(t)} \geq -\log \overline{\mathcal{L}(t)}$. Moreover $-\overline{\log \mathcal{L}(t)}$,

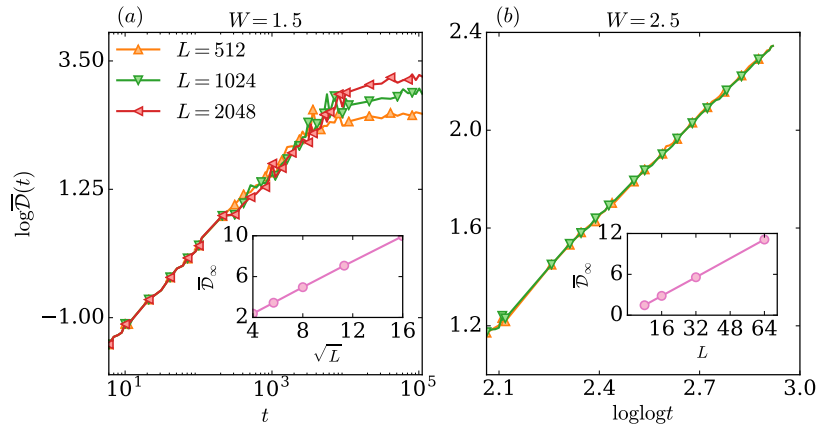


FIGURE 4.6: $\overline{\mathcal{D}}(t)$ for the AAH model in the two phases for different L . (a): $W = 1.5$, $\overline{\mathcal{D}}(t) \sim t^\alpha$ while its inset shows $\overline{\mathcal{D}}_\infty$ as a function of L ($\overline{\mathcal{D}}_\infty \sim \sqrt{L}$). (b): $W = 2.5$, $\overline{\mathcal{D}}(t) \sim \log^\alpha t$, its inset shows $\overline{\mathcal{D}}_\infty \sim L$. The averages have been performed over 2500 random configurations of disorder.

being the logarithm of the typical value of $\mathcal{L}(t)$, is less noisy than the logarithm of the arithmetic mean $-\log \overline{\mathcal{L}}(t)$. Nevertheless, to some extent the scaling of the algebraic decay β and of the time are the same for both ways of performing the disorder average.

4.2.2 Difference of the local density profile in non-interacting models

In this section, we probe the effect of local perturbation on the dynamics of local observables by studying $\overline{\mathcal{D}}(t)$ (DLDP). Figure 4.6 shows $\overline{\mathcal{D}}(t)$ for two different values of W for the AAH model. In the extended phase with $W = 1.5$, $\overline{\mathcal{D}}(t)$ shows an algebraic growth with time, $\overline{\mathcal{D}}(t) \sim t^\alpha$, $\alpha \approx 0.6$ for $W = 1.5$. The saturation point in time of $\overline{\mathcal{D}}(t)$ is consistent with the scale \sqrt{L} (inset, Fig. 4.6 (a)) with system size, indicating that in the long time limit the average over index sites of the DLDP ($\frac{\overline{\mathcal{D}}_\infty}{L}$) relaxes algebraically with system size. In the localized phase, $\overline{\mathcal{D}}(t)$ has a log-like slow growth, $\overline{\mathcal{D}}(t) \sim \log^\alpha t$ with $\alpha \approx 1.3$ for $W = 2.5$, so the effect of local perturbations on the dynamics is exponentially slow in time. Moreover, $\overline{\mathcal{D}}_\infty \sim L$ (inset, Fig. 4.6 (b)), so that the relaxation of $\frac{\overline{\mathcal{D}}_\infty}{L}$ never takes place. An analytical argument based on a random matrix approximation is possible to give, which will give a lower bound of \mathcal{D}_∞ as a function of L . Neglecting the time fluctuation of $\mathcal{D}(t)$ we get a lower bound of \mathcal{D}_∞ (diagonal ensemble)

$$\frac{1}{T} \int_0^T \mathcal{D}(s) ds \geq \frac{1}{T} \sum_x \left| \int_0^T \delta\rho(x, s) ds \right|. \quad (4.15)$$

Thus,

$$\lim_{T \rightarrow \infty} \frac{1}{T} \left| \int_0^T \delta\rho(x, s) ds \right| =$$

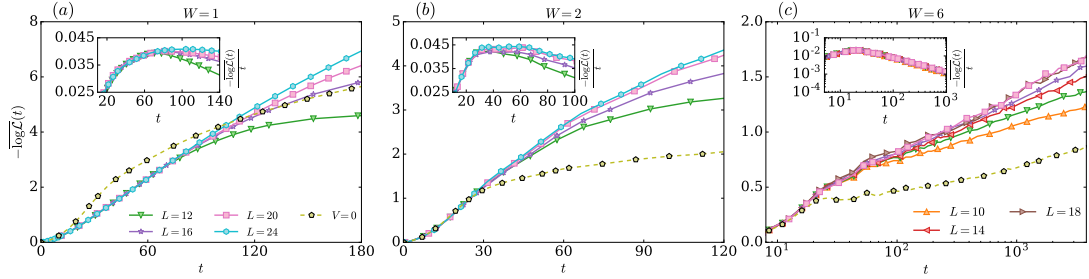


FIGURE 4.7: The panels show $-\overline{\log \mathcal{L}(t)}$ for different values of disorder strength W for the t-V model. (a): The system is in the ergodic phase $W = 1$ and the LE decays at least exponentially fast with time. (b): An intermediate disorder strength $W = 2$, $-\overline{\log \mathcal{L}(t)}$ (inset) forms a plateau with time which is enlarging with system size, showing that the range of times for which LE decays exponentially fast is expanding. (c): The system is in the localized phase $W = 6$ and the LE decays algebraically with time. We also show the LE for the non-interacting case ($V = 0$) for the largest system size in each panel ($L = 24$ for $W = 1, 2$ and $L = 20$ for $W = 6$). The averages have been performed over 10^4 random configuration for system size $L \leq 14$ and 5000 for $L = 16$ and 2500 for larger system sizes.

$$\begin{aligned}
&= \left| \sum_{\alpha} \sum_{s} |\phi_{\alpha}(x)|^2 |\phi_{\alpha}(s)|^2 - \sum_{\alpha} \sum_{s} |\phi_{\alpha}^{\epsilon}(x)|^2 |\phi_{\alpha}^{\epsilon}(s)|^2 \right| \\
&\sim \left| \sum_{\alpha} \sum_{s} \frac{|\tilde{\phi}_{\alpha}(x)|^2 |\tilde{\phi}_{\alpha}(s)|^2}{L^2} - \sum_{\alpha} \sum_{s} \frac{|\tilde{\phi}_{\alpha}^{\epsilon}(x)|^2 |\tilde{\phi}_{\alpha}^{\epsilon}(s)|^2}{L^2} \right|.
\end{aligned} \tag{4.16}$$

The sum over the index s runs over the index sites that are occupied at the initial time ($t=0$). $\{\phi_{\alpha}(x)\}_1^L$ and $\{\phi_{\alpha}^{\epsilon}(x)\}_1^L$ are the single-particle wavefunctions of $\hat{\mathcal{H}}$ and $\hat{\mathcal{H}}_{\epsilon}$ respectively. In first approximation in the extended phase, the single-particle wavefunctions can be approximated with $\{\frac{\tilde{\phi}_{\alpha}(x)}{\sqrt{L}}\}_1^L$ and $\{\frac{\tilde{\phi}_{\alpha}^{\epsilon}(x)}{\sqrt{L}}\}_1^L$, where $\{\tilde{\phi}_{\alpha}(x)\}_1^L$ and $\{\tilde{\phi}_{\alpha}^{\epsilon}(x)\}_1^L$ are independent random variables with a fixed mean and variance which do not scale with L , since their dependence on L has been already taken care with the normalization factor $\frac{1}{\sqrt{L}}$. Using the central limit theorem, we can estimate the scaling with L of the sum over the index s and α , e.g., $\sum_s' \frac{|\tilde{\phi}_{\alpha}(s)|^2}{L} \sim \text{constant}_1 + \mathcal{O}(\frac{1}{\sqrt{L}})$ and $\sum_{\alpha} \frac{|\tilde{\phi}_{\alpha}(x)|^2}{L} \sim \text{constant}_2 + \mathcal{O}(\frac{1}{\sqrt{L}})$. Since we have assumed that the perturbation does not change the statistical properties of the single-particle wavefunctions, we have that the difference of the local density profile $|\rho(x, t \rightarrow \infty)| \geq \mathcal{O}(\frac{1}{\sqrt{L}})$. This gives the result $\overline{\mathcal{D}}_{\infty} \geq \mathcal{O}(\sqrt{L})$. The argument can be repeated for the non-interacting localized phase. Indeed in the localized phase, taking the single-particle wavefunctions as box functions with a finite width randomly displaced, (e.g., $\phi_{\alpha}(x) \sim \frac{\chi_{[\alpha-\xi, \alpha+\xi]}}{\sqrt{2\xi}}$), it is easy to show that the lower bound $\overline{\mathcal{D}}_{\infty} \geq \mathcal{O}(L)$. Since $\overline{\mathcal{D}}_{\infty}$ can not be larger than L , we have $\overline{\mathcal{D}}_{\infty} \sim \mathcal{O}(L)$.

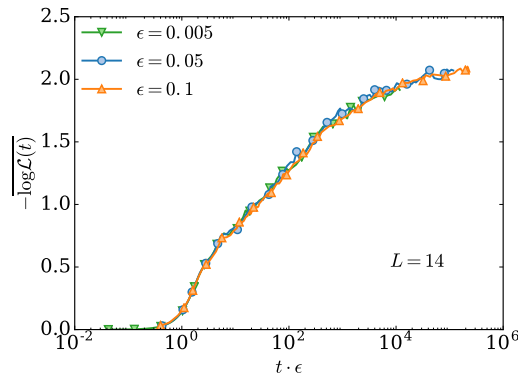


FIGURE 4.8: The panels show $-\log \mathcal{L}(t)$ averaged over disorder configurations for the interacting spinless t-V chain in the localized phase ($W = 6$) for a fixed system size $L = 14$ for several values of the perturbation strength ϵ .

4.3 Spinless t-V chain

4.3.1 Loschmidt echo for the t-V chain

In the previous section we have shown that the LE captures the salient features of the localization-delocalization transition in the AAH model, we now study $\mathcal{L}(t)$ for the interacting spinless t-V chain that has an MBL transition. We perform the time evolution using full diagonalization for small systems size $L \leq 16$, and using the Chebyshev integration technique (Appendix A) for larger L ($18 \leq L \leq 24$). Figure 4.7 (a-c) shows the behavior of the LE for the interacting model for different values of disorder strength W . The enhanced decay compared with the non-interacting problem is also shown in Fig. 4.7. Nevertheless, in the localized phase, the LE still decays algebraically as in the localized phase of the non-interacting models. For $W = 6$ the function $-\frac{\overline{\log \mathcal{L}(t)}}{t}$ (inset Fig. 4.7 (c)) does not present any systematic dependence on system size, indicating that the algebraic decay could be the asymptotic thermodynamic behavior. Moreover, the time can be rescaled with the strength of the perturbation ϵ like for the non-interacting case ($t \rightarrow t\epsilon$), as is shown in Fig. 4.8. In the ergodic phase with $W = 1$, the LE decays at least exponentially with time, and the function $-\frac{\overline{\log \mathcal{L}(t)}}{t}$ does not decay for times in which the decay of the LE is not affected by finite-size effects (inset Fig. 4.7 (a)). Figure 4.7 (b) also shows an intermediate disorder value $W = 2$, at which the function $-\frac{\overline{\log \mathcal{L}(t)}}{t}$ develops a plateau with respect to t , like in the extended phase, after which a slower decay sets in. This plateau is enlarging with increasing system size, which may indicate that in the thermodynamic limit ergodicity will be completely restored and the LE will decay exponentially with t . Figure 4.9 shows the behavior of the LE averaged over random product states ($\prod_{s=1}^N c_{i_s}^\dagger |0\rangle$) and disorder configurations for the interacting t-V chain for two different values of W , in the ergodic ($W = 1$) phase $\mathcal{L}(t) \sim e^{-\Gamma t}$ and in

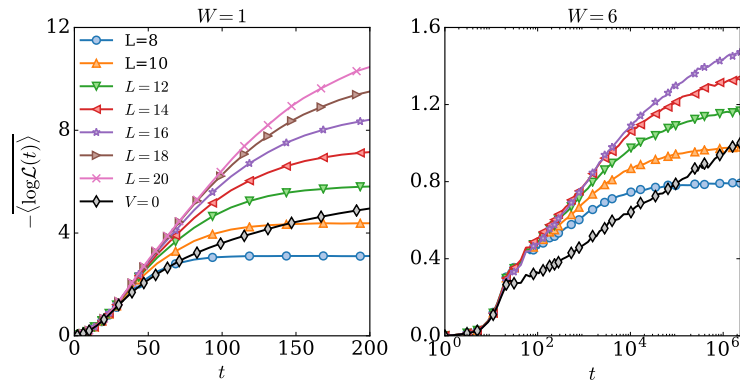


FIGURE 4.9: The panels show $-\log \mathcal{L}(t)$ averaged over random product states and disorder configurations for the interacting spinless t-V chain for two different W ($W = 1$ in the ergodic phase, $W = 6$ in the localized phase). For $V = 0$, $L = 20$.

the localized ($W = 6$) phase $\mathcal{L}(t) \sim t^{-\beta}$. We would like to stress that what we have done is only valid at infinite temperature (middle of the energy spectrum). Indeed the result will be completely different if we will repeat what we have done quenching for example the ground state (zero temperature $T = 0$) of $\hat{\mathcal{H}}$. Figure 4.10 shows $\bar{\mathcal{L}}(t)$ ($e^{\overline{\log \mathcal{L}(t)}}$) in the localized phase $W = 6$ where the initial state has been taken the ground state of $\hat{\mathcal{H}}$, in this case the LE does not decay in time. It is interesting to note that the same behavior of LE occurs also in the ergodic phase, since the ground state of $\hat{\mathcal{H}}$ is localized for any amount of disorder [62], as shown in Fig 4.11.

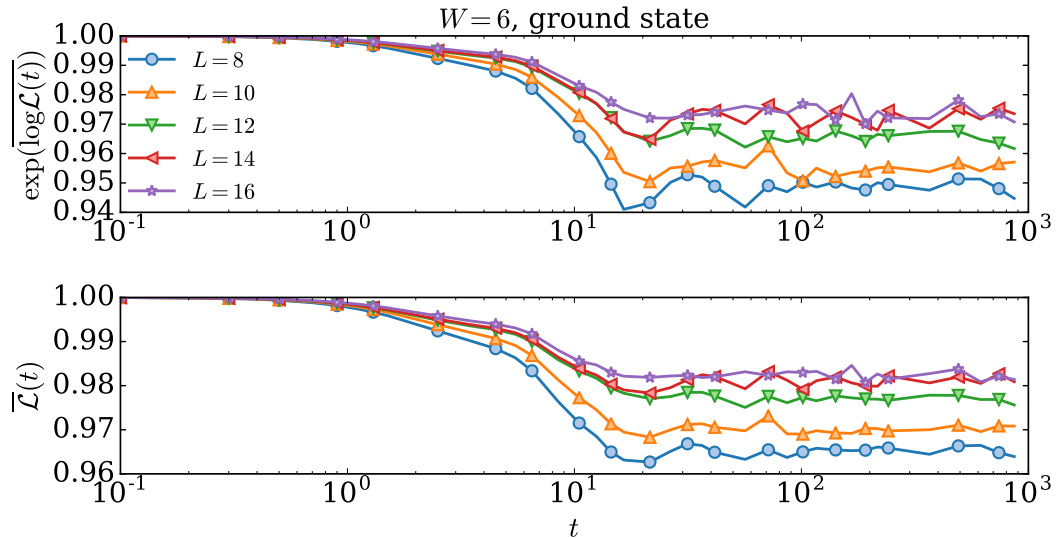


FIGURE 4.10: The panels show $\bar{\mathcal{L}}(t)$ ($e^{\overline{\log \mathcal{L}(t)}}$) in the localized phase ($W = 6$) for the t-V chain where the initial state has been taken the ground state of $\hat{\mathcal{H}}$.

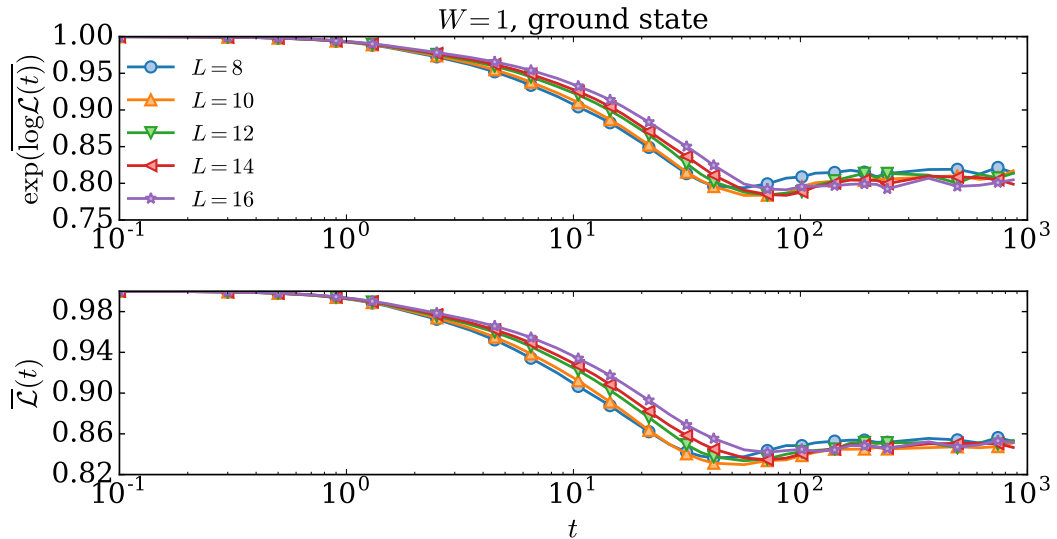


FIGURE 4.11: The panels show $\overline{\mathcal{L}}(t)$ ($e^{\overline{\log \mathcal{L}(t)}}$) in the ergodic phase ($W = 1$) for the t-V chain where the initial state has been taken the ground state of $\hat{\mathcal{H}}$.

4.3.2 Difference of the local density profile in the Spinless t-V chain

We now study the effects of perturbations in the dynamics of local observables by studying the DLDP for the t-V chain. Figure 4.12 shows $\overline{\mathcal{D}}(t)$ in the interacting model for two values of W . We give evidence that the behavior of $\overline{\mathcal{D}}(t)$ in the ergodic phase for long time is drastically different from the non-interacting case: $\overline{\mathcal{D}}(t)$ is not a monotonic function of t (inset, Fig. 4.12 (a)). For short times, $\overline{\mathcal{D}}(t)$ grows to a maximum value from which it starts to decay to a finite L -dependent value. The non-monotonic behavior is intimately connected with the thermalization of the system. Indeed, the long time expectation values of local observables for thermal systems at infinite temperature should be unchanged if the system is locally perturbed. The average time in which the decay of $\overline{\mathcal{D}}(t)$ starts, defines a time scale τ ; this is roughly the time at which $\overline{\mathcal{D}}(t)$ changes concavity and starts to decrease. For times much larger than τ , the expectation value of a local observable is given by the expectation value over a many-body random state (ETH at infinite temperature), so that $|\delta\rho(x, t \gg \tau)| \sim \left(\frac{L}{N}\right)^{-\gamma} \sim e^{-(\gamma \log 2)L}$. In the localized phase, the finite-size effects become more important, and for smaller system sizes it could seem that $\overline{\mathcal{D}}(t)$ has an unbounded slow growth similar to the localized phases for the non-interacting models. However, a careful analysis shows that the saturation value is merely an exponential decay such as in the extended phase, consisted with $\overline{\mathcal{D}}_\infty \sim L \left(\frac{L}{N}\right)^{-\gamma}$ (inset, Fig. 4.12 (b)). Compared with the ergodic phase, in the localized phase the exponent γ is small, so that for the considered system sizes, the behavior of $\overline{\mathcal{D}}_\infty$ is dominated by the linear prefactor L . In the thermodynamic limit we expect that the final shape will be similar to the one in the ergodic phase, so that $\overline{\mathcal{D}}(t)$

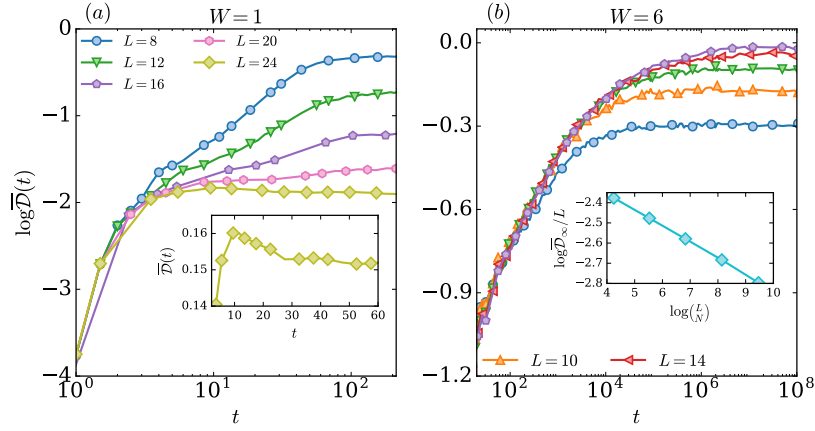


FIGURE 4.12: $\overline{\mathcal{D}}(t)$ for the spinless disordered t-V chain for different L and two values of W . (a) $W = 1$, the inset shows $\overline{\mathcal{D}}(t)$ for $L = 24$ to underline its non-monotonic dependence on t . (b) $W = 6$, the inset shows $\frac{\overline{\mathcal{D}}_\infty}{L}$ as function of L , it decays exponentially fast with L , $\frac{\overline{\mathcal{D}}_\infty}{L} \sim \left(\frac{L}{N}\right)^{-\gamma}$. The averages have been performed over 10^4 random configuration for system size $L \leq 14$ and 5000 for $L = 16$ and 2500 for larger system sizes.

will eventually also decay with time at long times. Note that the time scale at which this decay will take place is extremely large; the limitation on system size does not allow us to estimate an upper bound of the time scale τ , which leaves open the possibility that τ might shift to infinity with increasing L . The behavior of $\overline{\mathcal{D}}_\infty$ in the localized phase is reminiscent of the long time “volume-law” saturation of the entanglement entropy $\mathcal{S}(t)$ after a quantum quench. The distinction between the ergodic and the MBL phase lies only in the numerical value of the prefactor in front of the saturation value of $\mathcal{S}(t)$ (Chapter 2), while the scaling with L is the same in both phases (volume law).

We repeated our analysis for other values of W . Figure 4.13 shows the behavior of $\overline{\mathcal{D}}(t)$ for different system sizes in the two phases of the t-V chain. For $W = 2$, the system is in the ergodic phase, and $\overline{\mathcal{D}}(t)$ exhibits the same non-monotonic behaviour as a function of t as for the case $W = 1$. For $\overline{\mathcal{D}}(t)$ in the localized phase ($W = 5$), finite-size effects are important. Indeed, it is not possible to see the non-monotonic phase even in the ergodic phase for system sizes smaller than $L \leq 16$. However, Fig. 4.13 gives evidence that in both phases, $\overline{\mathcal{D}}_\infty \sim L \left(\frac{L}{N}\right)^{-\gamma}$. In the ergodic phase for $W = 2$, $\gamma \approx 0.26$. In the localized phase for $W = 5$, the exponent $\gamma \approx 0.1$. The exponent is small so that for system size $L \leq 16$ the behavior of the function $L \left(\frac{L}{N}\right)^{-\gamma}$ is dominated by the linear part L . Nevertheless, if this scaling persists in the thermodynamic limit, $\overline{\mathcal{D}}(t)$ in the long-time limit will go to zero.

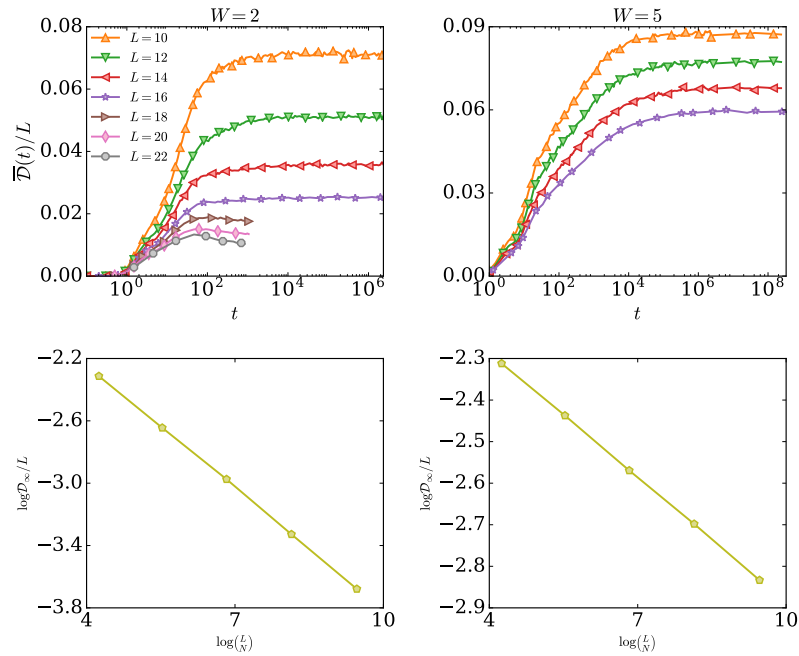


FIGURE 4.13: The top panel shows $\frac{\overline{D}(t)}{L}$ for $W = 2$ (ergodic) and $W = 5$ (localized) for the interacting t-V chain for several system sizes L . The bottom panels show that in both phases $\frac{\overline{D}_\infty}{L} \sim \left(\frac{L}{N}\right)^{-\gamma}$.

4.3.3 An effective model for many-body localized systems

In this section we introduce a general method which reproduces quantitatively and qualitatively the exact results of a many-body localized system in the limit of strong disorder. This method allows us to study system sizes and time scale that so far have not been observed in numerical simulations.

First, studying the growth of the entanglement entropy following a global quantum quench (Chapter 2), we show that this method is reliable in the limit of weak interactions ($W/V \gg 1$). Second, we confirm our speculation from the previous section: indeed, finite-scaling analysis suggests that in the MBL phase $\overline{D}_\infty \sim e^{-\alpha L}$. Nevertheless, due to limitation of available system sizes, we were not able to see the time scale in which $\overline{D}(t)$ starts to decay. Thus, in this section using our method we are able to give evidences of the existence of a time scale for which the decay of $\overline{D}(t)$ occurs.

Using first order perturbation theory on the interaction strength V (first order in the eigenenergies of $\hat{\mathcal{H}}$), it is possible to obtain the following effective Hamiltonian

$$\hat{\mathcal{H}}^{\text{eff}} = \sum_l \epsilon_l \hat{\eta}_l^\dagger \hat{\eta}_l + V \sum_{l,m} \mathcal{B}_{l,m} \hat{\eta}_l^\dagger \hat{\eta}_l \hat{\eta}_m^\dagger \hat{\eta}_m, \quad (4.17)$$

where $\hat{\eta}_l^\dagger = \sum_i \phi_l(i) \hat{c}_i^\dagger$ with $\{\phi_l\}$ and $\{\epsilon_l\}$ respectively the single-particle wavefunctions and the single-particle eigenenergies. The dephasing coefficients $\mathcal{B}_{l,m}$ are given by:

$$\mathcal{B}_{l,m} = \sum_{\langle i,j \rangle} [\phi_l(i) \phi_m(i) \phi_l(j) \phi_m(j) - |\phi_l(i)|^2 |\phi_m(j)|^2], \quad (4.18)$$

since the single-particle wavefunctions are localized in space, after a suitable relabeling of the indexes (l, m) , we have

$$\mathcal{B}_{l,m} \sim e^{-|l-m|/\xi_{\text{loc}}}. \quad (4.19)$$

The model $\hat{\mathcal{H}}^{\text{eff}}$ is in this representation a classical Ising model, and it is integrable (Chapter 2). Its eigenstates are the Slater-determinant states of the non-interacting model ($V = 0$).

The Heisenberg equation for the creation operators $\{\hat{\eta}_l^\dagger\}$ reads

$$\begin{aligned} \frac{d\hat{\eta}_l^\dagger}{dt} &= i[\hat{\mathcal{H}}^{\text{eff}}, \hat{\eta}_l^\dagger] \\ &= i\epsilon_l + iV \sum_m (\mathcal{B}_{m,l} + \mathcal{B}_{l,m}) \hat{\eta}_m^\dagger \hat{\eta}_m, \end{aligned} \quad (4.20)$$

defining $\tilde{\mathcal{B}}_{l,m} = \mathcal{B}_{m,l} + \mathcal{B}_{l,m}$ the solution of Eq. 4.20 is given by

$$\hat{\eta}_l^\dagger(t) = e^{+it\epsilon_l + itV \sum_m \tilde{\mathcal{B}}_{l,m} \hat{\eta}_m^\dagger \hat{\eta}_m} \hat{\eta}_l^\dagger. \quad (4.21)$$

Knowing the time evolution of the operators $\{\hat{\eta}_l^\dagger\}$, we can calculate easily the time expectation value of local observables (*e.g.*, \hat{n}_x).

As described in Chapter 2, the role of the term $\sum_{l,m} \mathcal{B}_{l,m} \hat{\eta}_l^\dagger \hat{\eta}_l \hat{\eta}_m^\dagger \hat{\eta}_m$ is to exponentially weakly correlate the eigenenergies of the non-interacting case, and reproducing the dephasing mechanism in an interacting localized phase. Figure 4.14 shows the average entanglement entropy $\bar{S}(t)$ calculated evolving a charge-density state ($\prod_{s=1}^N c_{2s}^\dagger |0\rangle$) first with the Hamiltonian $\hat{\mathcal{H}}$ (solid-lines) and then with the effective model $\hat{\mathcal{H}}^{\text{eff}}$. The effective model reproduces qualitatively the unbounded growth of the entanglement entropy observed in interacting localized systems. Moreover, the relative error between $S(t)$ calculated with $\hat{\mathcal{H}}$ and with $\hat{\mathcal{H}}^{\text{eff}}$ is a bounded function of time, implying that our method reproduces the exact results also qualitatively. It is interesting to note that despite being a perturbative expansion in V , our method reproduces the entanglement growth also for longer times than the range of validity of perturbation theory. A similar observation has been done also for $\mathcal{L}_A(t)$. It seems that perturbation theory is extremely stable in a localized phase.

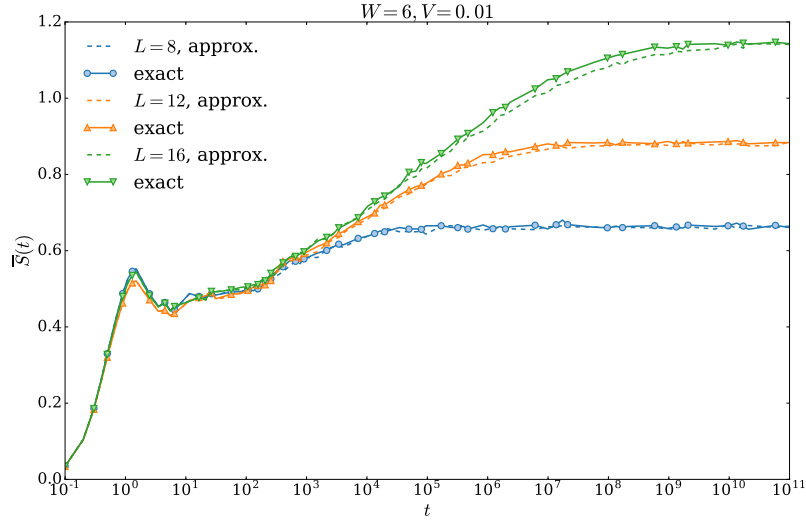


FIGURE 4.14: The panel shows the bipartite entanglement entropy $\bar{S}(t)$ after a global quantum quench for several systems sizes. The $\bar{S}(t)$ has been calculated using the exact Hamiltonian $\hat{\mathcal{H}}$ (solid-lines, exact) and the effective model $\hat{\mathcal{H}}^{\text{eff}}$ (dashed-lines, approx.).

Having shown that our model is suitable to study many-body localized systems, we now focus on $|\overline{\rho(x,t)}|$ using $\hat{\mathcal{H}}^{\text{eff}}$. In the previous section we predicted the existence of a time scale τ in which $\overline{D}(t) = \sum_x |\overline{\rho(x,t)}|$ changes concavity and starts to decrease. Figure 4.15 shows $|\overline{\rho(x,t)}|$ calculated using the effective model for a fixed system size $L = 96$, and fixed disorder and interaction strengths. Figure (a) 4.15 shows a clear change in the concavity of $|\overline{\rho(x,t)}|$ with time. This result confirms the existence of a time scale τ_x , in which $|\overline{\rho(x,t)}|$ starts to decrease. Moreover, the time has been rescaled to show that $\log \tau_x \sim x$ (x is the distance from the perturbation). Figure (b) 4.15 shows that $\log \tau_x \sim \xi_{\text{loc}}^{-1}$, here ξ_{loc}^{-1} is single-particle localization length which has been calculated using the transfer matrix technique (Chapter 1). Finally, we find the complete scaling form $\tau_x \sim e^{x/\xi_{\text{loc}}}$. Indeed, τ_x must be proportional to the time scale in which the site x starts to be entangled with the site $x = 0$ (site in which the system is perturbed) and so losing information about the existence of the perturbation,

$$\tau_x \tilde{\mathcal{B}}_{0,x} \approx 1 \Rightarrow \tau_x e^{-x/\xi_{\text{loc}}} \approx 1. \quad (4.22)$$

Furthermore, also the two-point correlation function

$$\mathcal{C}_x(t) = |\langle \hat{n}_x \hat{n}_0 \rangle - \langle \hat{n}_x \rangle \langle \hat{n}_0 \rangle|(t), \quad (4.23)$$

shows a similar behavior like as $|\overline{\rho(x,t)}|$. Figure 4.16 shows $\mathcal{C}_x(t)$ calculated with $\hat{\mathcal{H}}^{\text{eff}}$. Figure (a) 4.16 shows in a color plot the logarithmic light cone giving indications that correlations grow logarithmically with time as expected if $S(t) \sim \log(t)$. Nevertheless,

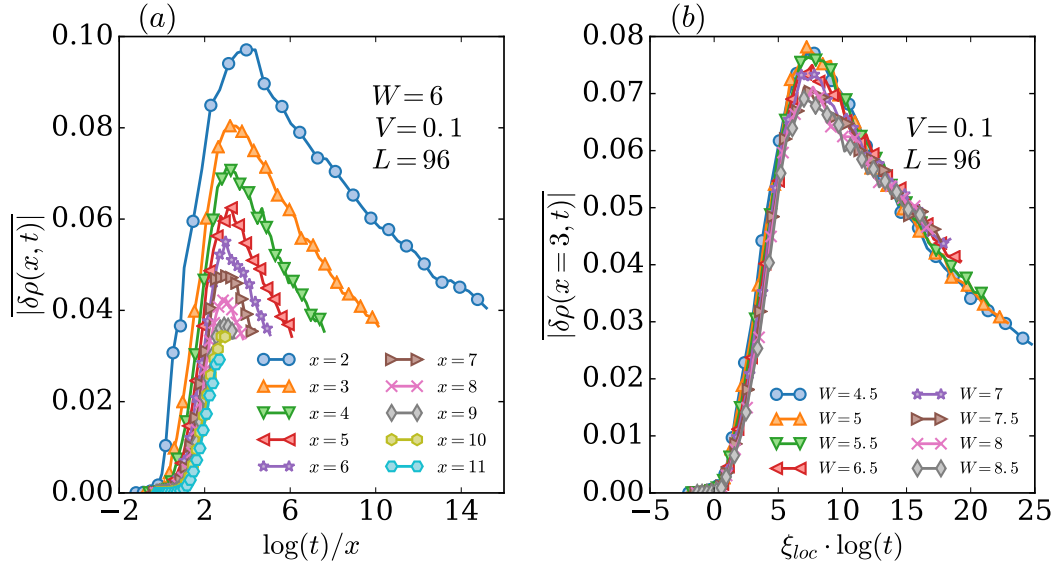


FIGURE 4.15: Panel (a): shows $|\overline{\delta\rho(x,t)}|$ calculated using $\hat{\mathcal{H}}^{\text{eff}}$ for a fixed system size $L = 96$, disorder strength $W = 6$ and interaction strength $V = 6$ for several x . The time has been rescaled to show that $\log \tau \sim x$ (τ_x : time scale in which $|\rho(x,t)|$ changes concavity and starts to decrease). (b): shows $|\overline{\delta\rho(x,t)}|$ for a fixed x ($x = 3$) for several disorder strengths W . It shows that $\log \tau_x \sim \xi_{\text{loc}}^{-1}$. For both panels $\epsilon = 0.05$ (perturbation strength).

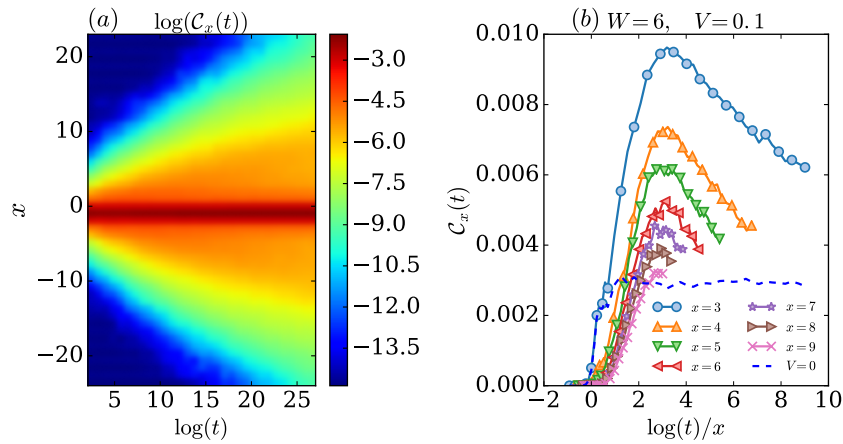


FIGURE 4.16: Panel (a): shows the logarithmically light-cone calculated using the $\mathcal{C}_x(t)$ for the effective model. Panel (b): shows $\mathcal{C}_x(t)$ as a function of time, the time has been properly rescaled to get the collapse of the curves. It also shows the non-interacting case ($V = 0$) (dashed-line). For both panels $L = 48$.

there exists a time in which also $\mathcal{C}_x(t)$ starts to decrease, as shown in Fig. (b) 4.16. Moreover, Fig. (b) 4.16 shows the non-interacting case ($V = 0$), in which $\mathcal{C}_x(t)$ does not decay. Thus, the two point correlation function could be a local measurement to distinguish an Anderson insulator from an interacting localized phase.

Recapitulating, our method gives strong evidence that the decay of the DLDP is only due to the dephasing mechanism, as we conjectured in the previous section.

4.4 Summary

In this chapter, we probed the effects of local perturbations on the dynamics of several disordered systems by studying the Loschmidt echo (LE) and the difference of the local density profile (DLDP). First, with a combination of analytical arguments and exact numerical simulations, we showed that the LE in the localized phase decays algebraically in time. Furthermore, we found, for the non-interacting models, that the exponent of the algebraic decay is proportional to the single-particle localization length, which diverges at the localization-delocalization transition. In the extended phase, the LE decays exponentially fast with time. The faster exponential decay in the extended phase compared with the algebraic decay in the localized phase implies that time-irreversibility is more strongly manifested in the extended phase than in the localized phase, at least for local perturbations. Second, we studied the DLDP for the same models, and we found that the long-time behavior saturates algebraically with system size in the extended phase of the Aubry-André-Harper model, while it never relaxes for the non-interacting localized phase. For the DLDP in the spinless disordered t-V chain, the relaxation is exponential in system size in both phases: in the ergodic phase this is due to thermalization, while in the MBL phase it could be due to the interaction-induced dephasing mechanism which also explains the long-time saturation values of the entanglement entropy after a quantum quench. We give evidence of our conjecture, testing it in an effective model. The study of the change in the expectation values of local observables when the system is perturbed, gives a different perspective concerning time-irreversibility as opposed to the LE. Indeed, the long-time expectation value of local observables in a thermal system at infinite temperature should be unchanged if the system is locally perturbed. We gave numerical evidence that this also happens in the MBL phase.

Part III

Study of Multifractal phases in Many-Body and Anderson localization on hierarchical tree-structures

In the next two chapters studying the quantum dynamics of an MBL system and of the Anderson model on a random regular graph, we will inspect the existence of an intermediate phase composed by multifractal states. These two models are intimately connected, due to the map between localization in Fock space and Anderson localization problems on hierarchical tree-structures. We question the existence of the intermediate phase for the MBL problem. We give indication of the possible existence of a multifractal phase for the Anderson problem on a random regular graph.

Chapter 5

Subdiffusion, mobility edges, and finite-size effects in many-body localized systems

In Chapter 2, we have discussed that the MBL transition for some values of the disorder strength can also occur as a function of energy density. In other words, for values $W \leq W_c(\epsilon = 0.5)$, the energy density spectrum of the system is divided in two parts: a part hosting delocalized (ergodic) eigenstates while the other one contains localized eigenstates. Moreover, as we discussed in Chapter 2, W. De Roeck et al. in a work entitled “Absence of many-body mobility edges” [42] claimed that the MBL transition can not happen as a function of energy density. In their work, using an argument based on perturbation theory, they indicate that local-fluctuations in an eigenstate will create hot-bubbles which will destabilize the localized phase. Furthermore, they also point out several mechanisms which could make the theory fail. This theory is in contrast with most of the exact numerical simulations (Chapter 2). Nevertheless, since numerical simulations can only be performed on relatively small system sizes, the validity of this theory in the thermodynamic limit is still not settled .

Moreover, numerical simulations in one-dimensional chains show that the transport close to the MBL phase within the ergodic phase could be subdiffusive [15, 60, 94, 96, 150], contradicting the expected diffusive transport behavior in a metallic phase. A phenomenological theory has been proposed to explain this unexpected anomalous propagation [60]. It has been claimed that the reason could be due to rare highly disordered regions (Griffiths regions) where the transport would be extremely slow. Nevertheless, this theory seems incomplete, since this subdiffusive dynamics has been observed also in an MBL model in which Griffiths regions are not possible (*i.e.* Aubry-André-Harper

model with short range interactions) [88]. This slow dynamic has also been observed for two dimensional systems [89], in which even the existence of Griffiths regions would not change the transport properties [151]. Additionally, two works [73, 139] show that the transport could indeed be diffusive.

In this chapter, with the aim to shed light on these two issues, we study the dynamics of an MBL system, restricting the dynamics only to selected windows of energy density. This chapter is organized as follows: In the first part we describe the model and the quantities considered to study the observed slow dynamics on the model. We focus on finite-size effects and we point out their importance.

5.1 Model and methods

We consider again the t-V model (Chapter 2)

$$\begin{aligned} \hat{\mathcal{H}} = & -\frac{t}{2} \sum_{x=-L/2}^{L/2-2} \hat{c}_x^\dagger \hat{c}_{x+1} + h.c. + \sum_{x=-L/2}^{L/2-1} \mu_x \left(\hat{n}_x - \frac{1}{2} \right) \\ & + V \sum_{x=-L/2}^{L/2-2} \left(\hat{n}_x - \frac{1}{2} \right) \left(\hat{n}_{x+1} - \frac{1}{2} \right), \end{aligned} \quad (5.1)$$

where L is the system size, $x=1, \dots, L$, with hopping ($t=1$) and interaction (V) between nearest neighbors. The uncorrelated on-site energies $\{\mu_x\}$ are being drawn from a box distribution $[-W, W]$. We work at half filling and with open boundary conditions. For $V=1.0$, the MBL transition is believed to be at $W_c \approx 3.5$ (Chapter 2). We investigate the charge propagation focusing on the delocalized region near the MBL transition. A common description of relaxation dynamics employs the density propagator ($C(r, t)$ in Chapter 2), $\Pi(x, t)$, that takes a simple Gaussian shape for diffusive systems:

$$\Pi(x, t) = e^{-\frac{1}{2}(x/\Delta x(t))^2} / \sqrt{2\pi} \Delta x(t), \quad \Delta x(t) = \sqrt{Dt}, \quad (5.2)$$

where D is the diffusion constant. As we discussed, aiming at the many-mobility edges (MBME)s, we actually study a variant of it, $\Pi_\varepsilon(x, t)$, that resolves the contribution to $\Pi(x, t)$ stemming from many-body states with energy densities ε . The specific correlator $\Pi_\varepsilon(x, t)$ is defined via its discrete Fourier space representation:

$$\Pi_\varepsilon(q, t) = \overline{\Phi_\varepsilon(q, t) / \Phi_\varepsilon(q, t=0^+)}, \quad (5.3)$$

where the disorder average is denoted by the overline. $\Phi_\varepsilon(q, t)$ is the Fourier transform of the energy-projected density relaxation functions

$$\Phi_\varepsilon(x, t) = [\langle \hat{n}_x(t) \hat{n}_0 \rangle_\varepsilon - \langle \hat{n}_x \rangle_\varepsilon \langle \hat{n}_0 \rangle_\varepsilon] \Theta(t). \quad (5.4)$$

The discrete Fourier transform of $\{x_n\}$ is defined by: $y_q = \sum_{n=0}^{L-1} x_n e^{-iqn}$, $q = \frac{2\pi aj}{L}$ and lattice spacing $a=1$.

The projection onto a narrow spectral range near ε is facilitated by taking the expectation value of an operator $\langle \hat{\mathcal{O}} \rangle_\varepsilon = \text{Tr}[\hat{\mathcal{O}} \hat{\rho}(\varepsilon)]$ with

$$\hat{\rho}(\varepsilon) = \mathcal{N}^{-1} \int_{\varepsilon - \Delta\varepsilon/2}^{\varepsilon + \Delta\varepsilon/2} d\varepsilon' \sum_{\gamma}^{\mathcal{N}} |\gamma\rangle \delta(\varepsilon_\gamma - \varepsilon') \langle \gamma|, \quad (5.5)$$

where $|\gamma\rangle$ denotes the eigenstates of the Hamiltonian (5.1) with energy density

$$\varepsilon_\gamma = (E_\gamma - E_{\min}) / (E_{\max} - E_{\min}), \quad (5.6)$$

where E_γ are the many-body energies and $E_{\max, \min}$ denote the extreme values of the energy spectrum. \mathcal{N} represents the number of states in the energy density window $\Delta\varepsilon$, and it is exponentially large in L . By definition, $\Pi_\varepsilon(q=0, t)=1$ and for a conventional diffusive system we have a Gaussian shape, $\Pi_\varepsilon(q, t) = \exp(-(\Delta x_\varepsilon(t)q)^2) \Theta(t)$, with $\Delta x_\varepsilon(t) = \sqrt{D_\varepsilon t}$. For the time evolution, Eq. (5.4), we employ a standard Chebyshev-polynomial propagation (Appendix A); traces over operators are performed stochastically as averages over random state vectors. The approach owes its efficiency to the fact that disorder averages converge very rapidly with the number of random states.

5.2 Mean square displacement

We begin the analysis of the propagator $\Pi_\varepsilon(x, t)$ with its second moment in real space,

$$\Delta x_\varepsilon(t)^2 = \langle x^2 \rangle_\varepsilon - \langle x \rangle_\varepsilon^2, \quad \langle x^n \rangle_\varepsilon = \sum_{x=-L/2}^{L/2-1} x^n \Pi_\varepsilon(x, t).$$

Figure 5.1 (a1-a3) shows the $\Delta x_\varepsilon(t)$ at $W = 2.5$ for both interacting ($V = 1$, dashed line) and non-interacting ($V = 0$, solid line) case for several values of energy densities ($\varepsilon = 0.1, 0.5, 0.875$). For these parameters the many-body mobility edges (MBMEs) have been reported near $\varepsilon \approx 0.2$ and near 0.8 with a delocalized regime in between [95], as is also explained in Chapter 2. Figure 5.1 (a1-a3) carries several messages:

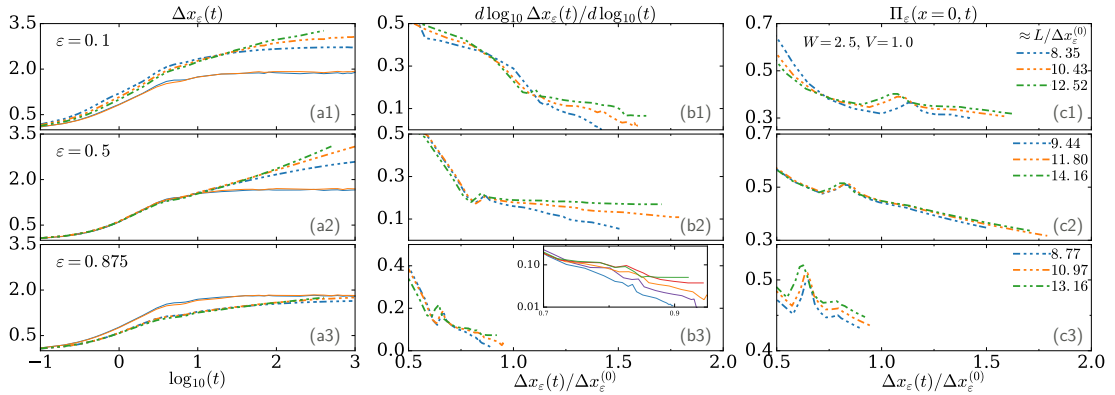


FIGURE 5.1: (a1)-(a3) The time evolution of $\Delta x_\varepsilon(t)$ at $W=2.5$ and $V=1$ near the lower band-edge (upper row, $\varepsilon = 0.1$) in the center region (center row, 0.5) and near the upper band-edge (lower row, 0.875) for system sizes $L = 16, 20, 24$ (dashed traces blue, red, green). Also shown are non-interacting reference traces for $L=16, 20$ ($V=0$, solid lines). (b1)-(b3) Re-plotting (a1)-(a3) as $d \ln \Delta x_\varepsilon(t) / d \ln t$ over $\Delta x_\varepsilon(t) / \Delta x_\varepsilon^{(0)}$ to highlight finite-size effects. Inset shows the blow up of the (b3) data for better visibility of trends including system sizes $L = 16, 18, 20, 22, 24$ (bottom to top). (c1)-(c3) Probability to return to the origin. The legends in this column also give the three system sizes in units of the bare localization length. (In all calculation we fix the width of the energy window $\Delta\varepsilon = 0.1$)

1. Finite size effects are very strong, indeed the system size, L , exceeds the non-interacting standard deviation, $\Delta x_\varepsilon^{(0)}$ (saturation value in time for $V = 0$), by a factor of 10-15 ($\approx L/\Delta x_\varepsilon^{(0)}$), but nevertheless the growth of $\Delta x_\varepsilon(t)$ changes with L by as much as 30%.
2. The interaction mediated delocalization process is very slow. Even after a time that typically corresponds to 0.1% of the inverse hopping ($t^{-1} = 1$) the width of the wavepacket has grown by less than a factor of two as compared to $\Delta x_\varepsilon^{(0)}$.
3. Depending on the spectral window, the transient dynamics is quite different. In particular, the spreading of $\Pi_\varepsilon(x, t)$ is enhanced by the interactions at low energy densities while it is hindered at high densities as compared to the non-interacting reference case.

5.3 Flowing of the dynamical exponent

In this section we quantify the time dependence of $\Delta x_\varepsilon(t)$ studying the exponent scaling function $\beta_\varepsilon(t)$, which is defined by:

$$\beta_\varepsilon(t) \equiv \frac{d \log \Delta x_\varepsilon(t)}{d \log t}, \quad (5.7)$$

which at long times quantifies the rate of growth of $\Delta x_\varepsilon(t) \propto t^{\beta_\varepsilon(t=\infty)}$. For diffusive systems $\beta_\varepsilon(t = \infty) = 1/2$, while $\beta_\varepsilon(t = \infty) < 1/2$ for subdiffusion. Figure 5.1 (b1-b3) shows the β_ε -function as a function of $\Delta x_\varepsilon(t)/\Delta x_\varepsilon^{(0)}$. It very clearly highlights the fact that beyond a certain transient time, τ_ε (set by the kink position), a slow dynamics sets in which reveals itself by a high degree of sensitivity to the system size, L . Always in Fig. 5.1 (b1-b3), all traces of $\beta_\varepsilon(t)$ experience a kink with a position evolving with the energy density ε that does not collapse after rescaling of the abscissa with $\Delta x_\varepsilon^{(0)}$. While the range of L -values available to us is not sufficient to study the asymptotic limit (in L and t), our data nevertheless gives a non-vanishing lower bound for $\beta_\varepsilon(t)$ and hence indicates delocalization, at least near the band-center. With this caveat, we notice that the qualitative behavior seen in all energy ranges is the same: with L increasing, there is a pronounced trend for $\beta_\varepsilon(t)$ to grow (at fixed long time), see Fig. 5.1 (b1-b3) and inset. Strictly speaking, we thus find no evidences for an upper bound to β_ε below the diffusion limit $1/2$, *i.e.* for genuine subdiffusion. Moreover, the growth (with L) being similar in all energy windows, suggests the lack of MBME at $W=2.5$ for the energy-densities inspected. The picture is similar for other choices of W ($\lesssim 3.0$). Indeed, Fig. 5.2 shows

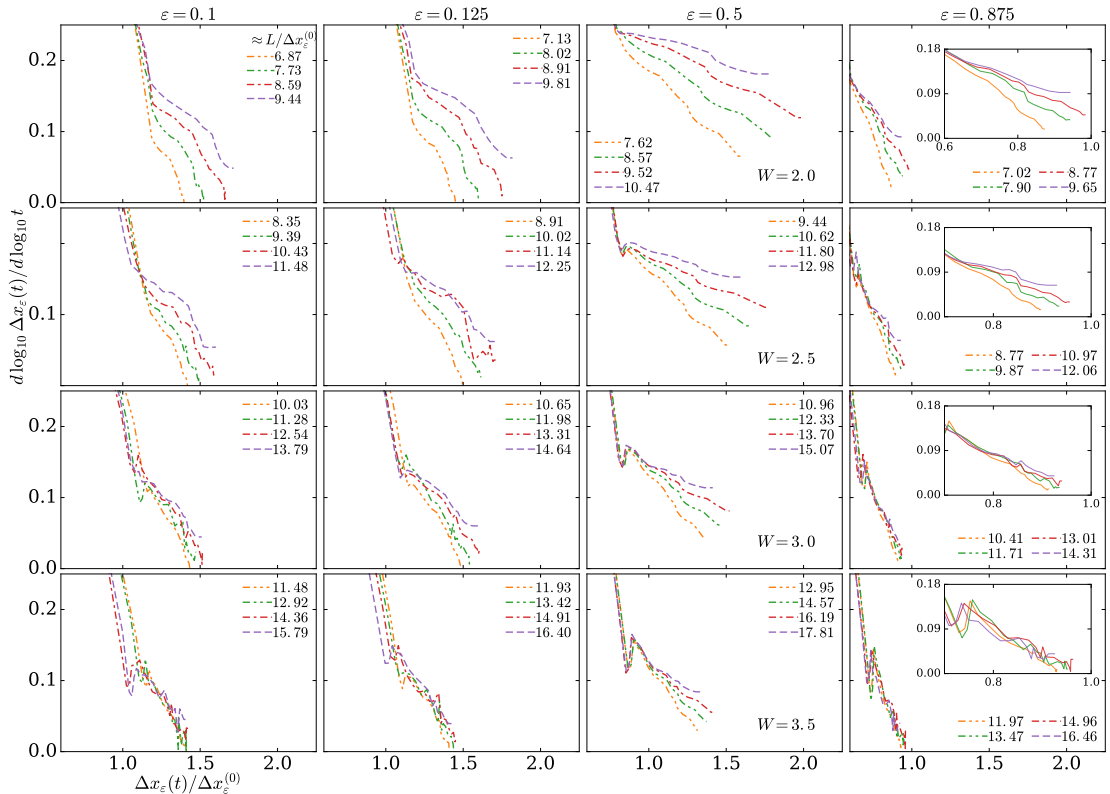


FIGURE 5.2: Time dependence of the exponent $\beta_\varepsilon(t) = d \ln \Delta x_\varepsilon(t) / d \ln t$ for different disorder $W = \{2.0, 2.5, 3.0, 3.5\}$ and system sizes ($L=16, 18, 20, 22$) at four different energy densities $\varepsilon = \{0.1, 0.125, 0.5, 0.875\}$ with $\Delta\varepsilon = 0.1$ and $V = 1.0$. Inset: Shows the same data as fourth column but zoomed for better visibility of the trend in the data with increasing system sizes.

the evolution of the $\beta_\varepsilon(t)$ over $\Delta x_\varepsilon(t)/\Delta x_\varepsilon^{(0)}$ for $L = \{16, 18, 20, 22\}$, at four energy densities and four disorder values close to the MBL transition ($W = \{2.0, 2.5, 3.0, 3.5\}$), which is believed to be around $W_c \approx 3.5$. For these data we usually perform around 10^6 disorder realizations for small system sizes ($L \lesssim 20$), while for larger system sizes the data is averaged over around 10^4 disorder samples. Furthermore, we give a detailed analysis of $\beta_\varepsilon(t)$ for several values of W and ε .

1. $\varepsilon=0.5$:

Figure 5.2 (3rd column) shows the result for values in the middle of the spectrum. In this regime the data clearly indicates that the dynamics is (transient) subdiffusive with an (effective) exponent, $\beta_\varepsilon(t) < 1/2$, which depends strongly on the system size L . The L -dependence is reflected via the upward movement of the $\beta_\varepsilon(t)$. We interpret this systematic trend as an indication to delocalization.

2. $\varepsilon = 0.1, 0.125$:

Fig. 5.2 (1st, 2nd column) shows the evolution of the exponent $\beta_\varepsilon(t)$ for different system sizes in the low energy density regime. Previous studies assigned this region to be many-body localized (at $W \gtrsim 2.0$, $V = 1.0$) as we have shown in Chapter 2 (Fig 2.9). However, for disorder strength below $W \lesssim 3.5$, the upward trend seen with these curves is similar to the one in the band center, suggesting the presence of a (slow) delocalization mechanism, which is inconsistent with the assignment to the MBL phase and the existence of a mobility gap in this parameter range. The proliferation of statistical noise precludes a further analysis about whether or not at even larger disorder, an MBME could exist.

3. $\varepsilon = 0.875$:

At disorder values below $W \lesssim 3.0$ a systematic delocalizing trend at largest times is seen, which we interpret as an indication of a very slow delocalization mechanism (Fig. 5.2, 4th column). Concerning statements about MBME at larger disorder values, we consider our data to be inconclusive due to strong statistical fluctuations.

Recapitulating, at larger disorder and close to the transition, $W \approx W_c$, the situation is numerically less conclusive due to residual statistical noise. Moreover, we have ascertained that our choice of the width $\Delta\varepsilon$ of the energy density shell was sufficiently narrow so that our results for $\Pi_\varepsilon(x, t)$ and its variance are (essentially) independent of it. In Fig. 5.3 we show the evolution of the exponent $\beta_\varepsilon(t)$ for two different values of the width $\Delta\varepsilon = 0.1, 0.2$ of the box function at energy density $\varepsilon = 0.25$. The data is averaged over $\gtrsim 10^4$ disorder configurations. As it is easily deferred from the figure, the curves are almost indistinguishable from each other. For this reason, we choose $\Delta\varepsilon = 0.1$.

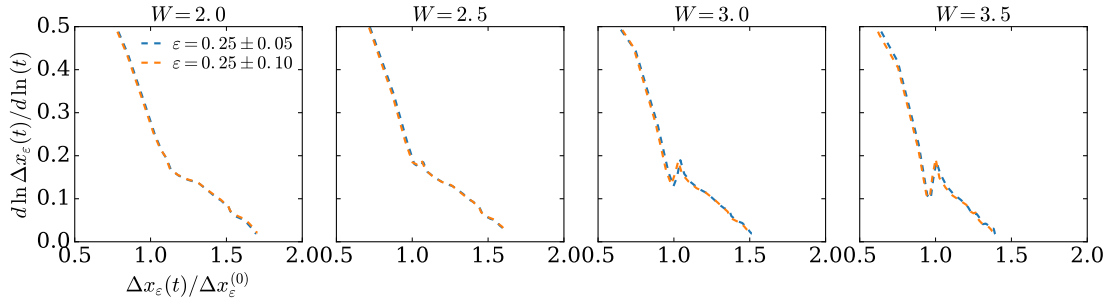


FIGURE 5.3: Evolution of the exponent $\beta_\varepsilon(t) = d \ln \Delta x_\varepsilon(t) / d \ln t$ for different values of the width of the energy density $\Delta\varepsilon$ for $L = 16$ and disorder strengths $W = \{2.0, 2.5, 3.0, 3.5\}$ and $\varepsilon = 0.25$.

5.4 Return probability

In the previous section, we studied the mean square displacement, which is a global quantity. In this section, we study the return probability, which is a local probe. In one dimensional diffusive systems the return probability associated with a spreading wavepacket relates to the variance $\Pi_\varepsilon(0, t) \sim 1/\Delta x_\varepsilon(t)$, merely stating that the wavepacket is internally homogeneous. The data displayed in Fig. 5.1 (c1 - c3) does not adhere to this fundamental idea: $\Pi_\varepsilon(0, t)$ is close to stationary and therefore does not follow the $1/\Delta x_\varepsilon$ law, most clearly seen in the low and high energy density regimes. This observation finds a natural explanation adopting the idea of strong disorder induced fractality.

Indeed it is well known that in the presence of (multi-)fractality the return-probability can be enhanced, $\Pi_\varepsilon(0, t) \propto \Delta x_\varepsilon^{-\alpha_\varepsilon}$, with $0 \leq \alpha_\varepsilon < 1$ [75]. A very slow decaying return probability can therefore also indicate a fractal-type behavior, *i.e.*, α_ε being significantly smaller than unity. Unfortunately, it is very challenging to extract α_ε reliably from our data, because our observation window for $\Delta x_\varepsilon(t)/\Delta x_\varepsilon^{(0)}$ does not exceed a factor of 2-3. Nevertheless, we still report a possible fitting for all values of W and ε which have been study. Fig. 5.4 shows the evolution of the $\Pi_\varepsilon(0, t)$ over $\Delta x_\varepsilon(t)/\Delta x_\varepsilon^{(0)}$ for $L = \{16, 18, 20, 22\}$, at four energy densities and four disorder values close to the MBL transition ($W = \{2.0, 2.5, 3.0, 3.5\}$). The slow decay of the return probability is clearly visible for disorder values not too far from the transition. A power law fit of the data is also provided to highlight the slowness of the decay. However, due to the small time window (only a factor of 2 in $\Delta x_\varepsilon(t)/\Delta x_\varepsilon^{(0)}$) the fit is not completely reliable and should be taken only as a guide to eye.

5.5 Density propagator

In the previous sections to characterize the slow dynamics, we studied two quantities, a local probe (return probability) and a global probe (mean square displacement). Nevertheless, only these two quantities are not able to describe completely the full propagation. Hence, to better understand the transient subdiffusive behavior, here we look at the time dependence of the full distribution function, Π_ε , both in real and q -space. Figure 5.5 (a1-a3) displays a density-propagator $\Pi_\varepsilon(x, t)$ that is far from Gaussian. To highlight its shape (curvature at small q , large x) we rewrite $\Pi_\varepsilon(q, t)$ employing an (inverse) memory kernel, $\kappa_\varepsilon(q, t)$,

$$\Pi_\varepsilon(q, t) = (1 + q^2/\kappa_\varepsilon(q, t))^{-1}, \quad (5.8)$$

where $-\partial_q^2 \Pi_\varepsilon(q, t)|_{q=0} = 2/\kappa_\varepsilon(0, t) \sim \Delta x_\varepsilon(t)^2$. A numerical example can be read off from Fig. 5.5 (b-c). It displays κ_ε at three different energy densities at intermediate disorder strength $W=2.5$. Notice that the non-interacting kernel, $\kappa_\varepsilon^{(0)}(q, t)$, is rapidly growing with wavenumber, q (Fig. 5.5(b1-b3)). This behavior reflects the presence of

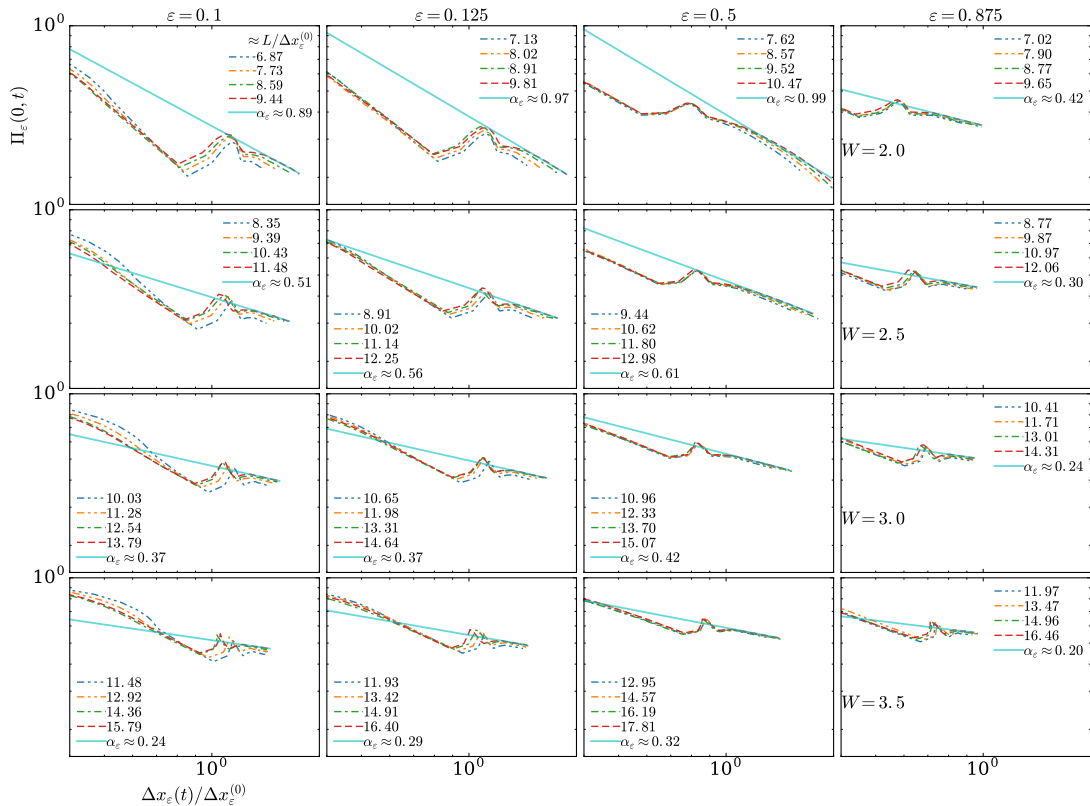


FIGURE 5.4: Time dependence of the return probability $\Pi_\varepsilon(0, t)$ in double log scale for different disorder $W = \{2.0, 2.5, 3.0, 3.5\}$ and system sizes ($L=16, 18, 20, 22$) at four different energy densities $\varepsilon = \{0.1, 0.125, 0.5, 0.875\}$ with $\Delta\varepsilon = 0.1$ and $V = 1.0$. The solid line serves as a guide of a power-law fit and also an estimate of the corresponding exponent α_ε is provided.

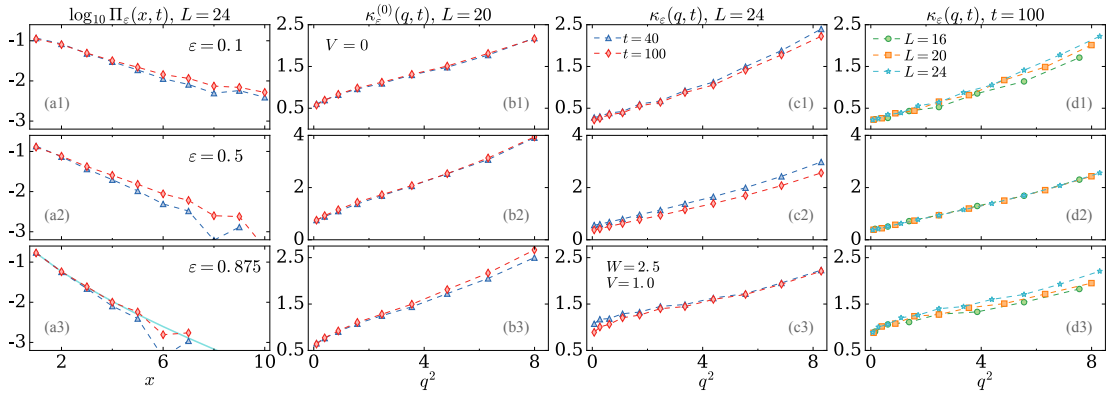


FIGURE 5.5: (a1)-(a3) The density propagator $\Pi_\varepsilon(x, t)$ in the delocalized regime ($\varepsilon=0.1, 0.5, 0.875$, $W=2.5$, $L=24$) at two times $t=40, 100$. The log-normal plot illustrates non-Gaussian shape. Solid line in (a3) shows a stretched exponential fit with an exponent ≈ 0.7 . (b1)-(d3) The corresponding memory kernel $\kappa_\varepsilon(q, t)=q^2/(\Pi_\varepsilon^{-1}(q, t) - 1)$, see also (5.8), for the case without (b1)-(b3) and with interactions (c1)-(d3). The structure at larger wavenumbers illustrates the (non-exponential) short-distance behavior. The absence of effects in time (and system size, not shown) highlights the localized character of the non-interacting kernel $\kappa_\varepsilon^{(0)}$. In contrast, the evolution of the interacting kernel is the hallmark of delocalization. (d1)-(d3) Shows the L -dependence of $\kappa_\varepsilon(t)$.

a short-distance cutoff, a , such as the lattice constant, terminating the long-distance, exponential tail. It exists in a similar way also in the interacting kernels $\kappa_\varepsilon(q, t)$ (Fig. 5.5 (c-d)). Moreover, we can notice that κ_ε in Fig. 5.5 (b1,b3) exhibits small oscillations in q that result from the finite system size. We would like to draw attention to a small additional feature that emerges for the high-energy kernel at very small wavenumbers; as seen in Fig. 5.5 (c3) with increasing time a cusp develops. It could be seen as a precursor indicating a stretched exponential shape in real space and the corresponding fit is shown in Fig. 5.5 (a3). The propagator can also be studied in the x -space. Indeed, Fig. 5.6 shows the distribution function $\Pi_\varepsilon(x, t)$ in real space taken in the subdiffusive phase at high energy density in the vicinity of the MBL transition. In the tail region a weak upturn is seen that indicates deviations from a simple exponential behavior. We describe the data on a phenomenological level employing a stretched exponential, three parameter fit $\Pi_\varepsilon(x, t) \approx \exp(-|x/\xi|^\eta)$. Indeed, the fitting suggests that the exponent η is significantly smaller than one, $\eta \approx 0.7$.

5.6 Numerical Tests

In this section we give few numerical tests, showing that our approximated methods are faithful. As we discussed, we have studied the energy-projected density relaxation

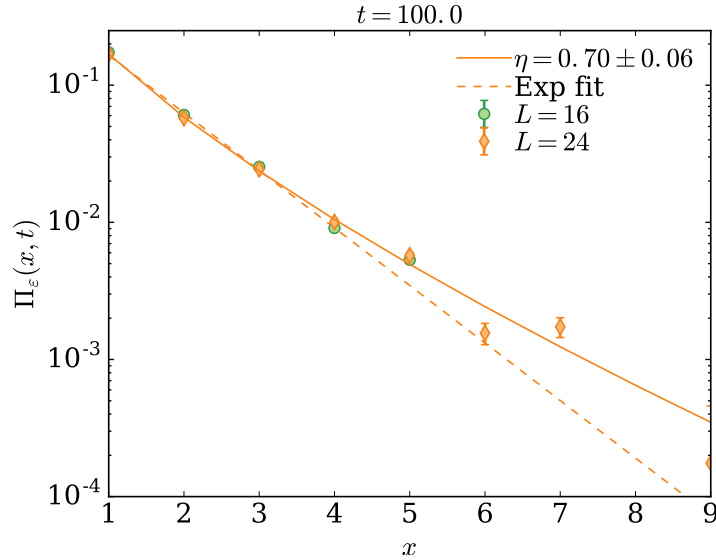


FIGURE 5.6: Distribution function $\Pi_\varepsilon(x, t)$ in real space exhibiting a decay slower than exponential in the tail region. Solid line represents a stretched exponential fit, $\exp(-(x/\xi)^\eta)$, with fitting parameters $\eta \approx 0.7, \xi = 0.464 \pm 0.12$. For comparison, the dotted line indicates a simple exponential. (Parameters: $\varepsilon = 0.875, L = 24, W = 2.5, V = 1.0$ at an intermediate time $t = 100$.) We have also shown the corresponding data for $L=16$ (green symbols) to ascertain that finite-size effects are negligible.

function

$$\Phi_\varepsilon(x, t) = [\langle \hat{n}_x(t) \hat{n}_0 \rangle_\varepsilon - \langle \hat{n}_x \rangle_\varepsilon \langle \hat{n}_0 \rangle_\varepsilon] \Theta(t), \quad (5.9)$$

where $\langle \hat{O} \rangle_\varepsilon = \text{Tr} \hat{O} \hat{\rho}(\varepsilon)$, and $\hat{\rho}(\varepsilon)$ projects into a narrow spectral range near energy density ε with width $\Delta\varepsilon$. To calculate the two-point space-time correlator Eq. (5.9) for large systems ($L=24$) and long times ($\approx 10^3$), we use three approximations:

1. The density matrix $\hat{\rho}(\varepsilon)$ is constructed using Chebyshev polynomials.
2. The energy projected trace denoted via the angular brackets $\langle \dots \rangle_\varepsilon$ is evaluated stochastically.
3. The time evolution is performed employing a standard kernel-polynomial method based on Chebyshev polynomials (Appendix A).

5.6.1 Chebyshev-representation of the density matrix $\hat{\rho}(\varepsilon)$

For the numerical evaluation we represent the density matrix $\hat{\rho}(\varepsilon)$ as a simple function of the Hamiltonian $\tilde{\mathcal{H}}$ ($\tilde{\mathcal{H}}$ is the rescaled $\hat{\mathcal{H}}$ so that its energy density is between $\{0, 1\}$) in the following way,

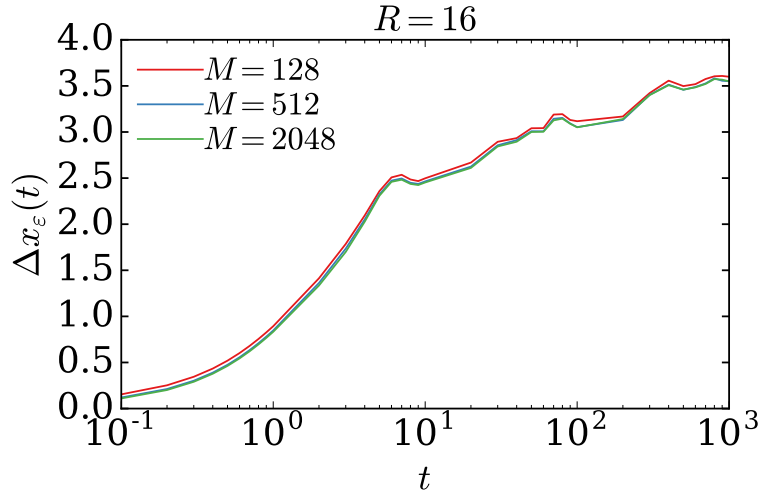


FIGURE 5.7: Convergence of the variance of the density propagator with respect to the number of moments, M , used in Eq. (5.11). R defines the number of random vectors taken for the trace evolution. Only 16 disorder samples are taken for averaging.

$$\hat{\rho}(\varepsilon) = \frac{R_{[\varepsilon-\Delta\varepsilon/2, \varepsilon+\Delta\varepsilon/2]}(\tilde{\mathcal{H}})}{\text{Tr } R_{[\varepsilon-\Delta\varepsilon/2, \varepsilon+\Delta\varepsilon/2]}(\tilde{\mathcal{H}})}, \quad (5.10)$$

where $R_{[a,b]}(x)$ is the box function of unit height in the interval $[a, b]$. We approximate $\hat{\rho}(\varepsilon)$ as a truncated Chebyshev series,

$$\hat{\rho}(\varepsilon) \approx \frac{\sum_{i=0}^M \mu_i T_i(\tilde{\mathcal{H}})}{\text{Tr } \sum_{i=0}^M \mu_i T_i(\tilde{\mathcal{H}})}, \quad (5.11)$$

where $\{T_i(x)\}$ denote the Chebyshev polynomials. M denotes the order of the expansion taken sufficiently large ($M \geq 3000$) to assure convergence Eq. (5.11) (see also Fig. 5.7 right panel). The expansion coefficients $\{\mu_i\}$ are given as follows: $\mu_0 = \frac{1}{\pi}(\arccos a - \arccos b)$, $\mu_1 = \frac{1}{\pi}(\sqrt{1-a^2} - \sqrt{1-b^2})$, $\mu_{n \geq 2} = \frac{1}{n\pi}(\sin(\arccos nb) - \sin(\arccos na))$. In Fig. 5.7 we display the convergence of the time evolution of our main observable, the variance $\Delta x_\varepsilon(t)$, with respect to the number of moments in the sum Eq. (5.11).

5.6.2 Stochastic trace evaluation and convergence

The expectation values $\langle \hat{\mathcal{O}} \rangle_\varepsilon$ of an operator $\hat{\mathcal{O}}$ has been calculated using *stochastic trace evaluation*. The idea is to represent a trace as an average over an ensemble of random state vectors $\{|r\rangle\}_{r=0}^R$:

$$\langle \hat{\mathcal{O}} \rangle_\varepsilon \sim \frac{1}{R} \sum_{r=0}^{R-1} \langle r | \hat{\rho}(\varepsilon) \hat{\mathcal{O}} | r \rangle, \quad \text{with } R \gg 1. \quad (5.12)$$

Truncating the sum at an upper cutoff, R , for global variables the relative error decays

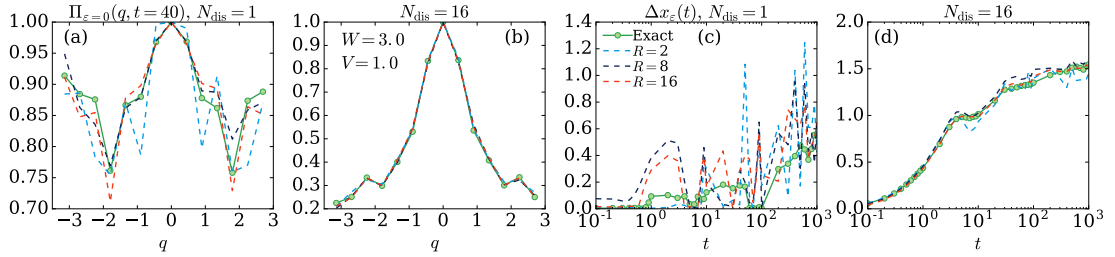


FIGURE 5.8: Trace evaluation: comparison between exact and stochastic methods for $\Pi_\varepsilon(q, t)$ and $\Delta x_\varepsilon(t)$. (Parameters: $L = 14$, middle of the band $\varepsilon = 0.5$ and $W = 3.0, V = 1.0$). (a) Density propagator $\Pi_\varepsilon(q, t = 40)$ in q -space for a single disorder realization. The (green) dots represent the exact data calculated using the full trace employing exact diagonalization; the dashed lines are evaluated with different number of random vectors $R = \{2, 8, 16\}$ (blue, black, red) employing the stochastic trace formula (5.12). (b) Density propagator $\Pi_\varepsilon(q, t)$ averaged over 16 disorder realizations. As can be seen, the average of $\Pi_\varepsilon(q, t)$ over the disorder realization converges rapidly in the number R of stochastic state vectors as opposed to $\Pi_\varepsilon(q, t)$ taken for a single disorder realization. (c),(d) A similar trend is also visible with real space data, here shown for the second moment of $\Pi_\varepsilon(x, t)$: $\langle \Delta x^2(t) \rangle$.

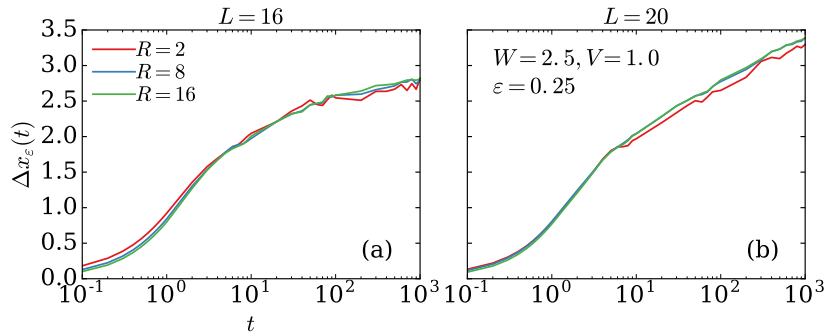


FIGURE 5.9: Shows the variance $\Delta x_\varepsilon(t)$ for three trace vectors $R = \{2, 8, 16\}$ after a small disorder averaging $N_{\text{dis}} = 32$ for two different system sizes $L = 16, 20$.

as $1/\sqrt{\mathfrak{D}R}$ (central limit theorem), with \mathfrak{D} denoting the dimension of the Hilbert space. Hence, the stochastic trace evaluation is more efficient in very high dimensions (for variables that sample the full system size). In our case, \mathfrak{D} is exponentially large in the system size, L , and is given by $\binom{L}{N}$, N being the particle number. For smaller system size, $L \lesssim 20$, we typically use $R=16$ random state vectors, while for larger system sizes we only keep $R=2$. The convergence properties are illustrated in Fig. 5.8 (a). The plot displays a comparison between the stochastic trace estimate and an exact trace evaluation. As is seen there, the convergence properties of the distribution $\Pi_\varepsilon(q, t)$ with R are actually quite poor; at $R=16$ deviations are still of the order of a few percent. However, note that the convergence with R is drastically improved for the traces averaged over the disorder ensemble, *i.e.* for $\overline{\langle \hat{O} \rangle_\varepsilon}$ Fig. 5.8 (b) shows that even for a relatively small ensemble of $N_{\text{dis}}=16$ samples a good convergence is reached already with $R=2$. The same behavior is seen at all times. To illustrate this we display similar data also for the variance, $\Delta x_\varepsilon(t)$. Again, the disorder averaged variance converges very rapidly

with the number R of random states kept for the trace evaluations. Figure 5.9 further illustrates the dependence of the variance on the averaging over trace vectors, now for two larger system sizes. As it is clear from both plots, the variance is well approximated at all times with only a small number of trace vectors. With increasing system size and improving disorder average the trace approximation becomes progressively efficient, this is because the error scales as $\propto 1/\sqrt{\mathfrak{D}}$.

5.7 Summary

In this section we summarize the results of this chapter:

1. Within our observation window, $\Pi_\varepsilon(x, t)$ exhibits a very pronounced non-Gaussian spatial shape that decays in a (simple) exponential fashion or even slower. It is tempting to associate this finding with the stretched exponential behavior of correlations that has been proposed to exist due to fractal Griffiths regions in the localized phase near the phase boundary.
2. The time dependence of its width $\Delta x_\varepsilon(t)$, is very sensitive to the system size, L . In order to highlight the effects of finite size in the time evolution, we studied the dynamical exponent $\beta_\varepsilon(t) = \frac{d \log \Delta x_\varepsilon(t)}{d \log t}$. In the ergodic phase at intermediate times $\beta_\varepsilon(t)$ grows in a subdiffusive manner with values $\beta_\varepsilon(t) < 1/2$ consistent with other reports [15, 60, 94, 96, 150]. However with increasing time, $\beta_\varepsilon(t)$ becomes progressively L -dependent. At these longer times a similar tendency of growing $\beta_\varepsilon(t)$ (with L) is observed in all spectral windows at low, intermediate and high energy density. This strong growth prevents us from confirming the existence of genuine subdiffusion that would exhibit a time-independent exponent $\beta_\varepsilon < 1/2$. We detect a slow growth of $\beta_\varepsilon(t)$ even in those regions of the phase diagram that have been identified previously as localized. Thus, the delocalized phase is larger than reported previously [95], which is associated with a very slow collective dynamics. Such a behavior is not entirely unexpected, perhaps signaling the breakdown of localization due to “hot bubbles” [42].
3. For the probability $\Pi_\varepsilon(0, t)$ to return to the origin one might have suspected $\Pi_\varepsilon(0, t) \propto 1/\Delta x_\varepsilon(t)$, suggesting $\Pi_\varepsilon(0, t) \propto t^{-\beta_\varepsilon(t=\infty)}$. Instead, our data indicates that the subdiffusive transients behavior coexists with an elevated return probability consistent with (possibly transient) weakly ergodic phases with fractal phenomenology, $\Pi_\varepsilon(0, t) \propto \Delta x_\varepsilon(t)^{-\alpha_\varepsilon}$ and $0 \leq \alpha_\varepsilon < 1$.

These results are summarized graphically in Fig. 5.10. Due to the finite resolution of our simulations, we could not rule out the possibility of the existence of MBME for low

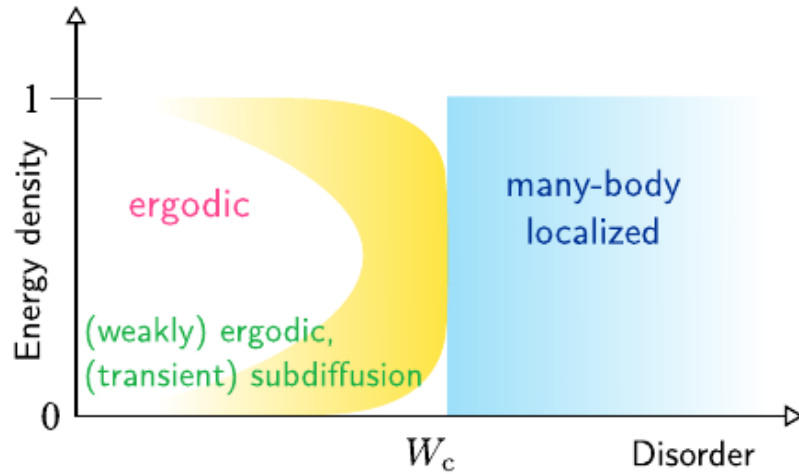


FIGURE 5.10: A qualitative phase diagram of different dynamical regions in the disorder energy density plane of the t-V model. At disorder strength W below the many-body localization transition W_c , we propose a transient subdiffusive, weakly ergodic dynamical regime with an anomalously slow decay of the return probability.

energy density values, thus this region of the phase-diagram (Fig. 5.10) has been left uncolored (white).

Based on these findings we propose the following scenario: There is a timescale τ_ϵ beyond which a slow dynamics kicks in together with diffusive behavior. Approaching the MBL transition from the delocalized side, this time scale diverges; simultaneously, $\beta_\epsilon(t)$ at times $t \lesssim \tau_\epsilon$ is rapidly decreasing, which might suggest a small value of β_ϵ at the MBL transition. In this scenario, the critical fixed-point would carry excited states that exhibit phenomenological features reminiscent of (strong) multifractality [51].

We conclude with two remarks relating our results to the most recent literature and with a problem that we will describe in the next chapter (Chapter 6).

1. Consistent with our findings, also Serbyn et al. observe very strong finite size effects in their study of the Thouless energy [132]. Like us, they interpret their results as indicating that the system sizes are too short for observing the asymptotic thermalized behavior. Unlike us, they go a step further proposing that the numerical data at small system sizes (below $L=20$) already reveals hydrodynamic properties of the critical fixed point, such as multifractality. This conclusion for us is difficult to draw, because one would expect system size independent exponents in the critical window, which we don't observe.
2. Studies of Anderson localization of random regular graphs (RRG) (Chapters 6) show the possible existence of a multifractal phase [7, 41, 82]. Nevertheless, recent works [57, 145] give indications that this phase could be a finite size effect, and that

with increasing system size ergodicity will be restored. When interpreting $\Delta x_\varepsilon(t)$ as an effective system size, then the transient subdiffusive behavior observed by us finds a natural interpretation within the RRG-perspective.

Chapter 6

Typical versus mean properties as a sensitive probe of multifractal states

As we have seen in the previous chapter (Chapter 5), an intermediate phase has been argued to exist for one-dimensional MBL systems, in which the transport is subdiffusive. We have questioned the existence of this phase, showing that the exponents characterizing the subdiffusive transport do not converge for the available system sizes, thus leaving the possibility to have diffusive transport in the thermodynamic limit.

Moreover, as discussed in the introduction (Chapter 2), an MBL problem can be mapped onto an Anderson problem in Fock space (tree-like structure). This mapping has constructed a fundamental link between Anderson localization in hierarchical tree structures and many-body physics [6]. In Chapter 1 we have also discussed the Anderson problem on the Bethe lattice and we have shown that a localization-delocalization transition (Anderson transition) occurs. A Bethe lattice has a special tree-like geometric structure (Fig. 1.2), and it is free of loops. Moreover most of its sites lie at the boundary, thus in principle different choices of boundary conditions could drastically change the physics of the system. A random regular graph (RRG) is a tree-like structure Fig. 6.1, which locally looks like a Bethe lattice, but without a boundary. Indeed, it is possible to obtain a RRG from a Bethe lattice by randomly closing its boundary condition, but keeping the local connectivity of the graph fixed. The RRG has an Anderson transition at the same disorder strength of the Bethe lattice (Eq. 1.27) [82]. The structure of a RRG is similar to the structure of the graph in Fock space (GFS) (Fig 2.3) to study an MBL problem. In fact both have loops, nevertheless there are also differences:

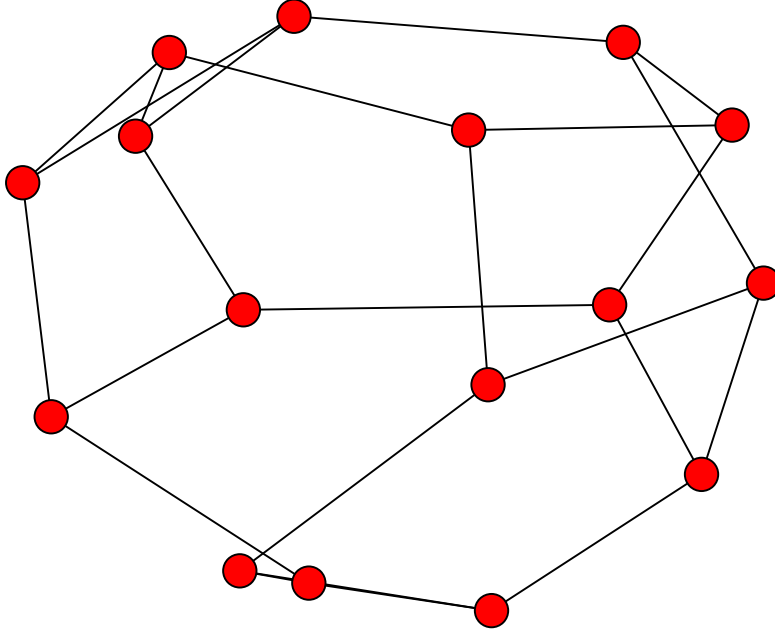


FIGURE 6.1: Random regular graph with 16 sites and with connectivity equal to three.

1. The connectivity of the GFS grows with the volume of the physical system, while in a RRG the connectivity is fixed.
2. The site energies in the GFS are correlated, and typical fluctuations between them scale as $\sqrt{\log \mathcal{D}}$ (\mathcal{D} is the dimension of the Hilbert space) but the difference of neighboring on-site energies are of order one, while the on-site energies of the Anderson model on a RRG are uncorrelated and neither their value nor their fluctuations have any scaling with system size.

In addition to these differences, the MBL problem in first approximation can be mapped onto an Anderson localization model on a RRG. Recently, it has been proposed that the Anderson model on a RRG might have a new phase transition [7, 82] between an ergodic phase, with states spanning uniformly the entire space, to a non-ergodic phase composed of multifractal states which present strong fluctuations in space (Chapter 1). Nevertheless, the existence of this new phase has been strongly questioned giving indication that it could be just a finite-size effect, and it is still generating an active debate [144, 145].

Understanding the existence of this non-ergodic phase in a RRG could shed light on the existence of this subdiffusive intermediate phase found in the most intriguing problem of an extensive interacting disordered many-body system (Chapter 5). In this chapter, we

study the quantum dynamics of a particle initially localized on one site of the system. We give a new characterization of multifractal states, emphasizing the importance of space and disorder fluctuations. The chapter is structured as follows. First, we define the models. We then explain the methods and the main idea of this new characterization. Second, we benchmark this characterization with two models having critical states, the power-law banded random matrix (PLBM) [51, 103] and the Rosenzweig-Porter random matrix model (RPRM) [83, 124]. Finally, we use the same concepts to study the Anderson model on a RRG to understand the existence of this putative new non-ergodic phase.

6.1 Models and methods

We study the Hamiltonian

$$\hat{\mathcal{H}} := \sum_{x,y}^L h_{x,y} |x\rangle\langle y|, \quad (6.1)$$

represented in the basis of the site states $|x\rangle$, where L is the number of sites in the system. We consider three different models that have a localization-delocalization transition with wavefunctions changing properties from ergodic to localized via multifractal ones.

1. The PLBM [51, 103], which is obtained from $\hat{\mathcal{H}}$ (Eq. 6.1) with $h_{x,y} = h_{y,x} = \mu_{x,y}/(1 + (|x - y|/b)^{2a})^{1/2}$. Henceforth $\mu_{x,y}$ are independent uniformly identically distributed random variables taken from $[-1, 1]$. This ensemble of matrices parameterized by a and b have a localization-delocalization transition at $a = 1$, for any b . For $a < 1$, the model shows an ergodic phase and for $a > 1$ the eigenstates are power-law localized. At the critical point ($a = 1$) all the states are multifractal and the parameter b tunes the multifractal properties of the states from strong ($b \ll 1$) to weak ($b \gg 1$) multifractality [90, 102, 103]. There is no mobility edge in this model, *i.e.* for any a, b all the states are either extended or localized.
2. The RPRM [83, 124] is obtained by choosing $h_{x,y} = h_{y,x} = \mu_{x,y}/L^{\gamma/2}$ for $x \neq y$, while for $x = y$, $h_{x,x} = \mu_{x,x}$. The RPRM, like the PLBM, has no mobility edge, but it has three distinct phases. For $\gamma < 1$ all the states are ergodic while for $\gamma > 2$ all the states are localized at a few sites. For $1 < \gamma < 2$ the fractal phase arises [83]. By fractal states we mean that the wavefunctions can be considered ergodic but in an extensive number of sites being still a zero fraction of the entire system. The consequence of this kind of multifractality is that the exponents τ_q defined by $\sum_x |\phi_E(x)|^{2q} \sim L^{-\tau_q}$ (Chapter 1) have the following form $\tau_q = (2 - \gamma)(q - 1)$, where $\phi_E(x)$ is an eigenstate of $\hat{\mathcal{H}}$ at site x .

3. The disordered RRG model which is obtained by taking $h_{x,x}$ independent uniformly identically distributed random variables between $[-W/2, W/2]$, $h_{x,y} = h_{y,x} = -1$ if the sites x, y are linked in the RRG with fixed local connectivity and $h_{x,y} = h_{y,x} = 0$ otherwise. The local connectivity is taken to be three like in Fig. 6.1. This model is believed to have a localization-delocalization transition called Anderson transition (AT) at $W_{AT} \approx 17.64$ (Chapter 1). Moreover, it is a matter of discussion [7, 57, 82, 145] the possibility of the existence of another transition at smaller disorder strength between ergodic states to multifractal states. This putative transition has been estimated to be around $W_{EMT} \approx 10$ (EMT, ergodic to multifractal) [7, 82]. Consequently, it implies the existence of an entire phase ($W_{EMT} < W < W_{AT}$) composed of multifractal states. The RRG has mobility edges, thus the spectrum of $\hat{\mathcal{H}}$ depending on the disorder strength can host separated bands of energies composed of extended or localized eigenstates.

We are interested in studying these different extended phases (ergodic, non-ergodic multifractal, fractal) by investigating their dynamical properties. In particular, we study the return probability starting from a state $|x\rangle$, defined by

$$\mathcal{R}(t) := \frac{|\langle x | \hat{P}_{\Delta E} e^{-i\hat{\mathcal{H}}t} \hat{P}_{\Delta E} |x\rangle|^2}{|\langle x | \hat{P}_{\Delta E} |x\rangle|^2}, \quad (6.2)$$

where $\hat{P}_{\Delta E} := \sum_{E \in \Delta E} |E\rangle\langle E|$ is the projector onto the eigenstates of $\hat{\mathcal{H}}$ whose energy E belongs to a small energy shell $E \in \Delta E = [-\delta E, \delta E]$ around the middle of the spectrum of $\hat{\mathcal{H}}$.

The reason to use the projector $\hat{P}_{\Delta E}$ is to avoid the mixing of states with different properties. Indeed, for the RRG, ΔE has been chosen small enough so that the eigenstates involved in the dynamics are all extended, while for the other models (PLBM, RPRM) $\hat{P}_{\Delta E} = \mathbb{I}$, since no mobility edge is present. The average over matrix ensemble and initial states $|x\rangle$ is indicated with a overline over the quantities considered. In particular, we are interested in the mean and the typical values of $\mathcal{R}(t)$, defined respectively as $\overline{\mathcal{R}(t)}$ and $e^{\overline{\log \mathcal{R}(t)}}$. The scaling of $\mathcal{R}(t)$ to zero with the system size L in the long-time limit is also within our main focus (both typical and mean averages)

$$\overline{\mathcal{R}_\infty} := \lim_{T \rightarrow \infty} \frac{1}{T} \int_0^T \overline{\mathcal{R}(t)} dt, \quad (6.3)$$

$$e^{\overline{\log \mathcal{R}_\infty}} := \lim_{T \rightarrow \infty} \frac{1}{T} \int_0^T e^{\overline{\log \mathcal{R}(t)}} dt. \quad (6.4)$$

These quantities $(\overline{\mathcal{R}_\infty}, e^{\overline{\log \mathcal{R}_\infty}})$ provide information on the properties (ergodicity or multifractality) of the eigenstates belonging to the energy shell ΔE , since the mean $\overline{\mathcal{R}_\infty}$

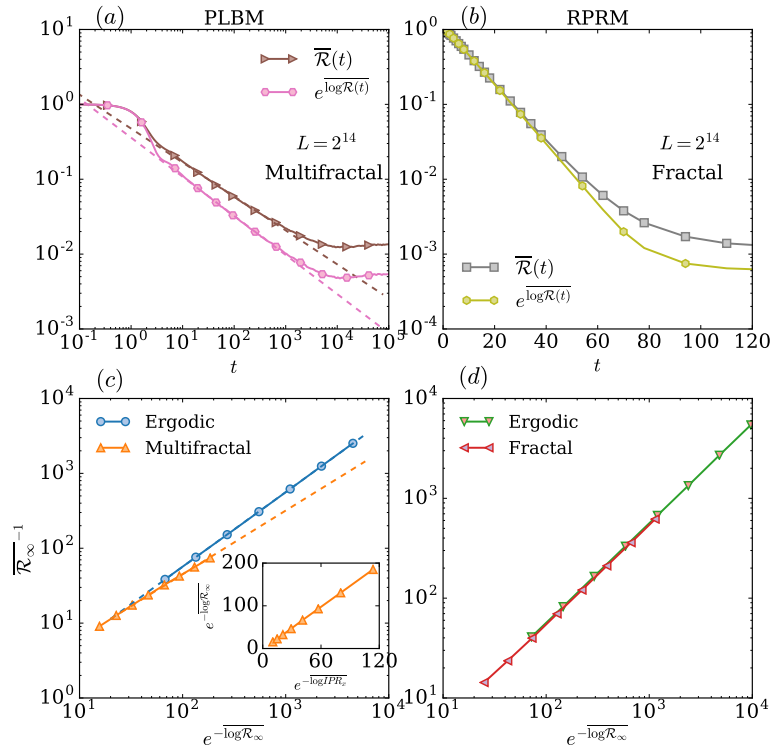


FIGURE 6.2: (a) $\overline{\mathcal{R}}(t)$ and $e^{\overline{\log \mathcal{R}}(t)}$ as a function of time t for the PLBM in a log-log scale in the multifractal phase ($a = 1, b = 0.5$) for a fixed $L = 2^{14}$. The dashed lines are guides for the eyes to emphasize the decay with time is different between $\overline{\mathcal{R}}(t)$ and $e^{\overline{\log \mathcal{R}}(t)}$. (b) $\overline{\mathcal{R}}(t)$ and $e^{\overline{\log \mathcal{R}}(t)}$ as a function of time t for the RPRM in the fractal phase ($\gamma = 1.25$) for $L = 2^{14}$, $\overline{\mathcal{R}}(t) \sim e^{\overline{\log \mathcal{R}}(t)} \sim e^{-E_{\text{Th}}t}$, with E_{Th} the Thouless's energy ($E_{\text{Th}} \sim L^{1-\gamma}$) [83]. (c) $\overline{\mathcal{R}}_{\infty}^{-1}$ as a function of $e^{-\overline{\log \mathcal{R}}_{\infty}}$ for the PLBM in two different phases of the PLBM: In the ergodic phase ($a = 0.5, b = 1$) $\overline{\mathcal{R}}_{\infty}^{-1} \sim e^{-\overline{\log \mathcal{R}}_{\infty}}$, while in the multifractal phase ($a = 1, b = 0.5$) $\overline{\mathcal{R}}_{\infty}^{-1} \sim e^{-\alpha \overline{\log \mathcal{R}}_{\infty}}$ with $\alpha < 1$. The inset shows the scaling of the typical IPR_x versus the typical $R(\infty)$. (d) $\overline{\mathcal{R}}_{\infty}^{-1}$ as a function of $e^{-\overline{\log \mathcal{R}}_{\infty}}$ for the RPRM in two phases: in the ergodic phase ($\gamma = 0.5$) and in the fractal phase ($\gamma = 1.25$), in both of them $\overline{\mathcal{R}}_{\infty}^{-1} \sim e^{-\overline{\log \mathcal{R}}_{\infty}}$.

can be expressed in terms of the inverse participation ratio (IPR) of wavefunctions $\{\phi_E\}$ of $\hat{\mathcal{H}}$,

$$\overline{\mathcal{R}}_{\infty} = \overline{IPR_x} = \frac{\overline{\sum_{E \in \Delta E} |\phi_E(x)|^4}}{(\sum_{E \in \Delta E} |\phi_E(x)|^2)^2}. \quad (6.5)$$

Note that contrary to the IPR defined in Chapter 1, $\overline{\mathcal{R}}_{\infty}$ is calculated summing over the energy index E . The typical value $e^{\overline{\log IPR_x}}$ of IPR_x is not equal to $e^{\overline{\log \mathcal{R}}_{\infty}}$ in general. This difference is due to the time fluctuations of $\mathcal{R}(t)$. Nevertheless for long-times (of the order of the saturation value for a finite system) the time fluctuations of $\mathcal{R}(t)$ scale to zero as a function of L . Therefore at first approximation, the corrections due to time fluctuations do not change the L -scaling $e^{\overline{\log IPR_x}} \sim e^{\overline{\log \mathcal{R}}_{\infty}}$. However, the scaling of $\overline{IPR_x}$ and $e^{\overline{\log IPR_x}}$ can, in principle, be different depending on the phase. Indeed, in an ergodic phase the envelope of the wavefunctions $\{\phi_E\}$ is in first approximation

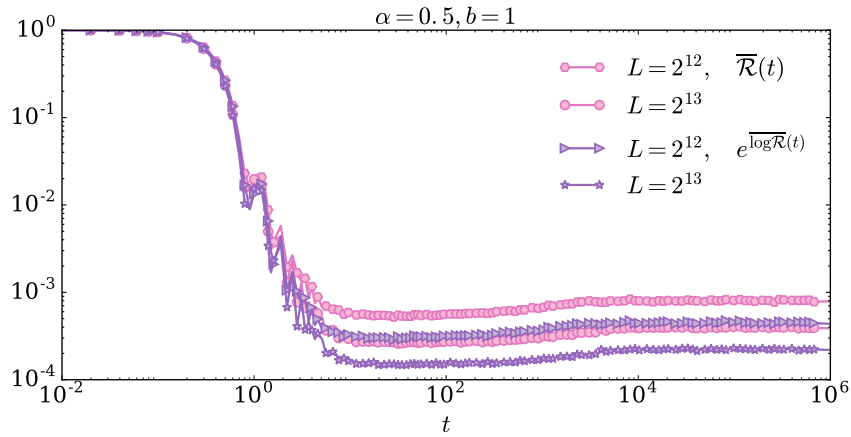


FIGURE 6.3: The figure shows $\overline{\mathcal{R}(t)}$ and $e^{\overline{\log \mathcal{R}(t)}}$ in the ergodic phase of the PLBM for two systems sizes.

uniformly distributed over the entire system ($|\phi_E(x)|^2 \sim 1/L$), thus it does not reveal strong spatial fluctuations. In this case, we do not expect any difference between the scaling of mean and typical values. In a fractal phase, like in the RPRM, the magnitude of wavefunctions in space does not have large fluctuations, since the fractality is only due to its support, *i.e.*, the wavefunctions are ergodic in a small portion of the entire system. Nevertheless, in a multifractal phase the wavefunctions $\{\phi_E(x)\}$ could have strong spatial dependence, which could imply a possible difference in scaling with L between $\overline{\mathcal{R}_\infty}$ and $e^{\overline{\log \mathcal{R}_\infty}}$.

6.2 Return probability for the power-law banded matrices and for the Rosenzweig-Porter random matrices

In this section we study $\mathcal{R}(t)$ and its long-time saturation value for the PLBM and RPRM. We perform the time evolution using exact full diagonalization. At the critical point of the PLBM, where all states are multifractal, both $\overline{\mathcal{R}(t)}$ and $e^{\overline{\log \mathcal{R}(t)}}$ decay algebraically, $\overline{\mathcal{R}(t)} \sim t^{-\alpha_1}$ and $e^{\overline{\log \mathcal{R}(t)}} \sim t^{-\alpha_2}$. Figure 6.2(a) shows the algebraic decay of $\overline{\mathcal{R}(t)}$ and $e^{\overline{\log \mathcal{R}(t)}}$ at criticality (multifractal phase). As observed, the two rates of decay (α_1, α_2) are different from each other due to the inequality between arithmetic and geometric mean $\alpha_1 < \alpha_2$. Instead, in the ergodic phase ($a < 1$) $\overline{\mathcal{R}(t)}$ and $e^{\overline{\log \mathcal{R}(t)}}$ decay asymptotically at the same rate, as shown in Fig 6.3. As a consequence of a different rate of decay between $\overline{\mathcal{R}(t)}$ and $e^{\overline{\log \mathcal{R}(t)}}$, in the multifractal phase the saturation values $\overline{\mathcal{R}_\infty}$ (Eq. 6.3) and $e^{\overline{\log \mathcal{R}_\infty}}$ (Eq. 6.4) may have different scaling to zero as functions of L , $\overline{\mathcal{R}_\infty} \sim L^{-D_2}$ and $e^{\overline{\log \mathcal{R}_\infty}} \sim L^{-D_{\text{typ}}}$ ($D_2 < D_{\text{typ}} < 1$), while in an ergodic phase $D_2 = D_{\text{typ}} = 1$. Figure 6.2(c) shows $\overline{\mathcal{R}_\infty}^{-1}$ as a function of $e^{-\overline{\log \mathcal{R}_\infty}}$ in a log-log plot

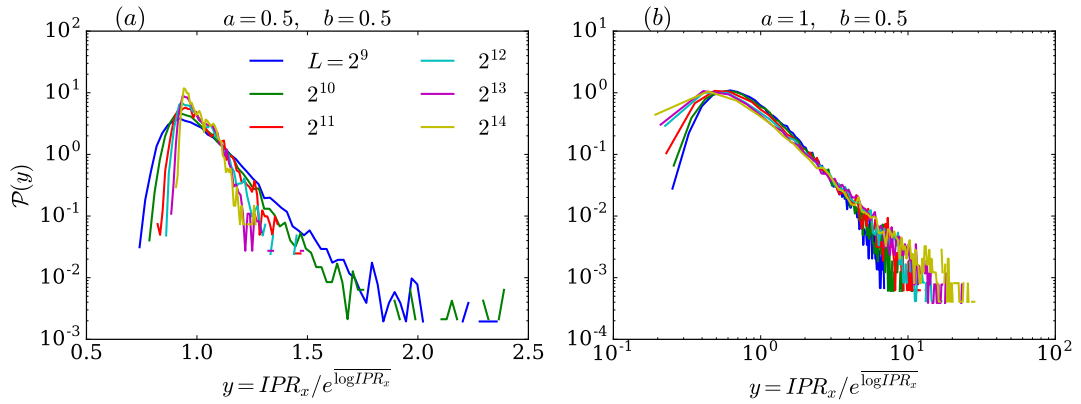


FIGURE 6.4: Panel (a) shows the probability distribution $\mathcal{P}(y)$ for the rescaled random variable $y = IPR_x / e^{\overline{\log IPR_x}}$ for PLBM in the ergodic phase ($a = 0.5, b = 0.5$) for several system sizes. Panel (b) shows the probability distribution $\mathcal{P}(y)$ in the multifractal phase ($a = 1, b = 0.5$), in this case $\mathcal{P}(y)$ has power-law tails, indicating that $\overline{IPR_x}^{-1} \sim e^{-\alpha \overline{\log IPR_x}}$ with $\alpha < 1$.

for two different values of a, b . One in the ergodic phase and another in the multifractal phase. In the ergodic phase $\overline{\mathcal{R}_\infty}^{-1}$ and $e^{-\overline{\log \mathcal{R}_\infty}}$ scale in the same way as a function of system size ($\overline{\mathcal{R}_\infty}^{-1} \sim e^{-\overline{\log \mathcal{R}_\infty}}$). In a multifractal phase $\overline{\mathcal{R}_\infty}^{-1}$ and $e^{-\overline{\log \mathcal{R}_\infty}}$ scale in a different way, $\overline{\mathcal{R}_\infty}^{-1} \sim e^{-\alpha \overline{\log \mathcal{R}_\infty}}$ with $\alpha = D_2/D_{\text{typ}} < 1$. The inset of Fig. 6.2(c) shows $e^{\overline{\log IPR_x}}$ as a function of $e^{\overline{\log \mathcal{R}_\infty}}$ in a linear scale, giving indication that $e^{\overline{\log \mathcal{R}_\infty}} \sim e^{\overline{\log IPR_x}}$. Furthermore, from the equality $\overline{\mathcal{R}_\infty} = \overline{IPR_x}$ (Eq 6.5) we have that $\overline{IPR_x}^{-1} \sim e^{-\alpha \overline{\log IPR_x}}$ with the same α as in $\overline{\mathcal{R}_\infty}^{-1} \sim e^{-\alpha \overline{\log \mathcal{R}_\infty}}$.

The difference in scaling between the mean and typical value is also possible to observe in the probability distribution of IPR_x (\mathcal{R}_∞). In the multifractal region the probability distribution of IPR_x becomes long-tailed giving the discrepancy in the scaling between mean and typical values as shown in Fig. 6.4 for the rescaled random variable $y = IPR_x / e^{\overline{\log IPR_x}}$. Instead, in the ergodic phase the probability distribution of \mathcal{R}_∞ has exponentially decaying tails and it shrinks with increasing system size, indicating that $\overline{IPR_x} \sim e^{\overline{\log IPR_x}}$.

In the RPRM both $\overline{\mathcal{R}(t)}$ and $e^{\overline{\log \mathcal{R}(t)}}$ decay exponentially ($\sim e^{-E_{\text{Th}}t}$) in time [83] in the non-ergodic phase, $1 < \gamma < 2$ (fractal phase). In the ergodic phase ($\gamma < 1$) $\overline{\mathcal{R}(t)} \sim e^{\overline{\log \mathcal{R}(t)}}$ decays algebraically with oscillations. Figure 6.5 shows $\overline{\mathcal{R}(t)}$ in the ergodic phase for the RPRM. In this case we use a projector $\hat{P}_{\Delta E} = \sum_{n \in [(1-\eta)\frac{L}{2}, (1+\eta)\frac{L}{2}]} |E_n\rangle \langle E_n|$ with $0 < \eta < 1$. It is possible to prove that $\overline{\mathcal{R}(t)} \sim e^{\overline{\log \mathcal{R}(t)}} \sim [\sin(\delta Et)] / (\delta Et)^2$ with $\delta E = \frac{\pi}{2} \eta L^{(1-\gamma)/2}$. Finally, Fig. 6.2(b) shows $\overline{\mathcal{R}(t)}$ and $e^{\overline{\log \mathcal{R}(t)}}$ in the fractal critical region. It provides evidence that both $\overline{\mathcal{R}(t)}$ and $e^{\overline{\log \mathcal{R}(t)}}$ decay exponentially in time with the same rate E_{Th} . The same dependence on time for mean and typical implies that their saturation values scale to zero as a function of L in the same manner. Figure 6.2(d)

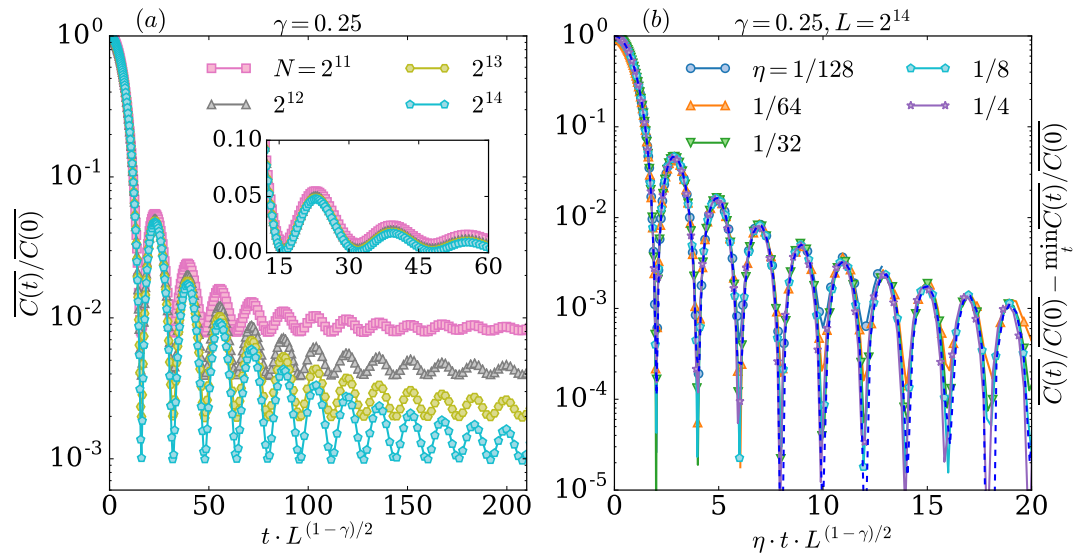


FIGURE 6.5: Panel (a) shows $\overline{\mathcal{R}}(t)$ as a function of time t for the RPRM for several L . The time has been rescaled with L , since in the ergodic phase the energy-band enlarges with L . Moreover, in the quantum evolution as been taken only $\eta = 1/8$ of the total number of states in the middle of the spectrum. Panel (b) shows $\overline{\mathcal{R}}(t) \sim [\sin(\delta Et)/(\delta Et)]^2$ (dashed line) for several η (fraction of eigenstates used in the dynamics).

shows $\overline{\mathcal{R}}_\infty^{-1}$ as a function of $e^{-\log \overline{\mathcal{R}}_\infty}$ for two values of γ , one in the ergodic phase and another in the fractal phase, in both phases $\overline{\mathcal{R}}_\infty^{-1} \sim e^{-\log \overline{\mathcal{R}}_\infty}$.

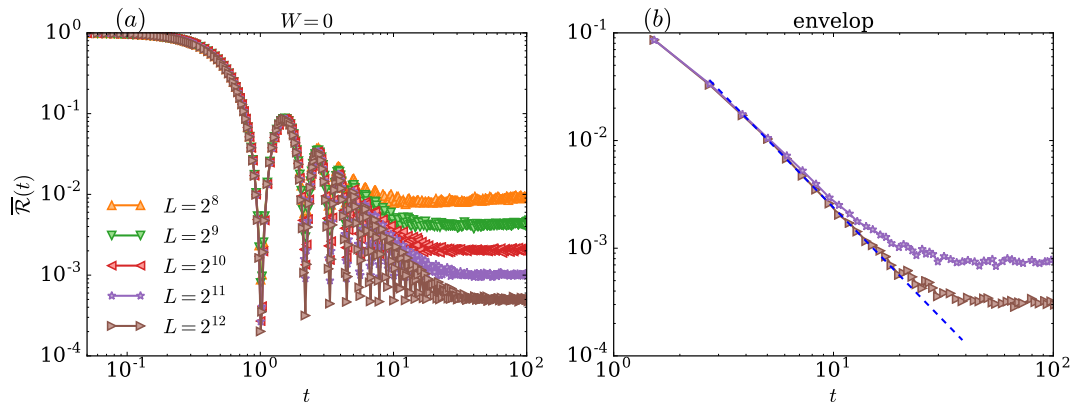


FIGURE 6.6: $\overline{\mathcal{R}}(t)$ for the disorder-free case $W = 0$ for several system sizes, $\overline{\mathcal{R}}(t) \sim t^{-2}$.

6.3 Return probability in a random regular graph

In the previous section we have shown that the difference in the behavior between the mean and the typical value of $\mathcal{R}(t)$ can be used to distinguish ergodic and multifractal

phases. We now study $\mathcal{R}(t)$ in the RRG, where the existence of a multifractal phase is under debate mainly because of the two following issues [82, 145].

1. The existence of a correlation length L_{cor} that diverges approaching the Anderson transition ($L_{\text{cor}} \sim e^{c/\sqrt{W_{AT}-W}}$) [30, 84, 162]. Recently, a different expression for L_{cor} , $L_{\text{cor}} \sim e^{c/(W_{AT}-W)}$ has been proposed [82]. For finite systems of size L smaller than L_{cor} the wavefunctions could share properties of both localized and ergodic states and thus they could be mistakenly classified as multifractal.
2. Even for $L > L_{\text{cor}}$, finite-size corrections for the IPR might be quite strong $\overline{\sum_x |\phi_E(x)|^4} \sim \log(L)^{\tilde{\eta}} L^{-D_2}$, with $\tilde{\eta} \geq 0$. The calculation of D_2 ($D_2 = 1$ for ergodic, $D_2 < 1$ for non-ergodic) is an extremely challenging problem [145].

RRG has a mobility edge, thus in our study we consider only the energies in the middle of the spectrum, choosing $|\Delta E| = 1$, thereby ensuring that all the states $\{\phi_E\}_{E \in \Delta E}$ share the same properties for our choice of the disorder strength W . We perform the time evolution using full diagonalization for small systems sizes $L \leq 2^{14}$, and using the Chebyshev integration technique (Appendix A) for larger $2^{15} \leq L \leq 2^{20}$. The projector $P_{\Delta E}$ has been constructed using full diagonalization for $L \leq 2^{14}$, for larger $2^{15} \leq L \leq 2^{20}$ it is constructed using a truncated Chebyshev expansion (Chapter 5). Figure 6.6 shows the return probability for the free case ($W = 0$), $\overline{\mathcal{R}}(t)$ decays algebraically with time ($\overline{\mathcal{R}}(t) \sim t^{-2}$) and oscillations are present. Instead, Fig. 6.7(a) shows time dependence of the mean of $\mathcal{R}(t)$ for a fixed disorder strength $W = 11$ for several system sizes. In a log-log scale $\overline{\mathcal{R}}(t)$ shows a clear bending which is consistent with a stretched exponential decay $\overline{\mathcal{R}}(t) \sim Ae^{-\Gamma t^\beta}$ (up to possible sub-leading polynomial prefactor). This stretched exponential behavior holds for all values of disorder strength W in the extended phase ($W < W_{AT}$) for $\overline{\mathcal{R}}(t)$, as shown in Fig. 6.7(b). Also the typical value of $\mathcal{R}(t)$ decays like a stretched exponent, $e^{\overline{\log \mathcal{R}(t)}} \sim A_{\text{typ}} e^{-\Gamma_{\text{typ}} t^{\beta_{\text{typ}}}}$, as shown in Fig. 6.7(c). In the considered range of disorder strengths $6 < W < 12$ the stretched exponential parameter β shown in Fig. 6.8(a) decays linearly. The prefactor Γ in front of t^β , Fig. 6.8(b), decays with disorder strength in a different manner. The linear extrapolation of $\beta(W)$ gives reasonable values of the Anderson localization transition W_{AT} , where $\beta(W_{AT}) = 0$, and the small disorder limit $\beta(W \rightarrow 0) = 1$ consistent with works on classical diffusion on the Bethe lattice [27, 36]). Thus, the point $W = 0$ is a singular point (Fig 6.6), for any infinitesimal amount of disorder the return probability will decay exponentially fast with time. It is important to underline that the time scale in which the decay of $\overline{\mathcal{R}}(t)$ can be distinguished from an algebraic decay diverges approaching the Anderson transition *e.g.*, for $W = 14$ the bending in a log-log plot is only visible for $t^* \approx 10^4$ and it requires having system size of $L = 2^{20}$, thus the decay of $\overline{\mathcal{R}}(t)$ for smaller times and smaller

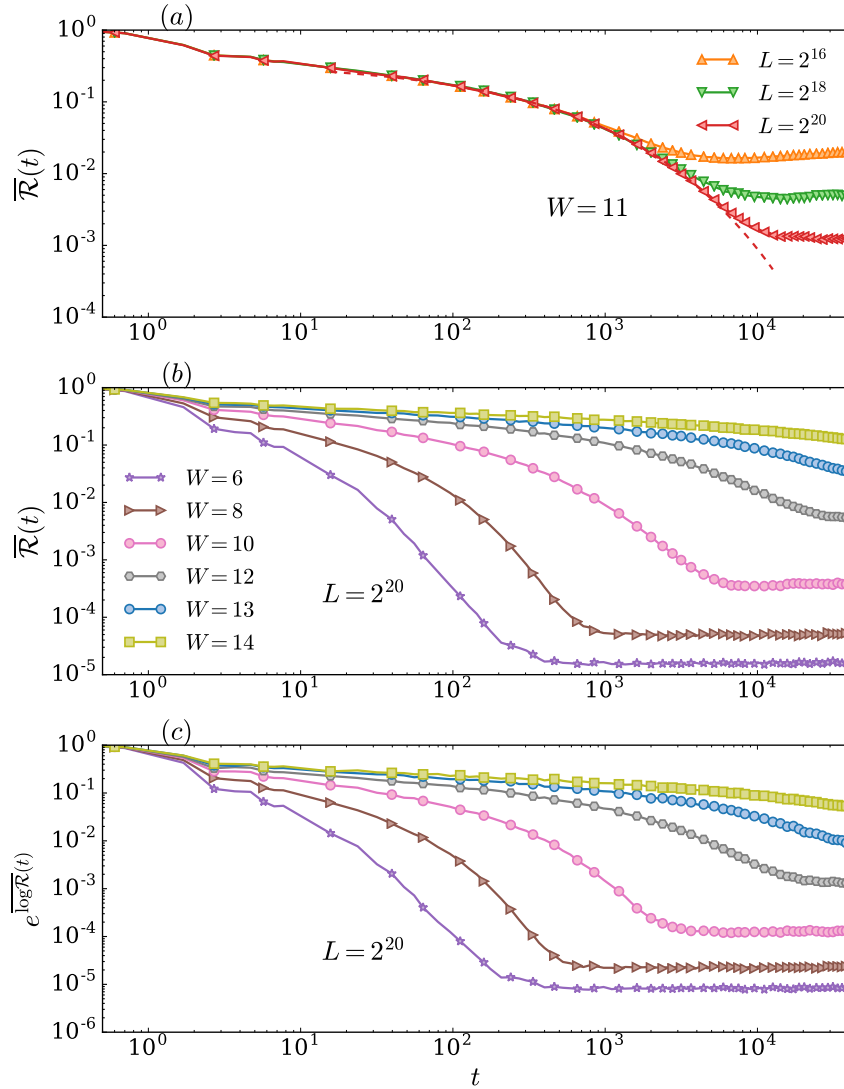


FIGURE 6.7: The Panel (a) shows $\overline{\mathcal{R}}(t)$ as a function of t for the RRG for a fixed disorder strength $W = 11$ and several system sizes $L = 2^{16}, 2^{18}, 2^{20}$. The dashed line has been obtained with a three parameter fit, $\mathcal{R}(t) = Ae^{-\Gamma t^\beta}$. The panel (b) shows $\overline{\mathcal{R}}(t)$ for a fixed system size ($L = 2^{20}$) and for several values of W . The panel (c) shows the typical value $e^{\overline{\log \mathcal{R}}(t)}$ for the same parameters of panel (b).

system sizes could be interpreted as a power law [21]. Moreover, in a recent work [21] it is shown numerically that a possible power law decay of $\overline{\mathcal{R}}(t) \sim t^{-\zeta}$ is consistent with an algebraic dependence of the overlap of different wavefunctions $\mathcal{K}(\omega) \sim \omega^{1-\zeta}$ defined as

$$\mathcal{K}(\omega) = \frac{1}{\mathcal{N}} \overline{\sum_{E, E' \in \Delta E} | \langle x | E \rangle |^2 | \langle E' | x \rangle |^2 \delta(\omega - E + E')} \quad (6.6)$$

with a normalization constant \mathcal{N} ensuring $\int d\omega \mathcal{K}(\omega) = 1$. Indeed, $\overline{\mathcal{R}}(t)$ and $\mathcal{K}(\omega)$ are related by $\overline{\mathcal{R}}(t) \sim \int d\omega \mathcal{K}(\omega) \cos(\omega t)$ [21]. However, using stationary phase approximation it is possible to show that for $\overline{\mathcal{R}}(t) \sim e^{-\Gamma t^\beta}$, the overlap decays as $\mathcal{K}(\omega) \sim \omega^{-\frac{1+(1-\beta)^{-1}}{2}}$

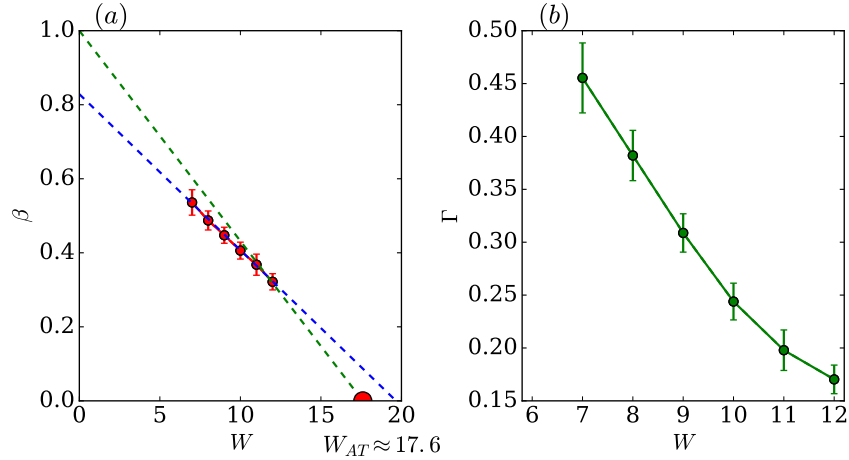


FIGURE 6.8: The parameters (a) β and (b) Γ of stretched exponential fit of the mean survival probability $\overline{\mathcal{R}}(t) \sim Ae^{-\Gamma t^\beta}$ extracted from the data at $L = 2^{18} \dots 2^{20}$.

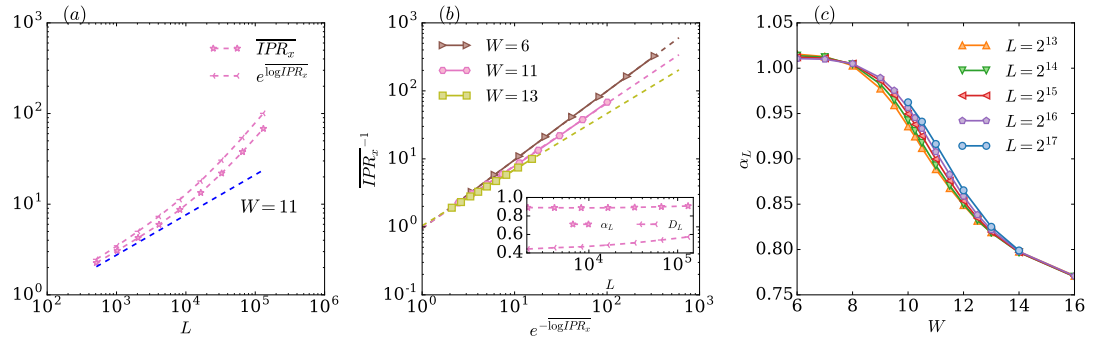


FIGURE 6.9: (a) \overline{IPR}_x and $e^{\overline{\log IPR}_x}$ as a function of L for a fixed disorder strength $W = 11$ for the RRG. (b) \overline{IPR}_x^{-1} as a function of $e^{-\overline{\log IPR}_x}$ ($\overline{IPR}_x \sim e^{-\alpha \overline{\log IPR}_x}$) for several W , each point of the curve indicates a different system size $L = 2^9 - 2^{17}$. (c) Panel shows α_L as a function of W . α_L has been extracted from the linear fitting of $\log \overline{IPR}_x$ versus $\log \overline{\log IPR}_x$ with an enlarging L . Here L indicate the largest system size considered in the fit starting with $L = 2^9$. The inset of panel (b) shows α_L and D_L as a function of L . D_L has been extracted from the linear fitting of $-\log \overline{IPR}_x$ versus $\log(L)$.

for moderately large ω and as $\mathcal{K}(\omega) \sim \omega^{-(1+\beta)}$ for very large ω . As for observed values of $\beta \lesssim 0.5$ the difference between above mentioned exponents is less than 7 %, a stretched exponential behavior for $\overline{\mathcal{R}}(t)$ could be also consistent in the first approximation with a power law behavior of $\mathcal{K}(\omega)$.

Aiming to shed light on the existence of the putative multifractal phase in a RRG, we analyze the dependence of the saturation values $\overline{\mathcal{R}}_\infty = \overline{IPR}_x$ (Eq. 6.5) and $e^{\overline{\log \mathcal{R}}_\infty} \sim e^{\overline{\log IPR}_x}$ on system size L . Due to shorter times, it is difficult to extract the saturation values of $\mathcal{R}(t)$ reliably. Therefore, we find it easier to analyze IPR_x , which has been calculated using a shift-inverse exact diagonalization technique. Figure 6.9(a) shows \overline{IPR}_x and $e^{\overline{\log IPR}_x}$ as a function of L in a log-log scale for fixed disorder strength

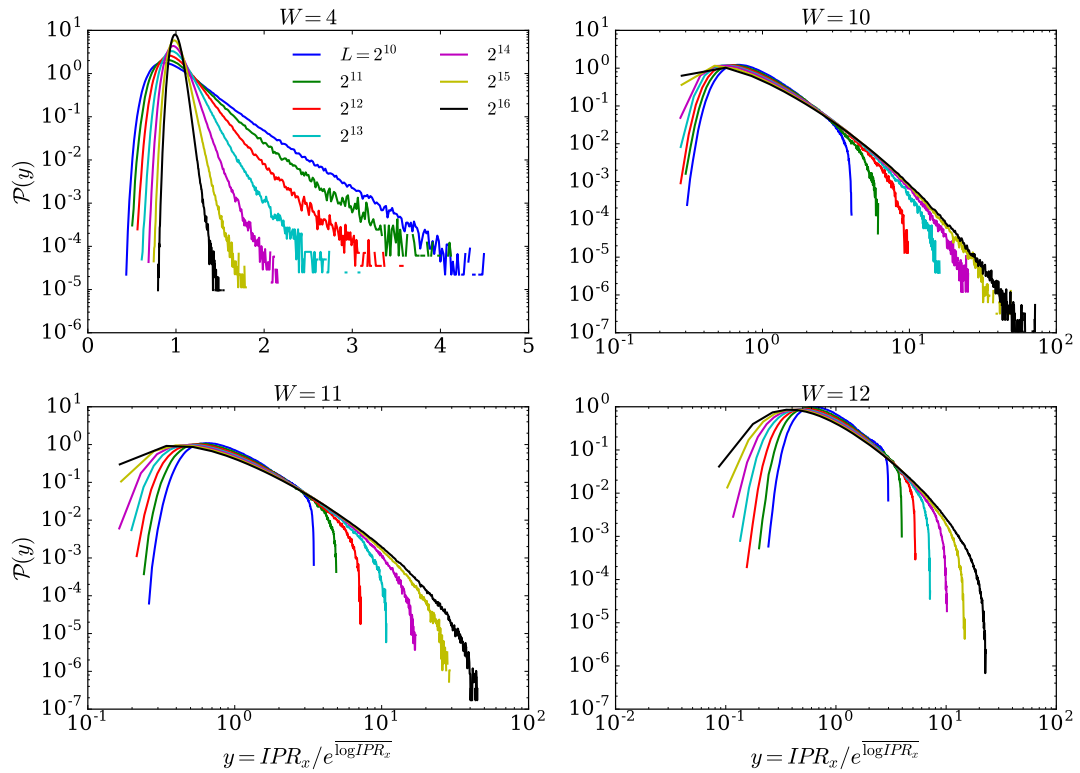


FIGURE 6.10: The Figure shows for four different values of W the probability distribution of the rescaled variable $y = IPR_x / e^{\log IPR_x}$.

$W = 11$. Strong finite-size effects are visible for available systems sizes, which makes the extrapolation of D_2 and D_{typ} nearly impossible. Nevertheless, $\overline{IPR_x}$ and $e^{\log IPR_x}$ seem to suffer from similar finite-size effects. Indeed, plotting $\overline{IPR_x}$ parametrically as a function of $e^{\log IPR_x}$ drastically reduces finite-size effects. Figure 6.9(b) shows $\overline{IPR_x}$ as a function of $e^{\log IPR_x}$ for several values of W , giving indication that $\overline{IPR_x} \sim e^{\alpha \log IPR_x}$. As we have already shown in the ergodic phase $\alpha = 1$, while in a multifractal phase we expect $\alpha = D_2/D_{\text{typ}} < 1$. Using an enlarging linear fitting procedure we are able to extract the exponent α as a function of system size L , α_L , (L here indicate the last system size that has been taken in consideration in the fit starting from $L = 2^9$) and disorder strength. The inset of Fig 6.9(b) shows for $W = 11$ the two exponents D_L and α_L as a function of L , extracted with the same procedure. D_L has a change of 30 % for available system sizes, while α_L changes only by 3 %. Figure 6.9(c) shows α_L for several L as a function of W . For $W < 10$, $\alpha \approx 1$ providing evidence that in this regime the phase is ergodic. For $W > 10 \approx W_{EMT}$, α drops to a smaller value confirming that for available systems sizes the system is not ergodic. The flow of α_L towards unity with increasing L is visible at least for $10 < W < 12$, while for $W > 12$ the data seems to be converged. Nevertheless, it is important to point out that the convergence could be due to finite system size small compared to the correlation length L_{cor} . We can also analyze

the full probability distribution of IPR_x . Figure 6.10 shows the probability distribution $\mathcal{P}(y)$ of the rescaled variable $y = IPR_x / e^{\overline{\log IPR_x}}$. In the ergodic phase $W = 2$, $\mathcal{P}(y)$ shrinks with L , indicating that $\overline{IPR_x} \sim e^{\overline{\log IPR_x}}$. For larger values of W , $\mathcal{P}(y)$ develops long tail (algebraically decaying tails), which is the main requirement to have a different scaling with L between the mean and the typical value.

6.4 Summary

In this chapter, we have studied the quantum dynamics of an initially localized particle in several disordered systems, giving a different characterization of multifractal phases. In particular, we study the return probability $\mathcal{R}(t)$: the quantum probability to return to the initial site. In a multifractal phase, fluctuations over disorder and initial site are so strong that the long-time limit of the mean and typical value of $\mathcal{R}(t)$ scale to zero differently as a function of system size, while in an ergodic phase the scaling is the same. First, we benchmark these ideas in the power-law banded random matrix ensemble. We show that the long-time limit of the mean and typical value of $\mathcal{R}(t)$ scale to zero in the same way in its ergodic regime, while at criticality, where all the states are multifractal, the scaling of these observables differ from each other. Second, we point out, analyzing the Rosenzweig-Porter random matrix model, that this difference in the scaling disappears in the case of only fractal states. Finally, we use this idea to tackle the disordered random regular graph, in which the existence of a multifractal phase is under debate. We present converged data, which could offer numerical evidence for the existence of this multifractal phase. Nevertheless, we discuss that this apparent convergence could also be due to the fact that system sizes are small compared to the correlation length of the system. Furthermore, we show that $\mathcal{R}(t)$ decays with time like a stretched exponential, so far the system is not in the localized phase, and extracted the parameters of this stretched exponential decay.

Part IV

Role of Symmetry and Correlation in the disorder

In the next chapter, we construct a non-interacting fermionic model with correlated disorder and particle-hole symmetry. We show how the interplay between correlated disorder and symmetry can lead the system to have subdiffusive charge propagation, whereas the growth of entanglement is logarithmically slow.

Chapter 7

The generalized Dyson model

We have already discussed that the interplay between interaction and quenched disorder can drive a quantum phase transition even at finite energy density (Chapter 2). Moreover, we have seen in Chapters 2,3, that the interaction creates a dephasing mechanism between degrees of freedom localized in space, generating a slow propagation of information in an MBL phase. Nevertheless, other mechanisms can also break localization in one-dimensional disordered systems. A possible example is the presence of symmetry in the system. It is known that the presence of particle-hole symmetry and disorder in a chain of non-interacting fermions, creates quasi-localized states [141, 161]. As a consequence, these quasi-localized states will produce an anomalous transport in the system. Another possible mechanism to modify the localization properties of a system is to introduce correlation in the disorder. Indeed, correlations between onsite energies can give a proliferation of resonant energies, thus a break down of localization [70]. In this chapter with the aim to understand the interplay between symmetry and correlation in the disorder, we define a model with particle-hole symmetry and correlated disorder. The defined model has two limiting cases, which recover two known models (Dyson I, Dyson II) [49]. We show that the interplay between symmetry and correlation can generate different kinds of transport. Particularly, we show that for this model the transport of particles is subdiffusive but nevertheless the growth of entanglement is logarithmically slow.

7.1 Model and localization length

In this section, we define the model that we study, and we explain several limiting cases. Moreover, we analyze the localization length as a function of the Hamiltonian's parameters.

The Hamiltonian $\hat{\mathcal{H}}$ is the non-interacting fermionic random hopping model, which is defined as,

$$\hat{\mathcal{H}} = - \sum_l [J_{2l-1} \hat{c}_{2l-1}^\dagger \hat{c}_{2l} + J_{2l} \hat{c}_{2l}^\dagger \hat{c}_{2l+1} + \text{h.c.}], \quad (7.1)$$

where $\{\hat{c}_l^\dagger\}$ ($\{\hat{c}_l\}$) are the fermionic creation (annihilation) operators at site l and $\{J_l\}$ are positive random hopping amplitudes. This model has a particle-hole symmetry. The Schrödinger equation for the single-particle modes reads

$$-J_{l-1}\psi_{l-1} - J_{l+1}\psi_{l+1} = E\psi_l, \quad (7.2)$$

and if $\{\psi_l(E)\}$ is a solution of Eq. 7.2 with energy E , then the wavefunction $\{\psi_l(-E) = (-1)^l \psi_l(E)\}$ is also a solution of Eq. 7.2 with energy $-E$.

The Hamiltonian Eq. 7.1 with uncorrelated disorder is called Dyson I model. It has a diverging mean density of states $\rho(E) \sim 1/E \log^3(E)$ as $E \rightarrow 0$ [26, 49, 108], which also leads to a logarithmic divergence in the localization length for $E \rightarrow 0$ [141, 161]. Using the Herbert-Jones-Thouless formulae (Chapter 1)

$$\xi_{loc}(E \rightarrow 0) \sim \lim_{E \rightarrow 0} \int_{-\infty}^{\infty} dE' \frac{\log |E' - E|}{|E'| \log^3 |E'|} \sim \lim_{E \rightarrow 0} \log E. \quad (7.3)$$

In dynamical properties, the quasilocal nature of the state manifests itself in extremely slow propagation of charge [81] ($\sim \log^2 t$) and bipartite entanglement growth $\sim \log(\log(t))$ [35, 152, 160]. Another interesting limiting case is when the random bonds $\{J_l\}$ are independent identically distributed but they appear in identical pairs $(J_1, J_1, J_2, J_2, \dots)$. This model is called Dyson II model [49]. Also in this case, the density of state has the same kind of divergence ($\rho(E) \sim 1/E \log^3(E)$), moreover also in this model the states close to $E = 0$ are anomalous, in the sense that they are delocalized, as we explain later.

We start by investigating the localization length of the model Eq. 7.1 using the transfer matrix technique (Chapter 1). With this aim, we define $\xi_L(E)$ as the localization length of a finite system of size L at energy E . We choose L odd with open boundary condition as it guarantees the existence of a $E = 0$ state due to the sub-lattice symmetry (Eq. 7.2). Nevertheless, due to the divergence in the density of state, the single-particle energy level spacing close to $E = 0$ becomes exponentially small with L , thus even-odd finite-size effect will not affect our result. As we have discussed in Chapter 1, $\xi_L(E = 0)$ can be expressed using the recursion relation between single-particle wavefunction Eq. 1.32 amplitudes as,

$$\xi_L^{-1}(E = 0) = \frac{1}{L} \overline{\log \left| \frac{\psi_{L-1}}{\psi_0} \right|} = \frac{1}{L} \sum_{l=1}^{\frac{L-1}{2}} \overline{\log \left(\frac{J_{2l}}{J_{2l-1}} \right)}, \quad (7.4)$$

where overline denotes the disorder average. For $\{J_l\}$ uncorrelated and equally distributed, *e.g.*, the Dyson I model, the average of the summation in Eq. 7.4 is zero. However, in a typical configuration the sum is divergent with system size L , which indicates that one needs to investigate the full probability distribution of the sequence under the sum rather than just the mean. Using the central limit theorem, it can be shown that the fluctuations grow as \sqrt{L} and therefore $\xi_L(E=0) \sim \sqrt{L}$ [34, 70]. On the contrary, in the presence of dimerization, $J_{2l-1}=J_{2l}$, the Dyson II model, the sum in Eq. 7.4 is zero for *each* configuration. Consequently $\psi_{L-1} = \psi_0$ implying that the $E=0$ state is extended in all samples [161]. With the motivation of interpolating between these two limits of quasilocalized (Dyson I) and extended (Dyson II) $E=0$ states, we choose the random couplings as

$$J_{2l-1} = B_{2l-1}^{(1)} \exp \frac{-\eta_{2l-1} B_{2l-1}^{(2)}}{(2l-1)^\alpha};$$

$$J_{2l} = B_{2l-1}^{(1)} \exp \frac{\eta_{2l} B_{2l}^{(2)}}{(2l)^\alpha},$$

where $B_l^{(1)}, B_l^{(2)}$ are random variables drawn from Gamma distributions with unit mean and variance $1/W_{(1,2)}$ defined as

$$P_W(x) = \frac{W^W}{\Gamma(W)} x^{W-1} e^{-Wx}; \quad x \geq 0, \quad (7.5)$$

where $\Gamma(W)$ is the Gamma function. $\{\eta_l\}$ are independent random variables with the probability distribution function $\tilde{p}(\eta) = p\delta(\eta-1) + (1-p)\delta(\eta+1)$ with $p \in [\frac{1}{2}, 1]$, and $\alpha \geq 0$. We can give few comments:

1. $\{J_l\}$ are short-range correlated random variables and inhomogeneous in space.
2. The inhomogeneity is predominantly in the edge of the sample, while in the bulk it is suppressed.

With this choice of $\{J_l\}$, Eq. 7.4 reduces to

$$\log \left| \frac{\psi_{L-1}}{\psi_0} \right| = \sum_{l=1}^{L-1} \frac{\eta_l B_l^{(2)}}{l^\alpha}. \quad (7.6)$$

In Eq. 7.6, α and p determine the asymptotic behavior of $\xi_L(E=0)$ as the thermodynamic limit is approached and also allows us to change the extension of the $E=0$ state almost continuously.

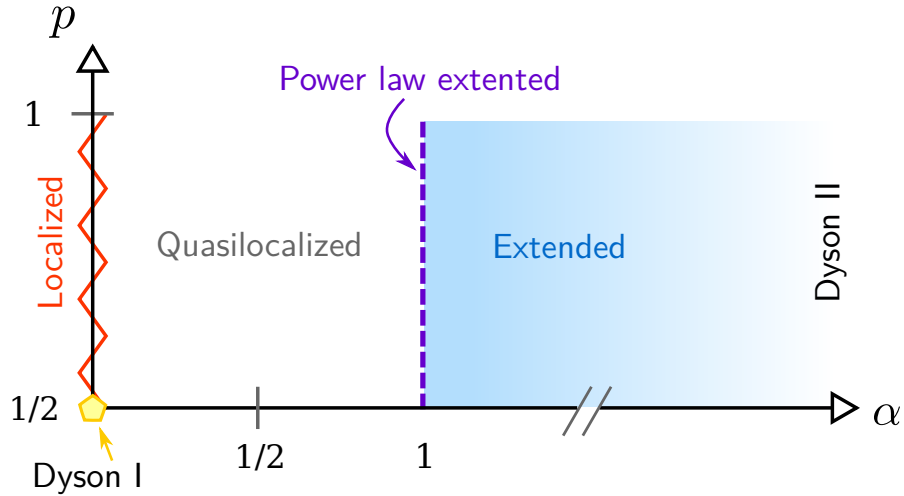


FIGURE 7.1: Phase diagram with regard to the asymptotic behavior of the $E = 0$ state. The regimes denoted by ‘Localized’ (‘Extended’) have localized (extended) $E = 0$ state. For $\alpha = 0$, $p = 1/2$ limit we recover the (uncorrelated) Dyson model and also for $\alpha > 1$, the dimerized Dyson II model is restored. See text for further details of the localization length in Eq. 7.7 and Eq. 7.9.

For $p \neq 1/2$ and $\alpha \geq 0$, averaging over the disorder and approximating the sum in Eq. 7.6 as an integral in the large L limit, we get

$$\xi_L(E = 0) \sim \begin{cases} (2p - 1)^{-1} L^\alpha, & 0 \leq \alpha < 1 \\ (2p - 1)^{-1} L / \log L, & \alpha = 1 \\ (2p - 1)^{-1} L, & \alpha > 1, \end{cases} \quad (7.7)$$

which immediately identifies four distinct regimes. For $\alpha = 0$, $\xi_L(E = 0)$ is finite, which leads to an exponentially localized state. In the range $0 < \alpha < 1$, the localization length diverges algebraically but slower than the system size, which we refer to as a quasilocalized state (see also Fig. 7.1). The logarithmic correction to $\xi_L(E = 0)$ at $\alpha = 1$ produces a polynomial spatial decay of the wavefunction. In the limit $\alpha \rightarrow \infty$, the correlation reveals itself via the dimerization of bonds, $J_{2l-1} = J_{2l}$, which is the Dyson II model with an extended $E = 0$ state.

For $p = 1/2$, the sign η_l appears with equal probability. Therefore, $\xi_L^{-1}(E = 0)$ defined in Eq. 7.4 goes to zero upon taking disorder average. Hence, in order to understand the asymptotic behavior of $\xi_L^{-1}(E = 0)$, we analyze the fluctuations of the sequence $\{\log |\psi_{L-1}/\psi_0|\}$, similar to the Dyson I model as follows. Let A_L be the random variable defined after averaging over $\{B_l^{(2)}\}$ in Eq. 7.6,

$$A_L = \overline{\left[\log \left| \frac{\psi_{L-1}}{\psi_0} \right| \right]} = \sum_{l=1}^{L-1} \frac{\eta_l}{l^\alpha}. \quad (7.8)$$

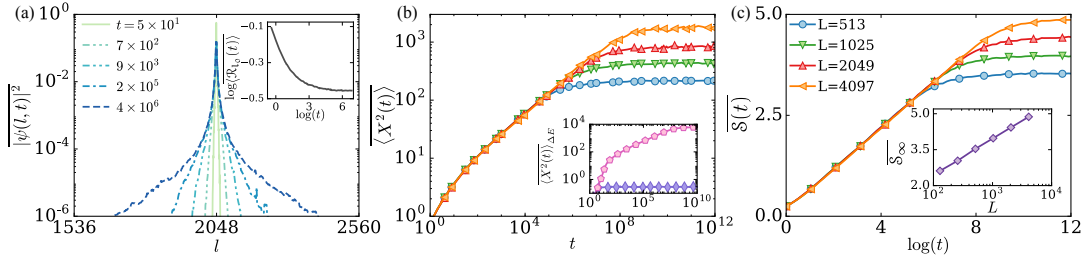


FIGURE 7.2: (a) The disorder averaged wavepacket at different times for the Dyson II model. The central core decays quickly and saturates after initial dynamics; whereas the tail of the distribution keeps spreading with time. Inset shows the return probability for $L = 4097$. (b) The growth of $\overline{X^2(t)}$ with time for $L = \{513, \dots, 4097\}$ in log-log scale. For finite systems it saturates to a value which grows linearly with the system size. Inset shows $\overline{X^2(t)}_{\Delta E}$ with $E = 0$ present in ΔE which grows subdiffusively and absent which saturates, hence confirming that the dynamics is governed by the states close to $E = 0$ ($L = 4097$). (c) The entanglement entropy shows a logarithmic growth in time $\overline{S(t)} \sim \log t$ and the saturation, $\overline{S_\infty}$, grows logarithmically with L as shown in the inset.

A_L is a sum of independent but not identically distributed random variables with zero mean and variance $\sigma_l^2 = 1/l^{2\alpha}$. The *Lyapunov Central Limit theorem* [79] then dictates that the probability distribution of A_L approaches to a Gaussian distribution with zero mean and variance, $\sigma_{A_L}^2 = \sum_{l=1}^{L-1} l^{-2\alpha}$, in the limit $L \rightarrow \infty$. The asymptotic behavior of $\sigma_{A_L}^2$ can then be used to extract the behavior of the localization length,

$$\xi_L(E = 0) \propto \frac{L}{\sigma_{A_L}} \sim \begin{cases} L^{\alpha+1/2}, & 0 \leq \alpha < 1/2 \\ L/\sqrt{\log L}, & \alpha = 1/2 \\ L, & \alpha > 1/2. \end{cases} \quad (7.9)$$

Three qualitatively different regimes can be identified. For $0 \leq \alpha < 1/2$, the localization length diverges algebraically, but slower than the system size. At the $\alpha = 0$, $p = 1/2$ point, we recover the Dyson I model, where the localization length diverges as $\sim \sqrt{L}$ solely due to fluctuations. Finally, for $\alpha > 1/2$, the state is extended with system size. The behavior of $\xi_L(E = 0)$ as a function of α and p is summarized in Fig. 7.1. Importantly, the phase diagram is stable against any local perturbations that do not break the original symmetry of the $\hat{\mathcal{H}}$, because it does not qualitatively change the structure of Eq. 7.4.

7.2 Dynamical properties

In this section we study the dynamical properties of the Hamiltonian $\hat{\mathcal{H}}$ (Eq. 7.1). We have established that the model (Eq. 7.1) with the random couplings Eq. 7.5 hosts several different natures of extended/quasilocalized state at $E = 0$. We now investigate

its effects on dynamical properties. First, we study charge propagation via wavepacket dynamics in the single-particle framework. The initial wavepacket is localized at a single point l_0 in the middle of the chain, $\psi(l, t=0) = \delta_{l,l_0}$. With time it spreads out and its amplitude at the initial site l_0 decays. We monitor the decay of the initial density via the return probability $\langle \mathcal{R}_{l_0}(t) \rangle = |\psi(l_0, t)|^2$ and quantify the spreading of the charge by the disordered average mean-square displacement $\overline{\langle X^2(t) \rangle} = \sum_l l^2 |\overline{\psi(l, t)}|^2 - (\sum_l l |\overline{\psi(l, t)}|)^2$. It is important to note, that the study of the wavepacket analysis is equivalent of the study of the density-density correlator function (Chapter 5)

$$\frac{4}{2L} \text{Tr} \left[\left(\hat{n}_l(t) - \frac{1}{2} \right) \left(\hat{n}_{l_0}(0) - \frac{1}{2} \right) \right] = |\psi(l, t)|^2, \quad (7.10)$$

where $\hat{n}_l = \hat{c}_l^\dagger \hat{c}_l$.

Furthermore, the growth of the bipartite entanglement entropy $S(t) = -\text{Tr}(\rho_L(t) \log(\rho_L(t)))$, between two halves of the system L and R is investigated using standard free fermion techniques (Appendix A), where $\rho_L(t) = \text{Tr}_R(|\psi(t)\rangle\langle\psi(t)|)$ and $|\psi(t=0)\rangle$ is a random product state at half-filling. Under time-evolution, L and R subsystems exchange information leading to the growth of $S(t)$, which is zero at $t = 0$. In our simulations, we use open boundary conditions with $W_1 = 0.4$ and $W_2 = 10$.

7.2.1 Dyson II

We expect that the dynamical properties of these localized systems will be dominated by the properties of the states close to $E = 0$, thus it is expected that the dynamics would be qualitatively different depending on which regime of the phase diagram they belong to. In this section, we focus on the Dyson II model with dimerized hopping. In Fig. 7.2(a) we show the probability distribution of the time dependent wavefunction at different times. At long times only the tail of the wavefunction keeps spreading, while the return probability saturates after an algebraic decay as seen in the inset. Finite $\overline{\langle \mathcal{R}_{l_0}(t) \rangle}$ at long times implies a finite density of exponentially localized states in the energy spectrum.

Fig. 7.2(b) shows the expansion of the width of wavepacket. The linear behavior of the width with time in log-log scale suggests $\overline{\langle X^2(t) \rangle} \sim t^\beta$, where the non-universal exponent β depends on the disorder strength, *e.g.*, $\beta \approx 0.35$ for $W_1 = 0.4$, which implies subdiffusion. For finite systems, the growth saturates, with the saturation value growing linearly with the system size reflecting the spatial extension of the $E = 0$ state Eq. 7.7. Note that due to the diverging nature of the density of states, the dynamics is always going to be dominated by a finite number of states in the vicinity of $E = 0$. We ascertain

this by projecting the initial wavepacket onto eigenstates within an energy window ΔE that includes $E = 0$ and also away from it as $|\psi_0\rangle_{\Delta E} = \hat{P}_{\Delta E}|\psi(l_0, t=0)\rangle$, where $\hat{P}_{\Delta E} = \sum_{E \in \Delta E} |E\rangle\langle E|$ and $|E\rangle$ is the eigenstate. We contrast the two situations by measuring the spread of the wavepacket as $\overline{\langle X^2(t) \rangle}_{\Delta E} = \overline{\langle \psi_0 |_{\Delta E} \hat{X}^2(t) | \psi_0 \rangle_{\Delta E}} - \overline{\langle \psi_0 |_{\Delta E} \hat{X}^2(0) | \psi_0 \rangle_{\Delta E}}$. As seen in Fig. 7.2(b, inset) the spectral decomposed wavepacket with the $E = 0$ state shows a subdiffusive propagation, whereas the wavepacket that has been projected away from the band center quickly saturates as one would expect for localized states.

Fig. 7.2(c) shows the growth of disorder averaged bipartite entanglement $\overline{S(t)}$ starting from a product state. We observe a logarithmic growth of $\overline{S(t)}$ in time, which is slower than the charge transport. For $W_1 = 0.4$ the prefactor of $\log(t)$ is $\approx \ln(2)/3$. In the inset of Fig. 7.2(c) the saturation value of $\overline{S(t)}$ at $t \rightarrow \infty$ ($\overline{S_\infty}$) is plotted in a log-linear scale, which shows logarithmic scaling with system size with a slope $\approx \ln(2)$. The logarithmic scaling of $\overline{S_\infty}$ is similar to entanglement scaling of critical states [148]. Unlike in an interacting localized phase, where entanglement is generated via dephasing due to interaction as we discussed in Chapter 2, here it is due to the extended nature of the $E = 0$ state, which implies that the saturation time of $S(t)$ is proportional to the localization length of the extended state. Note that, there is no qualitative change in our results at higher values of W_1 . Specifically for $W_1 > 1$, when the Gamma distribution Eq 7.5 becomes non-singular at zero, $\overline{\langle X^2(t) \rangle}$ and $\overline{S(t)}$ still show a subdiffusive and logarithmic growth in time respectively. Indeed, Fig. 7.3(top) shows the growth of $\overline{\langle X^2(t) \rangle}$ for the Dyson II model for $W_1 = 0.8$ and $W_1 = 1.2$. For both these values of W_1 , $\overline{\langle X^2(t) \rangle}$ grows algebraically with time ($\overline{\langle X^2(t) \rangle} \sim t^{\beta(W_1)}$), with $\beta(W_1 = 1.2) \approx 0.78$ and $\beta(W_1 = 0.8) \approx 0.59$, showing the subdiffusive dynamics. Fig. 7.3(bottom) shows that the growth of $\overline{S(t)}$ for the Dyson II model with $W_1 = 1.2$. It is still clearly visible that the entanglement growth in time is logarithmic, $\overline{S(t)} \sim \log(t)$.

7.2.2 Generalized Dyson model

For any finite α ($0 \leq \alpha \leq 1$), charge propagation is subdiffusive. The difference for different α is seen in the scaling of the saturation values of $\overline{\langle \mathcal{R}_{l_0, \infty} \rangle}$ and $\overline{\langle X_\infty^2 \rangle}$ with L , as the localization lengths depend on α . Fig. 7.4(a) shows the $t \rightarrow \infty$ value of the width of the wavepacket in a log-log plot as a function of system size. The leading behavior is given by L^α as one would expect from the extended nature of the $E = 0$ eigenstate described in Eq. 7.7. Crudely approximating the $E = 0$ eigenstate, $|\phi_0\rangle$, as a box-function of width $\xi_L(E = 0)$, one finds $\overline{\langle \phi_0 | \hat{X}^2 | \phi_0 \rangle} \propto \xi_L(E = 0)$. Similarly, in

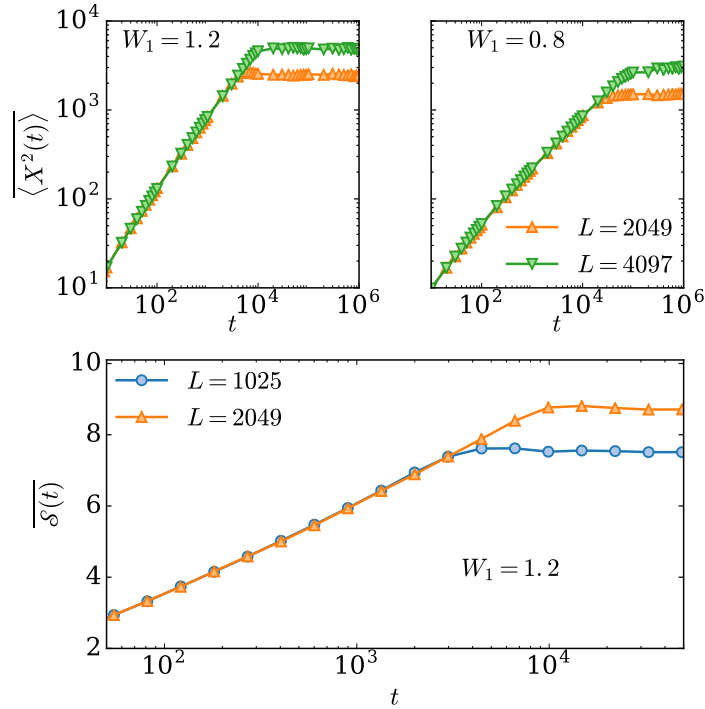


FIGURE 7.3: (Top) The subdiffusive growth of $\langle X^2(t) \rangle$ for the Dyson II model in log-log scale for two different values of W_1 and for two different system sizes $L = 2049, 4097$. (Bottom) Logarithmic growth of $\overline{\mathcal{S}(t)}$ for the Dyson II model for $W_1 = 1.2$ and $L = 1025, 2049$.

Fig. 7.4(b) we show the return probability at $t \rightarrow \infty$, defined as

$$\langle \mathcal{R}_{l_0}(t) \rangle = |\psi(l_0, t)|^2 \xrightarrow{t \rightarrow \infty} \sum_n |\phi_n(l_0)|^4, \quad (7.11)$$

which is the inverse participation ratio (IPR) of the single-particle eigenstates (Chapter 1). Two things are of note:

1. For $0 \leq \alpha \leq 1$, it converges with L , which emphasizes that most of the eigenstates are localized.
2. For $\alpha = 0$, the $\overline{\langle \mathcal{R}_{l_0, \infty} \rangle}$ converges at a different value than other α 's. This can be understood from the following decomposition of inverse participation ratio Eq. 7.11, $\sum_n |\phi_n(l_0)|^4 = \sum_{n < |\Delta E|} |\phi_n(l_0)|^4 + \sum_{n > |\Delta E|} |\phi_n(l_0)|^4$, where ΔE is the window of energies enclosing delocalized states around $E = 0$. Only for $\alpha \neq 0$ the first term in the sum is negligible because of the extended nature of the states within the interval ΔE , however for $\alpha = 0$, $\Delta E = 0$ as all states are localized Eq. 7.7. Therefore, it is expected that $\alpha = 0$ converges at a higher value as seen in Fig. 7.4(b) compared to other α .

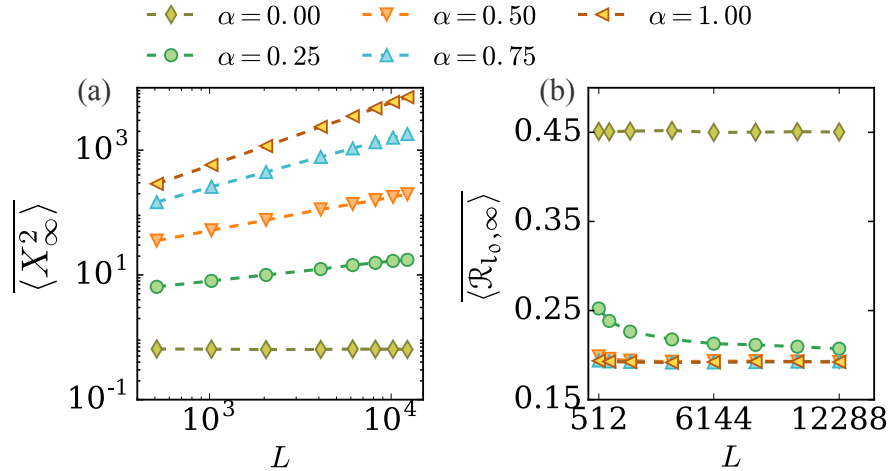


FIGURE 7.4: (a) $\langle X_\infty^2 \rangle$ for different values of α in a log-log scale to highlight the scaling $\propto L^\alpha$ as expected from the localization length calculation Eq. 7.7. (b) The return probability $\langle \mathcal{R}_{l_0, \infty} \rangle$ Eq. 7.11 for different α shows saturation with system size L . Dashed lines are given as guides to the eye.

Fig. 7.5(a) shows the time evolution of $\overline{S(t)}$ for different values of α after a global quench. The data shows a logarithmic growth of entanglement similar to Dyson II. Note that the slope at which $S(t)$ grows is almost independent of α , while the effect of α is clearly visible in the saturation. To highlight the dependence of the saturation with system size we plot $\overline{S_\infty}$ as a function of L in Fig. 7.5(b) in log-linear scale. For $\alpha > 0$ we see a logarithmic increase of $\overline{S_\infty}$ with a slope $\propto \alpha$. This is further confirmed in Fig. 7.5(c), where the saturation of entanglement is plotted as a function of α . The behavior suggests the following form of $S(t)$ with time and system size,

$$\overline{S(t)} \sim \log(t); \quad \overline{S_\infty} \sim \log[\xi_{L,\alpha}(E=0)], \quad (7.12)$$

where $\xi_{L,\alpha}(E=0)$ is the localization length and is $\propto L^\alpha$ (Eq. 7.7). For $\alpha = 0$, $p > 1/2$ the state is exponentially localized and therefore neither charge or entanglement propagate.

7.3 Summary

In summary in this chapter, we have constructed a generalized correlated one-dimensional random bond disorder model and studied its non-equilibrium dynamics. Even though the localization length of the $E = 0$ state is divergent, the state can be quasilocalized or extended and its spatial extent depends on the correlations in disorder. We have shown that the dynamical properties are dominated by the states close to $E = 0$. In all the parameter regimes studied we find subdiffusive transport, while logarithmically slow growth of entanglement. The saturation value of the wavepacket and entanglement

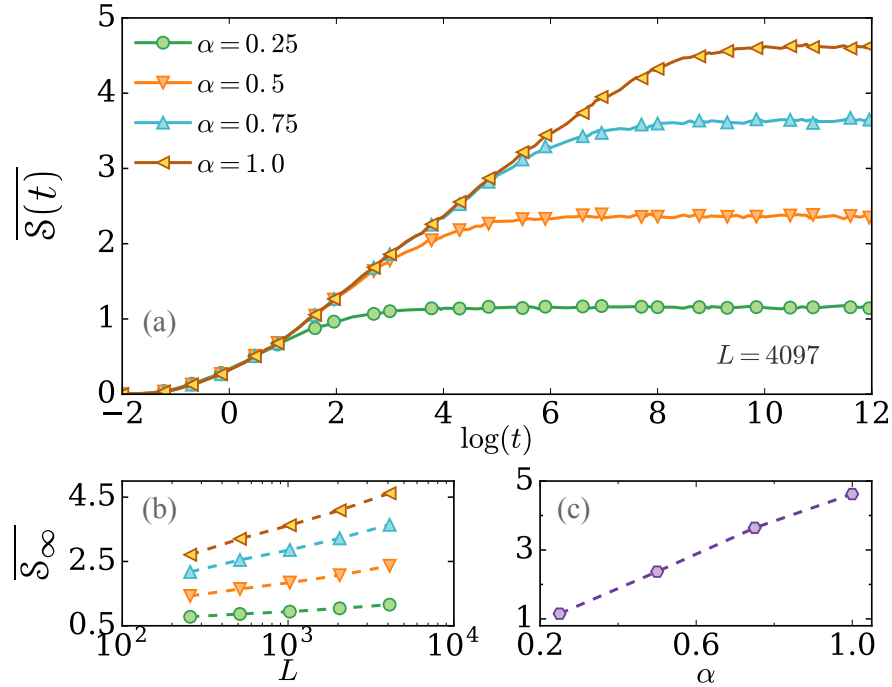


FIGURE 7.5: (a) Dynamics of entanglement for different values of α and $p = 1$ in a log-linear scale after a quench from a product state. The logarithmic growth of $\overline{S}(t)$ is visible for all values of α shown here. (b) The saturation value of $\overline{S}(t)$ at long time behaves as $\log(L)$ for all $\alpha \neq 0$. (c) The entanglement saturation \overline{S}_∞ shows a linear growth with α ($L = 4097$) Eq. 7.12.

depends on the finite-size localization length of the $E = 0$ state. In particular, \overline{S}_∞ grows logarithmically with the localization length of the $E = 0$ state. The scaling behavior is similar to the scaling of S in the excited state of uncorrelated random spin chain in the same universality class [148], except that in our generalized model disorder correlation enters in the \overline{S}_∞ scaling via the finite-size localization length of the $E = 0$ state.

Chapter 8

Conclusions and Outlooks

Understanding the fundamentals of statistical mechanics from the laws of quantum mechanics is one of the most intriguing questions in physics. The common belief that interactions in a quantum many-body system lead to ergodicity has been lately revisited showing the existence of a robust class of systems in which the laws of statistical mechanics break down [17]. Moreover, these systems have a new type of quantum phase transition, which can even happen at finite energy density. This phase transition distinguishes two phases [17, 62]: an ergodic phase which is governed by the laws of thermodynamics and a localized phase in which the degrees of freedom are frozen and thus statistical mechanics breaks down. The existence of a quantum phase transition at finite energy density has revolutionized the point of view of condensed-matter physics, whose previous focus was mainly on understanding low-temperature properties of many-body systems. These results have brought new emphasis and stimulated extensive research on the resulting many-body localization (MBL) [106].

The main focus of this thesis lies on understanding the phenomenon of MBL. We tackle the MBL problem with several methods and from different perspectives, ranging from the study of entanglement properties to the study of more conventional condensed-matter quantities (*e.g.* density-density propagator), including a detailed characterization of time-reversibility in quantum many-body systems. Most of our results have been obtained using numerical techniques, including exact diagonalization, Chebyshev kernel polynomial and transfer matrix techniques. Additionally, we always corroborate and support our analysis with analytical evaluations motivated by physical intuition.

Indeed, one of the main issues, especially in view of recent experiments, has been the possibility to distinguish an MBL phase from a non-interacting localized phase (Anderson insulator, AI). In Chapter 3, we show, using methods borrowed from quantum-information theory, a new way to distinguish an MBL phase from an AI phase. In

particular, we find that the quantum mutual information between two spins following the quantum-dynamics of a state can be used as a dynamical indicator for this distinction. The proposal of this quantity, being in principle measurable in an experimental setup (*e.g.* cold atoms, trapped ions), could give important insights on the interpretation of experimental results [24, 97, 129, 137]. In Chapter 4, with the aim of characterizing time-reversibility in MBL systems, we study the effect of local perturbations on the dynamics of observables. We propose an experimentally measurable quantity (*e.g.* with the use of a quantum gas microscope [14, 134]) which also allows us to distinguish an MBL phase from an AI phase. Moreover, this quantity gives important information on the long-time limit of the dynamics of an MBL system.

We also tackle another important open issue in MBL. Several works pointed out the possible existence of an intermediate phase. The transport in this intermediate phase has been argued to be sub-diffusive, contrary to the expected diffusive behavior of a metal [15, 60, 94, 96, 132, 150]. Moreover, this phase has been characterized to be multifractal, and believed to be explained with the existence of Griffiths regions, in which the transport would be highly suppressed. In Chapter 5, we criticize the existence of this phase. Studying the density-density propagator, including a careful analysis on finite-size effects, we show that the exponents defining the sub-diffusive phase do not converge for available system sizes. Our analysis confirms the existence of a sub-diffusive phase for these sizes, despite leaving open the possibility that diffusivity could be restored in the thermodynamic limit. We also point out that the propagation process is highly non-Gaussian, this could have important consequences for understanding the critical points of an MBL system. Indeed, the propagation of particles in classical glassy systems close to the frozen transition is also non-Gaussian even if the mean square displacement could show diffusive behavior [32, 101, 122, 154]. This analogy could be useful to build up an intuition for the MBL transition, and it could be an interesting future line of research. As we have discussed at several points of this thesis, an MBL problem can be mapped onto an Anderson problem in an effective local tree structure graph (localization in Fock space). In first approximation, due to this mapping, an MBL problem could be seen as an Anderson problem on a random-regular-graph (RRG). Recently, the existence of a multifractal phase has been argued also for the Anderson model on a RRG [7, 41, 57, 82, 145]. Thus, with the aim of understanding the existence of the putative intermediate phase in an MBL system, we also study the intermediate phase in a RRG. In Chapter 6, studying the quantum evolution of an initially localized particle in a RRG, we provide evidence of the possible existence of this multifractal phase. Our findings are more general, in the sense that our methods permit to give a new characterization of multifractal phases that we tested for several different models having critical phase. Nevertheless, it is not clear whether the existence of this phase for a RRG

implies the existence of an intermediate phase for MBL models. Therefore, in Chapter 6, we discuss in detail the main differences between the MBL problem and the RRG. One of the main approximations is to consider uncorrelated on-site energies in a RRG, while in an MBL they are strongly correlated. Thus, a first step could be to introduce in the RRG suitable correlations between on-site energies and try to understand the robustness of this intermediate phase. Moreover, we focus on local probes (survival probability).

It will be interesting to expand our work by studying the full propagation of the wavepacket, as we did for the MBL problem (Chapter 5). Finally, we believe that the existence of an intermediate phase in MBL models is still an open issue, that needs to be better analyzed. Also the phenomenological theory based on the existence of Griffiths [60, 152] phases could be incomplete for the following reasons. First, the probability distribution of the considered quantities is not consistent with the existence of rare regions (*e.g.* no difference between mean value and typical value). Second, the same physics is observed (numerically and experimentally) in a model with a quasi-periodic potential, but for this model rare Griffiths regions are not possible. Thus, a possible way to understand the existence of this intermediate phase could be by using more treatable toy models (*e.g.* RRG with correlated disorder).

The second law of thermodynamics seems to impose strong constraints on the time-reversibility of a natural process. In an MBL phase ergodicity breaks down, and thus a thermodynamic description is not possible anymore, leading to a major question: to what extent does this breaking of ergodicity influence time-reversibility? In Chapter 4, borrowing tools from quantum-chaos (*i.e.* Loschmidt echo), we attempt to answer this question. Our results support the idea that time-irreversibility is more strongly manifested in the ergodic phase than in the localized phase. Moreover, we support our conclusions with analytical approximated calculations, which give a reliable description of the analyzed quantity. As we discussed, an intermediate multifractal phase could exist, and therefore it will be interesting to use these methods to analyze the existence of this multifractal phase for both problems MBL and RRG. Also with the aim to understand how time-irreversibility is influenced in the presence of critical states.

In the last part of the thesis (Chapter 7), we study the interplay between symmetry (particle-hole) and correlated disorder for a non-interacting fermionic model. We construct a model in which we can tune the correlated disorder, showing that the resulting phase diagram is extremely rich. In particular, we study the non-equilibrium quantum dynamics, showing that information can propagate slower than charge. It would be interesting to analyze the presence of particle-hole symmetry in an MBL system and try to understand the effect on its dynamics. Preliminary results, which we have not reported in this thesis, show that in a disordered system composed by two interacting fermions,

the presence of particle-hole symmetry drastically changes the dynamics of the system. In the resulting system all the eigenstates are localized, but nevertheless these two particles can still propagate sub-diffusely through the system. This mechanism is strictly connected with the presence of the particle-hole symmetry and thus with the divergence of the single-particle density of states (Chapter 7). Whether this mechanism persists in the case of a finite density of particles still needs to be elucidated.

Appendix A

Appendix

A.1 Time evolution: Chebyshev expansion

In this part of the Appendix we explain how the quantum-evolution of a system can be performed using the Kernel polynomial techniques [156]. Let $\hat{\mathcal{H}}$ be the Hamiltonian of a quantum system. The idea is to expand the unitary time-evolution using Chebyshev polynomials $\{T_k(x)\}$ and then to truncate the expansion to some order which will bound the absolute error in time done with this approximated method.

$$U(t) \approx e^{-ibt} \sum_{k=0}^N \mu_k T_k(\tilde{\mathcal{H}}); \quad \mu_k = (-i)^k J_k(at), \quad (\text{A.1})$$

where $\tilde{\mathcal{H}} = e^{-it\hat{\mathcal{H}}} \frac{\hat{\mathcal{H}}-b}{a}$ denotes the rescaled Hamiltonian;

$$\begin{aligned} a &= (E_{\max} - E_{\min})/2, \\ b &= (E_{\max} + E_{\min})/2, \end{aligned} \quad (\text{A.2})$$

are the scaling factors and $J_k(x)$ denotes the Bessel function of order k . We typically take $N \gtrsim 2at$ to ensure convergence [155] of the truncated Chebyshev series $(T_k(x))$. Eq. (A.1) only requires sparse matrix multiplications. The iterative scheme scales as $\mathcal{O}(M)$ as compare to exact diagonalization which is $\mathcal{O}(M^3)$, M denoting the dimension of $\hat{\mathcal{H}}$. Therefore, for a chain of interacting spinless fermions, system sizes up to $L = 24$ can be treated for times of the order $\approx 10^3$ (in units of inverse hopping $t = 1.0$ for the interact).

A.2 Bipartite entanglement entropy for non-interacting spinless fermions

Let $\hat{\mathcal{H}}$ be the Hamiltonian of a chain of non-interacting spinless fermions

$$\hat{\mathcal{H}} = \sum_{i,j=1}^L \hat{c}_i^\dagger \Omega_{i,j} \hat{c}_j, \quad (\text{A.3})$$

where the $\{\hat{c}_i^\dagger\}$ ($\{\hat{c}_i\}$) are the creation (annihilation) fermionic operators and $\Omega_{i,j}$ a symmetric matrix with a bounded norm. The aim is to calculate the bipartite entanglement entropy (Chapter 2) (tracing out the portion $[1, \dots, \frac{L}{2}]$ for an eigenstate $|e\rangle$ of $\hat{\mathcal{H}}$). It is possible to prove [112] that the bipartite entanglement entropy is given by

$$S = - \sum_k (\lambda_k) \log(\lambda_k) - \sum_k (1 - \lambda_k) \log(1 - \lambda_k), \quad (\text{A.4})$$

where $\{\lambda_k\}$ are the eigenvalues of the matrix $A_{i,j} = \langle e | \hat{c}_i^\dagger \hat{c}_j | e \rangle$ with $\{i, j\} \in [1, \dots, \frac{L}{2}]$. Finally, the expectation value $\langle e | \hat{c}_i^\dagger \hat{c}_j | e \rangle$ can be calculated using the Wick's theorem [113].

Bibliography

- [1] Abou-Chacra, R., D. J. Thouless, and P. W. Anderson, 1973, Journal of Physics C: Solid State Physics **6**(10), 1734, URL <http://stacks.iop.org/0022-3719/6/i=10/a=009>.
- [2] Adamov, Y., I. V. Gornyi, and A. D. Mirlin, 2003, Phys. Rev. E **67**, 056217, URL <http://link.aps.org/doi/10.1103/PhysRevE.67.056217>.
- [3] Alba, V., 2015, Phys. Rev. B **91**, 155123, URL <https://link.aps.org/doi/10.1103/PhysRevB.91.155123>.
- [4] Alcaraz, F. C., and M. A. Rajabpour, 2013, Phys. Rev. Lett. **111**, 017201, URL <http://link.aps.org/doi/10.1103/PhysRevLett.111.017201>.
- [5] Altshuler, B. L., A. G. Aronov, and D. E. Khmelnitsky, 1982, J. Phys. C: Solid State Phys. **15**(36), 7367, URL <http://stacks.iop.org/0022-3719/15/i=36/a=018>.
- [6] Altshuler, B. L., Y. Gefen, A. Kamenev, and L. S. Levitov, 1997, Phys. Rev. Lett. **78**, 2803, URL <https://link.aps.org/doi/10.1103/PhysRevLett.78.2803>.
- [7] Altshuler, B. L., L. B. Ioffe, and V. E. Kravtsov, 2016, ArXiv e-prints [1610.00758](https://arxiv.org/abs/1610.00758).
- [8] Amico, L., R. Fazio, A. Osterloh, and V. Vedral, 2008, Rev. Mod. Phys. **80**, 517, URL <http://link.aps.org/doi/10.1103/RevModPhys.80.517>.
- [9] Anderson, P. W., 1958, Phys. Rev. **109**, 1492, URL <https://link.aps.org/doi/10.1103/PhysRev.109.1492>.
- [10] Anderson, P. W., 1967, Phys. Rev. Lett. **18**, 1049, URL <https://link.aps.org/doi/10.1103/PhysRevLett.18.1049>.
- [11] Anfossi, A., P. Giorda, A. Montorsi, and F. Traversa, 2005, Phys. Rev. Lett. **95**, 056402, URL <http://link.aps.org/doi/10.1103/PhysRevLett.95.056402>.
- [12] Aubry, S., and G. Andr'e, 1980, Ann. Israel. Phys. Soc. **3**, 133.

- [13] ben Avraham, D., and M. L. Glasser, 2007, Journal of Physics: Condensed Matter **19**(6), 065107, URL <http://stacks.iop.org/0953-8984/19/i=6/a=065107>.
- [14] Bakr, W. S., J. I. Gillen, A. Peng, S. Fölling, and M. Greiner, 2009, Nature **462**, 74 EP , URL <http://dx.doi.org/10.1038/nature08482>.
- [15] Bar Lev, Y., G. Cohen, and D. R. Reichman, 2015, Phys. Rev. Lett. **114**, 100601, URL <http://link.aps.org/doi/10.1103/PhysRevLett.114.100601>.
- [16] Bardarson, J. H., F. Pollmann, and J. E. Moore, 2012, Phys. Rev. Lett. **109**, 017202, URL <http://link.aps.org/doi/10.1103/PhysRevLett.109.017202>.
- [17] Basko, D., I. Aleiner, and B. Altshuler, 2006, Ann. Phys. **321**(5), 1126 , ISSN 0003-4916, URL <http://www.sciencedirect.com/science/article/pii/S0003491605002630>.
- [18] Bauer, B., and C. Nayak, 2013, J. Stat. Mech. Theor. Exp. (09), URL <http://stacks.iop.org/1742-5468/2013/i=09/a=P09005>.
- [19] Beugeling, W., R. Moessner, and M. Haque, 2014, Phys. Rev. E **89**, 042112, URL <https://link.aps.org/doi/10.1103/PhysRevE.89.042112>.
- [20] Beugeling, W., R. Moessner, and M. Haque, 2015, Phys. Rev. E **91**, 012144, URL <https://link.aps.org/doi/10.1103/PhysRevE.91.012144>.
- [21] Biroli, G., and M. Tarzia, 2017, Phys. Rev. B **96**, 201114, URL <https://link.aps.org/doi/10.1103/PhysRevB.96.201114>.
- [22] Bodyfelt, J. D., M. C. Zheng, T. Kottos, U. Kuhl, and H.-J. Stöckmann, 2009, Phys. Rev. Lett. **102**, 253901, URL <http://link.aps.org/doi/10.1103/PhysRevLett.102.253901>.
- [23] Bohigas, O., M. J. Giannoni, and C. Schmit, 1984, Phys. Rev. Lett. **52**, 1, URL <https://link.aps.org/doi/10.1103/PhysRevLett.52.1>.
- [24] Bordia, P., H. P. Lüschen, S. S. Hodgman, M. Schreiber, I. Bloch, and U. Schneider, 2016, Phys. Rev. Lett. **116**, 140401, URL <http://link.aps.org/doi/10.1103/PhysRevLett.116.140401>.
- [25] Bovier, A., 1992, Journal of Physics A: Mathematical and General **25**(5), 1021, URL <http://stacks.iop.org/0305-4470/25/i=5/a=011>.
- [26] Brouwer, P. W., C. Mudry, and A. Furusaki, 2000, Phys. Rev. Lett. **84**, 2913, URL <http://link.aps.org/doi/10.1103/PhysRevLett.84.2913>.
- [27] Cassi, D., 1989, EPL (Europhysics Letters) **9**(7), 627.

- [28] Caux, J.-S., and J. Mossel, 2011, *Journal of Statistical Mechanics: Theory and Experiment* **2011**(02), P02023, URL <http://stacks.iop.org/1742-5468/2011/i=02/a=P02023>.
- [29] Cerruti, N. R., and S. Tomsovic, 2003, *Journal of Physics A: Mathematical and General* **36**(12), 3451, URL <http://stacks.iop.org/0305-4470/36/i=12/a=334>.
- [30] Chalker, J. T., and G. J. Daniell, 1988, *Phys. Rev. Lett.* **61**, 593, URL <https://link.aps.org/doi/10.1103/PhysRevLett.61.593>.
- [31] Chandran, A., I. H. Kim, G. Vidal, and D. A. Abanin, 2015, *Phys. Rev. B* **91**, 085425, URL <https://link.aps.org/doi/10.1103/PhysRevB.91.085425>.
- [32] Chechkin, A. V., F. Seno, R. Metzler, and I. M. Sokolov, 2017, *Phys. Rev. X* **7**, 021002, URL <https://link.aps.org/doi/10.1103/PhysRevX.7.021002>.
- [33] Chen, Y.-X., and S.-W. Li, 2010, *Phys. Rev. A* **81**, 032120, URL <http://link.aps.org/doi/10.1103/PhysRevA.81.032120>.
- [34] Cheraghchi, H., S. M. Fazeli, and K. Esfarjani, 2005, *Phys. Rev. B* **72**, 174207, URL <https://link.aps.org/doi/10.1103/PhysRevB.72.174207>.
- [35] Chiara, G. D., S. Montangero, P. Calabrese, and R. Fazio, 2006, *Journal of Statistical Mechanics: Theory and Experiment* **2006**(03), P03001, URL <http://stacks.iop.org/1742-5468/2006/i=03/a=P03001>.
- [36] Chinta, G., J. Jorgenson, and A. Karlsson, 2015, *Monatshefte für Mathematik* **178**(2), 171.
- [37] Crisanti, A., G. Paladin, and A. Vulpiani, 1993, *Products of Random Matrices in Statistical Physics*, Springer Series in Solid-State Sciences (Springer-Verlag), ISBN 9783540565758, URL <https://books.google.de/books?id=mEcsAAAAYAAJ>.
- [38] Croy, A., Cain, P., and Schreiber, M., 2011, *Eur. Phys. J. B* **82**(2), 107, URL <http://dx.doi.org/10.1140/epjb/e2011-20212-1>.
- [39] Cucchietti, F. M., D. A. R. Dalvit, J. P. Paz, and W. H. Zurek, 2003, *Phys. Rev. Lett.* **91**, 210403, URL <http://link.aps.org/doi/10.1103/PhysRevLett.91.210403>.
- [40] D'Alessio, L., Y. Kafri, A. Polkovnikov, and M. Rigol, 2016, *Advances in Physics* **65**(3), 239, URL <http://dx.doi.org/10.1080/00018732.2016.1198134>.

- [41] De Luca, A., B. L. Altshuler, V. E. Kravtsov, and A. Scardicchio, 2014, Phys. Rev. Lett. **113**, 046806, URL <https://link.aps.org/doi/10.1103/PhysRevLett.113.046806>.
- [42] De Roeck, W., F. Huveneers, M. Müller, and M. Schiulaz, 2016, Phys. Rev. B **93**, 014203, URL <https://link.aps.org/doi/10.1103/PhysRevB.93.014203>.
- [43] Deng, D.-L., J. H. Pixley, X. Li, and S. Das Sarma, 2015, Phys. Rev. B **92**, 220201, URL <http://link.aps.org/doi/10.1103/PhysRevB.92.220201>.
- [44] Derrida, B., and E. Gardner, 1984, J. Phys. France **45**(8), 1283, URL <http://dx.doi.org/10.1051/jphys:019840045080128300>.
- [45] Deutsch, J. M., 1991, Phys. Rev. A **43**, 2046, URL <http://link.aps.org/doi/10.1103/PhysRevA.43.2046>.
- [46] Dóra, B., R. Lundgren, M. Selover, and F. Pollmann, 2016, Phys. Rev. Lett. **117**, 010603, URL <http://link.aps.org/doi/10.1103/PhysRevLett.117.010603>.
- [47] Dóra, B., F. Pollmann, J. Fortágh, and G. Zaránd, 2013, Phys. Rev. Lett. **111**, 046402, URL <http://link.aps.org/doi/10.1103/PhysRevLett.111.046402>.
- [48] Dunlap, D. H., H.-L. Wu, and P. W. Phillips, 1990, Phys. Rev. Lett. **65**, 88, URL <http://link.aps.org/doi/10.1103/PhysRevLett.65.88>.
- [49] Dyson, F. J., 1953, Phys. Rev. **92**, 1331, URL <http://link.aps.org/doi/10.1103/PhysRev.92.1331>.
- [50] Economou, E., 2006, *Green's Functions in Quantum Physics*, Springer Series in Solid-State Sciences (Springer), ISBN 9783540122661, URL <https://books.google.de/books?id=sOgsAAAAYAAJ>.
- [51] Evers, F., and A. D. Mirlin, 2008, Rev. Mod. Phys. **80**, 1355, URL <https://link.aps.org/doi/10.1103/RevModPhys.80.1355>.
- [52] Feenberg, E., 1948, Phys. Rev. **74**, 206, URL <https://link.aps.org/doi/10.1103/PhysRev.74.206>.
- [53] Flamm, D., 1998, ArXiv Physics e-prints [physics/9803005](https://arxiv.org/abs/physics/9803005).
- [54] Fleishman, L., and P. W. Anderson, 1980, Phys. Rev. B **21**, 2366, URL <http://link.aps.org/doi/10.1103/PhysRevB.21.2366>.
- [55] Flores, J. C., and M. Hilke, 1993, Journal of Physics A: Mathematical and General **26**(24), L1255, URL <http://stacks.iop.org/0305-4470/26/i=24/a=002>.

- [56] Furstenberg, H., and H. Kesten, 1960, *Ann. Math. Statist.* **31**(2), 457, URL <https://doi.org/10.1214/aoms/1177705909>.
- [57] García-Mata, I., O. Giraud, B. Georgeot, J. Martin, R. Dubertrand, and G. Lemarié, 2017, *Phys. Rev. Lett.* **118**, 166801, URL <https://link.aps.org/doi/10.1103/PhysRevLett.118.166801>.
- [58] Gol'dshtein, I. Y., S. A. Molchanov, and L. A. Pastur, 1977, *Funct. Anal. Appl.* **11**(1), 1, ISSN 1573-8485.
- [59] Goold, J., C. Gogolin, S. R. Clark, J. Eisert, A. Scardicchio, and A. Silva, 2015, *Phys. Rev. B* **92**, 180202, URL <http://link.aps.org/doi/10.1103/PhysRevB.92.180202>.
- [60] Gopalakrishnan, S., K. Agarwal, E. A. Demler, D. A. Huse, and M. Knap, 2016, *Phys. Rev. B* **93**, 134206, URL <https://link.aps.org/doi/10.1103/PhysRevB.93.134206>.
- [61] Gorin, T., T. Prosen, T. H. Seligman, and M. nidari, 2006, *Physics Reports* **435**(25), 33, ISSN 0370-1573, URL <http://www.sciencedirect.com/science/article/pii/S0370157306003310>.
- [62] Gornyi, I. V., A. D. Mirlin, and D. G. Polyakov, 2005, *Phys. Rev. Lett.* **95**, 206603, URL <http://link.aps.org/doi/10.1103/PhysRevLett.95.206603>.
- [63] Goussev, A., R. A. Jalabert, H. M. Pastawski, and D. Wisniacki, 2012, *ArXiv e-prints* **1206.6348**.
- [64] Haake, F., 2006, *Quantum Signatures of Chaos* (Springer-Verlag New York, Inc., Secaucus, NJ, USA), ISBN 3540677232.
- [65] Herbert, D. C., and R. Jones, 1971, *Journal of Physics C: Solid State Physics* **4**(10), 1145, URL <http://stacks.iop.org/0022-3719/4/i=10/a=023>.
- [66] Huang, Y., and J. E. Moore, 2014, *Phys. Rev. B* **90**, 220202, URL <http://link.aps.org/doi/10.1103/PhysRevB.90.220202>.
- [67] Imbrie, J. Z., 2016, *Communications in Mathematical Physics* **341**(2), 491, ISSN 1432-0916, URL <https://doi.org/10.1007/s00220-015-2522-6>.
- [68] Imbrie, J. Z., 2016, *Journal of Statistical Physics* **163**(5), 998, ISSN 1572-9613, URL <http://dx.doi.org/10.1007/s10955-016-1508-x>.
- [69] Islam, R., R. Ma, P. M. Preiss, M. Eric Tai, A. Lukin, M. Rispoli, and M. Greiner, 2015, *Nature* **528**(7580), 77, ISSN 0028-0836, URL <http://dx.doi.org/10.1038/nature15750>.

- [70] Izrailev, F., A. Krokhin, and N. Makarov, 2012, *Physics Reports* **512**(3), 125 , ISSN 0370-1573, URL <http://www.sciencedirect.com/science/article/pii/S0370157311002936>.
- [71] Izrailev, F. M., and A. A. Krokhin, 1999, *Phys. Rev. Lett.* **82**, 4062, URL <http://link.aps.org/doi/10.1103/PhysRevLett.82.4062>.
- [72] Jacquod, P., P. Silvestrov, and C. Beenakker, 2001, *Phys. Rev. E* **64**, 055203, URL <http://link.aps.org/doi/10.1103/PhysRevE.64.055203>.
- [73] Karahalios, A., A. Metavitsiadis, X. Zotos, A. Gorczyca, and P. Prelovšek, 2009, *Phys. Rev. B* **79**, 024425, URL <https://link.aps.org/doi/10.1103/PhysRevB.79.024425>.
- [74] Karbach, M., and G. Muller, 1998, eprint arXiv:cond-mat/9809162 [cond-mat/9809162](https://arxiv.org/abs/cond-mat/9809162).
- [75] Ketzmerick, R., K. Kruse, S. Kraut, and T. Geisel, 1997, *Phys. Rev. Lett.* **79**, 1959, URL <https://link.aps.org/doi/10.1103/PhysRevLett.79.1959>.
- [76] Khemani, V., R. Nandkishore, and S. L. Sondhi, 2015, *Nat Phys* **11**(7), 560, ISSN 1745-2473, article, URL <http://dx.doi.org/10.1038/nphys3344>.
- [77] Khemani, V., F. Pollmann, and S. L. Sondhi, 2016, *Phys. Rev. Lett.* **116**, 247204, URL <http://link.aps.org/doi/10.1103/PhysRevLett.116.247204>.
- [78] Kinoshita, T., T. Wenger, and D. S. Weiss, 2006, *Nature* **440**, 900 EP , URL <http://dx.doi.org/10.1038/nature04693>.
- [79] Koralov, L., and Y. G. Sinai, 2007, *Theory of probability and random processes* (Springer Science and Business Media).
- [80] Kramer, B., and A. MacKinnon, 1993, *Rep. Prog. in Phys.* **56**(12), 1469, URL <http://stacks.iop.org/0034-4885/56/i=12/a=001>.
- [81] Krapivsky, P. L., and J. M. Luck, 2011, *Journal of Statistical Mechanics: Theory and Experiment* **2011**(02), P02031, URL <http://stacks.iop.org/1742-5468/2011/i=02/a=P02031>.
- [82] Kravtsov, V., B. Altshuler, and L. Ioffe, 2018, *Annals of Physics* **389**, 148 , ISSN 0003-4916, URL <http://www.sciencedirect.com/science/article/pii/S0003491617303652>.
- [83] Kravtsov, V. E., I. M. Khaymovich, E. Cuevas, and M. Amini, 2015, *New Journal of Physics* **17**(12), 122002, URL <http://stacks.iop.org/1367-2630/17/i=12/a=122002>.

- [84] Kravtsov, V. E., and K. A. Muttalib, 1997, Phys. Rev. Lett. **79**, 1913, URL <https://link.aps.org/doi/10.1103/PhysRevLett.79.1913>.
- [85] Kuhl, U., F. M. Izrailev, and A. A. Krokhin, 2008, Phys. Rev. Lett. **100**, 126402, URL <http://link.aps.org/doi/10.1103/PhysRevLett.100.126402>.
- [86] Landau, L., E. Lifshits, J. Sykes, and J. Bell, 1976, *Mechanics*, Butterworth-Heinemann (Butterworth-Heinemann), ISBN 9780750628969, URL <https://books.google.de/books?id=e-xASAehg1sC>.
- [87] Landauer, R., 1970, Philos. Mag. **21**, 863.
- [88] Lev, Y. B., D. M. Kennes, C. Klckner, D. R. Reichman, and C. Karrasch, 2017, EPL (Europhysics Letters) **119**(3), 37003, URL <http://stacks.iop.org/0295-5075/119/i=3/a=37003>.
- [89] Lev, Y. B., and D. R. Reichman, 2016, EPL (Europhysics Letters) **113**(4), 46001, URL <http://stacks.iop.org/0295-5075/113/i=4/a=46001>.
- [90] Levitov, L. S., 1990, Phys. Rev. Lett. **64**, 547, URL <https://link.aps.org/doi/10.1103/PhysRevLett.64.547>.
- [91] Levstein, P. R., G. Usaj, and H. M. Pastawski, 1998, The Journal of Chemical Physics **108**(7), 2718.
- [92] Lifshits, I., S. Gredeskul, and L. Pastur, 1988, *Introduction to the theory of disordered systems*, A Wiley Interscience publication (Wiley), ISBN 9780471875338, URL <https://books.google.de/books?id=B6nvAAAAMAAJ>.
- [93] Luca, A. D., and A. Scardicchio, 2013, EPL **101**(3), 37003, URL <http://stacks.iop.org/0295-5075/101/i=3/a=37003>.
- [94] Luitz, D. J., and Y. Bar Lev, 2016, Phys. Rev. Lett. **117**, 170404, URL <https://link.aps.org/doi/10.1103/PhysRevLett.117.170404>.
- [95] Luitz, D. J., N. Laflorencie, and F. Alet, 2015, Phys. Rev. B **91**, 081103, URL <http://link.aps.org/doi/10.1103/PhysRevB.91.081103>.
- [96] Luitz, D. J., N. Laflorencie, and F. Alet, 2016, Phys. Rev. B **93**, 060201, URL <http://link.aps.org/doi/10.1103/PhysRevB.93.060201>.
- [97] Lüschen, H. P., P. Bordia, S. Scherg, F. Alet, E. Altman, U. Schneider, and I. Bloch, 2017, Phys. Rev. Lett. **119**, 260401, URL <https://link.aps.org/doi/10.1103/PhysRevLett.119.260401>.

- [98] Matsuda, H., 2000, Phys. Rev. E **62**, 3096, URL <http://link.aps.org/doi/10.1103/PhysRevE.62.3096>.
- [99] Matsuda, H., K. Kudo, R. Nakamura, O. Yamakawa, and T. Murata, 1996, Int. J. Theor. Phys. **35**(4), 839, ISSN 1572-9575, URL <http://dx.doi.org/10.1007/BF02330576>.
- [100] Melko, R. G., A. B. Kallin, and M. B. Hastings, 2010, Phys. Rev. B **82**, 100409, URL <http://link.aps.org/doi/10.1103/PhysRevB.82.100409>.
- [101] Metzler, R., 2017, Biophysical Journal **112**(3), 413 , ISSN 0006-3495, URL <http://www.sciencedirect.com/science/article/pii/S0006349516343235>.
- [102] Mirlin, A. D., and F. Evers, 2000, Phys. Rev. B **62**, 7920, URL <https://link.aps.org/doi/10.1103/PhysRevB.62.7920>.
- [103] Mirlin, A. D., Y. V. Fyodorov, F.-M. Dittes, J. Quezada, and T. H. Seligman, 1996, Phys. Rev. E **54**, 3221, URL <https://link.aps.org/doi/10.1103/PhysRevE.54.3221>.
- [104] Mondaini, R., and M. Rigol, 2017, Phys. Rev. E **96**, 012157, URL <https://link.aps.org/doi/10.1103/PhysRevE.96.012157>.
- [105] Mott, N., and W. Twose, 1961, Adv. in Phys. **10**(38), 107.
- [106] Nandkishore, R., and D. A. Huse, 2015, Annual Review of Condensed Matter Physics **6**(1), 15, URL <https://doi.org/10.1146/annurev-conmatphys-031214-014726>.
- [107] Oganesyan, V., and D. A. Huse, 2007, Phys. Rev. B **75**, 155111, URL <https://link.aps.org/doi/10.1103/PhysRevB.75.155111>.
- [108] Ovchinnikov, A., and N. Erikhman, 1977, JETP **46**, 340, URL <http://www.jetp.ac.ru/cgi-bin/e/index/e/46/2/p340?a=list>.
- [109] Page, D. N., 1993, Phys. Rev. Lett. **71**, 1291, URL <https://link.aps.org/doi/10.1103/PhysRevLett.71.1291>.
- [110] Pal, A., and D. A. Huse, 2010, Phys. Rev. B **82**, 174411, URL <http://link.aps.org/doi/10.1103/PhysRevB.82.174411>.
- [111] Peres, A., 1984, Phys. Rev. A **30**, 1610, URL <http://link.aps.org/doi/10.1103/PhysRevA.30.1610>.
- [112] Peschel, I., and V. Eisler, 2009, J. Phys. A **42**(50), 504003, URL <http://stacks.iop.org/1751-8121/42/i=50/a=504003>.

- [113] Peskin, M. E., and D. V. Schroeder, 1995, *An Introduction to quantum field theory* (Addison-Wesley, Reading, USA), ISBN 9780201503975, 0201503972, URL <http://www.slac.stanford.edu/~mpeskin/QFT.html>.
- [114] Pichard, J. L., 1986, *Journal of Physics C: Solid State Physics* **19**(10), 1519, URL <http://stacks.iop.org/0022-3719/19/i=10/a=009>.
- [115] Pollmann, F., S. Mukerjee, A. G. Green, and J. E. Moore, 2010, *Phys. Rev. E* **81**, 020101, URL <http://link.aps.org/doi/10.1103/PhysRevE.81.020101>.
- [116] P.W.Anderson, 1977, Nobel lectures, URL http://www.nobelprize.org/nobel_organizations/nobelfoundation/publications/lectures/index.html.
- [117] Rademaker, L., M. Ortuno, and A. M. Somoza, 2016, ArXiv e-prints [1610.06238](https://arxiv.org/abs/1610.06238).
- [118] Raghunathan, M. S., 1979, *Israel Journal of Mathematics* **32**(4), 356, ISSN 1565-8511, URL <https://doi.org/10.1007/BF02760464>.
- [119] Reif, F., 2009, *Fundamentals of Statistical and Thermal Physics*, McGraw-Hill series in fundamentals of physics (Waveland Press), ISBN 9781577666127, URL <https://books.google.de/books?id=gYpBPgAACAAJ>.
- [120] Rigol, M., 2016, *Phys. Rev. Lett.* **116**, 100601, URL <https://link.aps.org/doi/10.1103/PhysRevLett.116.100601>.
- [121] del Rio, R., S. Jitomirskaya, Y. Last, and B. Simon, 1995, *Phys. Rev. Lett.* **75**, 117, URL <https://link.aps.org/doi/10.1103/PhysRevLett.75.117>.
- [122] Roldan-Vargas, S., L. Rovigatti, and F. Sciortino, 2017, *Soft Matter* **13**, 514, URL <http://dx.doi.org/10.1039/C6SM02282K>.
- [123] Ros, V., M. Mller, and A. Scardicchio, 2015, *Nuclear Physics B* **891**, 420 , ISSN 0550-3213, URL <http://www.sciencedirect.com/science/article/pii/S0550321314003836>.
- [124] Rosenzweig, N., and C. E. Porter, 1960, *Phys. Rev.* **120**, 1698, URL <https://link.aps.org/doi/10.1103/PhysRev.120.1698>.
- [125] Roy, D., R. Singh, and R. Moessner, 2015, *Phys. Rev. B* **92**, 180205, URL <http://link.aps.org/doi/10.1103/PhysRevB.92.180205>.
- [126] Sakurai, J. J., 1994, *Modern quantum mechanics; rev. ed.* (Addison-Wesley, Reading, MA), URL <https://cds.cern.ch/record/1167961>.
- [127] Santos, L. F., and M. Rigol, 2010, *Phys. Rev. E* **82**, 031130, URL <https://link.aps.org/doi/10.1103/PhysRevE.82.031130>.

- [128] Scardicchio, A., and T. Thiery, 2017, ArXiv e-prints [1710.01234](https://arxiv.org/abs/1710.01234).
- [129] Schreiber, M., S. S. Hodgman, P. Bordia, H. P. Lüschen, M. H. Fischer, R. Vosk, E. Altman, U. Schneider, and I. Bloch, 2015, *Science* **349**(6250), 842, ISSN 0036-8075.
- [130] Serbyn, M., Z. Papić, and D. A. Abanin, 2013, *Phys. Rev. Lett.* **110**, 260601, URL <http://link.aps.org/doi/10.1103/PhysRevLett.110.260601>.
- [131] Serbyn, M., Z. Papić, and D. A. Abanin, 2014, *Phys. Rev. B* **90**, 174302, URL <http://link.aps.org/doi/10.1103/PhysRevB.90.174302>.
- [132] Serbyn, M., Z. Papić, and D. A. Abanin, 2017, *Phys. Rev. B* **96**, 104201, URL <https://link.aps.org/doi/10.1103/PhysRevB.96.104201>.
- [133] Serbyn, M., M. Knap, S. Gopalakrishnan, Z. Papić, N. Y. Yao, C. R. Laumann, D. A. Abanin, M. D. Lukin, and E. A. Demler, 2014, *Phys. Rev. Lett.* **113**, 147204, URL <http://link.aps.org/doi/10.1103/PhysRevLett.113.147204>.
- [134] Sherson, J. F., C. Weitenberg, M. Endres, M. Cheneau, I. Bloch, and S. Kuhr, 2010, *Nature* **467**, 68 EP , URL <http://dx.doi.org/10.1038/nature09378>.
- [135] Singh, R., J. H. Bardarson, and F. Pollmann, 2016, *New J. Phys.* **18**(2), 023046, URL <http://stacks.iop.org/1367-2630/18/i=2/a=023046>.
- [136] Singh, R. R. P., M. B. Hastings, A. B. Kallin, and R. G. Melko, 2011, *Phys. Rev. Lett.* **106**, 135701, URL <http://link.aps.org/doi/10.1103/PhysRevLett.106.135701>.
- [137] Smith, J., A. Lee, P. Richerme, B. Neyenhuis, P. W. Hess, P. Hauke, M. Heyl, D. A. Huse, and C. Monroe, 2016, *Nat. Phys.* **advance online publication**, ISSN 1745-2481, letter, URL <http://dx.doi.org/10.1038/nphys3783>.
- [138] Srednicki, M., 1994, *Phys. Rev. E* **50**, 888, URL <http://link.aps.org/doi/10.1103/PhysRevE.50.888>.
- [139] Steinigeweg, R., J. Herbrych, F. Pollmann, and W. Brenig, 2016, *Phys. Rev. B* **94**, 180401, URL <https://link.aps.org/doi/10.1103/PhysRevB.94.180401>.
- [140] Stéphan, J.-M., 2014, *Phys. Rev. B* **90**, 045424, URL <http://link.aps.org/doi/10.1103/PhysRevB.90.045424>.
- [141] Theodorou, G., and M. H. Cohen, 1976, *Phys. Rev. B* **13**, 4597, URL <http://link.aps.org/doi/10.1103/PhysRevB.13.4597>.

- [142] Thouless, D. J., 1970, *Journal of Physics C: Solid State Physics* **3**(7), 1559, URL <http://stacks.iop.org/0022-3719/3/i=7/a=012>.
- [143] Thouless, D. J., 1972, *Journal of Physics C: Solid State Physics* **5**(1), 77, URL <http://stacks.iop.org/0022-3719/5/i=1/a=010>.
- [144] Tikhonov, K. S., and A. D. Mirlin, 2016, *Phys. Rev. B* **94**, 184203, URL <https://link.aps.org/doi/10.1103/PhysRevB.94.184203>.
- [145] Tikhonov, K. S., A. D. Mirlin, and M. A. Skvortsov, 2016, *Phys. Rev. B* **94**, 220203, URL <https://link.aps.org/doi/10.1103/PhysRevB.94.220203>.
- [146] Um, J., H. Park, and H. Hinrichsen, 2012, *J. Stat. Mech. Theor. Exp.* **2012**(10), P10026, URL <http://stacks.iop.org/1742-5468/2012/i=10/a=P10026>.
- [147] Van Tiggelen, B. A., 1999, *Localization of Waves* (Springer Netherlands, Dordrecht), ISBN 978-94-011-4572-5, pp. 1–60, URL https://doi.org/10.1007/978-94-011-4572-5_1.
- [148] Vasseur, R., A. C. Potter, and S. A. Parameswaran, 2015, *Phys. Rev. Lett.* **114**, 217201, URL <http://link.aps.org/doi/10.1103/PhysRevLett.114.217201>.
- [149] Žnidarič, M., T. c. v. Prosen, and P. Prelovšek, 2008, *Phys. Rev. B* **77**, 064426, URL <http://link.aps.org/doi/10.1103/PhysRevB.77.064426>.
- [150] Žnidarič, M., A. Scardicchio, and V. K. Varma, 2016, *Phys. Rev. Lett.* **117**, 040601, URL <https://link.aps.org/doi/10.1103/PhysRevLett.117.040601>.
- [151] Vojta, T., 2013, in *American Institute of Physics Conference Series*, edited by A. Avella and F. Mancini, volume 1550 of *American Institute of Physics Conference Series*, pp. 188–247, [1301.7746](https://doi.org/10.1063/1.3631746).
- [152] Vosk, R., and E. Altman, 2013, *Phys. Rev. Lett.* **110**, 067204, URL <http://link.aps.org/doi/10.1103/PhysRevLett.110.067204>.
- [153] Wahl, T. B., A. Pal, and S. H. Simon, 2017, *Phys. Rev. X* **7**, 021018, URL <https://link.aps.org/doi/10.1103/PhysRevX.7.021018>.
- [154] Wang, B., S. M. Anthony, S. C. Bae, and S. Granick, 2009, *Proceedings of the National Academy of Sciences* **106**(36), 15160, ISSN 0027-8424, URL <http://www.pnas.org/content/106/36/15160>.
- [155] Weiße, A., and H. Fehske, 2008, *Computational Many-Particle Physics*, volume 739 of *Lecture Notes in Physics* (Springer Berlin Heidelberg, Berlin, Heidelberg), ISBN 978-3-540-74685-0, URL <http://link.springer.com/10.1007/978-3-540-74686-7>.

-
- [156] Weiße, A., G. Wellein, A. Alvermann, and H. Fehske, 2006, Reviews of Modern Physics **78**(1), 275, ISSN 0034-6861, URL <http://link.aps.org/doi/10.1103/RevModPhys.78.275>.
- [157] Wilms, J., J. Vidal, F. Verstraete, and S. Dusuel, 2012, J. Stat. Mech. Theor. Exp. (01), URL <http://stacks.iop.org/1742-5468/2012/i=01/a=P01023>.
- [158] Wolf, M. M., F. Verstraete, M. B. Hastings, and J. I. Cirac, 2008, Phys. Rev. Lett. **100**, 070502, URL <http://link.aps.org/doi/10.1103/PhysRevLett.100.070502>.
- [159] Yu, X., D. Pekker, and B. K. Clark, 2017, Phys. Rev. Lett. **118**, 017201, URL <https://link.aps.org/doi/10.1103/PhysRevLett.118.017201>.
- [160] Zhao, Y., F. Andraschko, and J. Sirker, 2016, ArXiv e-prints [1602.04380](https://arxiv.org/abs/1602.04380).
- [161] Ziman, T. A. L., 1982, Phys. Rev. Lett. **49**, 337, URL <http://link.aps.org/doi/10.1103/PhysRevLett.49.337>.
- [162] Zirnbauer, M. R., 1986, Phys. Rev. B **34**, 6394, URL <https://link.aps.org/doi/10.1103/PhysRevB.34.6394>.

Erklärung

Hiermit versichere ich, dass ich die vorliegende Arbeit ohne unzuläige Hilfe Dritter und ohne Benutzung anderer als der angegebenen Hilfsmittel angefertigt habe; die aus fremden Quellen direkt oder indirekt bernommenen Gedanken sind als solche kenntlich gemacht. Die Arbeit wurde bisher weder im Inland noch im Ausland in gleicher oder hnlicher Form einer anderen Prüfungsbehörde vorgelegt. Diese Arbeit wurde unter der wissenschaftlichen Betreuung von Prof. Dr. Roderich Moessner am Max-Planck Institut für Physik komplexer Systeme in Dresden angefertigt. Ich erkläre hiermit, dass keine früheren erfolglosen Promotionsverfahren stattgefunden haben. Ich erkenne die Promotionsordnung der Fakultät für Mathematik und Naturwissenschaften der Technische Universität Dresden an.

Signed:

Date:
